Author:
Kennedy-Asser, Alan

Title:
Climatic and oceanic changes across the Eocene-Oligocene Transition

Climatic and oceanic changes across the Eocene-Oligocene Transition

Alan Thomas Kennedy-Asser

A dissertation submitted to the University of Bristol in accordance with the requirements for award of the degree of PhD in the Faculty of Sciences

School of Geographical Sciences, July 2019

Word Count: 47,473

Abstract

The Earth system changed significantly at the Eocene-Oligocene Transition (EOT), around 34 Million years ago. After gradual cooling through the late Eocene, there was a rapid expansion of ice over Antarctica associated with global cooling, recorded by multiple proxy records. This cooling was likely driven by declining atmospheric pCO_2 levels; however, the underlying cause of the declining pCO_2 remains a relatively open question, with the role of changing ocean gateways such as the Drake Passage still debated. Using a fully coupled 3-D climate model, this thesis explores the climatic and oceanic response of the Earth system to some of the major changes that occurred across the EOT. This was done by simulating the equilibrium climate response to multiple different sets of boundary conditions, for example different Antarctic ice sheet states, palaeogeographic reconstructions and atmospheric pCO_2 levels. These simulations were used to address some fundamental questions regarding how the presence of the Antarctic ice sheet impacts on global and regional climate, and how sensitive palaeoclimate model simulations are to subtle changes in boundary conditions. It is shown that the inclusion of the Antarctic ice sheet in the model can result in high latitude warming, however, this response is highly sensitive to the boundary conditions used and the length of the model spin-up. To validate these model simulations (as well as simulations from other modelling groups) and to better understand the most plausible forcings and responses across the EOT, a large compilation of proxy temperature records was combined for the Southern Ocean and high latitude Southern Hemisphere. The evaluation suggests that modelled changes in response to opening of the Drake Passage are inconsistent with the temperature patterns recorded for the Southern Ocean, and that ice growth and pCO_2 decline represent a more realistic mechanism of explaining the changes observed in the proxy records.

Acknowledgements

There are so many people who deserve credit for helping me complete this thesis.

My principal supervisor, Dan Lunt, has been excellent at guiding me through the project, being very generous with time and advice. I know I am not the only person in the Geography Postgraduate (Browns) community that appreciates all the effort he puts in.

Additionally, I would like to thank co-supervisor Steph Cornford, who stuck with my attempts to model the early Oligocene Antarctic ice sheet. Unfortunately, I have no fruits to show for that labour in this thesis, but it provided a challenge and gave me a better appreciation of the uncertainties in modelling as a whole.

Of course, I have had so many creative and stimulating conversations with other great researchers from the University of Bristol and beyond, from professors to other students. For me, these interactions really brought the topic to life. These people are too many to name individually, but I owe you all a drink in the future.

Thanks, too, go to my family and friends, for putting up with me through the past four years. I'm sure many of them wonder how I am still just writing *one* essay after all this time. My experience of the final push to get this thesis finished was a very insular one, with endless hours and days lost in the depths of my own head. Although it has been hard to find the time in the past few months, interactions with friends and family have been vital for reminding me there's so much more out there. I am looking forward to having some open-ended time to catch up with you all again properly soon.

A special thanks go to my Mum, and Dad. Twenty-two years of subtle nudging with dinosaur books, walks in Northern Irish countryside and forced labour in the garden gave me a love of the outdoors and a curiosity in life that I suppose inevitably led me to committing four years to trying to understand how the natural world works.

Finally, I want to thank my beautiful wife, Georgina, who has been at my side every step of the way through this PhD. From forgiving me for upping-sticks and moving to Leeds for a work placement, to optionally sitting through my BRIDGE seminars on palaeoclimate, you have always supported me and kept a smile on my face through all of the ups and downs. I can't thank you enough.

I declare that the work in this dissertation was carried out in accordance with the requirements of the University's *Regulations and Code of Practice for Research Degree Programmes* and that it has not been submitted for any other academic award. Except where indicated by specific reference in the text, the work is the candidate's own work. Work done in collaboration with, or with the assistance of, others, is indicated as such. Any views expressed in the dissertation are those of the author.

Signed:

Date:

Table of contents

Chapter 3: Assessing mechanisms and uncertainty in modelled climatic change at the Eocene Oligocene Transition

Chapter 4: Changes in the high latitude Southern Hemisphere through the Eocene-Oligocene Transition

List of tables and illustrations

"High mountains, covered with snow"

Edward Bransfield, 1820, on the first sighting of the Antarctic Peninsula

Chapter 1: Introduction

1.0. The Eocene-Oligocene Transition

The Eocene-Oligocene Transition (EOT) marks one of the most significant shifts in the state of the Earth system of the past 65 million years (Kennett & Shackleton, 1976; Zachos et al., 2008), including the first major expansion of ice sheets over the Antarctic continent following several million years of gradually falling global temperatures (Zachos et al., 2001; Inglis et al., 2015). The Eocene-Oligocene Boundary (E/O) is officially marked in the geologic record by the extinction of the phytoplankton Family Hantkeninidae (Nocchi et al., 1986; Coccione, 1988; Silva & Jenkins, 1993), dated at 33.9 million years ago (Ma; Cohen et al., 2018); however, the changes generally associated with the EOT span over a time period ranging from 500,000 to several million years (e.g. Coxall et al., 2005; Coxall & Pearson, 2007; Scher et al. 2011; Bohaty et al., 2012; Coxall et al., 2018). Alongside the expansion of ice on Antarctica, there were changes in ocean circulation and overturning (e.g. Katz et al., 2011; Coxall et al., 2018), ocean biogeochemistry (e.g. Lear et al., 2008; Pälike et al., 2012), global climate (e.g. Liu et al., 2009), marine ecosystems (e.g. Villa et al., 2013; Houben et al., 2013), terrestrial fauna (e.g. Prothero, 1994; Kraatz & Geisler, 2010; Costa et al., 2011) and potentially ice expansion in the Northern Hemisphere (e.g. Eldrett et al., 2007; Bernard et al., 2016; Tripati & Darby, 2018).

The Eocene is a geological Epoch that spans from ~56-34 Ma. Throughout the Eocene and as far back as the Cretaceous Period (~146-66 Ma), the Antarctic continent resided over the South Pole, but remained relatively ice free (e.g. Francis & Poole, 2002; Markwick, 2007; Pross et al., 2012). Although there is some evidence for limited mountain glaciation (e.g. Birkenmajer et al., 2005) and some modelling studies which suggest glaciation was not impossible (e.g. Ladant & Donnadieu, 2016), generally the period from the Cretaceous through to the Eocene is described as a *greenhouse* world. This greenhouse world is associated with high atmospheric pCO_2 levels (estimates ranging from 500-2,000 ppmv; e.g. Foster et al., 2017) and much warmer temperatures globally (e.g. deep ocean temperatures up to 10 °C hotter; Zachos et al., 2001) and at the poles (Pross et al., 2012; Inglis et al., 2015). This allowed the expansion of paratropical forests – biomes resembling modern tropical forests but located at much higher latitudes – and temperate forest conditions at very high latitudes (Francis & Poole, 2002; Pross et al., 2012). Although Antarctica might have had some limited glaciation during this period, there is evidence for mixed vegetation ecosystems at least at the coast throughout the Eocene in the form of fossilised leaves, seeds and

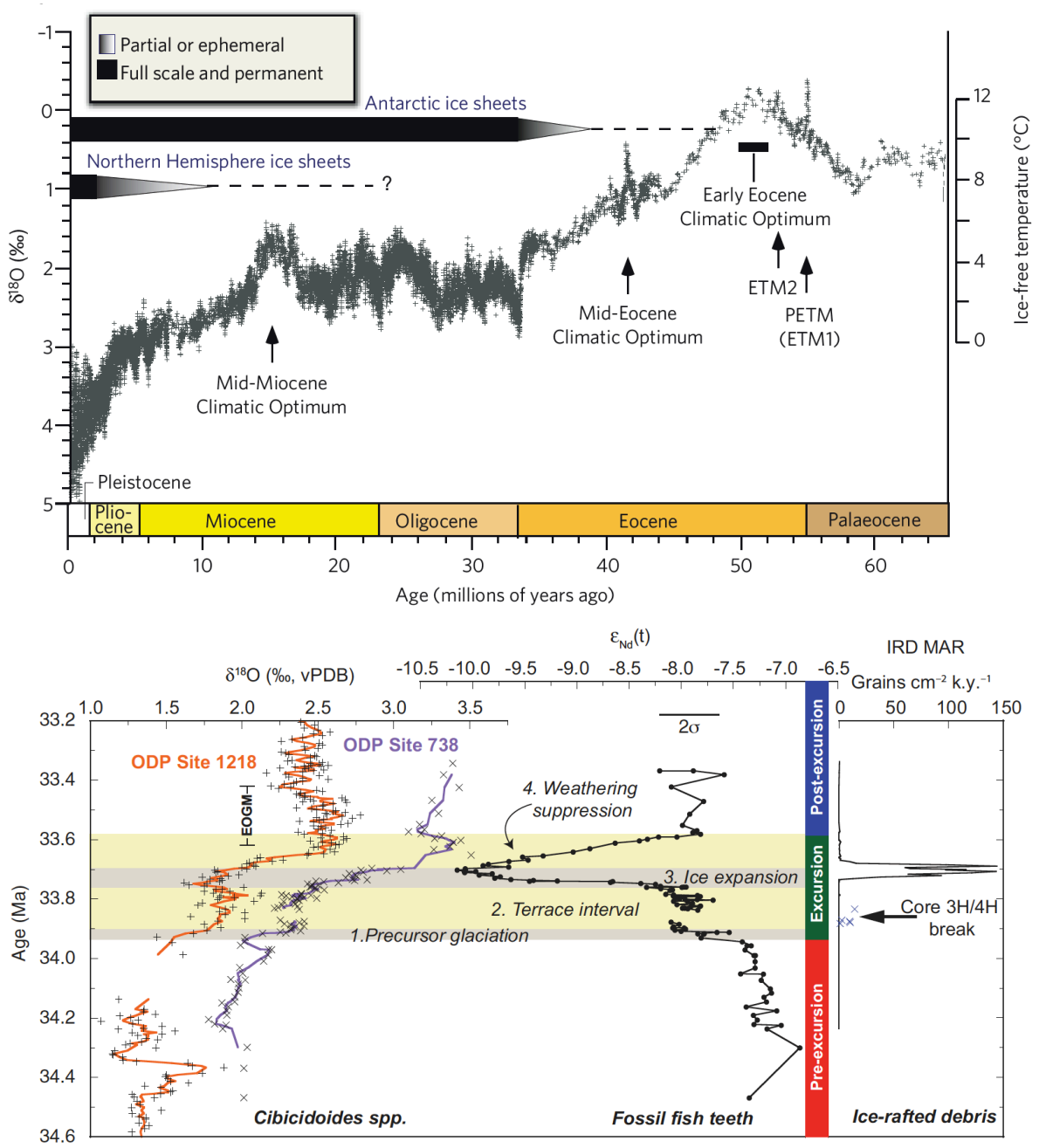

Figure 1.1: a) Global changes in oxygen isotope records show a cooling trend from the mid-late Eocene, followed by a rapid excursion at the Eocene-Oligocene Transition (figure from Zachos et al., 2008); b) the rapid oxygen isotope excursion is due to cooling and major glaciation of Antarctica, associated with increased glacial weathering products such as ice rafted debris (figure from Scher et al., 2011).

wood from various regions around Antarctica (e.g. Francis & Poole, 2002; Francis et al., 2009; Pross et al., 2012). Explaining these warm polar conditions has remained a challenge in palaeoclimate research, with most climate models failing to properly recreate such patterns, especially at reasonable atmospheric pCO_2 concentrations (Spicer et al., 2008; Huber & Caballero, 2011; Lunt et al., 2012). Although modern locations such as Patagonia may be broadly

representative of the climate of Antarctica during these greenhouse periods (Francis & Hill, 1996; Poole et al., 2005), the extreme seasonality of Antarctica still would have been a challenge for vegetation and finding modern day analogues remains challenging.

From the middle towards the end of the Eocene, global temperatures started to cool, shown in Figure 1.1a (Zachos et al., 2008). The culmination of this cooling was the relatively rapid expansion of glacial ice over much of Antarctica, evidenced by a large excursion in global oxygen isotope records (Zachos et al., 2008) synchronous with other proxies of glaciation such as ice rafted debris in ocean sediments off the coast of Antarctica, shown in Figure 1.1b (Zachos et al., 1992; Scher et al., 2011). It is not surprising nor coincidental that the geological definition of the E/O (based on species extinction) coincides with this change in the Earth's climate state, as such a major change in the atmospheric and oceanic temperatures would have forced many species out of their realms of survivability (e.g. Prothero, 1994; Meng & McKenna, 1998; Kraatz & Geisler, 2010). Following the formation of this large ice sheet at the beginning of the Oligocene geological Epoch, this period of the Earth's history is often referred to as an *icehouse* world. Although the AIS that formed at the EOT was still highly variable during the Oligocene (Pälike et al., 2006; Liebrand et al., 2017) and had not yet reached its full extent (e.g. Zachos et al., 2008; Huang et al., 2014), and the Northern Hemisphere is thought to have remained largely ice free until the Pliocene Epoch (~5.3-2.6 Ma; Zachos et al., 2008; DeConto et al., 2008), generally the Earth's climate remained much cooler than during the Eocene greenhouse. Vegetation persisted in Antarctica until the Miocene (~23-5.6 Ma), although diversity generally drops at the EOT and species become increasingly stunted as the icehouse climate cools (Askin & Raine, 2000). Elsewhere in the world, the global cooling during the icehouse eventually likely lead to the expansion of grasslands (e.g. Retallack, 2000; Edwards et al., 2010) as well as the large-scale glaciations of the Northern Hemisphere during the Pleistocene ice ages (Zachos et al., 2001), that shaped the natural world and species that we have on Earth today.

Understanding critical transitions in the Earth system from the geologic record such as the change from a greenhouse to an icehouse world at the EOT help us improve our understanding of tipping points and feedback mechanisms within the Earth's climate system (Valdes, 2011; von der Heydt et al., 2016). This is a key motivation for palaeoclimate research. The vast range of changes occurring around and across the EOT means there are many aspects of this period which still have not been researched in great depth and many questions about this significant shift remain unanswered. This thesis aims to address some of the uncertainties in our understanding of the climatic and oceanic response to the major changes that occurred at this time.

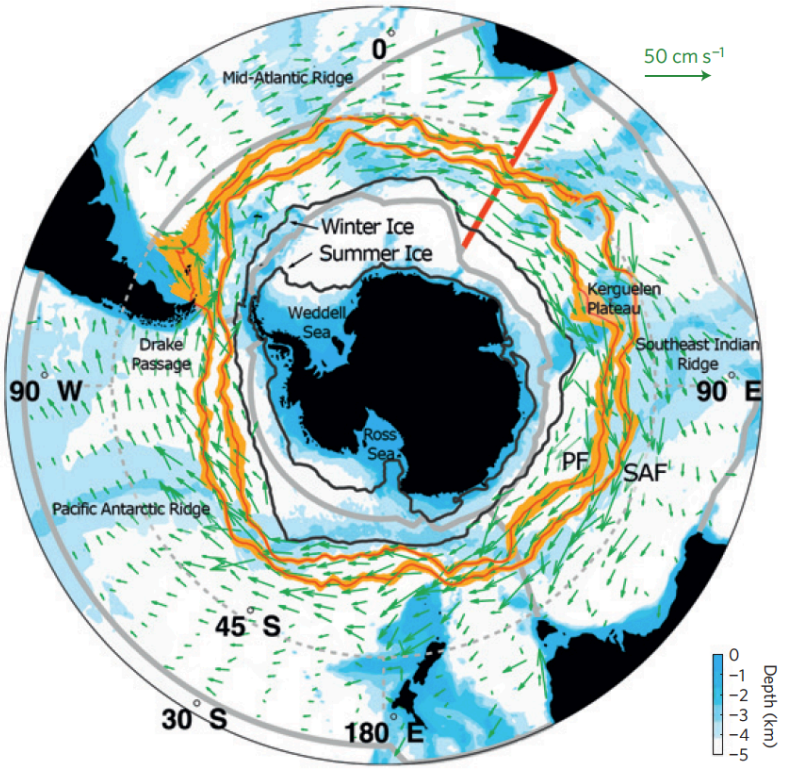

Figure 1.2: Summary of the key oceanographic features (e.g. Polar Front, PF; Subantarctic Front, SAF) of the present-day Antarctic Circumpolar Current (ACC; figure from Marshall & Speer, 2012). The initiation of the proto-ACC with the opening of ocean gateways between Antarctica and Australia and South America was proposed as the cause of the cooling and glaciation at the Eocene-Oligocene Transition (Kennett and Shackleton, 1976).

1.0.1. Why did the Eocene-Oligocene Transition occur?

On geological time scales, there are a number of *forcings* that can affect global climate and hence could be responsible for large transitions such as the EOT. A true forcing is something that is entirely external to the climate system, such as changes in the Earth's orbit around the Sun (Hays et al., 1976; Laskar et al., 2004), solar output (intensity; Caldeira & Kasting, 1992) or changes in the plate tectonics to volcanism (Hammer et al., 1980; Robock, 2000) or palaeogeography (Markwick, 2007). However, in addition to these forcings, other indirect processes may also influence the Earth's climate. Changes in atmospheric greenhouse gases (e.g. Foster & Rohling, 2013), the cryosphere (e.g. Ganopolski et al., 2010) or biological processes (e.g. Watson et al., 2000; Beerling & Osborne, 2006) are some examples of *long-term feedbacks* in the Earth system, although they may sometimes be considered as forcings to the climate.

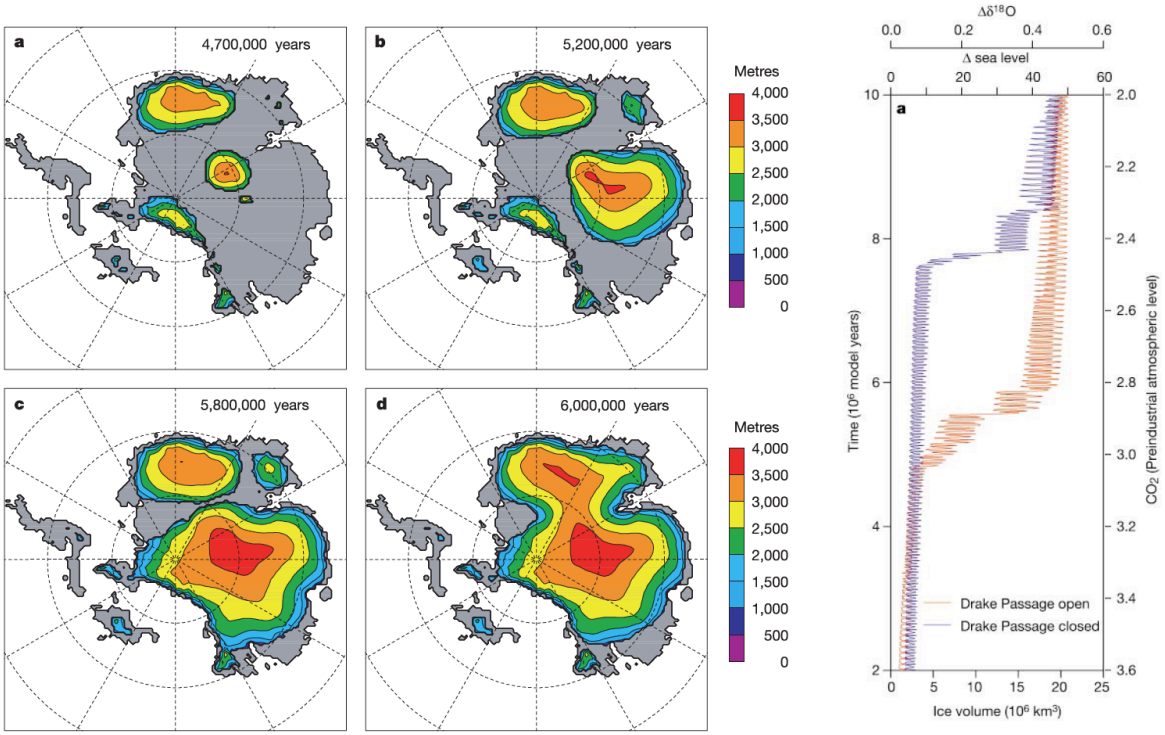

Figure 1.3: The modelling work by DeConto & Pollard (2003a) to asynchronously couple an ice sheet and climate model showed that the Antarctic ice sheet would form regardless of whether the Drake Passage was open or closed, if atmospheric pCO_2 is reduced enough (figure from DeConto & Pollard, 2003a).

When creating models of the Earth system for deep-time periods such as the EOT, regardless of whether these are numerical or conceptual models, it is important to consider the different roles of these forcings. Some numerical models will explicitly model changes in biogeochemistry and greenhouse gases (e.g. Armstrong McKay et al., 2016), while others have greater complexity in their modelling of the oceans and atmosphere, meaning they must prescribe variables such as the atmospheric greenhouse gases and so these are more representative of a forcing (e.g. Lunt et al., 2016).

Understanding of the underlying causes of the cooling and the eventual trigger of glaciation at the EOT has focussed on two main hypotheses. First, the *gateway hypothesis* proposes that the opening of the ocean gateways in the Southern Ocean between Antarctica and South America and Australia permitted the formation of the Antarctic Circumpolar Current (ACC), shown in Figure 1.2 (Marshal & Speer, 2012), leading to thermal isolation and glaciation of the Antarctic continent (Kennett & Shackleton, 1976; Kennett, 1977). Second, the *CO_2 hypothesis* proposes that declining atmospheric pCO_2 levels resulted in global cooling, which caused glaciation once a temperature threshold over Antarctica was reached (DeConto & Pollard, 2003a). For the latter hypothesis, the

precise timing of glaciation would have been affected by orbital cycles and the gateway configuration at the time (DeConto & Pollard, 2003a), but ultimately it is the pCO_2 decline that causes the major cooling, as shown in Figure 1.3. This is in broad agreement with proxy reconstructions of pCO_2 which also show a drop around the EOT (e.g. Pearson et al., 2009; Pagani et al., 2011). However, as atmospheric pCO_2 is a long-term feedback and not a true forcing, explaining what would have caused the pCO_2 to drop remains a relatively open question (e.g. Lefebvre et al., 2013; Fyke et al., 2015; Armstrong McKay et al., 2016; Elsworth et al., 2017).

Palaeoclimate research relies on a combination of modelling and proxy reconstruction work to build up evidence and explain major past events such as the EOT. Although the majority of recent evidence suggests that declining pCO_2 is the more likely driver of the cooling and Antarctic glaciation at the EOT, particularly from modelling studies (e.g. DeConto & Pollard, 2003a; Huber & Nof, 2006; Lefebvre et al., 2012; Ladant et al., 2014a; Goldner et al., 2014 etc.), the complexity of separating out the climatic feedbacks with atmospheric pCO_2 has left some debate regarding the true forcing of the EOT. Added to these issues untangling the cause and effect of changes around Antarctic glaciation, changes elsewhere around the world across the EOT are far from uniform in terms of magnitude and timing. In the oceans, cooling estimates range from negligible changes to drops of over 8 °C (Liu et al., 2009; Plancq et al., 2014) and there are large unknowns in the terrestrial response (Pound & Salzmann, 2017). Meanwhile, there are also known deficiencies in palaeoclimate modelling in explaining the proxy record, such as explaining the equable climate problem (Huber & Caballero, 2011; Lunt et al., 2012) and being too stable compared to some of the major swings in climate observed in the geologic record (Valdes, 2011).

The mid-Cenozoic period, within which the EOT lies, had many known changes of palaeogeography, such as the opening or widening of the Tasman Seaway (e.g. Stickley et al., 2004), illustrated in Figure 1.4 based upon the reconstructions of Getech Group plc. (as used in Kennedy et al., 2015). Also occurring was the early stages of uplift around the Tibetan Plateau (e.g. Sun & Windley, 2015), constriction of the Tethys Seaway (e.g. Ozsvárt et al., 2016), changes in the Central Asian Seaway or Turgai Strait (Rögl, 1999) and potential changes in Northern Hemisphere connections with the Arctic oceans (e.g. Hohbein et al., 2012). Although the precise timing of these changes is open to debate, they are expected to have some major implications for the Earth system, ranging from interaction of terrestrial species (potentially leading to extinction events; e.g. Kraatz & Geisler, 2010) to major perturbations in ocean circulation and overturning (e.g. Coxall et al., 2018). Clearly the true changes that occurred across the EOT were the result of a combination and the interaction between many of these different processes, without a solitary cause or forcing.

Figure 1.4: Illustration of how Antarctica might have looked prior to the Eocene-Oligocene Transition based upon the palaeogeographic reconstructions of Getech Group plc., used in Kennedy et al., (2015). An incipient ice sheet is spreading from the upland regions of the continent (DeConto & Pollard, 2003a), while low lying and coastal regions remain covered with mixed forest ecosystems (Francis et al., 2009). The narrow Tasman Seaway is just opening (Stickley et al., 2004) and marine ecosystems in the Southern Ocean are starting to shift from warmer to colder water taxa (Villa et al., 2013; Houben et al., 2013). Image designed by A.T. Kennedy, used in Lear & Lunt (2016).

1.0.2. Importance of the Antarctic ice sheet

The Antarctic ice sheet (AIS) is an important feature of the Earth system. It directly impacts upon global sea level (e.g. Alley et al., 2005; Dutton et al., 2015), circulation of the atmosphere and oceans (e.g. Hill et al., 2013; Goldner et al., 2014), global energy balance (e.g. Stap et al., 2017) and indirectly impacts biogeochemistry (e.g. by exposing shelf sediments or increasing weathering; e.g. Armstrong McKay et al., 2016) and polar marine ecosystems (e.g. Hawkings et al., 2014). Following its establishment at the EOT, the AIS would have had important implications for the Earth's climate and oceans and has since undergone periods of growth and decline on an array of timescales (Zachos et al., 2001; Pälike et al., 2006; Liebrand et al., 2017).

Given the uncertainty of future anthropogenic warming and the impact this could have on the Earth's ice sheets, which store more than 90 % of all fresh water on Earth, understanding the significance of changes in the AIS is of great importance to national and international policy makers (Church et al., 2013). Although complete collapse of the major polar ice sheets is likely to be beyond the lifespan of current generations, significant changes in the coming centuries cannot be ruled out (Joughin & Alley, 2011; Bamber & Aspinall, 2013; Vaughan et al., 2013; Golledge et al., 2015; DeConto & Pollard, 2016). Without a long observational record to base research on, deep-time case studies of change in the ice sheets and the implications this would have on global climate can provide useful tools (e.g. de Boer et al., 2015; DeConto & Pollard, 2016).

Given the vast differences in the Earth system today compared to these deep-time periods, describing past changes as an analogue of the future is likely exaggerating this research (not least in terms of the timescales over which the changes occurred). However, with only limited data available for the present, palaeoclimate work still provides an important check to constrain and validate our fundamental understanding of modern behaviour in the Earth system.

1.1. Palaeoclimate modelling

Models of the Earth system exist on a spectrum of complexity. The term *model* can essentially refer to any representation of the Earth system or its processes, with the simplest models being conceptual models that are essentially working hypotheses, possibly consisting of a small number of mathematical functions and parameters that often can be analytically solved. They generally are spatially simplified (e.g. being global or hemispheric, not 3-dimensional) but as a result are very quick to calculate for any combination of boundary conditions. Examples of conceptual models include the 1-dimensional ice accumulation models of Weertman (1976) and Oerlemans (2002) or the weathering-pCO_2 relationship of Elsworth et al. (2017).

At the other end of the spectrum of complexity are General Circulation Models (GCMs) that resolve the movement and transfer of heat and momentum in oceans and atmosphere in 3-dimensions. The spatial resolution of GCMs can vary significantly, but with increasing spatial resolution they become increasingly costly to run in terms of computing time and resources. These models are based on fundamental physical equations of thermodynamics and of motion in fluids (the Navier-Stokes equations) and often make up the core for weather prediction models. GCMs can be of the ocean, atmosphere or both (known as coupled models).

Although these models are reasonably complex, they represent the climate in 3-dimensions at a relatively coarse spatial resolution due to the computing power it requires to run such models. Certain small-scale processes that occur on more local scales than the models' spatial resolution (such as cloud formation or convection), as well as unknown processes in the real world, have to be parameterised in these models. This generally involves simplifying the process, so it can be represented by an empirical approximation that is tuned to fit modern day observations. Additionally, the complexity of the Navier-Stokes equations means they cannot be solved analytically on this scale, and so they must be simplified. As a result, most GCMs use the so-called Primitive Equations, which approximate the Navier-Stokes equations for use on thin fluid layers around a sphere. The Primitive Equations have highly traceable physics, meaning that the impact these approximations have on the resulting model output are reasonably well understood. Although a number of different GCMs exist and are used around the world, many are built on fundamentally the same numerical core, meaning they are often not totally independent of each other. Some examples of GCMs include HadCM3 (Gordon et al., 2000) and CESM (Gent et al., 2011).

In addition to these general extremes of the modelling spectrum there are Earth System Models (ESMs) and Earth system Models of Intermediate Complexity (EMICs). Both of these types of models incorporate other Earth system processes beyond just the climate of the atmosphere and oceans. This could include complex biogeochemistry for the oceans (e.g. cGENIE; Ridgwell et al., 2007) or an interactive and dynamic cryosphere (e.g. CLIMBER-SICOPOLIS; Ganopolski et al., 2010). ESMs incorporate these processes into GCMs and represent the state-of-the-art in modelling (e.g. UKESM, 2018). However, the sheer complexity of these models makes them prohibitively expensive to run for palaeoclimate research. In contrast, EMICs incorporate these other processes by simplifying their representation of the atmosphere and ocean dynamics, allowing the simulations to be run for long time periods while still including these processes that may be of great interest in palaeoclimate research. Examples of EMICs used in palaeoclimate research include the 2.5D model of Berger et al. (1990) that is used to simulate Northern Hemisphere glaciation over the last glacial cycle based on orbital forcings (but only simulates latitude and height in the atmosphere) and GENIE, a 3D model of the ocean with a simplified atmosphere, but very advanced representation of the ocean biogeochemistry (Ridgwell et al., 2007).

Simplifying the model physics for the dynamics in the ocean and the atmosphere can make the results less useful for certain applications (e.g. if interested in conditions over a specific region) and can also make the results significantly less traceable. However, these models come with the benefit of including other processes and being much more affordable to run for long periods, which can be of particular interest in palaeoclimate research when changes happen on a geological timescale. As a result, there is no perfect model and a model must be chosen based on the science question which it is being used to answer.

Although some palaeoclimate research might be able to run a realistic transient simulation of a past climatic event with a GCM (e.g. Shakun et al., 2012, model the last deglaciation from ~22.0-6.5 thousand years ago), generally for deeper time periods such as the EOT when the changes occur over timescales of 10^4-10^6 years, transient simulations would take too long to complete with a GCM. As a result, *snapshot* equilibrium climate simulations are generally carried out, where the model is run for as long as possible with generalised boundary and input conditions that are relevant for the period, until its output climate becomes acceptably stable (which can be defined in terms of ocean temperature trends or top of the atmosphere radiation balance, for example). The time it takes the model to reach this point is known as the *spin-up*. This equilibrium climate is then assumed to be broadly representative of the period that would have had similar boundary conditions to those used in the model. The boundary conditions include the palaeogeography (the past reconstructions of topography and bathymetry), atmospheric greenhouse gases and aerosols

and solar and orbital parameters. In reality, none of these boundary conditions will remain constant through time, meaning that this approach to palaeoclimate modelling represents an approximation of past periods, but again it is a necessary sacrifice to make due to computational constraints.

1.1.1. Modelling of the Eocene-Oligocene Transition

Modelling the climate, oceans and AIS of the EOT with GCMs has particularly developed over the past 15 years. Given the two main hypotheses of what drove Antarctic glaciation at the EOT being ocean gateway changes and atmospheric pCO_2 decline, a lot of modelling studies have focussed on the climatic response to these forcings. However, other questions have also been addressed, ranging from better understanding the greenhouse climates of the Eocene to modelling the variability of the AIS through the Oligocene. A brief summary of studies using some of the most frequently used GCMs is provided here.

The first major model that has been used extensively for palaeoclimate research around the EOT and for modelling changes in ice sheets through time is GENESIS (Thompson & Pollard, 1997). This is a 'slab ocean' GCM, meaning it does not have a dynamic 3-D ocean, instead having an ocean which is 50 m deep which can absorb heat from the atmosphere but has prescribed ocean heat transport. Once the ocean heat transport has been tuned to produce reasonable results, this simplified ocean makes it much quicker to run and spin-up than a fully-coupled GCM. Typically this has allowed it to be used in studies covering long time periods or combinations of boundary conditions, necessary for asynchronously coupling the model to an ice sheet model for example (e.g. DeConto & Pollard, 2003a; Pollard & DeConto, 2005; Pollard et al., 2013). Although the slab ocean of GENESIS means its climatic results can be scrutinised for not fully capturing feedbacks in the Earth system, its speed to run in combination with a relatively efficient ice sheet model (Pollard & DeConto, 2012) mean few models have provided as many results in terms of modelling the interaction between the climate and cryosphere.

The seminal work of DeConto & Pollard (2003a, b) used GENESIS, coupled asynchronously to an ice sheet model. This methodology produced multiple snapshots of the climate from relatively short GENESIS simulations, that were then used to force the ice sheet model for 10,000 year simulations. The resulting ice sheet geometry was then updated in GENESIS and used to produce an updated snapshot of the climate. Atmospheric pCO_2 in the model could be reduced over time, while opening of the Drake Passage is parameterised by increasing or reducing the ocean heat

transport, as the non-dynamic slab ocean does not explicitly model how changing ocean gateways would affect the climate. Studies with a similar setup (e.g. Pollard & DeConto, 2005; Pollard et al., 2005; Pollard et al., 2013) have been used to evaluate sensitivity in the expansion and collapse of the ice sheet and if it exhibits hysteresis, while climate only simulations have also been used assess the impact of vegetation on Antarctic climate around the EOT (Thorn & DeConto, 2006), for example.

Later work with GENESIS coupled to an ice sheet model also explored the potential of Northern Hemisphere ice growth at the EOT (DeConto et al., 2008). This study suggested that the pCO_2 threshold to allow ice to accumulate over Greenland is much lower than for Antarctica, meaning Northern Hemisphere glaciation seems unlikely at the pCO_2 levels recorded by most proxies for the EOT. Building upon this, Wilson et al. (2013) present revised estimates using GENESIS of how much ice could be accommodated on the Antarctic continent in the earliest Oligocene based on newer palaeogeographic reconstructions of Antarctica (Wilson et al., 2012). They suggest that the global ice volume thought to have formed at the EOT could have been situated entirely over Antarctica.

Another reduced complexity model that has been used to simulate the climate around the EOT is the EMIC, UVic (Weaver et al., 2001). This model has a 3-D ocean (the GFDL Modular Ocean Model 2.2; Pacanowski, 1995), coupled with a simplified energy-moisture balance atmosphere. Again, the reduced complexity of this model (in this case in the atmospheric domain) allow it to be run for long time periods and incorporate other processes, such as a dynamic carbon cycle.

The study of Sijp & England (2004) using UVic supported the hypothesis that changes in ocean gateways (specifically the Drake Passage) could cause significant changes in heat transport and cooling in the Southern Ocean. They also found that increasing the depth of an open Drake Passage could impact on North Atlantic overturning and thus affect Northern Hemisphere climate. The later study of Sijp et al. (2011) finds that although changes in ocean gateways (in that case a deepening of Tasman Seaway) do result in a strengthened ACC in UVic, associated with some regional temperature redistribution, there is limited cooling in the interior of Antarctica. However, this study does suggest that changes in the Tasman Seaways can cause deep ocean cooling as a result of increased sinking in the Southern Ocean, a conclusion that is shown again in Sijp et al. (2014) using both UVic and a fully coupled model, CCSM3. Coupling UVic with a carbon cycle model, Fyke et al. (2015) also find that gateway changes can have important implications for the Earth system, with changes in the Drake Passage and Panama Seaway affecting North Atlantic overturning and the distribution of dissolved inorganic carbon in the global oceans.

One of the fully-coupled GCMs most commonly used for EOT research is CCSM (Blackmon et al., 2001). This model has multiple versions of varying complexity, with the most recent version, CCSM 4 (also known as CESM 1; Gent et al., 2011) having higher resolution and improved parameterisation sof many elements of the Earth system over its predecessors. While not focussing on the modelling explicitly, multiple studies presenting novel EOT proxy results have been supplemented by model simulations from the CCSM group of models. For example, Eldrett et al. (2009) and Liu et al. (2009) use CCSM 3 results to explore spatial changes in surface air temperature and in the ocean with depth.

Early work by Huber et al. (2004) used CCSM 1 to investigate the effect of deepening of the Tasman Seaway in the model and found that it had little impact on continental Antarctic climate. They find that the East Antarctic Current does not extend significantly southwards even when the Tasman Seaway is closed and so does not result in a significant increase poleward heat transport. Huber & Nof (2006) further this result, bringing together results from other models (including atmosphere only variants of CCSM and simplified numerical ocean models). They find that across the range of model complexity, there was no strong evidence of greatly increased heat transport in the Eocene, or a significant enough change in ocean heat transport to cause the EOT.

The most recent version of the model, CESM is used by Goldner et al. (2013) in a slab ocean configuration to investigate the impact of Antarctic glaciation on climate. This study does not focus on the inception of glaciation; instead, they focus on the atmospheric feedbacks relating to cloud microphysics and how this affects the climatic fingerprint of the AIS in the modern compared to the Eocene. They find that the climate (and low clouds in particular) behave differently for the modern and Eocene setups of the model in response to glaciation, and that Antarctic glaciation at the EOT might have had limited impact on global temperatures due to negative feedback processes. Goldner et al. (2014) build on these results using the fully coupled version of CESM to show that the impact of Antarctic glaciation affected the structure of the ocean at depth due to changes in Southern Ocean overturning. They suggest that this results in a change that matches well with proxy data, potentially explaining the changes that had previously been best explained by ocean gateway changes (e.g. Sijp et a., 2014).

Other research groups have also used this model, for example Liakka et al. (2014) use the atmosphere only version of CESM in combination with a dynamic vegetation model and an offline ice sheet model to assess how Antarctic vegetation can impact on the pCO_2 threshold of Antarctic glaciation. They suggest that the vegetation effect on snow albedo and associated changes in

meridional heat transport play important feedback mechanisms in controlling glaciation. Finally, Baatsen et al. (2018a) use the fully coupled version of CESM to investigate the late Eocene climate and evaluate it against an extensive proxy database. They find that changes in cloud feedbacks, albedo, palaeogeographic land mass and ice sheets can reduce the latitudinal temperature gradient in the model to one that provides a reasonable fit with data, without having to increase the atmospheric pCO_2 to very high levels (e.g. Huber & Caballero, 2011).

FOAM is a relatively fast coupled climate model, that uses a reduced resolution version of the Community Climate Model atmosphere (4.5 x 7.5 °) coupled to the Modular Ocean Model ocean (Jacob et al., 2001). Its relatively efficient computational speed (at the expense of reduced resolution) allows FOAM to be used for long simulations with multiple setups, or with additional model components such as a carbon cycle module (known as GEOCLIM; Donnadieu et al., 2009).

Zhang et al. (2011) use FOAM with multiple palaeogeographic reconstructions varying various ocean gateways around the world (including the Drake Passage, Panama Seaway, the Tethys and connections to the Arctic). They find that changes in low latitude gateways can have effects on higher latitudes, causing cooling in the high latitude Southern Hemisphere by increasing deep water formation in the North Atlantic.

Other studies using FOAM, however, suggest pCO_2 is a more important driver of climate, with Lefebvre et al. (2012) and Ladant et al. (2014b) both suggesting that declining pCO_2 levels and glaciation of Antarctica can increase the strength of the ACC by increasing latitudinal temperature gradients and increasing deep water formation through expansion of sea ice. They therefore conclude that the ACC acts partly as a feedback with the changes occurring at the EOT, rather than as a forcing. Ladant et al. (2014a) carry out a similar study to DeConto & Pollard (2003a), using multiple climatic snapshot simulations with varying orbits, pCO_2 levels and AIS states, to then use a matrix approach to drive a higher resolution land surface model and a dynamic ice sheet model. The ice sheet model can be run transiently across the EOT by interpolating between the climatic snapshots and correctly recreates the two-step nature of the EOT shown in oxygen isotope records, with the glaciation paced by orbital and pCO_2 variations.

A third fully coupled GCM that is regularly used in palaeoclimate research is HadCM3L (Cox et al., 2001). Unlike CCSM, HadCM3L has not changed significantly with time; however, different modelling groups have implemented modifications to various aspects of the code from the original version (e.g. HadCM3BL used at the University of Bristol; Valdes et al., 2017). Higher resolution and more advanced versions of the model (e.g. HadCM3, Gordon et al., 2000; HadGEM3, Hewitt et al., 2011) are available, but due to the increased computational demands of these models, they

have been less widely used, with no studies focussing directly on the EOT. A specific example modelling the EOT using HadCM3L (Hill et al., 2013) focusses on changes in the ACC around the EOT, with varying palaeogeography and AIS state. In those simulations, the position of Australia is found to be important for determining the strength of the ACC even with open Southern Ocean gateways, which would be consistent with some proxy records that suggest the ACC continued to strengthen later in the Oligocene (e.g. Pfuhl & McCave, 2005). This study, however, does not discuss climatic changes in great depth.

Gasson et al. (2014) discuss the pCO_2 threshold for Antarctic glaciation based on the modelled climate from 7 different GCMs. Utilising the results from the Eocene Model Inter-comparison Project (EoMIP; Lunt et al., 2012), as well as various other studies, these climate models were used to drive an offline ice sheet model (GLIMMER; Rutt et al., 2009). The study showed that the threshold varies significantly between models and their setup, with GENESIS being the most likely to produce major glaciation (at around 3x pre-industrial pCO_2 levels), while HadCM3L was unable to produce any major ice over Antarctica until atmospheric pCO_2 was at or below pre-industrial levels. The fact that HadCM3L fails to glaciate is shown to be related to its extremely high seasonality over Antarctica; however, why the seasonality was so high was not identified. This study clearly shows the sensitivity of palaeoclimate model results, with potential inter- and intra-model uncertainties.

Finally, some more recent studies have focussed on the climate of the late Eocene and EOT using other models that have not been used as extensively in the literature. Using the ocean-only model POP, Baatsen et al. (2018b) show an example of bistability in the ocean circulation state using two similar palaeogeographic reconstructions, with a potential switch from North Pacific to South Pacific deep water formation. Elsworth et al. (2017) use the CM2Mc model, which is a 3 ° resolution version of the NOAA GFDL model, to look at the impact of a deepening Drake Passage on the Earth's oceans. They parameterise this based on a modern day topography and bathymetry with the only changes being to vary the Drake Passage depth and to open the Panama Seaway. They show this affects the stratification in the Southern Ocean and enhances overturning in the North Atlantic, with resultant impacts on climate which they propose could enhance weathering feedbacks and draw down atmospheric pCO_2. Hutchinson et al. (2018) use a much higher resolution version of the GFDL model with a 1 x 1.5 ° ocean and a late Eocene palaeogeography under three pCO_2 levels. Their simulations show overturning in the Southern Ocean and North Pacific, which they attribute to changes in salinity patterns due to using the late Eocene palaeogeography. The model can simulate reasonable global mean temperatures; however, the

model shows a steeper latitudinal temperature gradient compared to the proxy records compiled in Baatsen et al. (2018a).

There is a mixture of narratives through these various modelling studies. Clearly, the majority of GCMs show that pCO_2 plays a major role in controlling climate, particularly temperature, and so it is unsurprising that this provides a viable method to induce Antarctic glaciation. However, as Gasson et al. (2014) showed, the models are far from agreement in terms of what the climate sensitivity was or how latitudinal temperatures varied. Additionally, the effect of pCO_2 on other aspects of the Earth system (such as the ACC) is much more complex. Some studies suggest linkages between pCO_2, the AIS and various ocean gateways and the state of ocean circulation, with little clear consensus between all of these models.

A host of physical oceanographic studies have looked at changes in the ocean circulation that have some relevance to those that are thought to have taken place across the EOT. For example, research has focussed on the effect of Southern Ocean wind stress on ACC flow (e.g. Allison et al., 2010) and meridional overturning (e.g. Rahmstorf & England, 1997; Sijp & England, 2009; Abernathey et al., 2011), the implications of the latitudinal location of ocean gateways (e.g. Munday et al., 2015) or the processes of deep water formation at the Antarctic margin (e.g. Assmann & Timmermann, 2005; Petty et al., 2014). However, a comprehensive review of these papers is beyond the scope of this thesis.

1.2. Research objectives

Using a combination of Earth system modelling techniques and different proxy records for changes in Earth's climate, oceans, cryosphere, vegetation, ecology etc., a complex picture of changes across the EOT has been built up by years of research. In attempting to synthesise knowledge of how the climate changed across the EOT, this thesis contributes by addressing some fundamental questions particularly relating to climate modelling of the AIS and major past climatic events such as the EOT. The three main results chapters of this thesis address three core questions, within which there are also a number of more detailed sub-research questions.:

- What impact does the Antarctic ice sheet have on regional and global climate? (Addressed in Chapter 2.)
    - How does the impact of glaciation vary between two different palaeogeographic reconstructions?
    - How does the island definition in the model affect the climatic responses shown?
    - Why do the results differ from those of Hill et al. (2013) in terms of the change in ACC flow in response to Antarctic glaciation?

- How sensitive are palaeoclimate model simulations to subtle changes in boundary conditions? (Addressed in Chapter 3.)
    - What are the impacts and relative importance of three forcings on global and Antarctic climate at the EOT (including pCO_2 drop and palaeogeographic change)?
    - For each of these forcings, what is the range of uncertainty in the magnitude of certain modelled variables resulting from differences in the model boundary conditions?
    - How does the simulation spin-up time affect the modelled impacts associated with these forcings?

- How did the high latitude Southern Hemisphere climate change across the Eocene-Oligocene Transition? (Addressed in Chapter 4.)
    - What are the spatial patterns of temperature change inferred from proxy records for the high Southern Hemisphere before, after and across the EOT?
    - Which GCMs and model boundary conditions give the best fit to a range of qualitative and quantitative proxy records of temperature before, after and across the EOT?

Chapter 2 and Chapter 3 focus primarily on the climate model responses to large changes in the model boundary conditions. This is useful exercise for testing the model's sensitivity as well as biases or uncertainties that might be introduced in palaeoclimate studies more broadly. A full review of the proxy records of the EOT globally is beyond the scope of this thesis, but many inferred changes particularly relating to the high latitude Southern Hemisphere are presented in Chapter 4, where they are used to evaluate the climate model simulations of the EOT and build up a detailed picture of the changes that occurred at that time.

Although each of these chapters broadly build upon each other, they are presented in 'paper format', mostly with their own standalone introductions and methodologies. As a result, an extensive methodology is not included in this introductory chapter. However, throughout this thesis, the climate model HadCM3BL (Valdes et al., 2017) is used extensively and so a brief description of this model is presented in the rest of this chapter.

1.3. HadCM3BL description

HadCM3B (Valdes et al., 2017) is a fully coupled GCM that is used at the University of Bristol, derived with some minor modifications from the Met Office Unified Model (UM) HadCM3 (Gordon et al., 2000). The original HadCM3 was included in CMIP-3 (third Climate Model Inter-comparison Project; IPCC, 2007), contributed to CMIP-5 and variations of it (such as HadCM3B) are still used by multiple research groups around the UK. HadCM3 (and HadCM3B in Bristol) represents the standard version of the model, but there are various versions that include different model components or work at different resolutions, such HadAM3H, HadCM3L and FAMOUS. The HadCM3B family of models is described in depth in Valdes et al. (2017), of which I was a co-author, contributing primarily to the model evaluation (Section 5.1.1 of Valdes et al., 2017). Part of this evaluation is reproduced verbatim here in Section 1.3.6.

This research uses HadCM3BL, a version of HadCM3B with a lower resolution ocean. In HadCM3BL, the ocean and atmosphere both run at 2.5 ° latitude by 3.75 ° longitude, whereas in HadCM3B the ocean runs at 1.25 ° longitude and latitude. There are benefits and limitations from using a lower resolution model such as HadCM3BL. For a fully coupled model, it is relatively fast to run, allowing multiple different experiments to be carried out in a consistent framework. However, the low-resolution limits how well certain processes and features such as deep-water formation and ocean gateways can be resolved.

The original Met Office version of HadCM3L (Cox et al., 2001) was primarily designed for carbon cycle research and HadCM3BL varies significantly from the original description of the model. HadCM3BL instead uses the ocean corrections designed for FAMOUS (an even lower resolution variant of the UM; Jones, 2003) with the original HadCM3 atmosphere (Gordon et al., 2000). A full up-to-date description of the current University of Bristol UM setup can be found in Valdes et al. (2017). Given this recent comprehensive review, only details specific to HadCM3BL and relevant to the research in this thesis will be presented.

Appendix 1 gives a detailed description of each of the simulations carried out for this thesis, their setup and purpose for future reference. Appendix 1 also notes other simulations used in this thesis that were carried out by others at the University of Bristol.

1.3.1. Atmosphere

The HadCM3BL atmosphere has 19 hybrid vertical levels (merging between sigma and pressure levels with increasing height) and a 30-minute time step (Gordon et al., 2000). As mentioned, the resolution is 2.5 ° latitude by 3.75 ° longitude on a Cartesian grid. The model solves the Primitive Equations (White & Bromley, 1995), conserving angular momentum and energy on an Arakawa staggered B-grid (Arakawa & Lamb, 1977). As a regular latitude-longitude grid is used, Fourier filtering is utilised to remove sub-grid scale variability at high latitudes, necessary to retain stability in finite difference models, depending on the time step. There are many parameterisations of sub-grid scale processes in the atmospheric module, for approximating the vertical mixing (Gregory et al., 1998; Grant, 1998), horizontal diffusion (Valdes et al., 2017), precipitation (Gregory et al., 1997; Wilson, 1998), cloud formation processes (Bushell, 1998) and radiation balance (Edwards & Slingo, 1996; Ingram et al., 1997; Edwards, 1998). These are explained in greater technical detail in Valdes et al. (2017).

1.3.2. Ocean

The HadCM3BL ocean has 20 vertical levels at 2.5 ° latitude by 3.75 ° longitude resolution with a 1-hour timestep. Fourier filters are used to remove greater than grid-scale waves from the ocean fields at high latitudes (Rickard & Foreman, 2000). It is a *rigid-lid* ocean, meaning it is not affected by fast external mode gravity waves, allowing a longer time-step but prohibiting changes in ocean volume (Valdes et al., 2017). While this model is very similar in its mechanics to HadCM3, there are modifications due to the difference in ocean resolution. There are a number of parameterisations of sub-grid scale processes, such solar radiation penetration (Valdes et al., 2017), mixed layer mixing processes (Bryan & Cox, 1972; Foreman, 2005), horizontal eddies (Gent & McWilliams, 1990), isopycnal diffusion (Valdes et al., 2017) and salinity fluxes (representing ice calving from ice sheets; Valdes et al., 2017), all of which are explained in greater depth in Valdes et al. (2017).

Importantly for palaeoclimate applications, HadCM3 (and HadCM3B) does not require flux adjustments for modern day simulations (an improvement of HadCM3 over HadCM2; Cox et al., 2001). Flux adjustments are artificial parameterisations of energy or mass (additions or removals), which are included to keep the model stable in a realistic state for the modern day (e.g. to prevent the build-up of excessive sea ice). No flux adjustments are required for HadCM3L either, provided

Iceland is removed from the topography and land-sea mask (Jones, 2003). If Iceland is present, the lower resolution ocean mask prevents relatively warm water passing through the Greenland strait and there is an excessive build-up of sea ice in the far North Atlantic (Jones, 2003). The alteration of North Atlantic bathymetry is only possible given understanding of what the model should correctly simulate for the present-day Earth system based on observations. For palaeoclimate applications, when understanding of the state of the Earth (e.g. sea ice) may be limited, it is harder to know whether adjustments might be necessary.

Another important consideration about the ocean model component of HadCM3BL is that it requires *islands* to be defined by the user for the calculation of barotropic flow. Barotropic flow is flow along an equal pressure gradient (Mellor, 1996) and in the model it will allow flow in one direction through the entire depth of the water column. Land that is not manually defined as an island is prescribed a default barotropic stream function value of zero around its coastline, whereas land that is defined as a separate island can have a non-zero stream function around its coast. Flow through an ocean gateway will depend on the calculated values of barotropic stream function at the coasts on each of the gateway margins. Therefore, if no islands are defined in the model, all land areas must have a barotropic flow of zero at their margins and so there will be no net flow through any gateways, no matter how wide they are. This, however, does not rule out surface flow through a gateway with an equal return flow at depth or different directions of flow through the centre of a gateway cancelling out the net flow. As a result, at low model resolution where there are few islands and ocean gateways, apparently small differences in island definition can act to artificially constrain ocean circulation, as will be shown in Chapter 2.

1.3.3. Land surface and vegetation

The HadCM3BL simulations in this thesis model land surface processes using the Met Office Surface Exchange Scheme (MOSES; Essery et al., 2003), version 2.1a (Valdes et al., 2017). MOSES accounts for water and energy fluxes at the surface and in four soil layers, as well as for physiological effects of the atmosphere on vegetation (e.g. CO_2, temperature, water supply). MOSES version 2 allows dynamic vegetation (Cox, 2001), with 5 vegetation types and 4 other land surface types able to fractionally cover each grid cell. Subsequently, the surface moisture and energy fluxes are calculated and weighted based upon these surface fractions. There are variations between MOSES versions 2.1, 2.1a and 2.2 in terms of their code structure and also, to a lesser extent, the science within them; Valdes et al. (2017) expand in detail the differences between these model versions. Version 2.1a is used here as it has some scientific improvements over version 2.1

and provides a better representation of the modern Eurasian land climate and vegetation compared to version 2.2 (Valdes et al., 2017)

MOSES can be coupled with the dynamic vegetation model, TRIFFID (Top-down Representation of Interactive Foliage and Flora Including Dynamics; Cox, 2001), which also has the capacity to model terrestrial carbon storage. In the HadCM3BL simulations carried out for this thesis, TRIFFID is run in equilibrium mode. Although it is more scientifically correct to run TRIFFID in the fully coupled 'dynamic' mode, the asynchronous coupling of 'equilibrium' mode allows for a quicker spin-up of the model (Valdes et al., 2017). As vegetation processes are not of specific interest in this study, using equilibrium mode is sufficient. Using the grid box average fluxes from MOSES 2, TRIFFID calculates the fractional coverage of the 5 vegetation types (broadleaf and needleleaf trees, C3 and C4 grasses and shrubs). Variables such as net primary productivity and leaf area index are calculated by TRIFFID and it interacts with the atmosphere through changes in the surface albedo, evapotranspiration and aerodynamic roughness (Valdes et al., 2017).

1.3.4. Sea ice

The sea ice model in HadCM3BL has thermodynamic and dynamic components, but is relatively primitive, being the same as was used in HadCM2 (Gordon et al., 2000). As was noted in Section 2.1.2, the sea ice in HadCM3BL can be highly sensitive to model setup and can potentially produce very unrealistic results (Jones, 2003). Sea ice can form in the high latitudes in either hemisphere and is represented as a zero-layer, interacting with both the ocean and atmospheric components of the model. Gaps in the ice, or leads, are represented by a fraction of a grid cell. Ice concentration in each grid cell is capped just below one, as completely solid ice is rare in reality. Ice mainly freezes in the leads when the surface air temperature falls below freezing, but thickness can also increase in response to accumulation of snow. Melting then occurs on the ice surface when the temperature rises above freezing. Melting occurs all year round at the base of the ice, proportionally to the temperature gradient between the ocean top-layer temperature and that of the sea ice (constant at -1.8 °C; Gordon et al., 2000). Ocean surface salinity changes are input via leads and can come about through many methods, for example melting, freezing, precipitation and sublimation.

Sea ice albedo is parameterised based on surface temperature (reflecting the age of ice, formation ice pools etc.). Surface energy flux and temperature are calculated separately in the atmospheric model. Wind stress applies to the ocean surface beneath the sea ice, with ice thickness,

concentration and any accumulated snow then advected by the top layer ocean current (Gordon et al., 2000). Ice rheology is simply parameterised and does not allow ice to converge if it is more than 4 m thick, although it can exceed this thickness through additional freezing (Gordon et al., 2000).

This sea ice model is reasonably simplistic and, again, it is important to note that excessive sea ice build-up has been documented in HadCM3L for modern day simulations under specific model setups (Jones, 2003).

1.3.5. Land ice

In reality, ice sheets are a dynamic part of the Earth system, but they respond over very long time periods compared to atmospheric or even ocean circulation. Complexity in their behaviour also means it is generally not computationally feasible to dynamically and synchronously couple a GCM to an ice sheet model, requiring approximations or asynchronous coupling techniques (e.g. Pollard et al., 2013; Ladant et al., 2014a).

In this research, HadCM3BL is not coupled to an ice sheet model, nor is an ice sheet model run offline. Areas of land ice are simply prescribed a high topographic height, the land surface changed appropriately and a huge volume of snow added on top of it. The snow does not act as a physical barrier, but simply means that the evaporative store never runs out which could potentially cause excessive heating due to a lack of latent heat flux. The topography over Antarctica may be raised by 2,000-3,000 m and, typically, an arbitrary 50 m of snow depth is prescribed over the ice sheet, ensuring a thick enough layer that will not melt away under high summer temperatures and allow an ice-free, low albedo land surface to be present. In the HadCM3BL atmosphere, the standard deviation of the topography is used to scale drag parameterisations to reduce systematic errors in zonal winds (Milton & Wilson, 1996). However, the smoothness of the Antarctic ice sheet relative to its height (compared to the Tibetan Plateau for example) means that this parameterisation may overestimate the drag and zonal easterlies over Antarctica have been shown to be sensitive to this parameterisation (Milton & Wilson, 1996). This is one example of how this simplistic, parameterised ice sheet setup could be affecting the simulated climate, however it is beyond the scope of this thesis to rigorously test the sensitivity to such parameters.

1.3.6. HadCM3BL evaluation

HadCM3 and its derivative models have been tested during their development at the Met Office (e.g. Cox et al., 2001; Jones, 2003); however, as part of the description paper of HadCM3B (Valdes et al., 2017), a basic model-data comparison was also carried out. The evaluation of terrestrial surface air temperature involved comparing the *benchmark simulation* of pre-industrial climate (i.e. the standard HadCM3BL setup) to modern day observations from the University of East Anglia (the CRU CL v2.0 1960-1990 climatology; New et al., 2002). Although this is not a perfect comparison, as the model simulation and observational data are of different periods, the climatological difference is expected to be small (Valdes et al., 2017) and it is still useful to have an appreciation of modern day biases in the model before interpreting palaeoclimate results. The following extract highlights the general nature of the errors and biases the model shows, particularly the differences introduced by changing resolution and land surface scheme. Note, the figures and their numbering have been updated to be consistent with this thesis.

"HadCM3BL-M2.1a [Figure 1.5a] has a RMSE of 2.6 °C and a comparable cold bias to HadCM3B-M1. As with the HadCM3B model variants, using MOSES2 with HadCM3BL reduces the cold bias and RMSE compared to using MOSES1, with HadCM3BL-M1 having a much higher RMSE [Figure 1.5b]. … The high northern latitudes (particularly over Russia and Scandinavia) are too cold, which is the result of an exaggerated seasonal cycle due to an overly cold winter. This is also the case for other HadCM3B model variants [e.g. Figure 1.5c], but it is most pronounced for the HadCM3BL variants. Similarly to the other simulations using MOSES 2, the Amazon remains slightly warmer than the observations with slightly reduced broadleaf forest cover." (Valdes et al., 2017; p. 3729).

It is also important to note that the seasonality in all model versions is too high relative to the modern-day observations. This high seasonality was also identified in palaeoclimate studies of the EOT and Oligocene (Gasson et al., 2014; Li et al., 2018) and is particularly pronounced in the lower resolution model variants (e.g. HadCM3BL). This enhanced seasonal range is clearly shown in Figure 1.6, which was produced for but not included in Valdes et al. (2017). This shows that there is some degree of variation in the modelled seasonality with different combinations of land surface scheme and vegetation model mode (Figure 1.6b, showing variants all run with HadCM3BL), but a more major contributor to the high seasonality anomaly appears to be the model resolution, with HadCM3BL and FAMOUS performing particularly poorly, and HadAM3BH (a high-resolution atmosphere-only variant) performing the best (Figure 1.6a). The

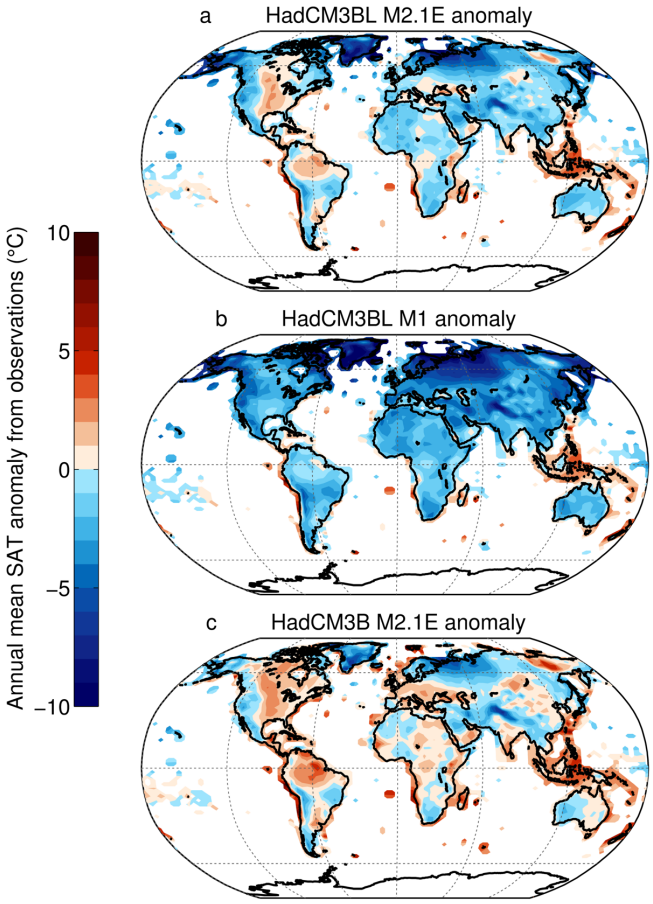

Figure 1.5: Anomaly in annual mean surface air temperature (°C) relative to CRU CL v2.0 data, comparing pre-industrial benchmark simulations with observations of 1960-1990; shown for HadCM3BL using the land surface schemes MOSES 2.1aE (a) and MOSES 1 (b), and for the higher resolution HadCM3B MOSES 2.1aE (c). Replotted from Valdes et al. (2017).

performance of HadAM3BH does not appear to be simply due to being an atmosphere-only model, as the standard resolution HadAM3B (the same resolution atmosphere as HadCM3B and HadCM3BL) also does not perform as well (Figure 1.6c). This is an interesting result which could partly be due to differences in the prescribed SST distribution between the simulations, but this requires further investigation. It is important to consider this high seasonality even for the modern day when interpreting the palaeoclimate results shown here, and to have some appreciation of the biases that might be introduced by changing the model resolution.

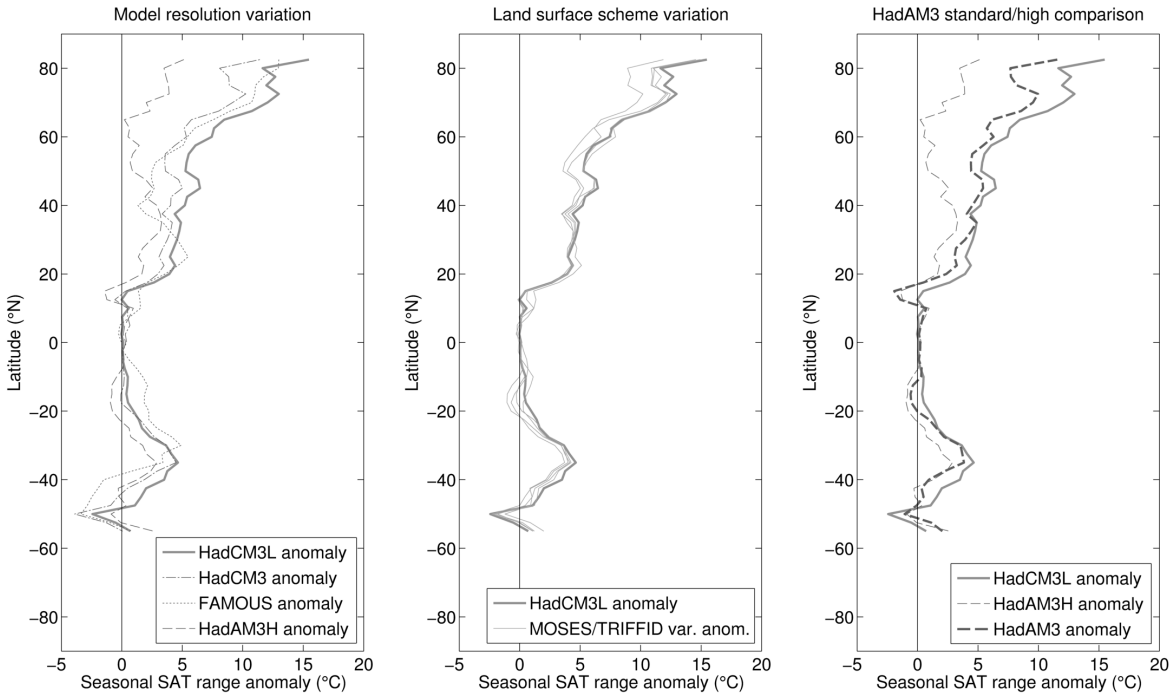

Figure 1.6: Zonal mean anomaly in surface air temperature seasonal range (°C) relative to CRU CL v2.0 data, comparing pre-industrial benchmark simulations with observations of 1960-1990. The anomaly varies for model variants of different resolution (a) and with different land surface schemes (b). The difference between resolution is also seen for the atmosphere only simulations (c).

Chapter 2: Modelling the climatic response to Antarctic glaciation using HadCM3BL

2.0. Introduction

The expansion of the Antarctic ice sheet was a major change in the state of the Earth system. In addition to the forcings driving the Eocene-Oligocene Transition, this glacial expansion in combination with multiple other feedbacks would likely have had a large impact on the Earth's atmosphere and oceans (Lear & Lunt, 2016; Scher, 2017). Using HadCM3BL-M2.1aE, some potential feedbacks and mechanisms of change in the Earth's climate and ocean systems are investigated to address the question: what impact does the Antarctic ice sheet have on regional and global climate?

The principal results from this chapter were published in a special issue of Philosophical Transactions of the Royal Society A (Kennedy A.T., Farnsworth A., Lunt D.J., Lear C.H. & Markwick P.J., 2015. Atmospheric and oceanic impacts of Antarctic glaciation across the Eocene–Oligocene transition. *Phil. Trans. R. Soc. A*, 373, 20140419, DOI: 10.1098/rsta.2014.0419). This special issue, entitled 'Feedbacks on climate in the Earth system' (Wolff et al., 2015), focussed on short and long-term climate feedbacks as well as feedbacks with the carbon cycle, with the discussion focussing on palaeo, present and future climate studies. Papers focussed on either describing the processes behind feedbacks, modelling the effect of the feedbacks or the proxy-evidence to support these. Kennedy et al. is reproduced verbatim in Sections 2.1 through to 2.5, with the supplementary figures included throughout the text to improve clarity. Section 2.6 addresses some of the outstanding questions from the paper: the importance of the island definition in HadCM3BL and reconciling the differences in results between Hill et al. (2013) and Kennedy et al. (2015). Concluding notes on this research will be made in Section 2.7.

I carried out the analysis of the results, 4 of the 6 model simulations used (see Appendix 1) and was the principle author of the paper. The remaining model simulations used were carried out by A. Farnsworth (University of Bristol; see Appendix 1), while Figure 2.1, its caption and paragraphs 3 and 4 of Section 2.1 (beginning "By way of introduction…" and "The first step…") were provided and written by C.H. Lear (Cardiff University).

Two errors in the original text were identified with further investigation into the results. Firstly, in Table 2.2 the stream function values for the Priabonian simulations (PriNO, PriEAIS and

PriFULL) were misquoted. Secondly, the caption for Figure 2.7 ('Changes in the northward heat flux in response to glaciation are shown for the Priabonian (b) and Rupelian (c)') has (b) and (c) incorrectly labelled: the Priabonian is actually shown in (c) and the Rupelian in (b). Neither of these fundamentally affect the discussion or conclusions and both have been corrected in the following version of the paper. It should also be noted that throughout the paper, the model used is referred to as HadCM3L, as the paper pre-dated the naming convention of Valdes et al. (2017). References to 'in press' and 'in prep.' papers have been updated, the abstract expanded to include conclusions from the additional work and Supplementary Figure 2.3 updated to improve clarity.

2.0.1. Abstract

The glaciation of Antarctica at the Eocene-Oligocene transition (~34 million years ago) was a major shift in the Earth's climate system, but the mechanisms that caused the glaciation, and its effects, remain highly debated. A number of recent studies have used coupled atmosphere-ocean climate models to assess the climatic effects of Antarctic glacial inception, with often contrasting results. Here, using the HadCM3L model, we show that the global atmosphere and ocean response to growth of the Antarctic ice sheet is sensitive to subtle variations in palaeogeography, using two reconstructions representing Eocene and Oligocene geological stages. The earlier Stage (Eocene; Priabonian), which has a relatively constricted Tasman Seaway, shows a major increase in sea surface temperature over the Pacific sector of the Southern Ocean in response to the ice sheet. This response does not occur for the later Stage (Oligocene; Rupelian), which has a more open Tasman Seaway. This difference in temperature response is attributed to reorganisation of ocean currents between the stages. Following ice sheet expansion in the earlier stage, the large Ross Sea gyre circulation decreases in size. Stronger zonal flow through the Tasman Seaway allows salinities to increase in the Ross Sea, deep-water formation initiates and multiple feedbacks then occur amplifying the temperature response. This is potentially a model dependent result, but it highlights the sensitive nature of model simulations to subtle variations in paleogeography, and highlights the need for coupled ice sheet-climate simulations to properly represent and investigate feedback processes acting on these timescales. Further model simulations show that the starkly contrasting sea surface temperature responses to glaciation between the Stages are at least in part due to using an inconsistent island definition in the model for the Priabonian and Rupelian. However, other correctly setup simulations show similar patterns, suggesting the mechanisms described are not entirely unrealistic. Finally, differences between this research and that of Hill et al. (2013) are shown to be due to differences in the model spin-up.

2.1. Introduction

The Eocene-Oligocene transition (EOT), ~34 million years ago (34 Ma), represents one of the major climatic transitions in the past 65 million years (Zachos et al., 2008). A steady decline in temperatures from ~50 to ~34 Ma culminated in the rapid expansion of permanent ice over Antarctica (Zachos et al., 2001; Katz et al., 2008; Lear et al., 2008). Previous work has generally focused on two main causes of the EOT: the CO_2 hypothesis and the ocean-gateway hypothesis. The first suggests the global decline in CO_2 (itself due to increased biological uptake and carbon cycling, and/or increased silicate weathering, and/or decreased volcanic emissions) caused the drop in global temperature (Zachos & Kump, 2005) which, due to polar amplification through ice-albedo and topographical feedbacks, led to the growth of the Antarctic ice sheet (AIS; e.g. DeConto & Pollard, 2003a; Pearson et al., 2009; Pagani et al., 2011; Foster & Rohling, 2013). The second hypothesis is that the opening of the ocean passages around Antarctica – the Drake Passage (DP) between South America, and Tasman Seaway (TS) between Australia – allowed for the initiation of the Antarctic circumpolar current (ACC) which reduced poleward heat transfer and so led to glacial inception (Kennett, 1977; Sijp & England, 2004). Although there is geological and modelling evidence for both hypotheses, recently an increasing body of evidence has given precedence to falling atmospheric CO_2 as being the chief driver of the EOT, with the precise timing influenced by orbital variations (e.g. DeConto & Pollard, 2003a; Huber et al., 2004; Coxall et al., 2005; Pearson et al., 2009; Pagani et al., 2011; Sijp et al., 2011 Lefebvre et al., 2012; Goldner et al., 2014; Ladant et al., 2014a).

The remainder of this section summarises proxy records of palaeoclimate through the EOT, the results of a number of recent modelling studies exploring the effects of Antarctic ice sheet expansion on global climate, and develops the motivation for our own work.

By way of introduction, the EOT is recorded as a two-stepped, orbitally-paced, ~1.5 ‰ increase in deep ocean benthic foraminiferal oxygen isotope ($\delta^{18}O$) records (Kennett & Shackleton, 1976; Zachos et al., 1996; Coxall et al., 2005). Benthic and low latitude planktonic $\delta^{18}O$ changes are shown in Figure 2.1a. These records reflect both an increase in continental ice volume and a decrease in ocean temperature, due to concentration of ^{16}O in ice sheets by the hydrological cycle and isotopic fractionation during the calcification process respectively. Attempts to deconvolve the EOT $\delta^{18}O$ increase into its ice volume and temperature components require the use of palaeotemperature proxies such as benthic foraminiferal Mg/Ca ratios. Further uncertainties arise in using Mg/Ca ratios due to a simultaneous ~1 km deepening of the calcite compensation depth (Lear et al., 2004; Coxall et al., 2005; Lear et al., 2010; Peck et al., 2010; Pusz et al., 2011), as well

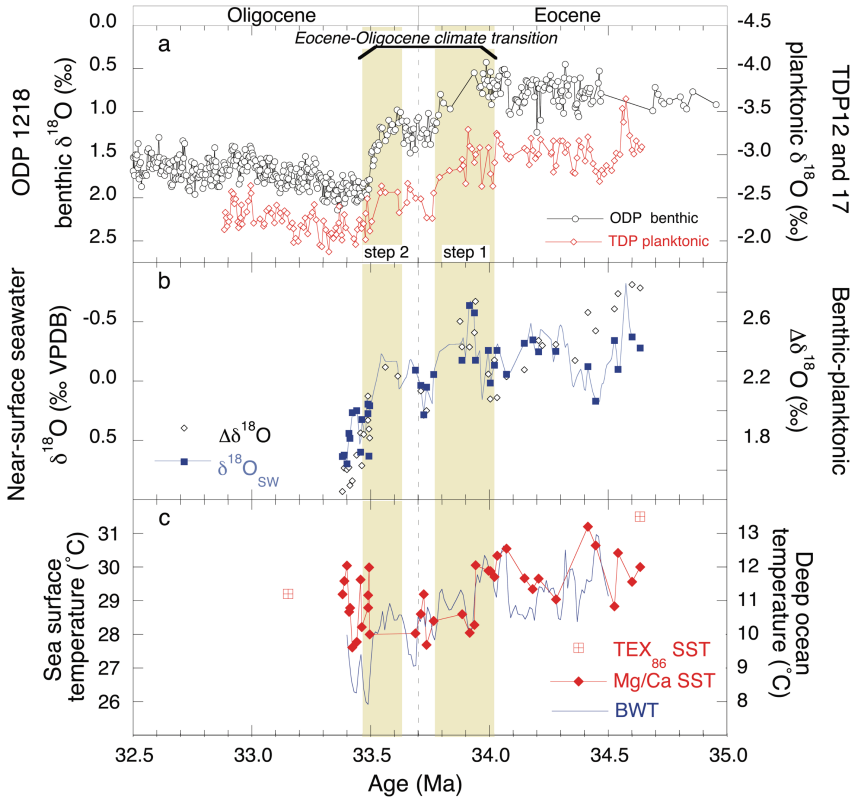

Figure 2.1: Multi-proxy records of climatic and palaeoceanographic change across the Eocene-Oligocene transition. Foraminiferal $\delta^{18}O$ records (a): black circles - benthic foraminiferal $\delta^{18}O$ from ODP Site 1218 (Coxall et al., 2005), red diamonds - planktonic foraminiferal $\delta^{18}O$ from TDP Sites 12 and 17 (Pearson et al., 2008). Proxy records of ice growth (b): blue line - near-surface $\delta^{18}O_{sw}$ calculated by interpolating TDP planktonic Mg/Ca and $\delta^{18}O$ records, solid blue squares – near-surface $\delta^{18}O_{sw}$ calculated using TDP planktonic Mg/Ca temperatures and interpolated TDP planktonic $\delta^{18}O$ record, open black diamonds – TDP benthic-planktonic $\delta^{18}O$ gradient, in part reflecting local water depth, calculated from *Epistomina* sp. $\delta^{18}O$ and interpolated *T. ampliapertura* $\delta^{18}O$ (Lear et al., 2008). Sea surface and deep ocean temperature (c): Red diamonds - SSTs based on TDP planktonic foraminiferal Mg/Ca (red diamonds), red hatched squares – SSTs based on TDP TEX86, blue line – deep ocean temperature calculated using the ODP Site 1218 benthic foraminiferal $\delta^{18}O$ record (Coxall et al., 2005) with the $\delta^{18}O_{sw}$ record derived from TDP sites (Lear et al., 2008) and the palaeotemperature equation of Marchitto et al., 2014. Yellow shaded bars highlight the two "steps" of the oxygen isotope shift (Coxall et al., 2005), and vertical dashed black line marks E/O boundary as defined by extinction of the Family Hantkeninidae.

as error in the Mg/Ca value chosen for Eocene-Oligocene seawater and its relationship with foraminiferal Mg/Ca. Uncertainty due to calcite compensation depth deepening is reduced by using continuously paired $\delta^{18}O$ and Mg/Ca records, such as those from Tanzania Drilling

Program (TDP; Pearson et al., 2008; Lear et al., 2008). Additionally, the long residence times of Mg and Ca in the oceans (~10 Myr and ~1 Myr respectively) mean that calculated changes in temperature and $\delta^{18}O_{sw}$ across the transition are more robust than absolute estimates (Lear et al., 2008).

The first step in the $\delta^{18}O$ record (Figure 2.1a) predominantly reflects an ocean cooling in low latitude surface waters with a small component of ice volume growth (~0.2‰ $\delta^{18}O_{sw}$ equivalent; Lear et al., 2008). Cooling ranges from ~2.5 °C at TDP (Lear et al., 2008) to ~3-4 °C in a multi-proxy Gulf of Mexico record (Wade et al., 2012; note, however, that the second step is absent for this record). High latitude Mg/Ca records from the Kerguelen Plateau in the Southern Ocean (SO) also suggest a 2.5 °C cooling (Bohaty et al., 2012). The second step is dominated by an increase in ice volume (~0.4‰ $\delta^{18}O_{sw}$ equivalent), supported by a decrease in the low latitude TDP benthic-planktonic foraminiferal $\delta^{18}O$ gradient, as shown in Figure 2.1b. This is interpreted as reflecting global sea level fall as ice sheets advanced (Lear et al., 2008). There is also evidence for some further deep ocean cooling at the second step (totalling ~4 °C across the EOT) that is not present at the surface in low latitude TDP records (assuming minimal change in local surface salinity), as shown in Figure 2.1c (Pearson et al., 2008; Lear et al., 2008; Coxall et al., 2005). A multi-site study using the TEX_{86} and $U^{K'}_{37}$ organic temperature proxies suggests there was a heterogeneous SST response at the EOT (Liu et al., 2009). Modelling results, however, are generally consistent with an overall deep-water cooling of ~4 °C and an overall increase in ice volume of 10-30 x 10^6 km^3 across the EOT (Liu et al., 2009).

Modelling is important in fingerprinting the driving mechanisms behind the EOT. Although often studies have chiefly been concerned with the trigger of glacial inception or the ACC, the range of results and simulation setups in the literature pose interesting questions about the role of palaeogeography and the presence of the AIS on global climate. Indeed, several modelling studies in the past two years have explored the effects of AIS expansion on global climate, and we summarise these here:

Goldner et al. (2013) simulated the climate of the modern-day and the Eocene, both with and without an AIS, using the NCAR CESM1.0 global climate model with a slab ocean. They find a contrasting response to the formation of the AIS between the modern and Eocene, which they attributed to differing cloud feedbacks. In the Eocene the feedback is negative, causing warming when the AIS forms, whereas the cloud feedback is weakly positive in the modern. They acknowledge that this result is likely to be model dependent.

Building on their earlier work, Goldner et al. (2014) used the same model (NCAR CESM1.0) but with a more realistic three-dimensional fully dynamic ocean and also included simulations with different CO_2 concentrations. They suggest that changes found in the high-latitude ocean core records at the EOT, previously explained only by the gateway hypothesis and not the CO_2 hypothesis, could be an outcome of the formation of the AIS itself. The formation of the AIS increased the meridional pressure gradient around the continent, in turn increasing the surface winds that affect the surface mixing in the Southern Ocean. This led to enhanced northward transport of Antarctic Intermediate Water (AIW) and invigorated Antarctic Bottom Water (ABW) formation. Around the Antarctic coastline, the SST was found to have areas of both increases (in the Indian Ocean sector) and decreases (in the Pacific and Atlantic sectors).

Knorr & Lohmann (2014) carried out a similar study with a fully coupled climate model (ECHAM5/MPIOM) with a 3D ocean, but looked at a different time period and hence palaeogeography, that of the Middle Miocene ~14 Ma. Their work indicates that the addition of the AIS causes a contrasting response in the SST around Antarctica to that of Goldner et al. (2014), with strong warming in the Atlantic and Indian Ocean sectors (particularly in the Weddell Sea) and mild cooling in the Pacific sector. These changes in SST between glaciated and unglaciated simulations they attribute to winds affecting ocean circulation, deep-water formation and sea ice cover.

Hill et al. (2013) present results using the same climate model as used in this paper, HadCM3L. They look at several scenarios and palaeogeographies (the Rupelian and Chattian stages, and pre-industrial modern) with differing boundary conditions (AIS presence and an open or closed DP, but not every combination thereof). Although the Rupelian is also used in the current study, the palaeogeography has since been updated (for example in West Antarctica). They suggest that although the ACC starts to initiate with the opening of the DP and the TS, an ACC of present-day strength does not develop until after the Chattian due to the proximity of the Australian continent to Antarctica prior to this time. They argue this result is consistent with geologic data (Pfuhl & McCave, 2005; Lyle et al., 2007).

There are several recurring points that emerge from these studies. Firstly, the response of the climate system to an expansion in Antarctic ice appears to vary significantly between models. However, it is also possible that the results are strongly dependent on the time period (i.e. palaeogeography) examined - Goldner et al., 2014, Knorr & Lohmann, 2014, and Hill et al., 2013 all examine differing time periods and/or palaeogeographies. The significance of palaeogeography cannot be underestimated, particularly when there is such large debate over the timings of key

events such as the opening of the DP (Barker & Thomas, 2004; Stickley et al., 2004; Barker et al., 2007). Additionally, it seems that the effect of changing ocean circulation is a significant driver of the global climate at the EOT, even if it was not the ultimate trigger of Antarctic glaciation (Goldner et al., 2014; Lefebvre et al., 2012; Sijp et al., 2011 etc.). Palaeogeography, ocean circulation, CO_2 and climatic change are all therefore inter-connected and each warrants a complete understanding at this major climatic shift.

Here, we model and describe the global atmospheric and oceanic response to the glaciation of Antarctica in the HadCM3L model and compare this to previous studies. This experiment may therefore be indicative of the climatic changes that occurred during the second 'ice growth' step of the EOT. We do this for two successive periods over the EOT: the Priabonian during the Eocene (~38-34 Ma), and the Rupelian during the Oligocene (~34-28 Ma). These stages have subtly different palaeogeographies; for example the Tasman Seaway is wider in the Rupelian than the Priabonian in our reconstructions (see next section). We do not attempt to model the inception of glaciation in a transient simulation, like the studies of DeConto & Pollard (2003a) or Ladant et al. (2014a), but instead, through steady-state simulations we aim to explore the importance of the palaeogeography on the regional and global response to glaciation, and the associated feedbacks. Our experimental design is briefly outlined in Section 2.2, descriptive results in Section 2.3, analysis and discussion of the physical mechanisms and implications in Section 2.4, and conclusions and future direction of work in Section 2.5.

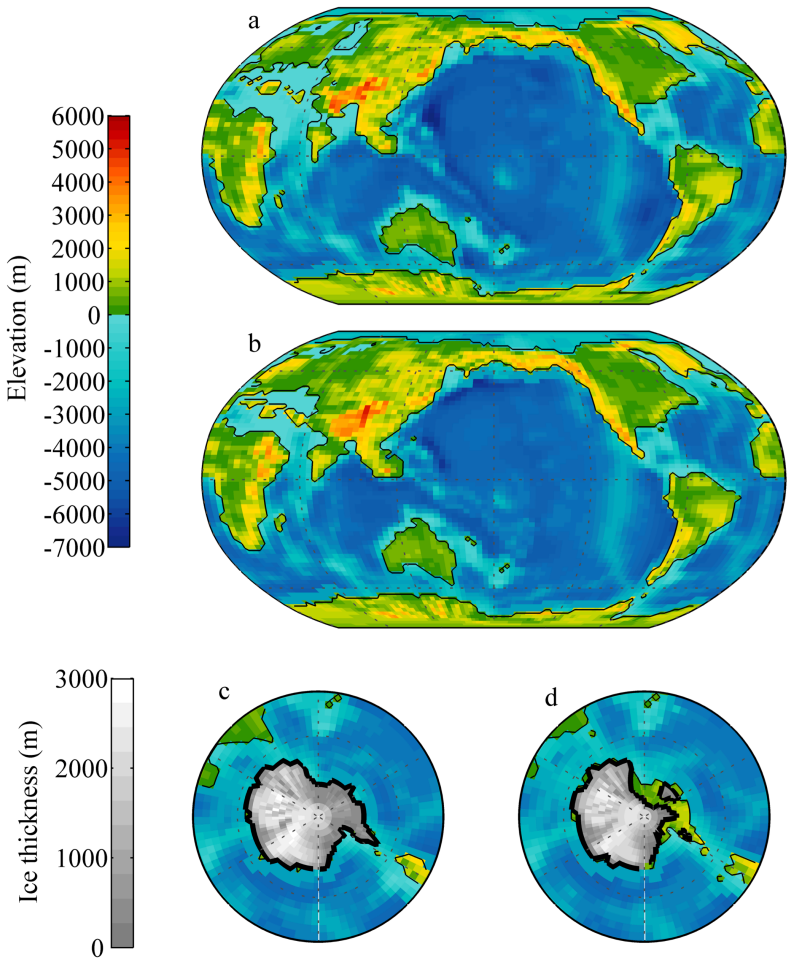

Figure 2.2: Palaeogeographic reconstructions of topography and bathymetry (m) for the Priabonian (a) and Rupelian (b) stages shown at model resolution. The thickness (m) and extent of the reconstructed full (c) and East Antarctic ice sheets (d) are also shown.

2.2. Experimental design

To investigate the model sensitivity to AIS expansion and subtle variations in the palaeogeography, the model HadCM3L was run towards a steady state using high-resolution palaeogeographic reconstructions of the stages, with and without reconstructed ice sheets. HadCM3L is a fully coupled atmosphere-ocean general circulation model (GCM; Cox et al., 2001). HadCM3L is a lower-resolution version (3.75 ° × 2.5 °) of the HadCM3 model (Gordon et al., 2000), with a few changes in parameterisations (see Cox et al., 2001 and Jones, 2003 for example) compared to HadCM3. No ice sheet model was included; the AIS was simply prescribed with an appropriate land surface albedo and topography. The ice sheet topography, as well as global bathymetry and topography was supplied by Getech Plc. at a 0.25 ° resolution. These were based upon tectonic, lithologic and fossil studies and DSDP/ODP deep-sea data (Markwick,

2007). The principle ice sheet used is a reconstruction for the Rupelian and is similar to the full modern extent (~17 x 10^6 km^3 in size). A smaller ice sheet was also used for cross-examination, similar to only the East AIS (EAIS; ~14 x 10^6 km^3 in size). These reconstructions are shown in Figure 2.2, and experiments listed in Table 2.1.

Model spin-up was carried out in four phases consistently across the simulations. First, in Phase 1, the model was initialised with pre-industrial CO_2 levels and a zonally symmetric SST and deep ocean distribution, uniform vegetation and the different ice-free palaeogeographies, and run for 50 years. In Phase 2, the vegetation model TRIFFID (Cox, 2001) was activated, CO_2 was increased to four times pre-industrial, the prescribed ozone concentration was adjusted (Lunt et al., 2007), and the model run for 319 years. In Phase 3, prescribed lakes were added to the land surface and the ice sheet added in simulations requiring it, and the model run for 53 years. Finally, in Phase 4, barotropic flow in the ocean is calculated (prior to this point, only the baroclinic component was calculated), the CO_2 is reduced to two times pre-industrial (560 ppm), and for ice sheet sensitivity simulations the ice sheet is adjusted (differences are noted in Table 2.1). This final phase is run for 1,000 years. This combined spin-up of 1,422 years produces quasi-stable results for atmospheric and surface ocean characteristics as deep as 670 m, as shown in Supplementary Figure 2.1. There is still, however, a trend in deep ocean temperatures >1000 m and so these are not the focus of this study. More details of the experimental design can be found in Inglis et al. (2015), and Lunt et al. (2016).

There are a number of points we would like to note about the methodology for clarity. Firstly, because the land-sea and ice masks do not align exactly between the stages, a small number of grid cells which should be prescribed as 'ice' lie off the continental margin of Antarctica during the Priabonian. It was deemed more important not to influence the bathymetry by changing the land-sea mask and so these occasional cells of ice sheet were omitted. Secondly, adjustments to the ice

Table 2.1: Key details of each model simulation carried out. Those experiments marked with an * are the principle experiments around which the results and discussion are based.

Simulation name	Palaeogeography	Ice sheet configuration	Spin-up phase with final ice sheet state	CO_2
PriNO*	Priabonian	Ice-free	3	560 ppm
PriEAIS	Priabonian	East Antarctic ice only	4	560 ppm
PriFULL*	Priabonian	Full Antarctic ice sheet	4	560 ppm
RupNO*	Rupelian	Ice-free	3	560 ppm
RupEAIS	Rupelian	East Antarctic ice only	4	560 ppm
RupFULL*	Rupelian	Full Antarctic ice sheet	3	560 ppm

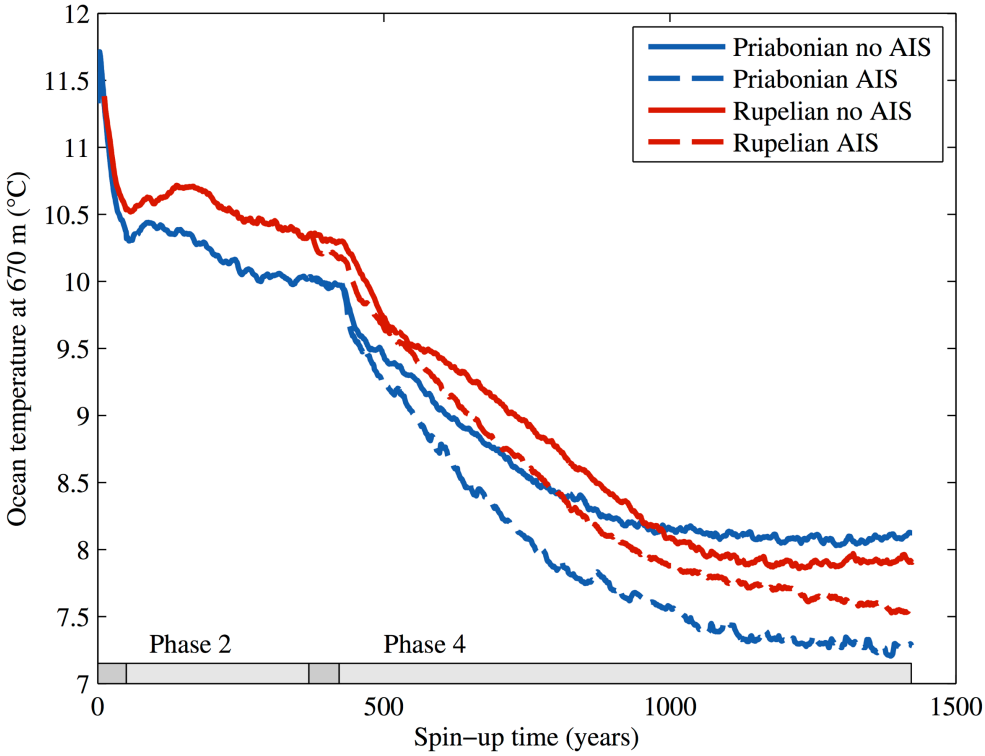

Supplementary Figure 2.1: Model spin-up trends of mean ocean temperature at 670 m depth (°C) for the four main simulations. The four phases of spin-up (detailed in section 2) are indicated by the grey bars.

sheet states for sensitivity simulations (PriEAIS, PriFULL and RupEAIS) were made only in the fourth Phase of spin-up. These three simulations therefore have a slightly shorter spin-up (by 53 years) with their final ice sheet configuration than RupFULL. Thirdly, in our HadCM3L setup, the standard deviation of topography (used in the gravity-wave drag scheme) is estimated as a constant factor of the topographic height. This is a fair assumption over mountainous regions, but exaggerates the standard deviation over the AIS, potentially altering atmospheric dynamics. Fourthly, the solar constant varies fractionally between the stages (1360.86 and 1361.35 kW m^{-2} for the Priabonian, and Rupelian respectively). It is not believed that any of these points should have a major impact on the findings of the study.

Finally, the solution of the barotropic component of ocean circulation requires the user to define islands around which the net flow can be non-zero. Any continent and its coastline that is not defined as an island is assigned a barotropic stream function value of 0. For the Rupelian we define Australia, South America and Antarctica to be islands in this sense, whereas in the Priabonian, with a more constricted TS, we only define Australia and South America as islands. As such, there is zero net flow around the Antarctic coastline in the Priabonian, despite the presence of a (albeit

small) TS. By assigning the same value of stream function to Antarctica as the Eurasian and North American continents we provide a coupling between the Southern Ocean and tropical Pacific gateways in the Priabonian that is not present in the Rupelian (see Figure 2.5, shown later). This should not have a major effect on flow through the TS or the high latitude response during the Priabonian, but may potentially affect the climate response at low latitude.

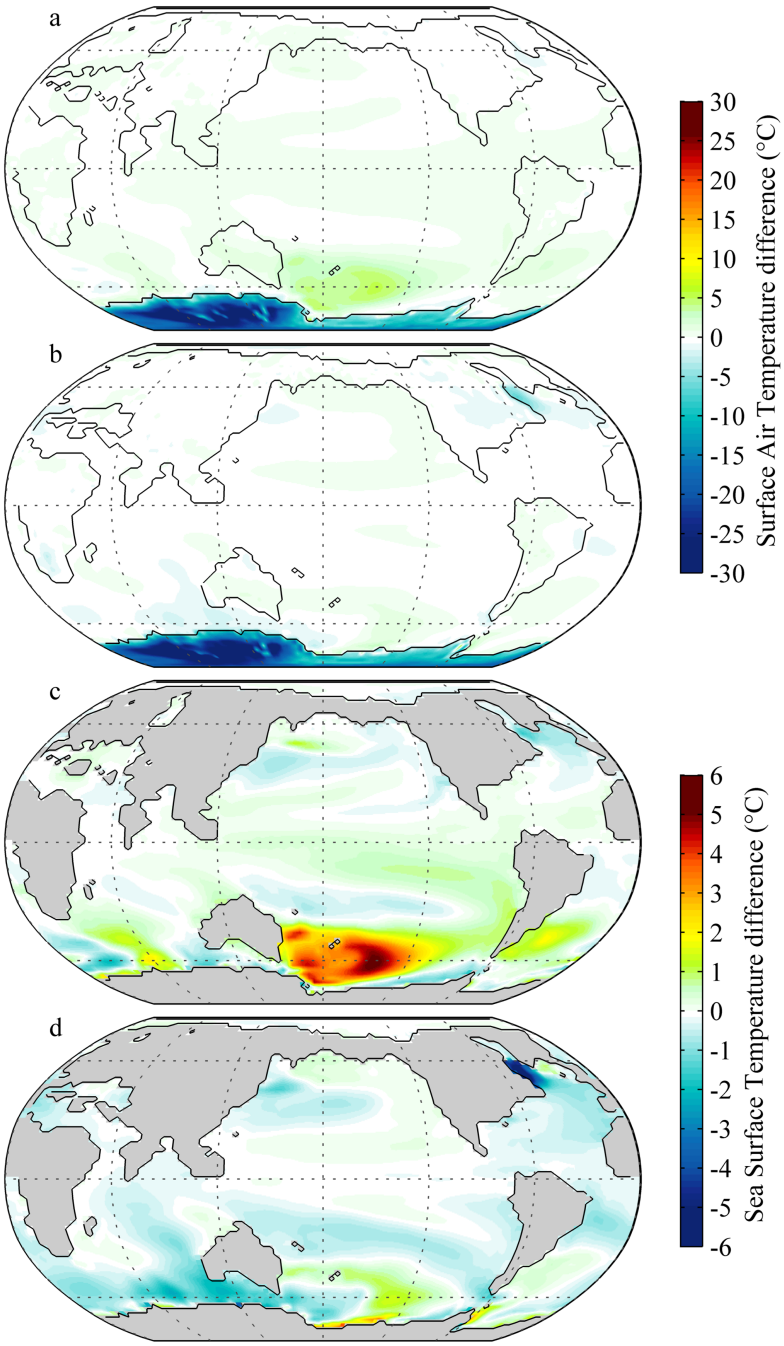

Figure 2.3: Annual mean surface air temperature response (°C) to Antarctic glaciation for the Priabonian (a) and Rupelian (b), and annual mean sea surface temperature response (°C) to glaciation for the Priabonian (c) and Rupelian (d).

2.3. Results

Here, oceanic and atmospheric response to the expansion of the full AIS (Δ_{glac}) will be the primary focus (i.e. FULL – NO), discussed in terms of temperature, atmospheric and ocean circulation, and meridional heat flux changes. The discussion of mechanisms follows in Section 2.4.1.

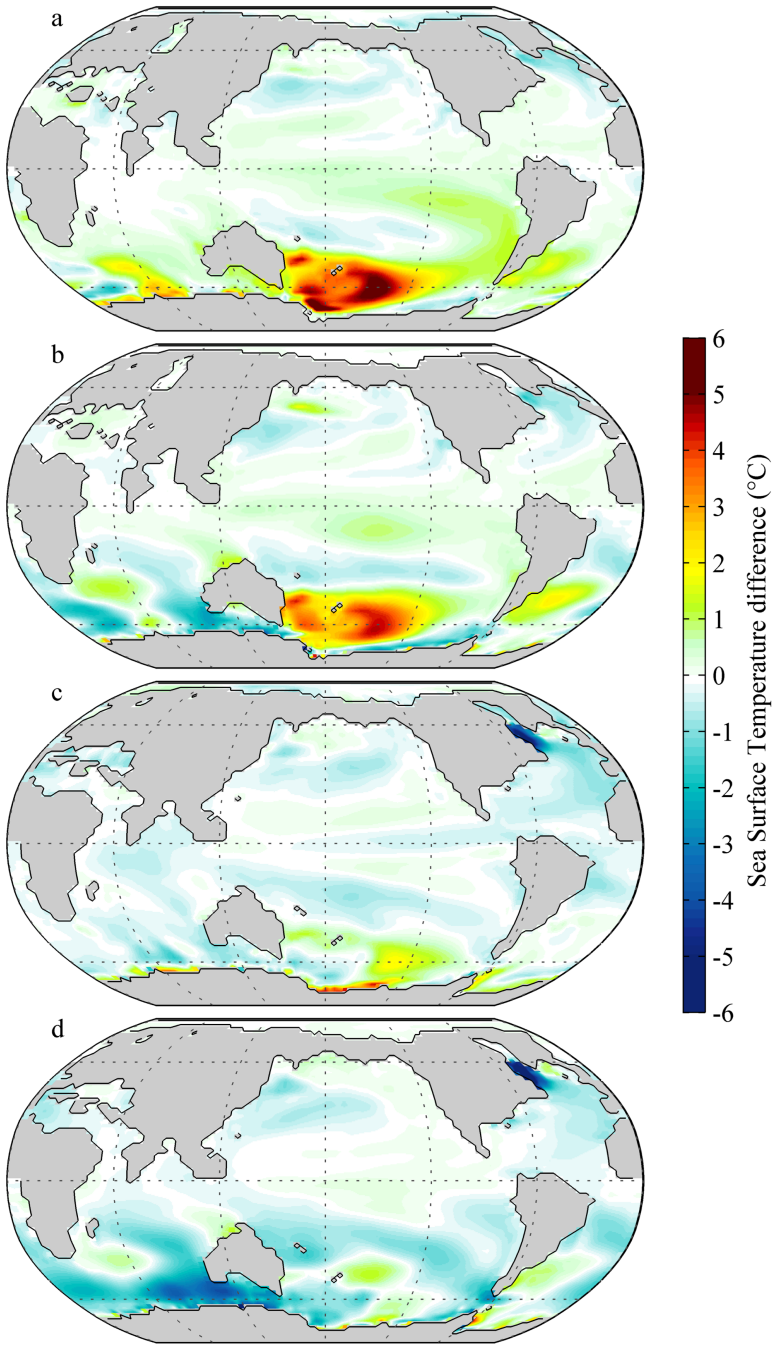

Supplementary Figure 2.2: Seasonal mean sea surface temperature response to Antarctic glaciation (°C) for the Priabonian winter (a), Priabonian summer (b), Rupelian winter (c) and Rupelian summer (d). Summer is defined December, January and February; winter is June, July and August.

Annual mean global surface air temperature (SAT) Δ_{glac} response is dominated by the cooling of up to 30 °C over the Antarctic continent in both stages, as shown in Figures 2.3a and 2.3b. The annual mean SST Δ_{glac} response varies substantially between the stages. The Priabonian shows a large area of warming of up to 6 °C over the Pacific sector of the SO, while there is cooling of up to 1.5 °C in the North Atlantic, NW Pacific and Bellingshausen Sea (Figure 2.3c). In contrast, the

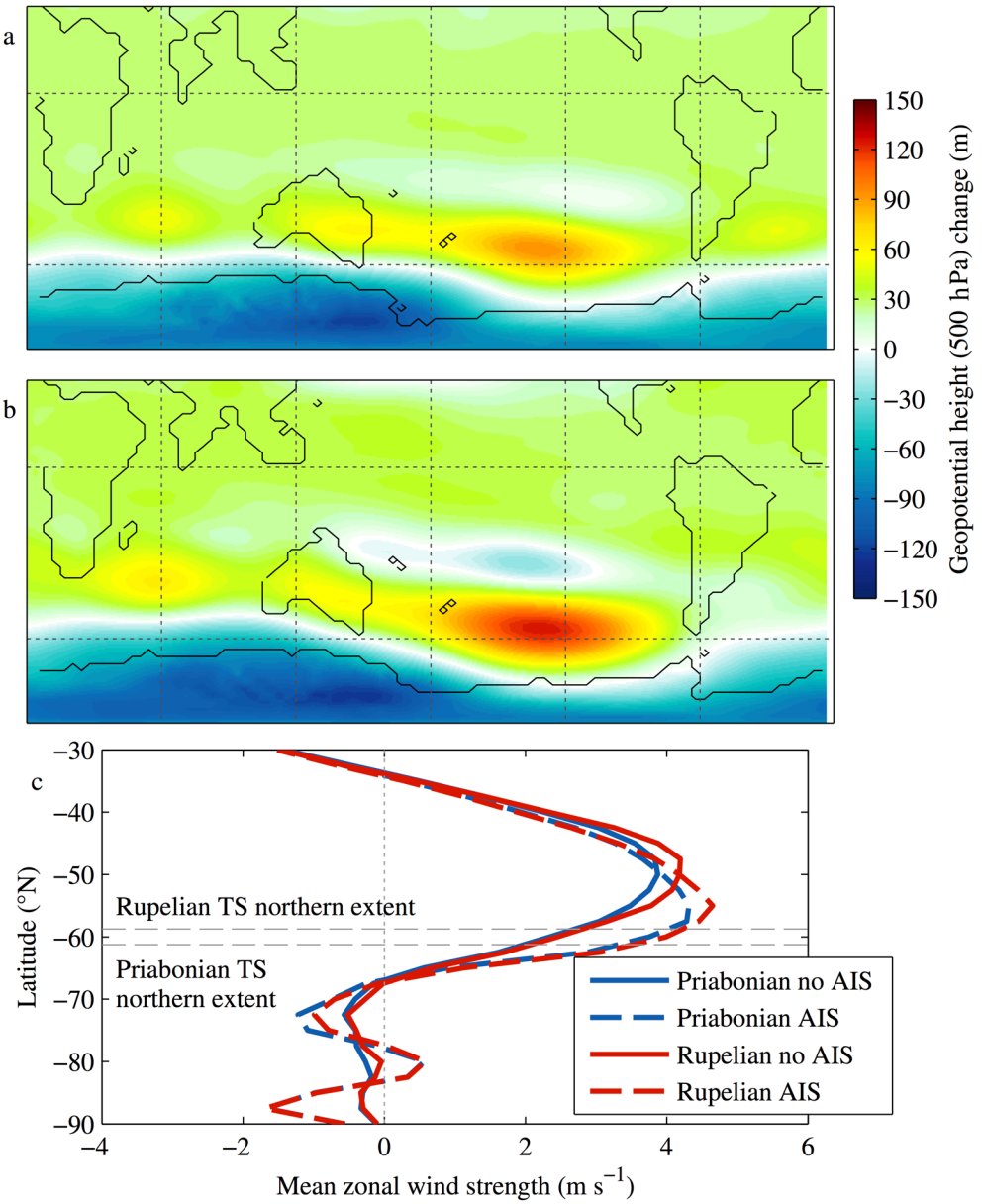

Figure 2.4: Changes in annual mean 500 hPa geopotential height (m) in response to Antarctic glaciation for the Priabonian (a) and Rupelian (b), and mean zonal westerly wind strength (m s^{-1}) for each stage and ice sheet configuration (c).

Rupelian shows more subtle variations and is more zonally heterogeneous in the Southern Hemisphere (SH), as shown in Figure 2.3d. Cooling occurs in much of the SH, particularly in the Indian Ocean sector of the SO by ~2 °C, while warming of up to 1.5 °C occurs in the South Pacific sector of the SO and some localised coastal areas by >3 °C. There is also year round cooling of ~6 °C in the North Atlantic. In both stages there is seasonality in the SST Δ_{glac} response, with warming being stronger during the winter (JJA) and cooling being stronger in the summer (DJF) as shown in Supplementary Figure 2.2. The only Δ_{glac} change in average annual sea ice concentration in

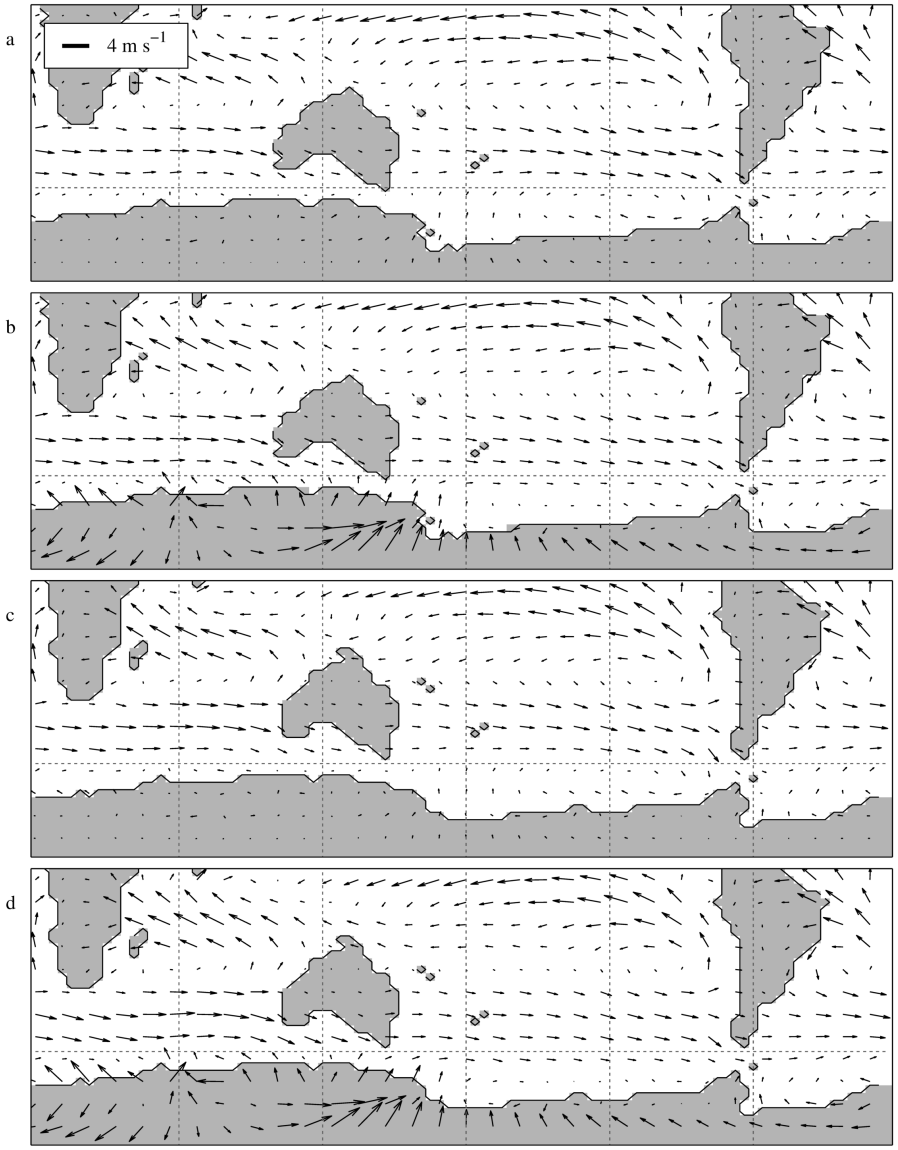

Supplementary Figure 2.3: Vectors of Southern Hemisphere surface wind strength (m s^{-1}) for the unglaciated Priabonian (a), glaciated Priabonian (b), unglaciated Rupelian (c) and glaciated Rupelian (d). Vector scale is located in (a).

either stage is a partial retreat of the sea ice in the Ross Sea during the Priabonian (figure not shown).

Annual mean mid-atmospheric pressure (*P*; expressed as the 500 hPa geopotential height) Δ_{glac} response is shown for both stages in Figures 2.4a and 2.4b. *P* decreases significantly over Antarctica and the SO and increases in southern mid-latitudes between 40-60 °S, increasing the *P* gradient at 60 °S. Changes are more pronounced for the Rupelian than the Priabonian. This response is also seasonally dominated, mostly occurring during the summer with only slight decreases in *P* over the Ross Sea edge of East Antarctica and some increases over the South Pacific and SO during winter (figure not shown). The changes in *P* result in Δ_{glac} changes in zonal winds,

as shown in Figure 2.4c (see also Supplementary Figure 2.3 for annual mean wind vectors before and after glaciation). The largest changes in wind field are off the AIS due to the initiation of katabatic winds and these are persistent throughout the year. Elsewhere, changes in winds are generally geostrophic in nature, aligning with changes in the pressure gradient contours. Over the Pacific sector of the SO at 60 °S, the increased summer pressure gradient leads to strengthening and a poleward shift in the geostrophic westerlies in both stages.

Annual mean ocean zonal flow through the TS and DP for each stage and ice sheet configuration is listed in Table 2.2, and the depth integrated stream functions for the principle experiments (PriNO, PriFULL, RupNO, RupFULL) shown in Figure 2.5. There are clear differences in the ocean circulation patterns between the stages, regardless of ice sheet state. The Pacific at this time is a basin with four gateways: the DP, the TS, the Indonesian Seaway (IS) and the Panama Seaway (PS). During the Priabonian, the western gateways (TS and IS) make up the majority (68-77 %) of the flow through the Pacific, whereas during the Rupelian, the southern gateways (TS and DP) represent the majority (76-86 %) of the total flow. Large gyre systems dominate the Indian, South Pacific and SO during the Priabonian. During PriNO, there is a huge Ross Sea gyre extending to ~35 °S and along the entire Antarctic coastline between the TS and DP. With the addition of the ice in PriFULL the Ross Sea gyre shrinks considerably, reaching ~45 °S and contracting westwards, no longer influencing the Bellingshausen Sea. Simultaneously, flow in the South Pacific and Indian Ocean gyres (and flow between them) strengthen. In the Rupelian, flow through the SO is zonal, dominated by a proto-ACC. Addition of the ice sheet strengthens this proto-ACC but has limited impact on the rest of the global ocean. Total flow through all Pacific gateways increases by 97 % during the Priabonian but only 27 % during the Rupelian in response to Δ_{glac}.

Mixed layer depth (MLD) in the SO and North Atlantic for the four principle experiments is shown in Figure 2.6. There are increases of 200-1,000 m in the Ross Sea for both stages and increases along the Atlantic and Indian Ocean sectors of the East Antarctic coastline by up to 1,000 m in

Table 2.2: Annual mean ocean transport through Pacific Ocean gateways for each simulation.

Simulation	Tasman Seaway through flow (Sv)	Drake Passage through flow (Sv)	Total flow through Pacific gateways (Sv)
PriNO	12.7	2.5	30.4
PriEAIS	20.3	7.9	56.4
PriFULL	21.7	8.7	60.8
RupNO	52.6	46.2	130.1
RupEAIS	71.3	64.5	159.0
RupFULL	75.2	68.0	165.8

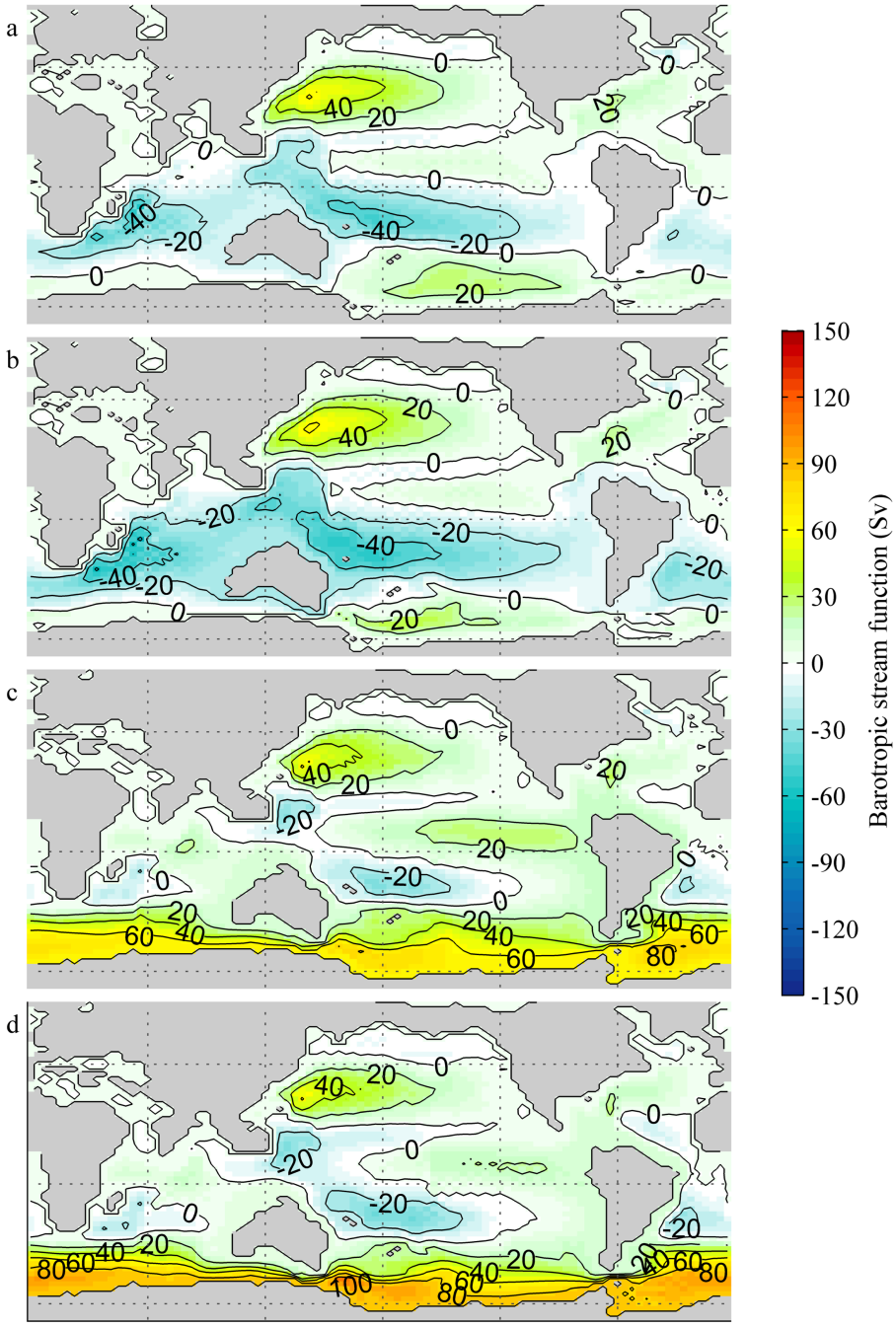

Figure 2.5: Annual mean barotropic stream function (Sv) for the Priabonian: unglaciated (a) and glaciated (b); and Rupelian: unglaciated (c) and glaciated (d).

the Priabonian and 500 m in the Rupelian. There are decreases in the Weddell Sea of the Priabonian (up to 670 m) but increases in the region during the Rupelian (up to 600 m). There is a decrease in MLD in the North Atlantic in both stages. The increase in the Ross Sea MLD during the Priabonian is important, as PriNO has a very shallow MLD of <100 m, which increases up to 1,000 m in PriFULL. Additionally, increased surface winds at 60 °S result in seasonal Δ_{glac} changes in the wind driven mixing in the SO, with increased upwelling to the south and increased

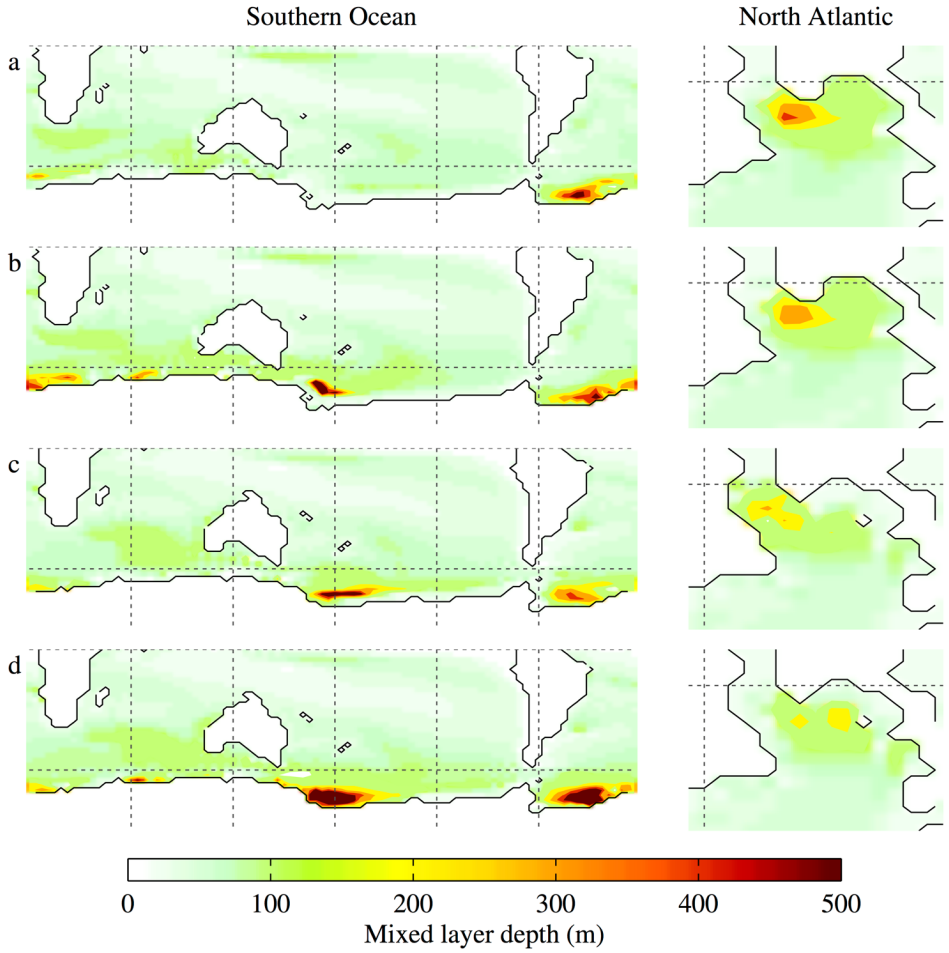

Figure 2.6: Annual mean mixed layer depth (m) in the Southern Ocean (left) and North Atlantic (right) for the Priabonian: unglaciated (a) and glaciated (b); and Rupelian: unglaciated (c) and glaciated (d). The mixed layer is very shallow in the North Pacific in all simulations.

downwelling to the north of the peak wind strength and current change. This causes a summer seasonal deepening of the MLD throughout the SO by up to 25 m (figure not shown), but this is small compared to the coastal increases previously mentioned. The global meridional overturning stream function is not shown due to the insufficient spin-up time for the deep ocean.

The meridional heat flux has the same general form for all ice sheet configurations (and stages), shown by the example of RupNO in Figure 2.7a. The oceanic and total heat fluxes increase southwards at all latitudes for both stages in response to Δ_{glac}, as shown in Figures 2.7b and 7c. The largest increases in the total southward heat flux (0.4 PW in the Priabonian; 0.3 PW in the Rupelian) occur in the SO at 65 °S, as a result of strong oceanic and atmospheric components at this latitude. The maximum increases in oceanic southward heat flux (0.4 PW in the Priabonian at ~40 °S; 0.2 PW in the Rupelian at ~60 °S) are similar in magnitude to those found in previous studies (e.g. Huber & Nof, 2006; Goldner et al., 2014). Changes due to gateway opening (i.e. the

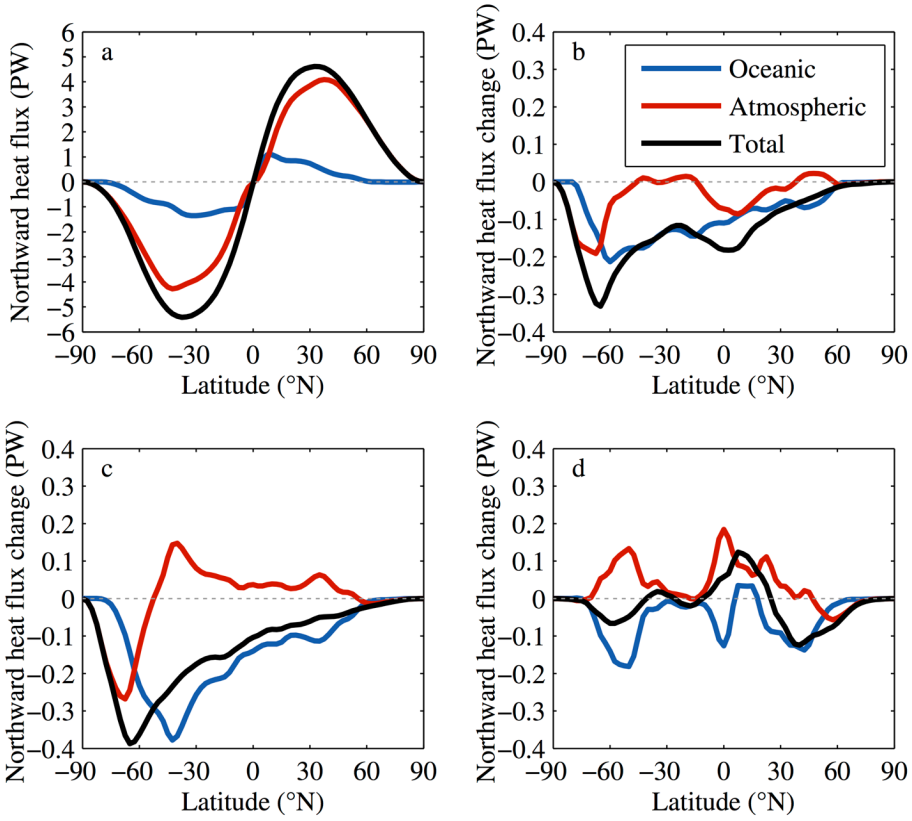

Figure 2.7: General form of the global meridional (northward) heat flux (PW), shown for the unglaciated Rupelian (a). Changes in the northward heat flux in response to glaciation are shown for the Rupelian (b) and Priabonian (c), and changes in response to gateway opening (unglaciated Rupelian – unglaciated Priabonian) are shown in (d). In all figures, black lines show total, red lines show atmospheric and blue lines show oceanic heat fluxes.

RupNO – PriNO; Figure 6d) show little net change in the SH total southward heat flux, with the (northwards) atmospheric component mostly balancing the (southwards) oceanic component.

2.4. Discussion

2.4.1. Mechanisms

Due to the complexity of GCMs, and in particular the feedbacks which act between many aspects of the system, diagnosing the mechanisms behind changes seen in the model in response to a change in boundary conditions is challenging. The only way to confidently assess mechanisms is to carry out sensitivity studies in which particular aspects of the system are kept constant, and/or feedback loops are cut. However, due to the computational cost of additional simulations, this is rarely carried out. Here, the mechanisms behind the observed responses will be discussed qualitatively. We aim to provide plausible mechanistic explanations for the changes seen in both stages, but without additional sensitivity studies these mechanisms remain somewhat speculative.

Two fundamental factors of Antarctic glaciation affect climate: 1) the increased surface albedo over the continent, reducing the solar radiation absorbed at the surface, and 2) the increased height of the new ice sheet topography, changing the reference height and modifying atmospheric pressure and circulation. The combined effect of these two factors causes the dramatic SAT cooling over Antarctica (Figure 2.3). The gravitational potential of this cold air initiates katabatic winds off the ice sheet (e.g. Parish & Waight, 1987). The outflow of the katabatic winds enhances polar circulation over Antarctica, and so between 60-80 °S air is rising to replace that flowing off the AIS leading to reduced *P* (Figure 2.4). It would be expected that cooling air over the AIS would lead to sinking and be associated with increasing *P* (similar to Goldner et al., 2014). However, the strong temperature seasonality of HadCM3L over Antarctica (Gasson et al., 2014) negates this pressure effect with large decreases in summer *P*. It should be noted, however, in terms of mean sea level pressure, *P* is found to increase over Antarctica (figure not shown; similar to Goldner et al., 2014). This is subject to interpolation that may be unrealistic when adding a thick AIS.

Regardless of the mechanism of *P* change over the AIS, the Δ_{glac} decrease over the SO is expected and results in an increased north-south pressure gradient at the polar front, ~60 °S. This causes increases in westerly winds over the Pacific sector of the SO (Figure 2.4c) that result in slight changes in the wind-driven eastward flow (Allison et al., 2010). The change in zonal wind stress over the SO leads to some increased wind driven upwelling south of 60 °S and downwelling north of 60 °S (figure not shown). Some of this wind driven overturning change would be expected to be balanced by an increased eddy field, however, the relatively coarse model resolution means that these eddies are not resolved (Abernathey et al., 2011; Munday et al., 2015).

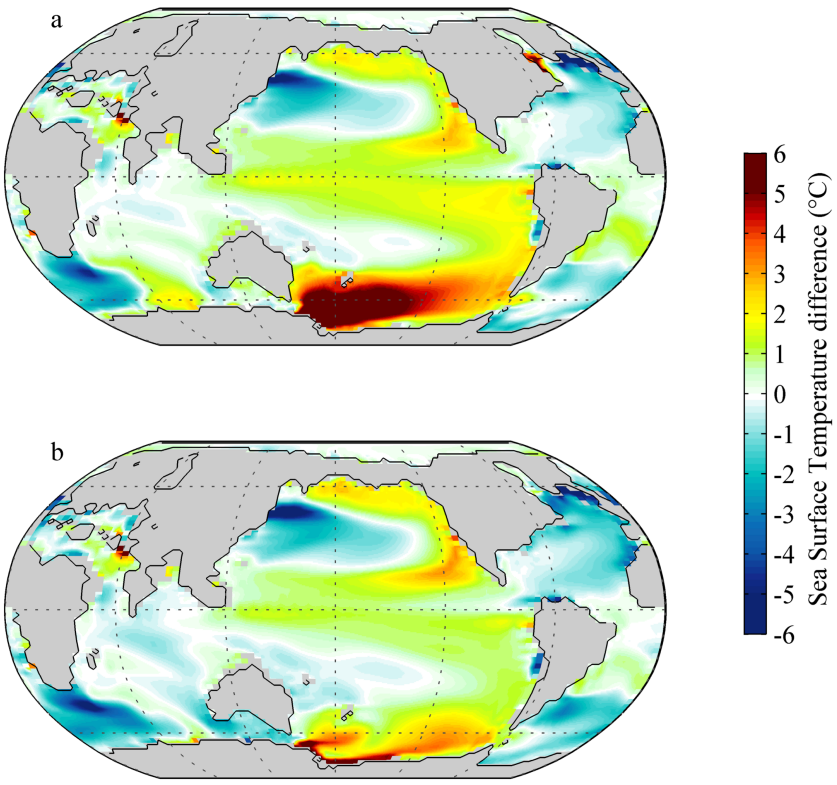

Supplementary Figure 2.4: Sea surface temperature difference between the stages for the same ice sheet configuration (°C), shown for the unglaciated Rupelian – unglaciated Priabonian (a) and the glaciated Rupelian – glaciated Priabonian (b).

By comparing the Δ_{glac} SST response with the change in SST observed between the stages with the same ice sheet states (Supplementary Figure 2.4), it is possible to identify PriNO as having an anomalously cold Ross Sea and South Pacific sector. This sensitive stratified ocean state is associated with a lack of deep-water formation in the region, indicated by the very shallow MLD (Figure 2.6a). Deep-water formation draws water from lower latitudes, releasing heat as it sinks. The interconnectivity of the causes and changes associated with deep-water formation make untangling these results particularly challenging, but a potential explanation of why this process is absent during PriNO is offered here.

During the Priabonian, constricted ocean gateways do not allow a strong barotropic circumpolar current to form around Antarctica, with eastward flowing water in the Pacific sector being part of larger South Pacific or Ross Sea gyre circulations (Figures 2.5a and 2.5b). The sluggish zonal circulation prior to glaciation allows the Ross Sea gyre to expand both northwards and eastwards across the width of the Pacific sector of the SO (similar to Sijp et al., 2011 with a closed TS). As a result, water is transferred to high latitudes along the eastern boundary of the Pacific and returns westwards along the Antarctic coastline, and is very cold upon reaching the Ross Sea. Combined

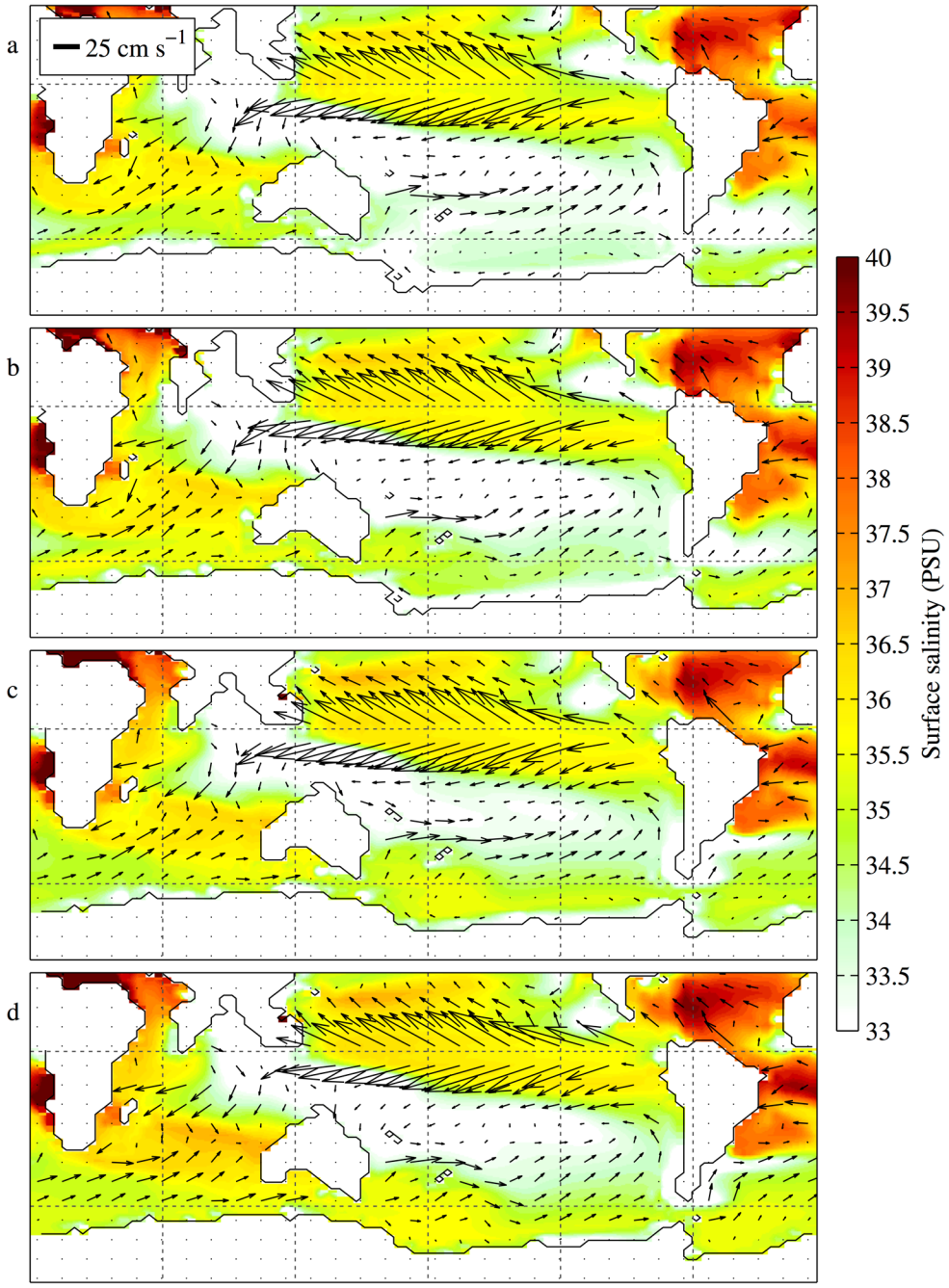

Supplementary Figure 2.5: Ocean surface currents (vectors) and sea surface salinity (PSU) for the unglaciated Priabonian (a), glaciated Priabonian (b), unglaciated Rupelian (c) and glaciated Rupelian (d). Vector scale is located in (a).

with the lack of deep-water formation and a sea ice albedo feedback, this causes the region to be anomalously cold compared to the other simulations. Deep-water formation in the polar regions is strongly affected by salinity (Assmann & Timmermann, 2005), so despite the low Ross Sea SST in PriNO water density and deep-water formation are suppressed by low salinities (Supplementary Figure 2.5a). With the addition of the AIS (or expansion of the gateways), the salinity in the Ross Sea increases (Supplementary Figure 2.5b), initiating sinking. This salinity change could be the

result of changes in sea ice formation, changes in net evaporation and precipitation (*E-P*) and/or changes in ocean circulation.

Changes in sea ice formation are ruled out as being an important driver of the Ross Sea Δ_{glac} salinity response, because sea ice extent reduces with the inclusion of the ice sheet, which will result in less brine rejection. Sea ice causes a seasonal increase in salinities but this effect diminishes once the ice sheet forms. The South Pacific and SO experience net precipitation (*P*>*E*) in all simulations, contributing to the low salinities found there. In the SO the highest salinities are close to the TS and decrease with distance east (Supplementary Figure 2.5). The *E-P* Δ_{glac} response shows an increase in evaporation over the Ross Sea of the Priabonian, but there is still net precipitation over the region. This may not be the driver of change but will act as a positive feedback with deep-water formation (whereby enhanced evaporation increases salinity, potentially increasing deep-water formation, which in turn releases heat and further enhances evaporation). Pacific sector salinity shows a strong correlation with flow through the TS from the high salinity Indian Ocean. It is plausible that the low salinity in PriNO is due to the greatly reduced flow through the TS. Once flow is increased, either by opening the gateway or adding the ice sheet, high salinity water penetrates into the Ross Sea, initiating deep-water formation.

A combination of the latter two processes is likely to have brought about the change in the Ross Sea salinity, with advection of water through the TS potentially triggering and enhanced *E* consolidating the increase (Sijp et al., 2011). Deep-water formation then enhances meridional transport of water, causing the large Ross Sea gyre to contract westwards away from the Bellingshausen Sea. As a result, the Bellingshausen Sea coast cools (less meridional transport to the region) and the Ross Sea warms. The warming is strong and extensive in contrast to the results of Sijp et al. (2011), who compared a fully open and closed TS but with no change in ice sheet. Further feedbacks may have contributed to this strong response: firstly with the collapse of sea ice and associated albedo effect enhancing the temperature anomaly in the region; secondly with the smaller Ross Sea gyre reducing the transport time of water within the gyre, reducing the freshening effect of the negative net *E-P* in the region; and thirdly with steepening of the isopycnals in the SO resulting in a stronger zonal depth integrated stream function through thermal wind.

The Rupelian SST Δ_{glac} response is not as strong as the Priabonian, but there are still some clear spatial and seasonal patterns. The warming and cooling responses can be explained by separate mechanisms. The summer SST cooling over the Indian Ocean sector of the SO appears to be a direct result of glaciation through atmospheric cooling and katabatic winds. The proximity of the Indian Ocean sector to the EAIS, where there is Δ_{glac} cooling of >30 °C and katabatic winds to

transfer this extremely cold air over the SO, affects the summer SST. The Δ_{glac} change in southward heat flux (Figure 2.7c) shows a global increase in the oceanic component, suggesting that the cooling has a local source and is not the result of changes in ocean circulation (i.e. reduced southward heat flux). Future work will aim to confirm this by comparing results to simulations with a slab ocean with a fixed ocean heat flux (which we hypothesise to show the same signal). In the winter, the Δ_{glac} warming response found in the South Pacific sector of the SO is caused by circulation changes. Stronger westerlies and seasonally persistent katabatic winds intensify the Ross Sea gyre (shown by the sharper 'kink' in the depth integrated stream lines in Figure 2.5d and the surface currents in Supplementary Figure 2.5d), transferring waters meridionally and bringing heat southwards. The signal is not as clear during the summer, however, because the increased westerly winds at 60 °S transfer colder water from the Indian Ocean sector to the Pacific sector of the SO and Ross Sea, overprinting the signal. Some stronger warming occurs along coastlines where there is enhanced deep-water formation, shown by the increases in MLD between Figures 2.6c and 2.6d.

It should be noted that the responses and mechanisms outlined here are also consistent for glaciation of only East Antarctica, with the main area of Ross Sea warming still present during the Priabonian but having a slightly lower magnitude (exhibiting maximum warming values of ~4.5 °C; figure not shown). There are only subtle variations in the Weddell Sea MLD and SST responses to East Antarctic glaciation compared to those discussed here, showing the effect of the WAIS is small and localised.

2.4.2. Implications

These results would suggest that prior to an established proto-ACC (or sufficient TS opening) there is a negative feedback on AIS growth, in which increases in Antarctic ice volume lead to large increases in SST in the Pacific SO, potentially inhibiting further Antarctic ice growth. If this were the case, it may have and contributed to the temporality of ephemeral ice sheets during the Eocene (Miller et al., 2008). This feedback wanes once the TS and DP widen and the ACC becomes stronger, with cooler summer SO temperatures, particularly in the Indian Ocean sector. There is also a potential mild positive feedback with winter warming in the coastal SO, which may enhance evaporation and Antarctic ice growth. However, there is evidence for a limited effect of SST changes on the interior of the Antarctic continent within models (Huber & Nof, 2006)

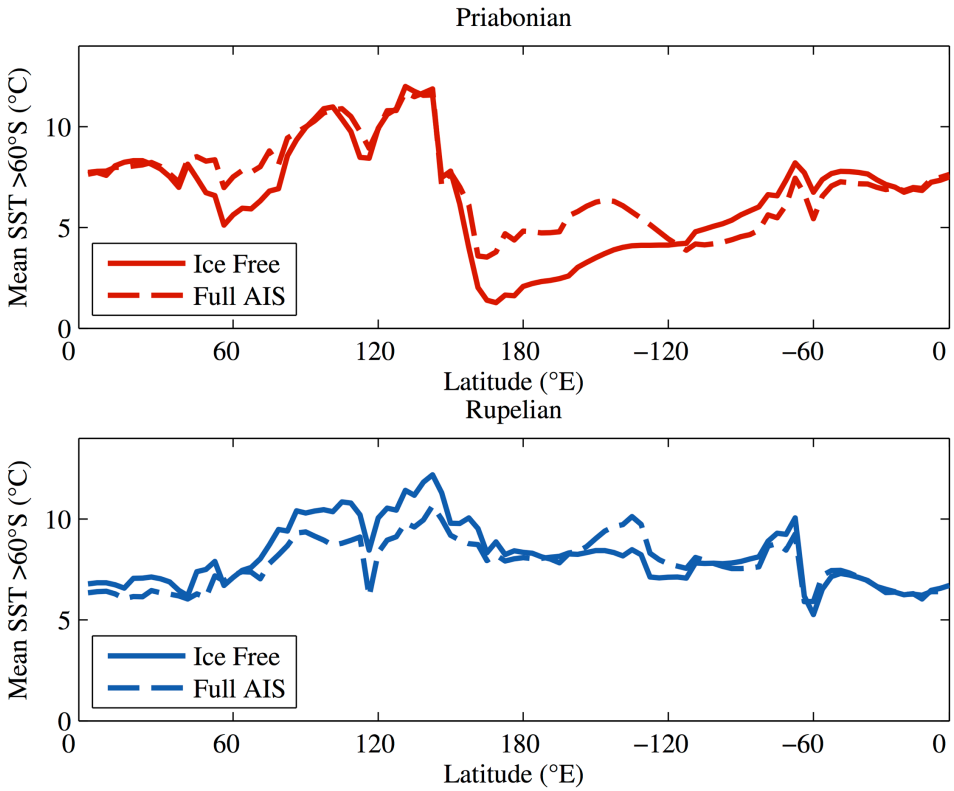

Supplementary Figure 2.6: Meridionally averaged sea surface temperature profile (°C) for the Southern Ocean (>60 °S). The Priabonian is shown in red and the Rupelian in blue. The solid lines show the unglaciated and the dashed lines the glaciated simulations.

Additionally, the unglaciated Priabonian results are inconsistent with some of the (albeit limited) proxy datasets available. Douglas et al. (2014) find a zonal gradient in SST proxies between the warmer southwest Pacific and the cooler south Atlantic of 7 °C during the middle-to-late Eocene. A similar temperature gradient is found here for the Rupelian, but not for the Priabonian (see Supplementary Figure 2.6). During the Rupelian, the gradient is greater when Antarctica is unglaciated (4 °C), reducing slightly with glaciation (3 °C) due to the cooling and transfer of Indian Ocean sector waters reducing the peak temperatures found in Pacific sector. It should be noted the absolute values are ~15 °C cooler than the simulations and proxy reconstructions of Douglas et al. due to the different atmospheric CO_2 levels used (their simulations used 2,400 and 1,600 ppm, representative of the mid-to-late Eocene). We suggest, therefore, the key implication of these results is that subtle changes in palaeogeography and model setup can result in substantially different regional climate responses: potentially of great importance when interpreting model results. Hence, it is not surprising that the results differ from those of Goldner et al. (2014) and Knorr & Lohmann (2014).

This conclusion is further corroborated by comparing the zonal flow Δ_{glac} response for the Rupelian with the results of Hill et al. (2013). In our study, adding the AIS in the Rupelian increases zonal flow by >20 Sv (10^6 m^3 s^{-1}) whereas Hill *et al.* found it reduced flow through the DP and TS by 2 and 10 Sv respectively. Although their simulations were also carried out using the same model (HadCM3L) and atmospheric CO_2 levels, their spin-up procedure, model setup and palaeogeographic reconstructions were different, highlighting how experimental design can impact results, even using the same model.

A number of additional experiments were carried out with the same spin-up procedures as those discussed here. One of these was an ice-free Priabonian simulation with four times pre-industrial CO_2 levels (more physically realistic for the late Eocene; Pearson et al., 2009; Pagani et al., 2011). This experiment also showed a very cold Ross Sea with no deep-water formation, so while we note this result is likely to be model dependent, it is robust to a change in CO_2 concentration. Another set of simulations was carried out for the Chattian stage (~28-23 Ma) that follows the Rupelian (~34-28 Ma). In this stage there was further widening of the TS and DP by another grid cell in the model, and the same ice sheet and ice-free configurations were used. With this additional opening of the southern gateways flow approximately doubles compared to the Rupelian, and with the addition of the AIS there is an established ACC and flow through the DP of 103.5 Sv (a similar order of magnitude to present day measurements of ~130 Sv; Meredith et al., 2004). This would support studies suggesting the ACC strengthened in the mid-to-late Oligocene (Pfuhl & McCave, 2005; Lyle et al., 2007). It is also worth noting the zonal flow through the DP and TS is once again different to the results of Hill et al. (2013), being 10-20 Sv higher in our study.

All stages (including the Chattian) show that enhanced zonal ocean circulation due to Antarctic glaciation and gateway opening causes increased poleward heat transport in the Southern Hemisphere, contrary to traditional theory (e.g. Gill & Bryan, 1971; Kennett, 1977; England, 1993) but similar to the results of Goldner et al. (2014). These results suggest that the enhanced circulation does not act as a barrier to inhibit poleward heat transport. As noted previously, these increases are similar to those found in previous studies (Huber & Nof, 2006; Goldner et al., 2014), however, it remains to be seen if it is great enough to have a significant effect on Antarctic climate (Huber & Nof, 2006).

2.5. Conclusions

This study identified the climatic and oceanic response to glaciation in the HadCM3L model for two geological stages on either side of the EOT. The climatic response to glaciation varied significantly between the two stages, due to a complex network of feedbacks acting to cool the Ross Sea during the unglaciated Priabonian simulation. The sensitive, cold ocean state in this simulation is easily destabilised with the onset of deep-water formation in response to either Antarctic glaciation or gateway opening. This response is likely to be very model dependent (it does not match with the limited proxy data available for the region for example), but it highlights how, through multiple feedbacks, subtle changes in palaeogeography and model setup can produce very different modelled climatic responses to Antarctic glaciation.

Future research can expand in multiple directions. Initial work could carry out a slab ocean model run for the Rupelian to affirm the conclusions about Indian Ocean cooling being due to the proximity with the AIS. Running similar experiments with different coupled climate models will be essential in assessing if this sensitive behaviour is a feature of other models, or if this is specific to HadCM3L. Further work will also include more detailed comparison of the modelled response to the geological record. Finally, using these high-resolution palaeogeographic reconstructions, it would be interesting to carry out transient simulations under changing CO_2 forcing with a coupled ice sheet model (similar to those of DeConto & Pollard, 2003a and Ladant et al., 2014a) to model glacial inception and examine if regional sensitivity exists in this case also, and to properly explore the feedbacks between Antarctica and global climate.

2.6. Outstanding questions

The research presented in Kennedy et al. (2015) highlighted some interesting responses to Antarctic ice growth, including the importance of feedbacks in the model (and possibly the real world) for influencing the spatial patterns and magnitudes of change. However, outstanding questions remained, particularly relating to some of the inconsistencies in the model setup and how much of an influence this would have on the results. Three main outstanding questions will be focussed on in greater depth:

1. How does the island definition in the model affect the climatic responses shown?
2. Why do the results differ from those of Hill et al. (2013) in terms of the change in ACC flow in response to Antarctic glaciation?
3. How representative of other boundary condition states are these four simulations?

The first two questions are discussed in this section and the third question is addressed in Chapter 3.

2.6.1. Island definition

In Kennedy et al. (2015) it was noted that the island definition varied between the Priabonian and the Rupelian simulations, whereby in the Priabonian, Antarctica was erroneously not defined as a separate island, whereas in the Rupelian it (correctly) was. Further simulations carried out since the publication of Kennedy et al. find this difference to be an important one.

The Priabonian simulations in Kennedy et al. had neither Antarctica nor the Northern Hemisphere (the single or inseparable land mass of Europe, Africa, Asia and North America) defined as islands, whereas, Australia and South America were defined as separate islands. The original island definition used in Kennedy et al. is shown in Figure 2.8a and the correct definition as it should have been simulated is shown in Figure 2.8b. The islands of the Rupelian and Chattian simulations are also shown for reference in Figures 2.8d and 2.8e respectively.

For all of these Stages, there are four gateways into the Pacific Ocean: the Tasman Seaway and Drake Passage at high latitude (TS and DP respectively) and the Indonesian and Panama Seaways

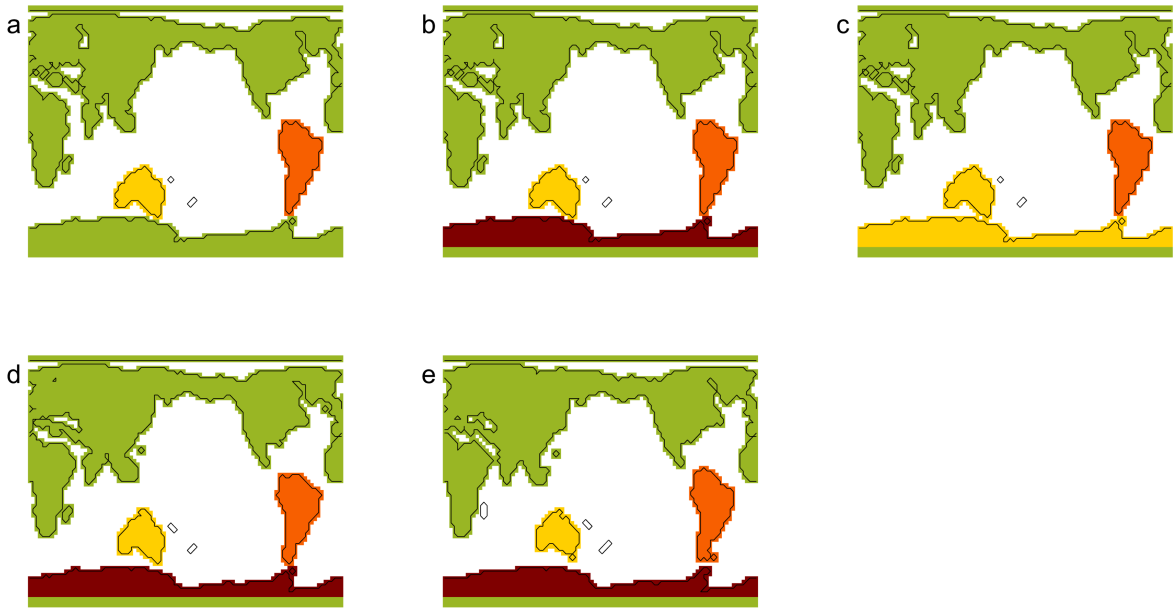

Figure 2.8: Island definition used in various model runs, including a) the Priabonian simulations of Kennedy et al. (2015), b) the corrected Priabonian simulations, c) the Priabonian with a combined Antarctic-Australian island, d) the Rupelian simulations and d) the Chattian simulations. Islands of the same colour must have the same stream function value. (Note: smaller islands, e.g. New Zealand and Madagascar, were included, but are not shaded here.)

at low latitude (IS and PS respectively). The flow through each of these gateways for the Priabonian simulations with and without a full AIS, with the islands defined as in Figures 2.8a and 2.8b, is shown in Table 2.3. Figure 2.9 shows the depth integrated stream function for each experiment.

There are a number of differences in the circulation between the island setups worth noting. Firstly, if Antarctica is defined as an island (i.e. gateway flow is unconstrained) the flow through high latitude gateways is much greater than that at low latitude (approx. 2-3 times greater). If Antarctica is not defined as an island, the coupling between the low and high latitude gateways acts to decrease the flow through all gateways and reverse the direction of the low latitude flow (in the unconstrained setup flow is eastward, whereas the constrained flow is westward). This numerical

Table 2.3: Eastward flow through all Pacific gateways (Sv) in the Priabonian simulations with and without a full AIS and with Antarctica defined as a continent and as an island.

Simulation	IS flow (Sv)	PS flow (Sv)	TS flow (Sv)	DP flow (Sv)
No ice, incorrect islands	-12.7	-2.5	12.7	2.5
Glaciated, incorrect islands	-21.7	-8.7	21.7	8.7
No ice, correct islands	18.1	17.1	37.4	38.4
Glaciated, correct islands	23.1	14.1	53.7	62.7

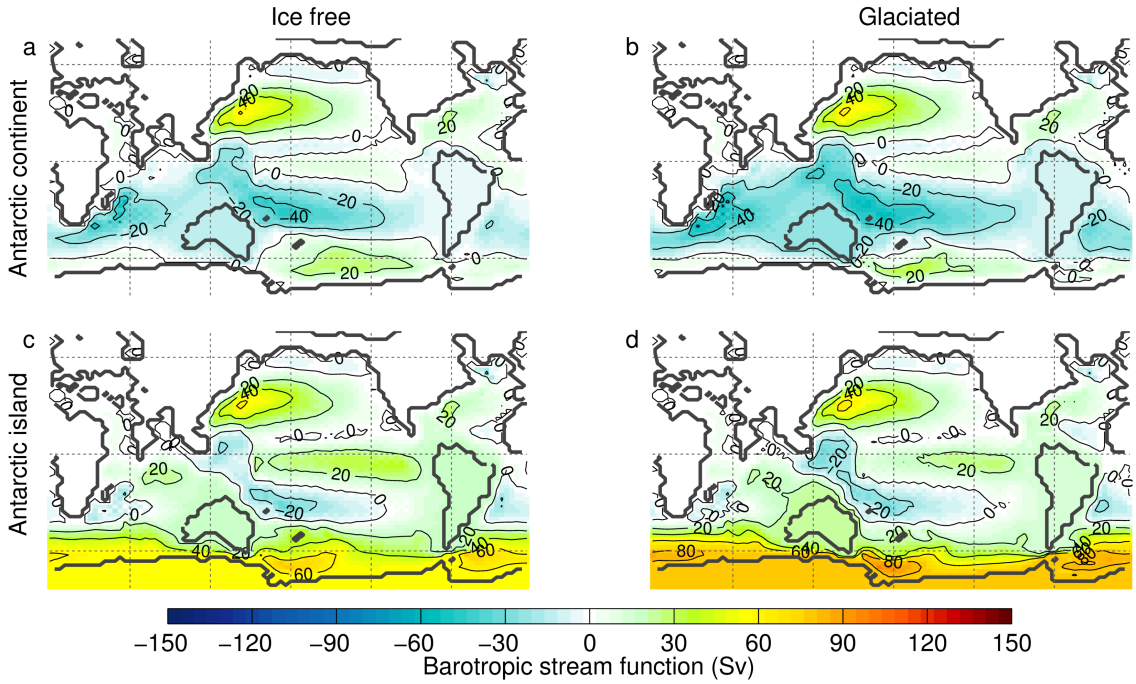

Figure 2.9: Mean annual barotropic stream function (Sv) for the (a) ice free and (b) glaciate Antarctic continent simulations (as in Kennedy et al., 2015) and the (c) ice free and (d) glaciated Antarctic island (corrected) simulations.

artefact is an interesting result, as some modelling studies (e.g. Baatsen et al., 2018b) show a flow pattern more similar to the incorrect continental definition, with westward flow at low latitudes, while others (e.g. Zhang et al., 2011) show net eastward flow through at least the Panama Seaway. Fewer studies focus on low latitude gateways and it is unclear what the consensus is in past-research. Secondly, because the zonal flow through the Southern Ocean is enhanced when Antarctica is an island, the large Ross Sea gyre noted in Kennedy et al. (2015) is suppressed under both ice-free and glaciated conditions and deep-water formation occurs in the Ross Sea (figure not shown). Thirdly, there is a large difference in the flow through the Atlantic sector of the Southern Ocean between the island setups, firstly being much more strongly zonal and also having a larger Weddell Sea gyre when Antarctica is an island. Northern hemisphere oceans show broadly similar circulation patterns in all simulations.

The changes in ocean circulation have some large-scale implications for atmospheric conditions. Figure 2.10 shows the SAT and SST response to glaciation for the Priabonian and Rupelian (the same as Figure 3 of Kennedy et al.) but with the corrected Antarctic island definition for the Rupelian. With the correct island definition, the extremely cool Ross Sea state for the ice-free Priabonian ceases to exist and, as a result, the Ross Sea and Pacific sector of the Southern Ocean is up to 9 °C warmer than the incorrect simulation (figure not shown).

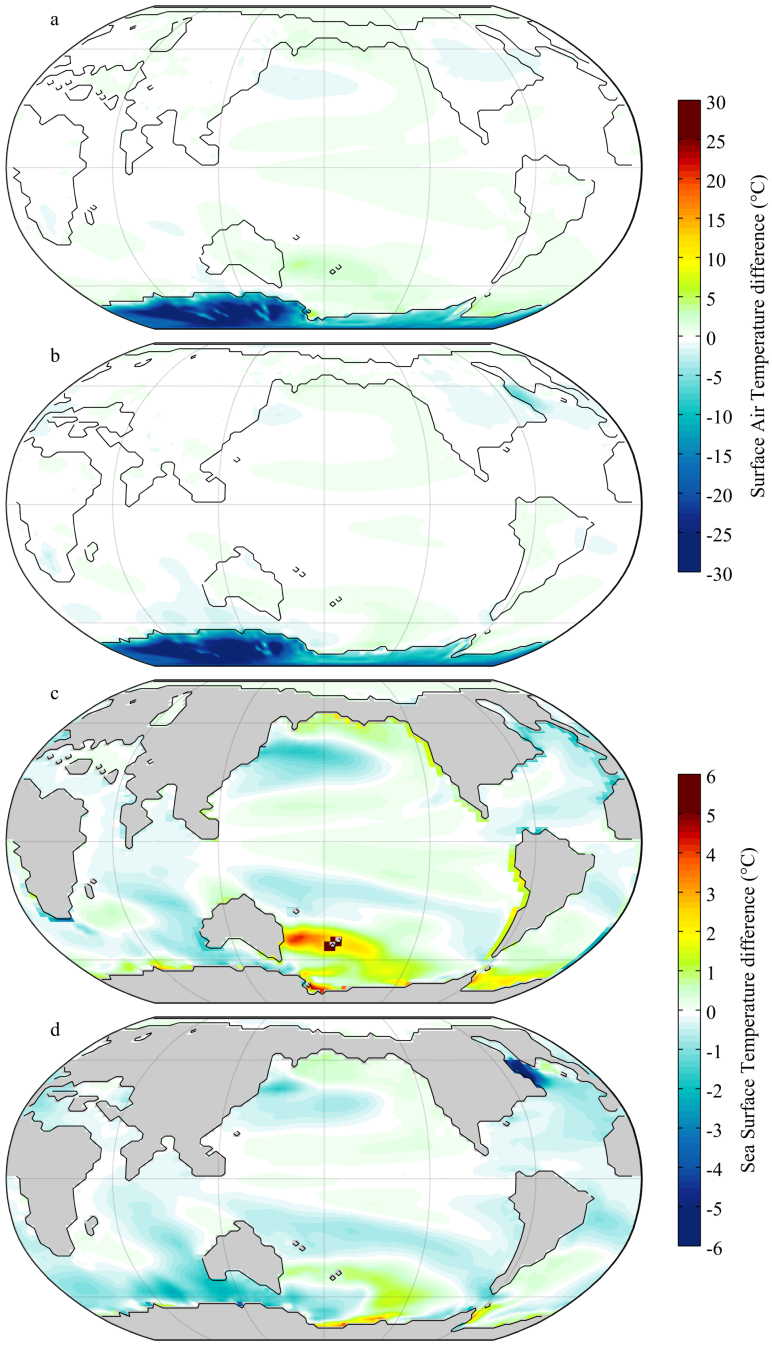

Figure 2.10: As Figure 3 of Kennedy et al. (2015) but with the corrected island definition for Antarctica in the Priabonian simulations (a and c).

Clearly, these supplementary results have important implications for the research presented in Kennedy et al., where the principle result was that the Priabonian showed a very different climatic response to glaciation than the Rupelian. Correcting the island definition produces results for both Stages that are much more similar (Figure 2.10) and it is important to consider if the results based on the original simulations used in Kennedy et al. are still relevant.

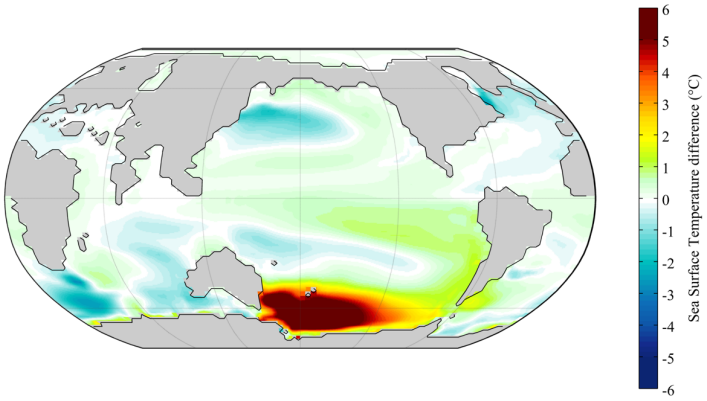

Figure 2.11: The sea surface temperature response to glaciation (°C) if Antarctica and Australia are modelled as one combined island using the Priabonian palaeogeography.

Given that the island definition is controlling the amount of flow through the TS, it is possible that the mechanisms discussed in Kennedy et al. could represent a realistic response through a restricted, narrow gateway. HadCM3BL is limited by its resolution in terms of how it can resolve these small-scale features in the model, as east-west gateways are effectively limited to being >500 km wide (two latitudinal grid cells). The actual gateway expansion would have had times when it was much narrower than this, but this is impossible to model with a consistent island definition in HadCM3BL. Presumably, however, a narrower gateway would have had reduced flow, so it is possible that the simulations with an incorrect Antarctic island could represent this scenario (despite the gateway not actually changing dimensions). In this case, technically, the correct way to define the islands would combine Antarctica and Australia into one island box (as shown in Figure 2.8c). Additional simulations doing this have a very similar spatial SST response to glaciation as the results in Kennedy et al., shown in Figure 2.11, with a maximum warming over the Southern Ocean of 8 °C. This island configuration, shown in Figure 2.8c, is what should be used for earlier Getech reconstructions which have a narrower TS than the Priabonian (e.g. for the Bartonian or Lutetian Stages). The results shown in Kennedy et al., therefore could still hold for an earlier palaeogeography.

To further explore if this is truly a realistic response, a different modelling approach would need to be taken using higher resolution models and possibly physically based eddy resolving ocean models, with much better representations of fluid dynamics. This is, however, well beyond the scope of this thesis.

2.6.2. Differences compared to Hill et al.

It was also noted in Kennedy et al. (2015) that despite using the same GCM as Hill et al. (2013) and carrying out a qualitatively similar experiment (comparing the steady-state climate with and without an AIS with a 'Rupelian' palaeogeography), there was a different ACC response to glaciation between the studies. Hill et al. found that adding the AIS reduced flow through the DP and the TS, but Kennedy et al. find that flow through the DP and TS increases in response to glaciation.

The simulations used in Hill et al. were carried out at the University of Bristol by P.J. Valdes (completed around 2010) and so the model results were available to be investigated further. They were part of a series of simulations that have been continued since and it appears that differences in the spin-up procedure are responsible for the differences in responses between the two studies. The ice free and glaciated simulations used in Hill et al. were TBOYH and TBOYQ respectively (D.J. Hill, personal communication, 2016), although identifying the precise version of these simulations (e.g. TBOYH or TBOYH1) has not been possible. Table 2.4 shows the spin-up details and flow through the TS and DP for the Hill et al. and Kennedy et al. Rupelian simulations. Differences in the method of calculating the throughflow are believed to be the cause of the difference in the stream function values given here compared to those in Table 2 of Hill et al. (D.J. Hill, personal communication, 2016).

As shown, TBOYH and TBOYQ have very different total lengths of spin-up (1,510 vs 3,100 years respectively). The simulation TBOYR, also listed in Table 2.4, is a continuation of the ice-free TBOYH, which brings the total spin-up to be more in line with TBOYQ, the glaciated simulation. Once the ice-free simulation is spun-out to a similar length, its flow through the Southern Ocean gateways decreases to a value that is less than the glaciated simulation, similar to the results of Kennedy et al. Although the absolute values are lower for the Hill et al. simulations, comparing TBOYR to TBOYQ suggests that flow through the Southern Ocean gateways increases by ~50 % with glaciation, a similar value to that shown in the Kennedy et al. simulations. Chapter 3 will further investigate the change in ACC strength in response to the appearance of an AIS, with additional simulations supporting the results presented in Kennedy et al. that glaciation causes an increase in the ACC strength.

Table 2.4: Spin-up details for the ice-free and glaciated Rupelian simulations used in Hill et al. (2013) and Kennedy et al. (2015), showing previous simulation experiments in the spin-up and the Southern Ocean gateway throughflow for each simulation. Note: all of these simulations have used the correct island definition.

Simulation	Expt. name	Previous expt. names	Final phase length/Total spin-up length (years)	Tasman Seaway throughflow (Sv)	Drake Passage throughflow (Sv)
Hill et al. ice-free (published)	TBOYH	-	1,510/1,510	64.6	45.5
Hill et al. ice-free (continued)	TBOYR	TOBYH	1,395/ 2,905	37.5	28.8
Hill et al. glaciated (published)	TBOYQ	TBOYE, TBOYG	1,933 / 3,100	56.5	43.3
Kennedy et al. ice-free	TDLUT	TDKAH, TDLCH, TDLUN	416 / 1,422	52.6	46.2
Kennedy et al. glaciated	TDLUP	TDKAH, TDLCL	1000 / 1,422	75.2	68.0

2.7. Conclusions

This chapter of research and the results of Kennedy et al. (2015) shows that a complex web of feedbacks is involved with changes in the cryosphere, before even dynamic ice, solid earth or biogeochemical processes are considered (e.g. Rugenstein et al., 2014; Armstrong McKay et al., 2016; Elsworth et al., 2017). Model simulations using HadCM3BL with different ice sheet states, palaeogeographies and island definitions were tested. Comparisons between simulations showed that the addition of the AIS can, under certain conditions, cause a large warming in Southern Ocean sea surface temperatures in the South Pacific sector. This effect is found because the simulation with the Priabonian palaeogeography, when Antarctica is defined as a continent and is ice free, is anomalously cold in this region. This cooling is at least partly related to internal model processes and feedbacks, for example this simulation has very low flow through the Tasman Seaway and as a result, there is low salinity, no deep-water formation and an expansion of sea ice in the Ross Sea area. Other simulations which have greater flow through the Tasman Seaway (either when Antarctica is defined as an island or is glaciated in the Priabonian, or for all simulations with the later Rupelian palaeogeography) do not show such cold temperatures in the South Pacific sector of the Southern Ocean.

It is possible that the anomalously cold Priabonian simulation is simply a model artefact and does not represent a real state that the Earth system ever would have been in. If it is a real process, such a major change should be expected to be present in proxy records, requiring a detailed regional model-data comparison, which will follow in Chapter 4. If this is a model artefact, it is important to understand why it is occurring. One possibility is that it is due to an incomplete spin-up. Given that deep water formation in the region is important yet conspicuously absent, it is possible that with more spin-up the model will start to generate deep water and over turning in the Ross Sea region. The specific conditions of the Priabonian simulation with the ice-free Antarctic continent are possibly slower to equilibrate or their initial conditions further from equilibrium than the other simulations. This will be investigated further in the Chapter 3, as well as a much wider investigation into the modelled changes at the EOT, which will show if any other simulations with a wider range of boundary conditions behave similarly.

Further to the work of Kennedy et al., this chapter showed that the effect of island definition in the model is very important. All subsequent model simulations in later chapters will ensure that the correct island definition is consistently used. It is hard to definitively say whether or not the simulations with the incorrect island definitions are entirely unrealistic or not. The effect of the incorrect definition at high latitudes is to slow the ocean flow in the Southern Ocean. Given the

ocean gateways in the Southern Ocean during the Priabonian are already close to the limit of what is resolvable due to the model resolution, the slowing of the ocean flow might be a reasonable approximation for a further constricted gateway. However, another major impact of the island definition is the reversal of flow at low latitudes into and out of the Pacific (either westward or eastward flow through the Panama and Indonesian Seaways). Given there is little focus in the literature on these gateways, with some examples contradicting each other, it is hard to know what might be expected to occur in these seaways during around the EOT, and to comment on this further would require more research.

The contradiction between the results of Kennedy et al. and the results of Hill et al. (2013) in terms of the change in Drake Passage throughflow in response to the addition of the AIS was investigated in more depth, with differences in the spin-up procedure identified as the likely cause of the difference. The published Hill et al. ice-free and glaciated simulations have very different lengths of spin-up. Direct continuations of the ice-free simulation to increase its length to be comparable with the glaciated simulation produces a different result. Once further spun-out, the ice-free Southern Ocean gateway throughflow is much lower, approximately a third less than the glaciated simulation – a similar result to the Kennedy et al. simulations.

It is very important to consider how sensitive these results are to the model setup and to reflect on how these feedbacks might have been manifested in the real world during the EOT. How would these processes have interacted with other forcings and feedbacks not considered in this research? What evidence is there from proxy records to support any of these changes? Chapters 3 and 4 will address some of these questions.

Chapter 3: Assessing mechanisms and uncertainty in modelled climatic change at the Eocene-Oligocene Transition

3.0. Introduction

This research chapter is written in paper format. It was published in a special issue of *Paleoceanography and Paleoclimatology* themed around the Climatic and Biotic Events of the Paleogene (CBEP) 2017 conference, held in Utah, September 2017 (Kennedy-Asser, A.T., Lunt, D.J., Farnsworth, A. & Valdes, P.J., 2019. Assessing mechanisms and uncertainty in modelled climatic change at the Eocene-Oligocene Transition. *Paleoceanography and Paleoclimatology*, 34, pp. 16-34, DOI: 10.1029/2018PA003380).

This work directly builds upon Kennedy et al. (2015) and Chapter 2 of this thesis. It was shown that, through a series of feedback mechanisms, the response to Antarctic glaciation can vary significantly between different model simulations depending on their boundary conditions (palaeogeography, in the case of Kennedy et al., 2015). However, it was unclear how representative the few model simulations used in Kennedy et al. are of the potential spectrum of boundary conditions more broadly. The general motivation of this research aims to answer the question: how sensitive are palaeoclimate model simulations to subtle changes in boundary conditions? This was investigated by greatly expanding the number of model simulations to cover a much wider range of boundary condition changes. Following the work in Chapter 2, it was also ensured that all simulations carried out and assessed for this chapter (and Chapter 4) had a consistent island definition in the model.

The text of this chapter is taken mostly verbatim from the most recent version of the paper. The only differences from the version that has been submitted are that supplementary figures and a table are shown in the text where they are referred to and the spelling has been changed to UK English rather than US English. At the request of the examiners of this thesis, the axes of Figure 3.6 have been modified from the published version of the paper, however the data is unchanged. I was the author of the text and carried out all of the analysis, with co-authors providing advice and guidance on structuring the work. Of the 23 model simulations used, 7 were run by me, 8 were run by A. Farnsworth and 8 were run by P.J. Valdes (see Appendix 1).

3.0.1. Abstract

The Earth system changed dramatically across the Eocene-Oligocene Transition (EOT) on a variety of spatial and temporal scales. Understanding the many complex and interacting factors affecting the Earth's atmosphere and oceans at the EOT requires the combination of both data and modelling approaches, and an understanding of the uncertainty in both of these elements. Here, uncertainty in the Earth system response to various imposed forcings typical of changes at the EOT is assessed. By using an ensemble of simulations from the fully-coupled GCM, HadCM3L, the uncertainty due to differences in the boundary conditions and insufficient model spin-up is quantified. The surface temperature response in high latitude ocean regions, particularly where deep water formation occurs, is found to be highly sensitive to differences in boundary conditions (i.e. have the greatest magnitude of uncertainty), while low latitude oceans are the most insensitive to differences in boundary conditions (i.e. have the lowest magnitude of uncertainty). The length of spin-up (or how far the model is from equilibrium) can have a significant effect on the response to some forcings and on the magnitude of uncertainty due to differences in boundary conditions. These findings are important to consider for future modelling work and for interpreting previous published simulations.

3.1. Introduction

The Eocene-Oligocene Transition (EOT) occurred approx. 34 million years ago and was a time of major global environmental change (Zachos et al., 2001). The EOT marks an abrupt end to gradual cooling during the late Eocene (Inglis et al., 2015), with significant ice sheet growth over Antarctica (Galeotti et al., 2016) and upheaval in some marine ecosystems (Houben et al., 2013). Other major changes occur around the same time as, but not necessarily coincident with, the EOT; for example, changes in ocean biogeochemistry (Pälike et al., 2012) and ocean circulation (Scher et al., 2015), suggesting possible but unclear linkages and the presence of complex feedbacks in the Earth system.

Arguably the most significant event to occur at the EOT is global cooling followed by the growth of a semi-permanent Antarctic ice sheet (AIS) to near modern-day proportions (Kennett, 1977; Zachos et al., 2001). This is usually observed in oxygen isotope proxy records as a 1.5 ‰ increase in two steps, the first representing benthic cooling and the second representing ice growth (Coxall et al., 2005; Lear et al., 2008). This oxygen isotope shift could represent a benthic ocean cooling of 2-3 °C and an expansion of the AIS to 60-130 % of its modern volume (Bohaty et al., 2012), with uncertainties due to the unknown isotopic composition of the AIS, for example. Evidence of Antarctic glaciation is further supported by changes in clay minerology of sediments around Antarctica and appearances of ice rafted debris at the EOT (Carter et al., 2017; Galeotti et al., 2016).

Not all changes that occurred around the time of the EOT, however, are so clearly marked. Some changes are more gradual, starting during the late Eocene and continuing through the EOT. This is the case for oceanographic changes such as the initiation of the Antarctic Circumpolar Current (ACC) and the formation of deep water in the North Atlantic. Traditionally, the former was cited as the cause of Antarctic glaciation, through the thermal isolation of the continent (Kennett, 1977). However, revised proxy estimates of the opening of Southern Ocean gateways (the Tasman Seaway and Drake Passage) and proxies of ocean circulation suggest changes in the ACC occurred gradually, with some changes during the Eocene but the ACC not reaching its full strength until the mid-late Oligocene (Lyle, et al., 2007; Scher, et al., 2015; Stickley, et al., 2004) suggesting other mechanisms were also fundamentally important. The formation of North Atlantic deep water shows changes broadly around the EOT but with some uncertainty on the timing (Katz et al., 2011; Via & Thomas, 2006). Particularly, recent studies show the deep-water formation started occurring in advance of the EOT (Coxall et al., 2018; Hohbein et al., 2012).

Additionally, terrestrial studies show a range of responses during this period of time, although these records are subject to weaker age control than ocean records. On one hand, there is strong evidence for continental aridification in central Asia (Sun & Windley, 2015) and the western interior of North America (Sheldon & Retallack, 2004; Zanazzi et al., 2007), likely due to uplift of mountains and changing moisture supply. In contrast, compiled records of vegetation ecosystem change show few clear changes globally over the EOT (Pound & Salzmann, 2017) nor regionally through the Oligocene (Li et al., 2018). This suggests changes to the terrestrial system occurred at a different rate to other climatic changes at the EOT with potentially complex driving mechanisms.

Numerical climate modelling has been very important for understanding the mechanisms behind these changes occurring at the EOT. DeConto & Pollard (2003a) provided the first strong evidence that declining atmospheric pCO_2 was more important for glaciation than changes in ocean gateways, a finding that has been echoed by a number of studies since (Huber & Nof, 2006; Ladant et al., 2014a; Sijp et al., 2011). However, processes and feedbacks within the Earth system could mean that even a small change in the ocean gateways around this time could have an effect on climate in other ways (Elsworth et al., 2017). Meanwhile, Gasson et al. (2014) showed that the pCO_2 threshold to induce glaciation is highly model dependent, while small changes in the setup and palaeogeography of a single model can affect the modelled climate (Kennedy et al., 2015) and ocean circulation (Baatsen et al., 2018b). Goldner et al. (2014) showed the Earth system may respond in a similar way to different forcings (in that case opening of the Southern Ocean gateways and formation of the AIS) and this could have impacts for how proxy records should be interpreted.

These modelling studies offered useful findings but cannot be taken without scrutiny. It is not uncommon to use idealised simulations to test palaeogeographic sensitivity to specific changes, such as open and closed ocean gateways to isolate their impact on climate (Huber & Nof, 2006; Hill et al., 2013). In these cases, palaeogeography outside the immediate region of interest is possibly assumed to have little effect on the climate, but this may not be the case. Currently, no studies have assessed the sensitivity in modelled climate that can arise from a range of dissimilar global palaeogeographies in a general circulation model (GCM). Here, we aim to provide an estimate of the degree of uncertainty that would be introduced to climate model simulations if subtle changes were made to the global palaeogeography and other boundary conditions.

Another typical issue faced in paleoclimate modelling is insufficient spin-up. Spin-up is the period of time over which a model simulation adjusts to the imposed boundary conditions before the climate of the model is calculated. Ideally this should be longer than the adjustment time of the

slowest-responding component of the system, usually the deep ocean. In general, the further the model initial conditions are from the true equilibrium state for a given climate variable, the longer the required spin-up. However, computational constraints mean that often the spin-up period is stopped before the model reaches equilibrium (which can be defined in terms of net radiative imbalance or deep ocean temperature and/or salinity drift over a given period of time). Furthermore, the large number of potential model parameters (e.g. paleogeography, greenhouse gas levels, orbital configurations etc.) can require a number of boundary condition sets to be used, further limiting computational resources available for spin-up. As a result, usually a compromise must be made between sampling the parameter space and the length of the spin-up (e.g. Lunt et al., 2016, used a large ensemble of simulations but a relatively short spin-up). This insufficient spin-up could produce misleading results.

While many proxy data studies include error bars or other measures of uncertainty in their results, often the meaning of uncertainty in model simulations is not clearly defined. Models will produce different answers with different boundary conditions, and different models (or identical models with different internal parameters) will produce different answers with the same boundary conditions. Furthermore, differing periods of spin-up will produce different results from the same model with the same boundary conditions. Here, efforts are made to understand the uncertainty due to boundary conditions and the uncertainty due to length of spin-up in the response to three idealised model forcings at the EOT: Antarctic glaciation, palaeogeographic change and atmospheric pCO_2 reduction. We focus on three research questions:

- What are the impacts and relative importance of these three forcings on global and Antarctic climate at the EOT?
- For each of these forcings, what is the range of uncertainty in the magnitude of certain modelled variables resulting from differences in the model boundary conditions?
- How does the simulation spin-up time affect the modelled impacts associated with these forcings?

The methods described in Section 3.2 outline the model, the ensemble of simulations and the statistical methods used. Results addressing the research questions follow in Section 3.3. Discussion, including a model-data comparison, are in Section 3.4 and conclusions in Section 3.5.

3.2. Methods

3.2.1. Model

All simulations carried out here used the fully-coupled GCM HadCM3BL-M2.1aE (Valdes et al., 2017). This is a specific setup used at the University of Bristol of the unified model, HadCM3L, created by the UK Met Office. The model runs at 2.5 x 3.75 ° horizontal resolution in both the ocean and atmosphere, with 19 vertical levels in the atmosphere and 20 in the ocean. Included in the model are representations of sea ice and land surface processes, and it is coupled with the land surface scheme MOSES and the vegetation model TRIFFID. Ice sheets in the model are not interactive, meaning they cannot melt or expand. They are prescribed by raising the topography, changing the TRIFFID land fraction to 'ice' (which affects the surface albedo and roughness length, for example) and covering it with a layer of snow (which is applied as a thick layer so that it does not completely melt).

3.2.2. Boundary condition ensemble

To investigate the intra-model uncertainty due to boundary conditions, results were used from a collaboration between the University of Bristol and Getech Group Plc., modelling multiple palaeogeographic reconstructions with a consistent but relatively short spin-up procedure (Lunt et al., 2016). Rather than modelling an idealised change in palaeogeography, here a range of realistic palaeogeographic uncertainty is tested based on the assumption that the Priabonian, Rupelian and Chattian geologic Stage reconstructions (shown in Supplementary Figures 3.1a-f) are all reasonable representations of the palaeogeography around the time of the EOT or early Oligocene, given dating uncertainties in the reconstructions. All of these reconstructions are qualitatively similar, in that they all have the same ocean gateways and similar continental positions, but they are subtly different globally. Along with different palaeogeographic boundary conditions, simulations also vary in terms of their pCO_2 level (either 1,120 or 560 ppmv) and AIS state (either Antarctica is ice free, has an East AIS or has a full AIS covering the whole continent). In Kennedy et al. (2015) it was noted that some simulations had inconsistencies in their island definition (required for the HadCM3BL ocean barotropic solver). Here, we have corrected those simulations and ensured that all of the simulations in this analysis have consistent islands.

In total this gives a boundary condition model ensemble of 15 simulations, detailed in Table 3.1. Each simulation is run with a consistent four phase spin-up procedure lasting 1,422 years, outlined

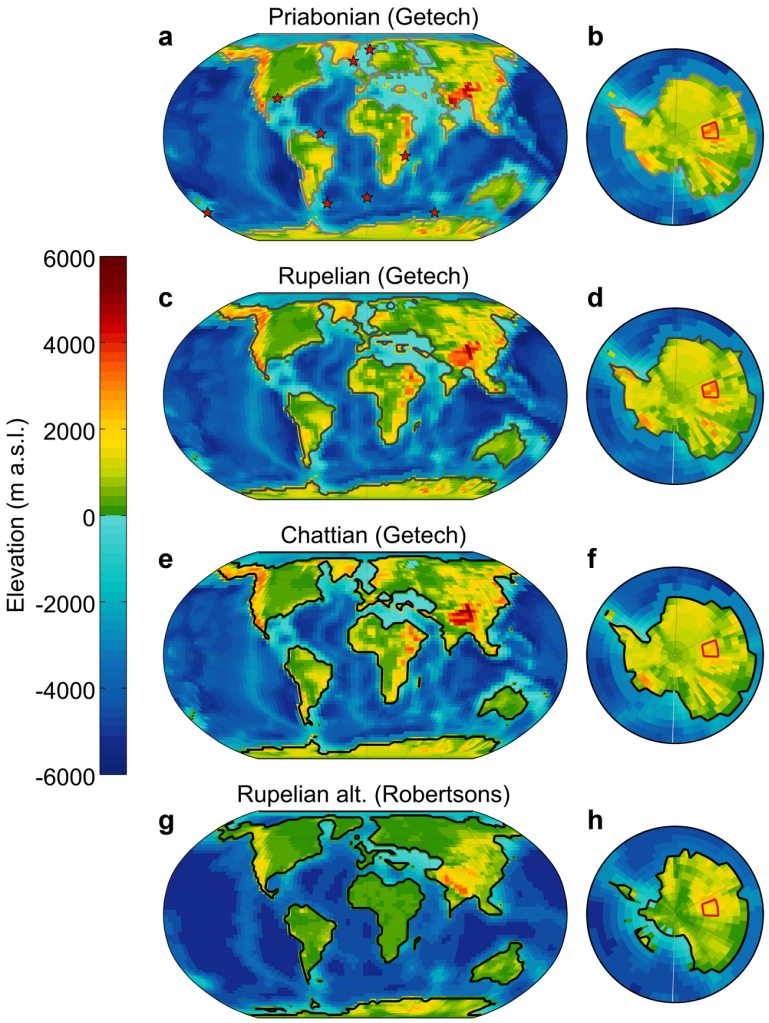

Supplementary Figure 3.1: Palaeogeographic reconstructions used. The red stars on the Priabonian reconstruction show the proxy data locations listed in Supplementary Table 3.1. The area marked in red in the polar projection plots over Antarctica shows the region of the Gamburtsev mountains, which is discussed in Figure 3.2. The different shades of the land-sea mask are the same as those used in Figure 3.1, with the Priabonian having the palest lines and the Chattian having the darkest lines.

in Lunt et al. (2016). Briefly summarised, the models are initialised for each palaeogeography with pre-industrial pCO_2 levels, uniform vegetation and a zonally symmetric sea surface temperature distribution. The ocean is initially stationary with a constant salinity of 35 ppt and an idealised zonal mean temperature structure that is a cosine function of latitude and depth (Lunt et al., 2016). The spin-up procedure then involves three initial phases totalling 422 years, in which the pCO_2 and ozone levels, lakes, ice sheets and (interactive) vegetation are adjusted, before there is a final 1,000 year phase of spin-up in which the model and boundary conditions stay constant. According to Lunt et al. (2016) by the end of the fourth phase the properties of the land and surface ocean are "approaching equilibrium", and as can be seen in Figure 4c of Lunt et al., the short early period

of spin-up with pre-industrial pCO_2 levels has little effect on the long-term ocean temperature trends. Some of these simulations will have coincidentally been initialised closer to their equilibrium state and hence will be exhibiting more gradual trends. The range in distances these model simulations are from equilibrium introduces another element of uncertainty to the simulations that is investigated as discussed in Section 3.2.3.

Table 3.1: Model simulation details. The highlighted 'Rupelian (alternate palaeogeog.)' simulations are those in the spin-up ensemble and all others are in the boundary condition ensemble. Simulations with an * are updated versions of the simulations in Kennedy et al. (2015) with corrected islands.

Epoch	Age (Ma)	Stage (palaeogeog.)	pCO_2 (ppmv)	AIS state	Drake Passage	Total spin up (years)	Simulation
Oligocene	28.1-23.0	Chattian	1,120	No ice	Open	1,422	TDLUY
				EAIS			TDLUX
				Full AIS			TDZSE
			560	No ice	Open	1,422	TDLUU
				EAIS			TDLUQ
				Full AIS			TDWQF
	33.9-28.1	Rupelian	1,120	No ice	Open	1,422	TDLUV
				Full AIS			TDLUW
			560	No ice	Open	1,422	TDLUT
				EAIS			TDWQE
				Full AIS			TDLUP
		Rupelian (alternate palaeogeog.)	840	Full AIS	Open	6,921	TECQS
					Closed	13,557	TECQT
				No ice	Closed	10,385	TECQU
					Open	6,493	TECQV
			560	Full AIS	Open	6,550	TECQN
					Closed	9,350	TECQO
				No ice	Closed	10,182	TECQP
					Open	6,121	TECQQ
Eocene	38.0-33.9	Priabonian	1,120	No ice	Open	1,422	TDZSC
				Full AIS			TDZSD
			560	No ice	Open	1,422	TDWQK*
				Full AIS			TDWQV*

3.2.3. Spin-up ensemble

A further set of eight model simulations outlined in Table 3.1 assess the model uncertainty due to insufficient spin-up. These simulations use an alternative palaeogeographic reconstruction of the Rupelian provided by Robertsons, shown in Supplementary Figure 3.1d, which has some notable differences to the Getech Rupelian reconstruction in terms of its connection between the Atlantic and Arctic oceans, the Paratethys and in West Antarctica. These simulations were run independently (Li et al., 2018) to those detailed in Section 3.2.2 and as a result have a different spin-up procedure. The simulations were continuations of older palaeoclimate simulations (themselves thousands of years long) that originally were initialised with a pre-industrial ocean, with ocean variables extrapolated to fill gaps whenever the palaeogeography was changed. These latest continuations of the simulations were run until the volume integrated ocean temperature was nearly stable (<0.1 °C drift over 1,000 years) with negligible top of the atmosphere energy imbalance. Given the length of these simulations, the specific initial conditions are expected to have little effect on the final climate, assuming that there is not bistability in the model (a condition which we are unaware of ever being found in HadCM3BL). Due to the long simulation times, only one palaeogeography is used, but there are variations in the AIS (either ice free or full AIS), pCO_2 level (either 840 or 560 ppmv) and idealised changes in the Drake Passage (either open or closed). 100 year climatologies are taken 1,000 years into the simulation as well as at the end, allowing changes in the mean response due to a more complete spin-up to be assessed. Because these simulations were run independently to the boundary condition ensemble (i.e. with different forcings and a different spin-up procedure), the two ensembles are not directly compared. Although the forcings are qualitatively similar between the ensembles, they are not identical and so should be thought of as independent experiments for each part of the analysis. It is still useful, however, to see how the uncertainty varies between the two ensembles.

Unlike the boundary condition uncertainty, the 'uncertainty' due to an un-equilibrated climate state could be seen as model 'error', with the fully equilibrated model taken as the correct answer that could be achieved if only more time was available. Regardless of how this uncertainty is defined, it is still useful to have an approximate measure of how much a lack of spin-up might affect results.

3.2.4. Analysis and assessment of uncertainty

Analysis of the climate forcing mechanisms (Antarctic ice growth, palaeogeographic change and pCO_2 reduction) compares all pairs of simulations that keep all boundary conditions the same, except for those relating to the forcing being analysed. For example, if analysing the effect of pCO_2 reduction, pairs of simulations that have the same palaeogeography and ice sheet state but different pCO_2 levels will be compared. The Antarctic ice growth forcing refers to the difference between either the EAIS or full AIS simulations and the ice-free simulations. Both EAIS and full AIS simulations were counted as 'glaciated', given the uncertainty in the state of the ice sheet present after the EOT (Bohaty et al., 2012). Finally, the palaeogeographic change forcing is taken as the difference between any Stage and the Stage immediately previous, i.e. Rupelian-Priabonian or Chattian-Rupelian. The Chattian and Priabonian are not differenced as this would constitute an unrealistically large jump in palaeogeography.

It should be noted that in the real Earth system, the growth of the AIS is actually a response to a forcing, and not a forcing in its own right. However, the presence of the ice would likely have a large impact on the Earth's climate that is important to understand when interpreting proxy records (i.e. it is a major feedback mechanism; Goldner et al., 2014). The GCM used here has no interactive ice sheet module, meaning the ice sheet must be prescribed and so in model terms Antarctic ice growth acts like a forcing. It is worth bearing in mind the distinction between model and true Earth system forcing when interpreting these results and those of similar studies (Goldner et al., 2014; Kennedy et al., 2015).

The boundary conditions used in any model simulation will always contain some uncertainty. For example, the palaeogeographies will contain uncertainties primarily relating to proxy reconstructions used in their construction (e.g. dating uncertainty and calibration error). Furthermore, there is also uncertainty in the assumptions driving different plate models used to reconstruct palaeogeographies, such as the reference frame, plate spreading rates and mantle convection rates (Baatsen et al., 2016). Uncertainties in ice sheet volume reconstructions and atmospheric pCO_2 levels will also come about through proxy dating and assumptions in calibration calculations (Bohaty et al., 2012; Pearson et al., 2009).

In the model, each of these potential sets of boundary conditions will have its own realization in climate space, and together all of the potential realised climates can be thought of in statistical terms as the 'population'. Assuming the climate predicted by the model is reasonably linear in response to each of the changes in boundary conditions, all of these idealised simulations making

up the population should be expected to fall on a normal distribution, i.e. holding with central limit theorem. In reality, it is not practical to model every single possible combination of boundary conditions, so instead a limited number of simulations, n, must act as a representative sample of the population. This sample of model simulations can be used to infer the underlying nature of the population from which they are drawn, in terms of the mean and spread of the normal distribution if the sample size is large enough (typically greater than 30).

The mean response, $\overline{x}$, of all pairs of simulations for each forcing (where n is the number of pairs) can be calculated. An estimate of the uncertainty of this sampled mean value, $\overline{x}$, compared to the true population mean can then be calculated based upon a t-distribution. A t-distribution, which has a similar shape to a normal distribution but is slightly wider, is used here because the number of simulations is less than 30 (Burt et al., 2009). This uncertainty, U_t, is defined as such:

Equation 3.1:

$$U_t = \frac{s}{\sqrt{n}} \times t_{(\alpha/2,\ n\text{-}1)}$$

Where s is the standard deviation of the sample simulation pairs and t is the value that defines the width of the t-distribution and its confidence intervals, taken from a look-up table for the desired confidence level (1-α) with n-1 degrees of freedom (Burt et al., 2009). Throughout this work, we use ± 95 % confidence intervals as standard.

Theoretically, this kind of analysis could be done for many parameters or combination of parameters in the model to better describe the model climate space. However, it is important to consider when the assumptions made in this analysis do not hold. A key assumption is the linearity of the climate response to the boundary condition uncertainty, which would ensure the theoretical climate space is normally distributed. This may not be the case for aspects of the model where there are tipping points and different modal states (von der Heydt et al., 2016; Lucarini & Bódai, 2017). If, for example, deep water formation has an 'off' and an 'on' state in a specific ocean basin, the potential climate space could be expected to be bimodal, with potentially non-linear transitions between the states. In the case of a bimodal or multimodal climate space, the uncertainty range provided by this analysis will likely be an underestimation, and the concept of $\overline{x}$ will not be valid as the true population should be described in terms of modal, not mean, states. In the case of variables that are particularly non-linear, it could be more appropriate to describe the uncertainty in terms of the range in the model responses. This produces a much larger uncertainty margin but makes no assumptions about the linearity of the response.

Although in certain cases (such as deep-water formation) it seems likely that the climate response is non-linear, because we only have a limited sample size available, it is not possible to definitively state whether the climate state is linear with a normally distributed response to the various perturbations or not. It is important to bear in mind the assumptions behind the methods used and where potential non-linearities could be causing an underestimation of the uncertainty. Additionally, given that only three boundary condition parameters are partially sampled, this uncertainty analysis is by no means exhaustive. For example, the uncertainty due to differences in the palaeogeographic boundary conditions could be found to be much greater if simulations with random variation around the reconstructions used here, or with entirely different palaeogeographic reconstructions (Baatsen et al., 2016), were also carried out. The potential impacts of non-linearity on this analysis are discussed further in Section 3.4.1.

3.3. Results

3.3.1. Boundary condition sensitivity

The effect on mean annual surface air temperature (SAT) of Antarctic ice growth, palaeogeographic change and pCO_2 reduction for the multiple simulations with varying boundary conditions is shown in Figure 3.1. The mean change for the three forcing mechanisms is shown Figures 3.1a, c and e, and the ± 95 % U_t of each mean response shown in Figures 3.1b, d and f.

Figure 3.2 shows a range of climatic variables (in terms of both absolute values from individual simulations and the mean changes for each forcing) for all the simulations used in this study. The climatic variables assessed here are annual mean Drake Passage throughflow (Figures 3.2a, b), annual mean sea surface temperature (SST) in the Southern Ocean (south of 60 °S; Figures 3.2c, d), mean annual precipitation over Antarctic land areas (Figures 3.2e, f) and summer (DJF) mean SAT approximately over the Gamburtsev mountains in Antarctica (Figures 3.2g, h). The absolute values from all simulations for these variables and several others (e.g. global mean SAT) are available for reference in the Appendix 2.

Likewise, Figure 3.3 shows absolute values and mean changes for variables relating to ocean overturning; specifically the maximum depth of the mixed layer in the Southern Ocean (Figures 3.3a, b) and North Atlantic (Figures 3.3c, d), and maximum overturning strength in the Southern (Figures 3.3e, f) and Northern (Figures 3.3g, h) Hemispheres. Unlike the results of Hutchinson et al. (2018), none of the simulations here suggest overturning in the North Pacific. The simulations here generally have lower sea surface salinities and a much shallower mixed layer depth in the Pacific than in the Atlantic, suggesting overturning is absent from this region (figures of North Pacific mixed layer depth and salinity not shown). Given that oceanic overturning may be more susceptible to non-linear behaviour, the range of all responses for these simulations are also shown, as U_t could potentially be underestimating uncertainty.

Antarctic ice growth causes a strong cooling of the SAT over Antarctica due to the imposed change in albedo and topographic height, but generally a low cooling response globally that is often less than the uncertainty (i.e. many regions have grey hatching; Figure 3.1a). Globally, the resultant change in planetary albedo accounts for approximately half of the total temperature change based upon a simple energy budget calculation. The only areas with mean changes greater than ± 1 °C are in the Southern Ocean (where there is warming) and North Atlantic (where there is cooling) that are associated with changes in deep water formation. These same areas, however, have higher

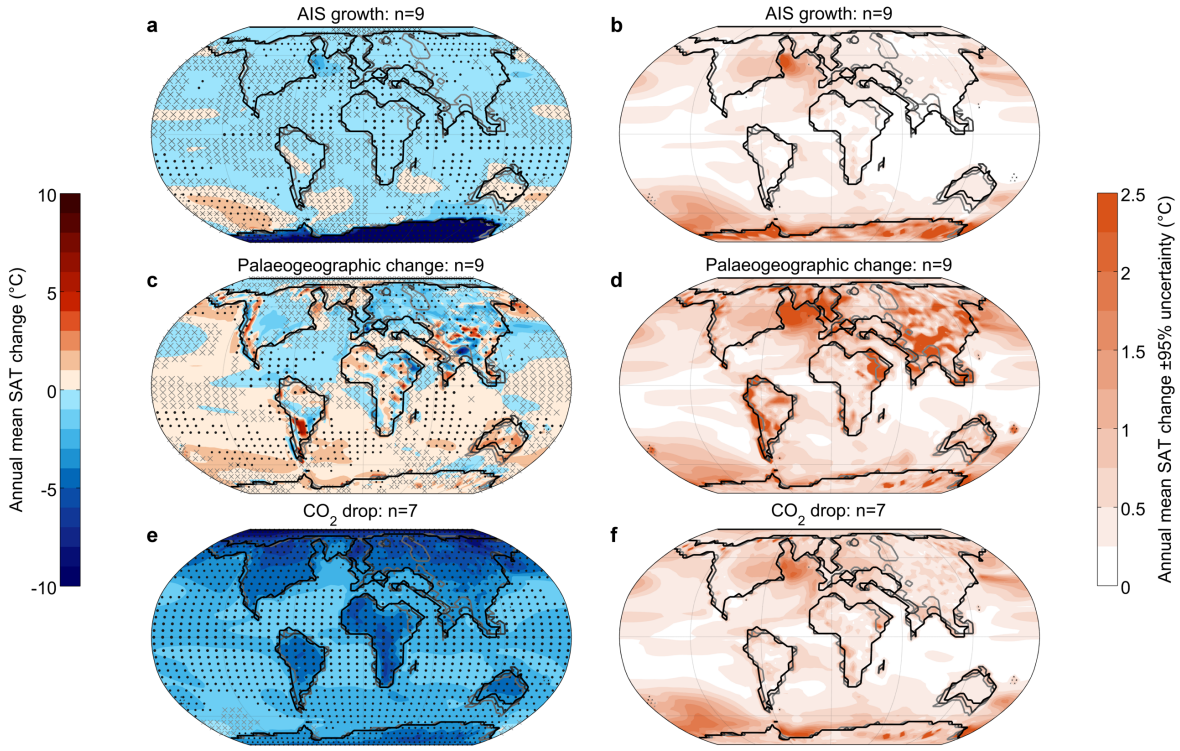

Figure 3.1: The modelled annual mean surface air temperature (SAT) response to various forcings and its ±95 % uncertainty due to boundary condition differences; a) mean response to Antarctic ice growth; b) uncertainty in (a); c) mean response to palaeogeographic change; d) uncertainty in (c); e) mean response to pCO_2 reduction (1,120-560 ppmv); f) uncertainty in (e). Black stippling indicates where all n pairs of simulations agree on the direction of change and grey crosses indicate where the mean change is less than the uncertainty. The land-sea masks are shown for each Stage (Priabonian = palest; Chattian = darkest).

uncertainties of up to ± 2 °C, which could potentially be an underestimation if there is non-linear behaviour in the system here. There is relatively limited agreement within the models on the direction of change, with black stippling over 27 % of the globe. The main regions where there is agreement between the models (i.e. there is stippling) are in the North Atlantic, Africa and in the Indian Ocean, South Pacific and Southern Ocean around Australia.

In terms of the other variables shown in Figures 3.2 and 3.3, Antarctic ice growth causes an increase in the strength of the ACC through the Drake Passage for all pairs of simulations. The average increase is 22.8 ± 3.6 Sv (Figure 3.2b). This increase is related to increased pressure gradients around 60 °S (not shown), that intensify the westerly winds and ACC flow in the Southern Ocean (Kennedy, et al., 2015). The effect on mean Southern Ocean SST varies, with the earlier Stages (Priabonian and Rupelian) showing a warming in response to ice growth and the Chattian showing cooling in response to ice growth (Figure 3.2c), resulting in a mean change close

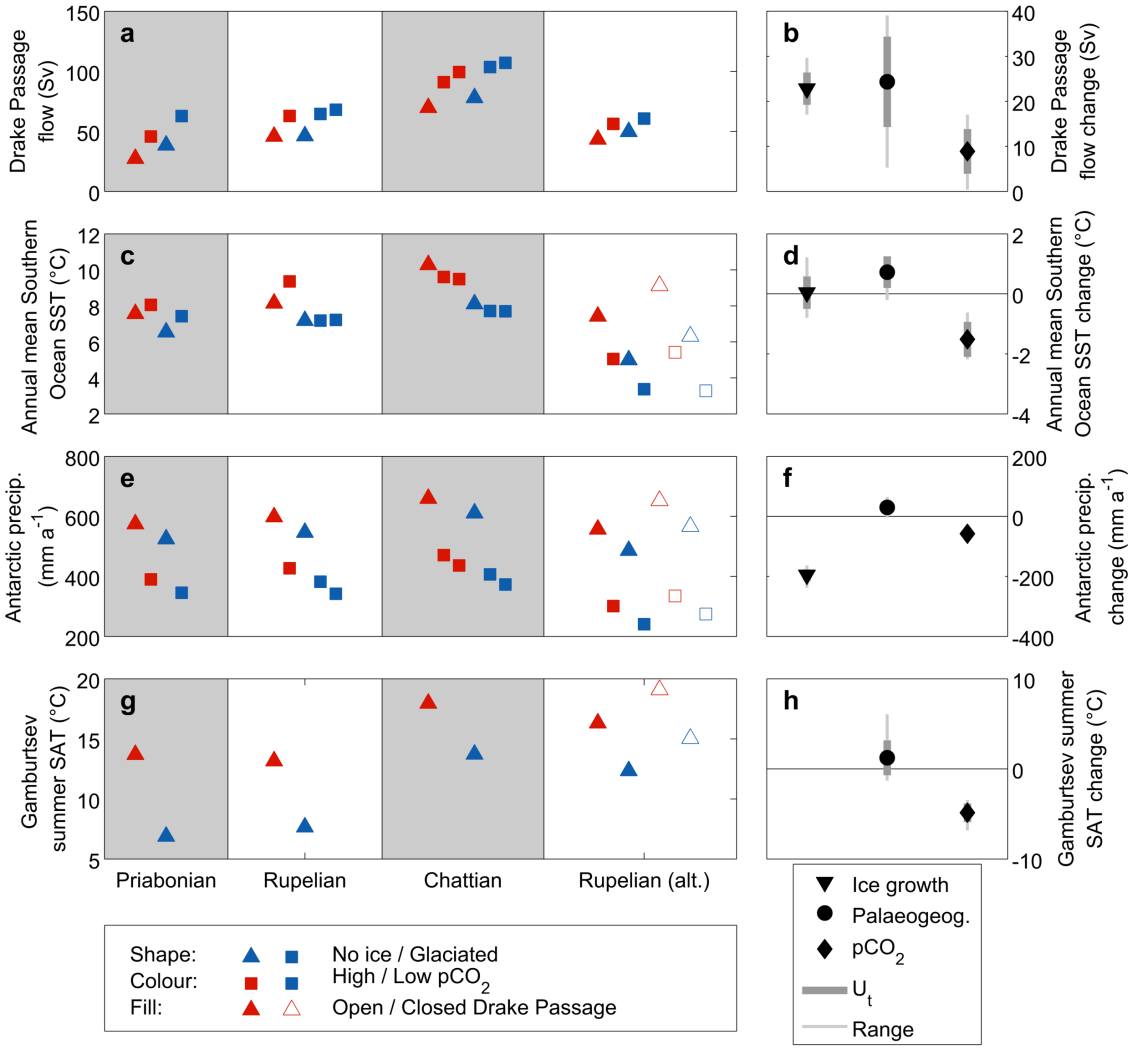

Figure 3.2: Absolute values for individual model simulations and mean changes in response to forcings of four climatic/oceanic variables; a) annual mean Drake Passage throughflow (Sv); b) mean changes in (a) due to forcings; c) annual mean Southern Ocean SST (°C); d) mean changes in (c) due to forcings; e) Annual Antarctic precipitation (mm a-1); f) mean changes in (e) due to forcings; g) summer mean SAT over the Gamburtsev mountains; h) mean changes in (g) due to forcings. The Priabonian, Rupelian and Chattian columns show simulations from the boundary condition ensemble; the Rupelian (alt.) column shows simulations from the spin-up ensemble. The mean changes in (b), (d), (f) and (h) are only for the boundary condition ensemble. Shape, colour and fill of markers in (a), (c), (e) and (g) detail the model simulation, while grey error bars in (b), (d), (f) and (h) highlight ±95 % U_t and the range in responses to forcings. The absolute summer SAT over the Gamburtsev mountains (which are highlighted in Supplementary Figure 1) is only shown for ice free simulations.

to zero (Figure 3.2d). Precipitation decreases significantly over Antarctica with ice growth, due to reduced transfer of moisture over the continent from its increase in topographic height and cooling.

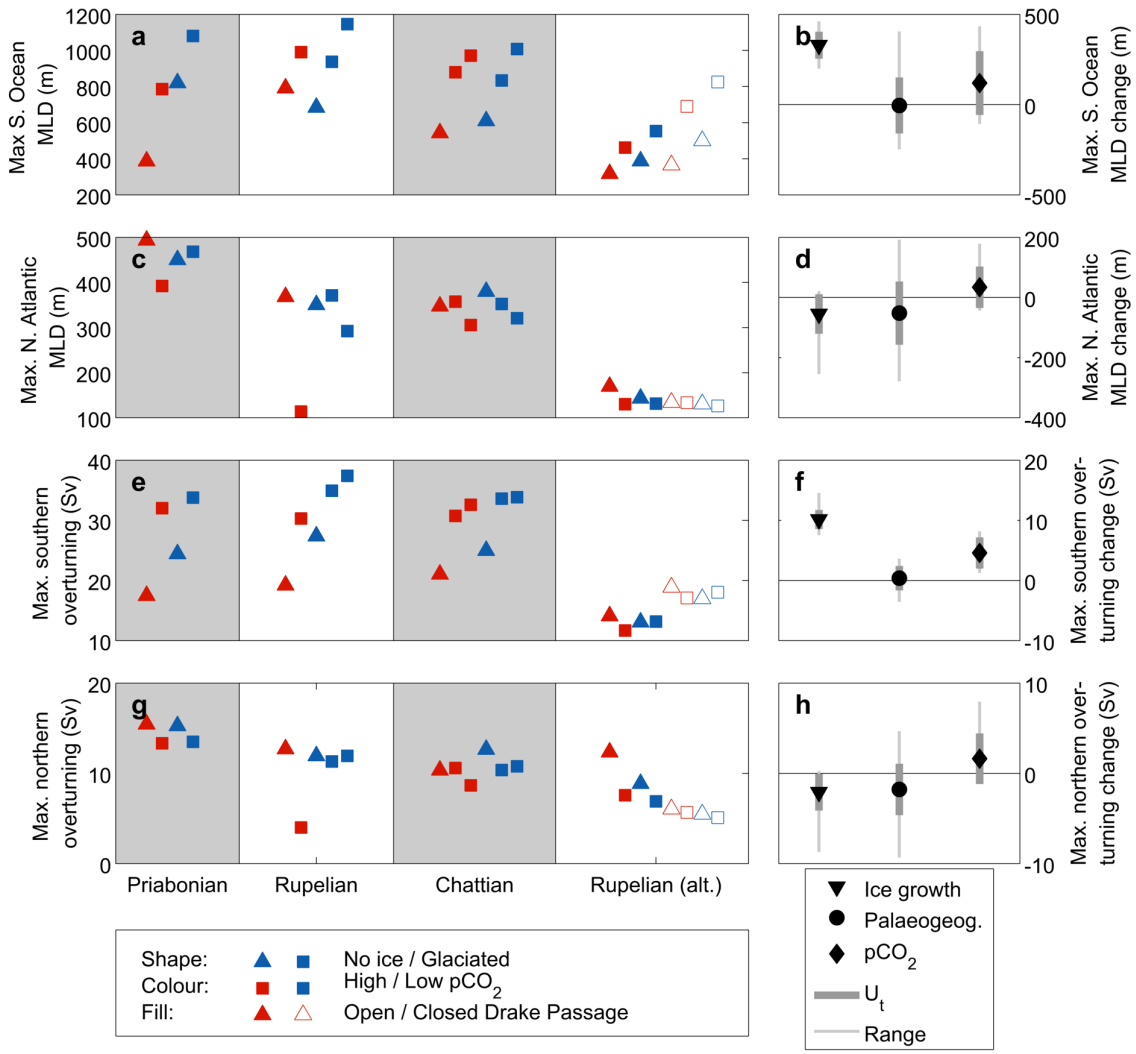

Figure 3.3: As Figure 2 for oceanic overturning variables; a, b) maximum annual mean mixed layer depth (MLD) in the Southern Ocean (m); c, d) maximum annual mean MLD in the North Atlantic (m); e, f) maximum Southern Hemisphere overturning (Sv); g, h) maximum Northern Hemisphere overturning (Sv).

The effect of ice growth on overturning is pronounced in the Southern Hemisphere, with both maximum Southern Ocean mixed layer depth (MLD) and overturning strength increasing, even when considering the larger uncertainty from the range (Figures 3.3b and 3.3f respectively). This is likely due to the resulting heat loss from the presence of the ice sheet demanding greater meridional heat transport, with increased temperature and pressure gradients in the region also resulting in strengthened westerly winds, more vigorous ocean circulation and colder waters at the Antarctic margin contributing to more intense deep water formation. Changes in the Northern Hemisphere MLD and overturning are more varied, with U_t and ranges that cover zero change (Figures 3.3d, h).

Palaeogeographic changes have a hemispheric mean annual SAT response with greater uncertainty than the Antarctic ice growth response (Figure 3.1c, d). Generally, palaeogeographic changes result in an intensification of Southern Ocean circulation (by 24.3 ± 10.0 Sv; Figure 3.2b) and a warming of the Southern Hemisphere (in the Southern Ocean by 0.72 ± 0.53 °C; Figure 3.2d) at the expense of cooling in the Northern Hemisphere, potentially due to a different mode of ocean circulation. Once again, there is relatively limited agreement between the models in the mean SAT response, with stippling over 28 % of the globe. All simulation pairs agree on this oceanic warming in the Southern Hemisphere over mid-latitudes as well as some cooling in the Caribbean and North Atlantic. Over land, patterns of change are more varied and highly dependent on changes in palaeoelevation, which can change a lot between reconstructions where there is horizontal movement of mountain ranges and coastlines. The Rocky Mountains for example show a temperature change dipole running north-south due to the westward movement of the mountain range with successive Stages. There is some agreement on cooling over central Asia and warming over Australia as it moves equatorward. Uncertainties in the modelled temperatures are generally up to ± 1.5 °C, with some terrestrial regions and areas of deep-water formation well exceeding ± 2.5 °C. There is a subtle increase in precipitation over Antarctica (Figure 3.2f) and mean summer SAT over the Gamburtsev mountains is greatest for the Chattian, while the Priabonian and Rupelian are more similar (Figure 3.2g). This is mainly due to elevation changes between the Stages, as can be seen in Supplementary Figure 3.1.

None of the ocean overturning metrics in Figure 3.3 shows a coherent response to palaeogeographic change, with the U_t estimates and range in responses being very large. The largest North Atlantic MLD and Northern Hemisphere overturning values are generally found for the Priabonian simulations (Figure 3.3c, g), with the Rupelian and Chattian simulations being more similar. The Southern Ocean MLD and overturning are similar for all three Stages, with no significant change in response to the forcing. The high pCO_2, glaciated Rupelian simulation shows a near-complete shutdown of North Atlantic deep-water formation, suggesting potential non-linearity in the system here. The reasons behind the lack of deep-water formation for this specific simulation are not fully understood.

Finally, pCO_2 reduction has a global cooling effect. Generally, it is greater over land and shows polar amplification, particularly in the Northern Hemisphere (Figure 3.1e). This is largely associated with increased sea ice coverage in the Northern Hemisphere with reduced pCO_2, which reflects more shortwave radiation across the region (figure not shown). Model agreement is generally good, with stippling over 95 % of the globe. The only regions where the model simulation pairs diverge in their direction of response are deep water formation regions or areas of major

ocean currents at high latitudes, namely the North Atlantic, Weddell Sea, Ross Sea/South Pacific and Kuroshio Current region. These areas also have an elevated uncertainty of ± 2 °C, compared to other regions that are generally less than ± 1 °C (Figure 1f). The Ross Sea is the only area where the modelled change is less than the uncertainty (i.e. it is hatched), once again showing this region is highly sensitive. It is possible that this variability is due to the averaging period over which the climate is calculated, as deep-water formation areas can show multi-decadal variability even in fully equilibrated simulations (Armstrong, et al., 2017).

The other climatic variables suggest declining pCO2 has a small effect of increasing ACC flow through the Drake Passage (by 8.8 ± 5.0 Sv; Figure 3.2b). Predictably, it causes a cooling of the mean Southern Ocean SST and of the Gamburtsev summer SAT, by 1.5 ± 0.6 and 4.9 ± 1.0 °C respectively (Figures 3.2d, h), and causes a slight decrease in Antarctic precipitation (Figure 3.2f). In the ocean, a pCO_2 reduction modestly increases Southern Hemisphere overturning (Figure 3.3f), while MLD in both hemispheres and Northern Hemisphere overturning are more variable with large U_t and ranges.

Supplementary Figure 3.2 shows the mean SAT response for each individual model pairing averaged in Figure 3.1, allowing deeper analysis of the results described here. Under the Antarctic ice growth forcing, the Chattian shows the least Southern Ocean warming, while the Priabonian and Rupelian simulation pairs at 1,120 ppmv pCO_2 show greater Southern Ocean warming. For the palaeogeographic change forcing, there is less consistency as to where some simulations warm and others cool in the same areas and by how much. Under the pCO_2 forcing, the Chattian simulations are the only ones not to show any areas of warming; however, the Priabonian and Rupelian simulations show pockets of warming in different areas where major ocean currents are or deep-water formation occurs.

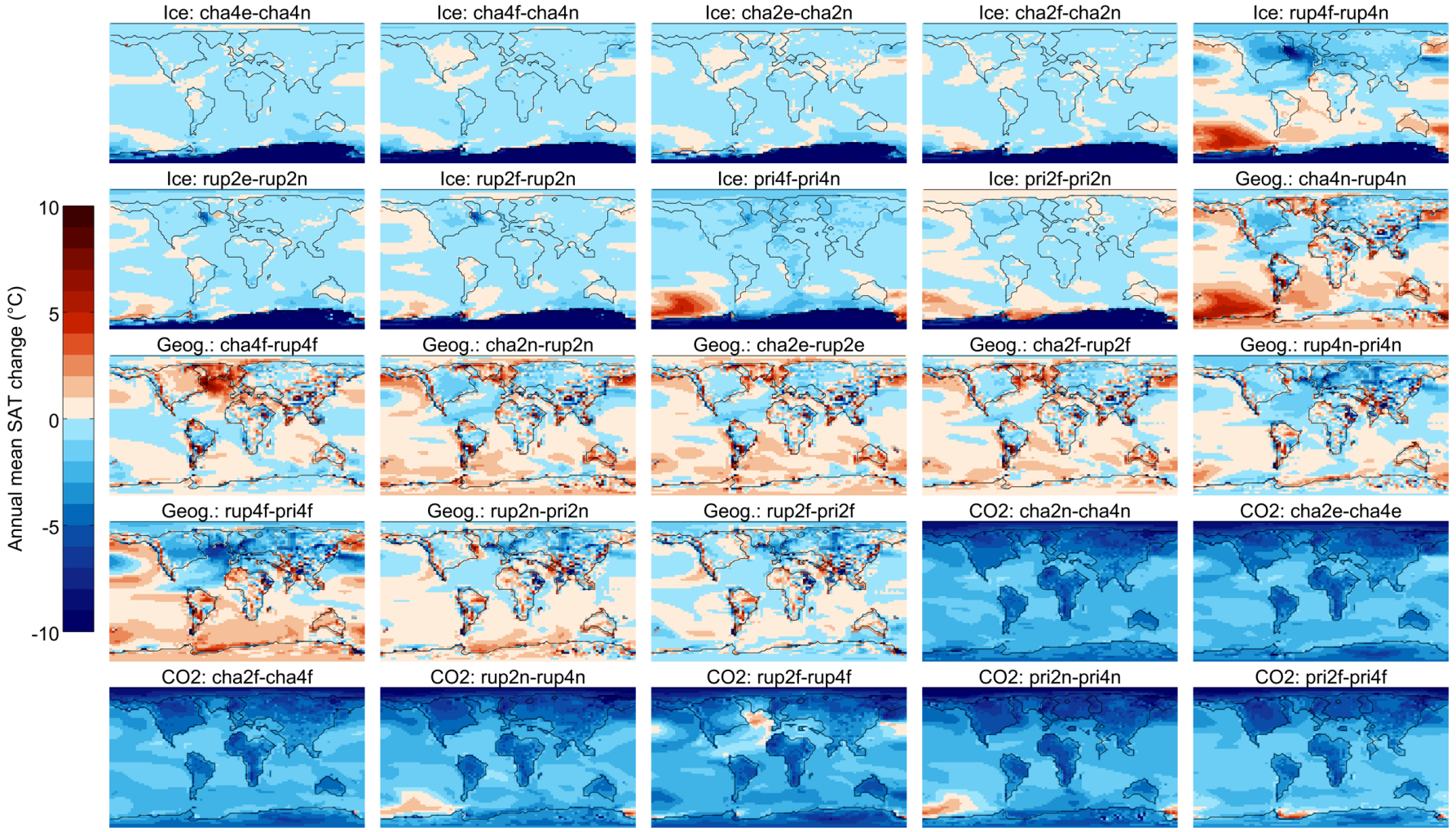

Supplementary Figure 3.2: Mean annual SAT response for each model simulation pair used in Figure 3.1. The figure titles show the forcing mechanism (ice, geog. and CO2) and the names of the simulations used in the differencing: the first 3 letters refer to the Stage (pri, rup or cha), the number refers to the pCO_2 level (x pre-industrial levels) and the final letter refers to the AIS state (n = no ice, e = EAIS and f = full AIS).

3.3.2. Spin-up uncertainty

One possible reason for the differences between individual simulation pairs shown in Supplementary Figure 3.2 could be how close the simulations are to reaching equilibrium, requiring further investigation into the effect of spin-up. Certain combinations of boundary conditions could coincidentally be initialised in greater balance between the surface and deep oceans, having further implications for deep water formation and the spatial patterns of SAT. The effect of spin-up on the modelled mean annual SAT response to Antarctic ice growth, opening of the Drake Passage and pCO_2 reduction is shown in Figure 3.4. The increasing prevalence of stippling for all forcings at the end of the spin-up (Figures 3.4b, d, f), shows model ensemble agreement generally improves once the simulations are fully spun-up. Although these simulations are independent from those in Figure 3.1 and Supplementary Figure 3.2, it is possible that the boundary condition ensemble simulations could also converge with increased spin-up. Besides improved model agreement with increased spin-up, there are also important implications for the spatial patterns of SAT change for some forcings.

The Antarctic ice growth simulation pairs at 1,000 years (Figure 3.4a) have a similar spatial response to the boundary condition ensemble (Figure 3.1a) and the results of Kennedy et al. (2015), both of which have qualitatively the same forcing. However, by the end of the spin-up, the area of 1-3 °C warming over the South Pacific sector of the Southern Ocean ceases to exist, instead showing 1-3 °C of cooling, with good model agreement (Figure 3.4b). This warming mid-way through the spin-up could be due to a larger imbalance between the surface and deep ocean at this point in the simulation, compared to the equilibrium state. Early in the spin-up, there are major differences in the deep water formation between the ice-free and the glaciated simulations (similar to that described in Kennedy et al., 2015), however the overturning converges later in the spin-up (figure not shown) causing the change in response to glaciation shown in Figure 3.4. Additionally, this suggests that the results described in Kennedy et al. (2015) could be an artefact of insufficient spin-up and that under a complete spin-up, Antarctic ice growth causes surface cooling over most regions due its effect on the global net radiation through increased reflectance of solar radiation (not shown).

In contrast to the reversal of the response to Antarctic ice growth in this region with increasing spin-up, with opening the Drake Passage, increased spin-up causes an amplification of the warming shown in the high latitude South Pacific early in the spin-up. There is 1-2 °C warming at 1,000 years with poor model agreement (Figure 3.4c), increasing to 2-4 °C warming with good model agreement at the end of the spin-up (Figure 3.4d). In this case, there is a zonal redistribution

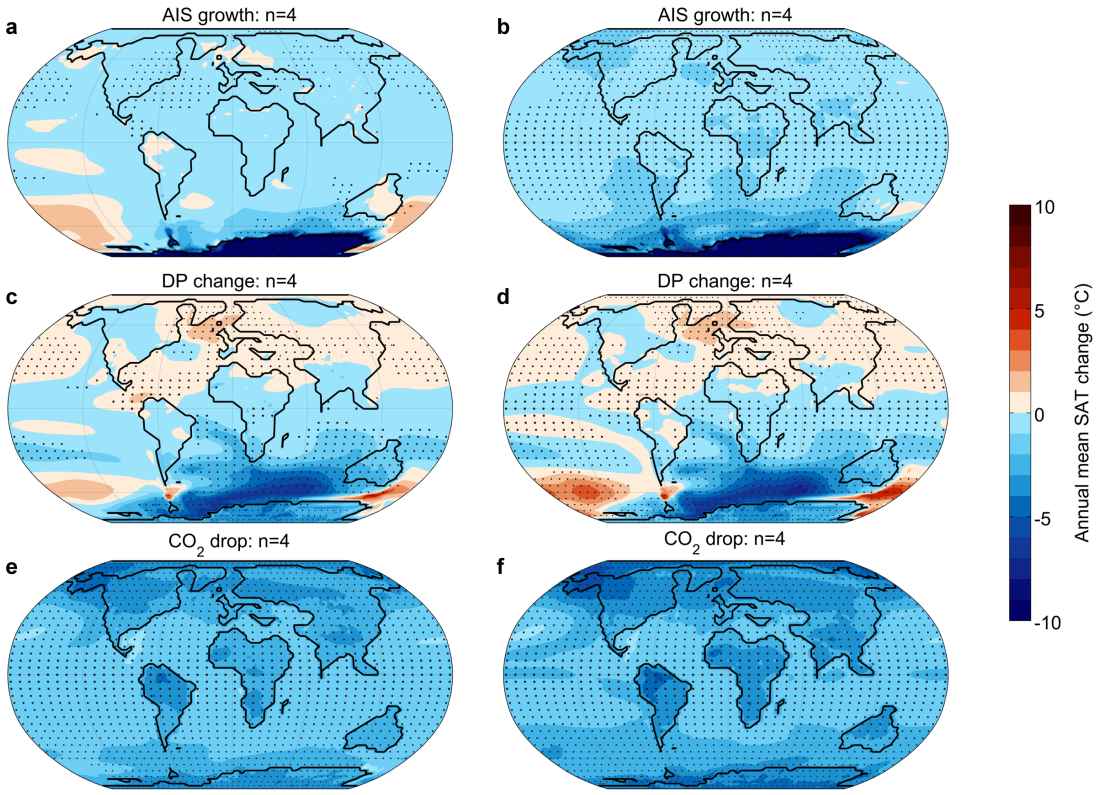

Figure 3.4: The modelled annual mean surface air temperature (SAT) response to forcings mid-way through the spin-up (after 1,000 years) and at the end of the spin-up (once the model is fully equilibrated). Shown are the responses to Antarctic ice growth a) mid-way through and b) at the end of the spin-up; opening of the Drake Passage c) mid-way through and d) at the end of the spin-up; and pCO_2 reduction from 840-560 ppmv e) mid-way through and f) at the end of the spin-up. Black stippling indicates where all n pairs of simulations agree on the direction of change.

of heat in the Southern Ocean when the gateway is opened with a shift in deep water formation region from the Weddell to the Ross Sea, which takes some time to reach its full magnitude. All other regions outside the high Southern Hemisphere show very little change (< 1 °C) between the middle and end of the spin-up, with ensemble agreement improving globally.

The effect of pCO_2 reduction changes the least with increasing spin-up (Figure 3.4e, f) and, like the boundary condition ensemble (Figure 3.1e), already has good model agreement early in the simulation. This is possibly due to the global nature of this forcing requiring less reorganisation of oceanic flow from the initial state. The model agreement in the direction of change improves in the Ross Sea (the only region where there was disagreement early in the spin-up). The global mean SAT cooling in response to the pCO_2 reduction increases from 2.06 °C midway through the spin-up to 2.38 °C at the end of the simulation (global mean SAT values not shown).

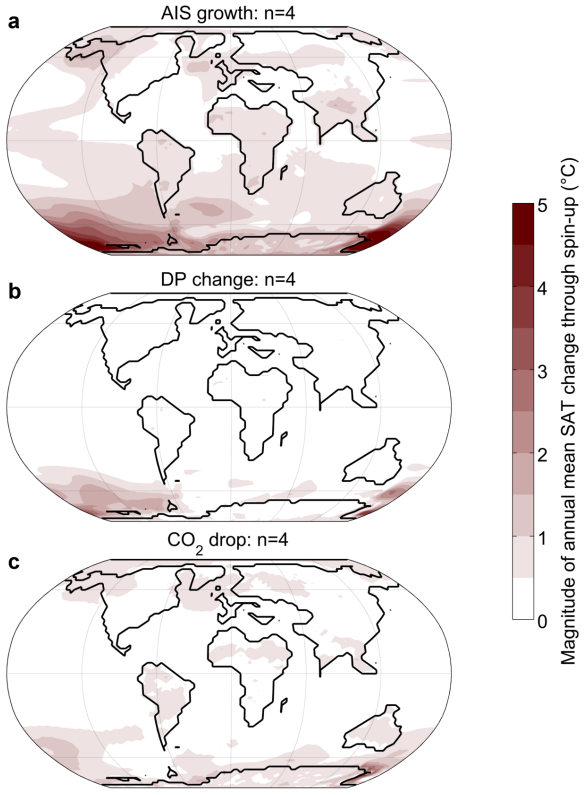

Figure 3.5: The magnitude of mean annual SAT change between the middle and end of the spin-up for the three forcings shown in Figure 4.

For all forcings, outside of deep-water formation regions, areas where there is model agreement in the mean SAT early in the spin-up tend to persist once fully equilibrated. However, in deep water formation regions it remains challenging to generalise how the model response changes with increased spin-up, with different responses showing stability, intensification and reversal depending on the region and forcing. This again highlights the potential non-linear nature of the behaviour of the model in these regions. The magnitude of changes between the mid- and end-points of the spin-up for each of these forcings are shown in Figure 3.5, highlighting that the uncertainty due to spin-up is greatest for the Antarctic ice growth forcing, least for the pCO_2 reduction and most localised for the Drake Passage opening. Like the boundary condition uncertainty plots shown in Figure 3.1, the areas with the greatest spin-up uncertainty also tend to be found at higher latitudes.

The 'Rupelian (alt.)' columns of Figures 3.2 and 3.3 show the absolute values of the climate variables for these simulations once they are fully spun-up. These simulations have similar absolute Drake Passage throughflow values compared to the Priabonian and Rupelian simulations from the boundary condition ensemble (Figure 3.2a). The mean responses to Antarctic ice growth and

pCO_2 reduction are slightly lower than the boundary condition ensemble, causing an increase in flow of 11.9 and 5.4 Sv respectively (mean change from spin-up ensemble not shown). Absolute annual mean Southern Ocean SSTs (Figure 3.2c) are generally lower for these simulations than those in the boundary condition ensemble due to having reduced Southern Ocean overturning, differences in the palaeogeographic reconstructions (with the Robertsons reconstruction having more ocean area at higher latitude) and due to being better equilibrated (with the boundary condition ensemble simulations generally showing cooling trends at the end of their spin-up periods; not shown). Also, due to being closer to equilibrium, there is a slightly stronger cooling in this ensemble, of 2.7 and 2.3 °C in response to Antarctic ice growth and pCO_2 reduction respectively (not shown). Finally, Antarctic precipitation and Gamburtsev summer mean SAT have similar absolute values and responses to the boundary condition ensemble (Figures 3.2e and 3.2g respectively), both decreasing with glaciation and reduction of pCO_2.

Absolute maximum MLD and overturning values are generally less for the fully equilibrated simulations compared to those in the boundary condition ensemble (Figure 3a, c, e, g). Additionally, North Atlantic MLD and overturning in both hemispheres are relatively unaffected by either Antarctic ice growth or pCO_2 reduction. For both forcings, North Atlantic MLD shoals by < 20 m, southern overturning reduces by < 1 Sv and northern overturning reduces by < 2 Sv (mean changes from spin-up ensemble not shown). Southern Ocean MLD shows the greatest changes in response to the forcings, deepening by 240 m in response to Antarctic ice growth and 108 m in response to pCO_2 reduction (not shown). For certain model simulations, the MLD changes significantly with increased spin-up, for example in the ice free setups it takes some time to deepen in the Ross Sea (i.e. for overturning to increase) and to converge with the equivalent glaciated simulation (figure not shown). A similar increase in MLD is found for the ice free simulations in the boundary condition ensemble that exhibit deep-water formation in the Ross Sea (figure not shown). Although the two ensembles used here were run independently with different spin-up procedures and are not directly comparable, it is possible that some of the spread in responses for these variables in the boundary condition ensemble will reduce with increased spin-up as the simulations approach steadier equilibrium states.

Similar to Figures 3.1b, d and f, the U_t for each of the forcings in the spin-up ensemble can be calculated, shown for the middle and end of the spin-up in Supplementary Figure 3.3. For this ensemble, U_t is generally large as it is calculated based upon a very small sample size of only four simulation pairs for each forcing, which increases the value of t in Equation 3.1. With the exception of the North Atlantic, generally U_t decreases with spin-up for all forcings and in some cases the reduction is significant, suggesting that the lack of spin-up can be a major contributor to

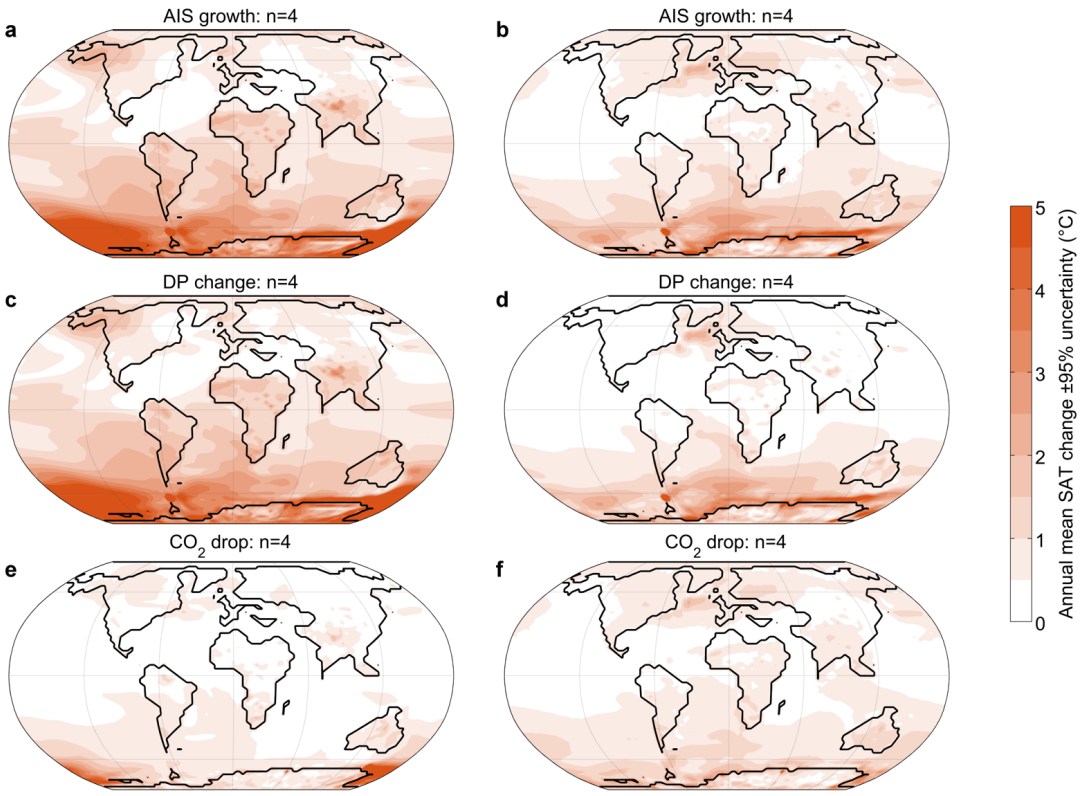

Supplementary Figure 3.3: U_t in the mean annual SAT responses for the Antarctic ice growth, Drake Passage opening and pCO_2 decline forcings 1,000 years into the spin-up (left hand side) and at the end of the spin-up (right hand side).

the magnitude of U_t. However, the fact that a similar spatial pattern persists between the middle and end of the spin-up suggests that not all of the U_t in the responses is due to lack of spin-up and the uncertainties in boundary conditions are still important to consider. Work is currently ongoing to run the boundary condition ensemble simulations further to properly quantify how much of the U_t in each response in Figure 3.1 is due to the lack of spin-up.

3.4. Discussion

3.4.1. Generalising spatial patterns of model uncertainty (U_t)

Although the forcings assessed here in both simulation ensembles are very different in terms of their regional vs. global extent and how they impact on the climate system, they have similar characteristics in their spatial patterns of SAT U_t. The exact magnitude of the U_t depends on the forcing, how close the model is to equilibrium and the ensemble size, but these generalised spatial patterns appear robust for the changes typical of the EOT. Low and mid-latitude oceans are the most consistent regions with low U_t, typically < 1 °C (i.e. we have higher confidence in modelled results in these regions). Most continental regions have a moderate degree of U_t, typically 1-2 °C (i.e. we have medium confidence in modelled results in these regions). Finally, high latitude oceans, particularly deep water formation regions, and mountainous regions are the most sensitive with high U_t, typically > 2 °C (i.e. we have low confidence in modelled results in these regions).

These high latitude ocean regions are the most uncertain as they generally have high variability (e.g. on inter-annual, decadal and longer timescales) and are sensitive to small differences in the forcings due to multiple feedback mechanisms. In the case of the Ross Sea and South Pacific sector of the Southern Ocean, subtle changes in ocean gateways of only one model grid cell can significantly alter the flow of the ACC and the subsequent mixing between Indian and Pacific Ocean basins in the Southern Ocean (Kennedy, et al., 2015). The resulting changes in salinity can influence the strength of deep-water formation in the region which then has further impacts on oceanic heat transfer, particularly if model spin-up is short and it is further from equilibrium. Finally, sea ice feedbacks with the atmosphere can amplify the changes so the resulting U_t is large. Likewise, changes in ice sheet state can affect the zonal winds over the Southern Ocean and pCO_2 reduction can affect the heat transfer, interacting further with this network of feedbacks. In the Northern Hemisphere, although there are no differences in terms of ice sheets, differences in the runoff basins in each paleogeography may be having an effect on the salinity of the North Atlantic and subsequently affecting the surface density and deep water formation. It is also important to note that the Getech reconstructions have an isolated Arctic Ocean, whereas the Robertsons Rupelian reconstruction has a connection the North Atlantic and the Arctic (see Supplementary Figure 3.1). This results in a much lower salinity and reduced overturning (shown in Figure 3.3) in the North Atlantic in the simulations with the Robertsons reconstruction.

Because of the multiple processes and feedbacks involved in deep water formation, this aspect of the Earth system response is likely to be particularly non-linear and could be bistable (Baatsen et

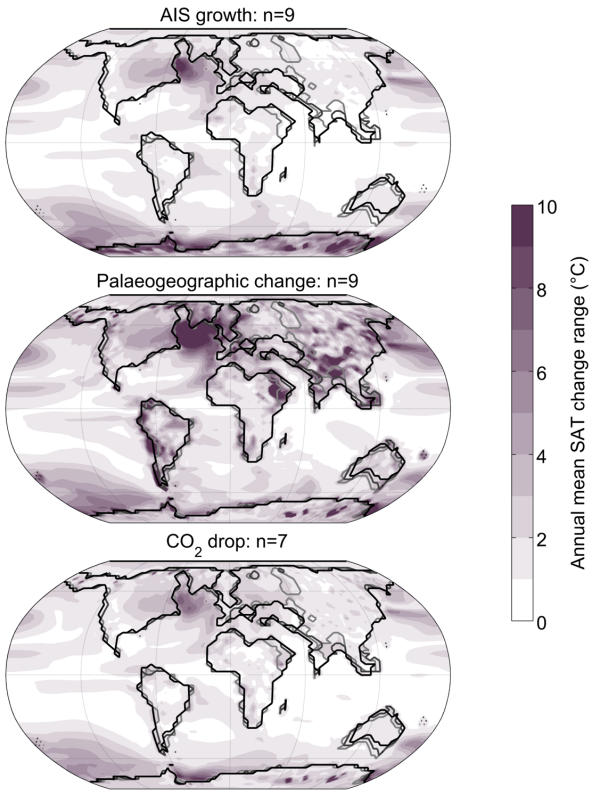

Supplementary Figure 3.4: The range in responses of individual model simulation pairs for each of the three forcings in Figure 3.1. By visualizing the spread of simulation responses using the range rather than U_t, no assumptions are made about the linearity of the climate response.

al., 2018b). In that regard, the assumptions behind the *t*-distribution method used here may be invalid for variables directly affected by deep water formation. It is important to consider the evidence for and implications of non-linearity. If one ocean state can be definitively ruled out by other evidence (i.e. if there was or was not deep-water formation without doubt), then all simulations that exhibit the incorrect state should be excluded from the analysis. The remaining simulations (showing the correct state) however could be expected to behave linearly, and so the methods used here could be appropriate for that selective sub-sample.

If there is no strong evidence to confirm if either one state or another is correct and no simulations can be ruled out, then true quantification of the uncertainty would require a different method, and portraying the mean response becomes inappropriate. The method used here would result in an underestimated uncertainty around a mean that is between the two modal states or sub-samples. A possible alternative method is to show the range between the maximum and minimum responses, as shown in Supplementary Figure 3.4 for the annual mean SAT of the boundary condition ensemble. This simplified method makes no assumptions about linearity but produces a

much larger estimation of the uncertainty. It is important to note that the spatial patterns of the magnitude of range match those of U_t, suggesting the generalised regions of low, medium or high confidence discussed above are robust.

No statistical test will be without assumptions which are invalidated in certain circumstances and we argue that the U_t method is still appropriate to use for many variables in many regions. It is not possible to exhaustively validate the individual responses for all variables on the required range of spatial and temporal scales, so it is important to be aware of the potential issues that non-linearity could cause and that the uncertainties reported here may be an underestimation.

Although it may not be possible for all studies to use an ensemble like this to quantify the U_t, consideration should be given to the broad spatial U_t (confidence) patterns. When interpreting model output for deep-time periods it is worth considering how much the model simulations could vary with only minor differences in the boundary conditions or increased spin-up, particularly if there is interest in these highly uncertain regions. In this regard, the results shown in Kennedy et al. (2015; their Figure 3) should not be seen as surprising; the large area of warming in the Southern Ocean identified in that study is shown here to be the artefact of a sensitive region of the model, exacerbated by a lack of spin-up. Although outside the scope of this study it is also worth considering inter-model uncertainty. Different model constructs will have a dissimilar array of model physics, parameterizations and resolutions that can also add further uncertainty, which could compound the uncertainty derived from the model boundary conditions.

Supplementary Table 3.1: Proxy data used in the model-data comparison. For some sites where multiple proxies were averaged or where different studies contributed the absolute values and magnitudes of change, the combined records used in the main text (Figure 3.6) are highlighted in the grey rows. Palaeolocations are given as the nearest model grid cell to the site, with published palaeolocations (where available) and the back-rotated position according to the Getech Group plc. plate model lying within 1 grid cell for all sites.

Site	Description	Palaeo-latitude (± 2.5 °)	Palaeo-longitude (± 3.75 °)	Palaeo-depth (m)	Proxy method	Pre-EOT SST (°C)	Post-EOT SST (°C)	SST change (°C)	Change error (°C)	Pre-EOT time period (Ma)	Pre-EOT time period error (Ma)	Post-EOT time period (Ma)	Post-EOT time period error (Ma)	Reference
ODP 913	Sub-Arctic	70 °N	5.625 °E	0-55	UK'37	18.30	11.50	-6.80	2.60	35.10	0.40	32.90	0.30	Liu et al. (2009) supplementary data
ODP 336	High North Atlantic	60 °N	13.125 °W	0-55	UK'37	20.00	17.90	-2.10	2.00	35.20	0.00	33.30	0.10	Liu et al. (2009) supplementary data
SSQ	St Stephen's Quarry, Alabama	30 °N	80.625 °W		TEX86	30.43	28.30	-2.13		33.95	0.15	33.60	0.10	Wade et al. (2012) supplementary data, table DR4
SSQ	St Stephen's Quarry, Alabama	30 °N	80.625 °W		Mg/Ca	31.15	27.67	-3.48		33.95	0.15	33.60	0.10	Wade et al. (2012) supplementary data, table DR2
SSQ	St Stephen's Quarry, Alabama	30 °N	80.625 °W	0-55	Combined	30.79	27.99	-2.81		33.95	0.15	33.60	0.10	
ODP 925	Ceara Rise	2.5 °N	39.375 °W	0-55	TEX86	28.30	27.80	-0.50	2.30	35.80	0.80	33.40	0.30	Liu et al. (2009) supplementary data
TDP	Tanzania Drilling Project	15 °S	39.375 °E	0-55	TEX86	31.50	29.20	-2.30		33.75		33.65		Pearson et al. (2007) supplementary information, table 2
ODP 1090	Agulhas Ridge	47.5 °S	1.875 °E	0-55	UK'37	23.60	20.00	-3.60	2.50	35.40	1.40	33.40	0.20	Liu et al. (2009) supplementary data
ODP 511	Falklands Plateau	52.5 °S	39.375 °W		UK'37	19.50	11.10	-8.40	2.50	35.20	1.90	33.40	0.30	Liu et al. (2009) supplementary data
ODP 511	Falklands Plateau	52.5 °S	39.375 °W		TEX86	18.40	11.20	-7.20	2.40	35.20	1.90	33.40	0.30	Liu et al. (2009) supplementary data
ODP 511	Falklands Plateau	52.5 °S	39.375 °W	0-55	Combined	18.95	11.15	-7.80	2.50	35.20	1.90	33.40	0.30	
ODP 277	New Zealand	60 °S	174.375 °W		TEX86	25.90	23.80	-2.10	0.80	34.50	0.90	33.50	0.10	Liu et al. (2009) supplementary data
ODP 277	New Zealand	60 °S	174.375 °W		UK'37	25.60	22.40	-3.20	1.30	34.50	0.90	33.50	0.10	Liu et al. (2009) supplementary data
ODP 277	New Zealand	60 °S	174.375 °W	0-55	Combined	25.75	23.10	-2.65	1.30	34.50	0.90	33.50	0.10	
ODP 689	Maud Rise				d18O	11.6 (± 1.8)				34.00	0.10			Petersen & Schrag (2015) table 2
ODP 748	Kerguelen Plateau	60 °S	76.875 °E		d18O	13.6								Bohaty et al. (2012), section 4.1
ODP 748	Kerguelen Plateau	60 °S	76.875 °E		Mg/Ca			-2.6	0.8	34.00		33.20		Bohaty et al. (2012), section 4.2
ODP 748	Kerguelen Plateau	60 °S	76.875 °E	80-550	Combined	13.6	11.0	-2.6	0.8	34.00		33.20		

3.4.2. Comparison to data

In addressing the first research question into the impacts and relative importance of these forcings on global and Antarctic climate at the EOT, it is worthwhile comparing the GCM simulations with proxy records for the period. To this end, all of the model simulation pairs that have gone into the boundary condition uncertainty analysis are compared with SST records from nine locations for the EOT (Pearson et al., 2007; Liu et al., 2009; Bohaty et al., 2012; Wade et al., 2012). In addition to the three main forcings described so far, the combined effect of ice growth and pCO_2 reduction (for which $n = 5$) is also compared to the data. Figure 3.6 plots the pre-EOT proxy SST against the post-EOT proxy SST at each location. Plotting this way shows if the individual model simulations have a general warm or cold bias (a cold bias will shift the point below and left of the proxy data, whereas a warm bias will shift the point above and right of the proxy data), as well as if the forcing produces the correct magnitude of change (which should fall on or close to the solid diagonal line if the magnitude is the same as the proxy records, even if there is a warm or cold bias). If simulations fall above and to the left of the zero change (dotted) line, it suggests they are simulating the wrong direction of change (i.e. warming over the EOT) and are performing particularly poorly.

The proxy records of change across the EOT used here are taken from papers or their supplementary information with uncertainty in the change plotted where available. There are some notable uncertainties in these records. In some cases, multiple proxies have been averaged, for example the St Stephens Quarry record (Wade et al., 2012) is an average of TEX_{86} and Mg/Ca records while the Kerguelen Plateau data uses absolute values from Petersen & Schrag (2015), with the change calculated using Mg/Ca and $\delta^{18}O$ from Bohaty et al. (2012). Additionally, the time definition of pre- and post- EOT varies slightly by site. To account for some uncertainty in the proxy location, the average ocean temperature is taken over a 3 by 3 grid cell area in longitude and latitude, which encompasses both the published palaeolocations and the possible range of locations computed by back rotation of the Getech plate model. Temperature is averaged in the top 55 m of the ocean (the top five ocean layers), except for the Kerguelen Plateau which is taken deeper in the water column (~100-500 m) to account for the deeper habitat of the foraminifera species used (Bohaty et al., 2012). Full details of the sites and proxy data used can be found in Supplementary Table 3.1 and proxy locations are shown in Supplementary Figure 3.1a.

In terms of absolute values, many data locations (e.g. sub-Arctic, high North Atlantic, St Stephen's Quarry, Agulhas Ridge, New Zealand, Kerguelen Plateau) show a cold bias of up to 15-20 °C, particularly with increasing latitude of the sites. The Falklands Plateau is found to be too cold

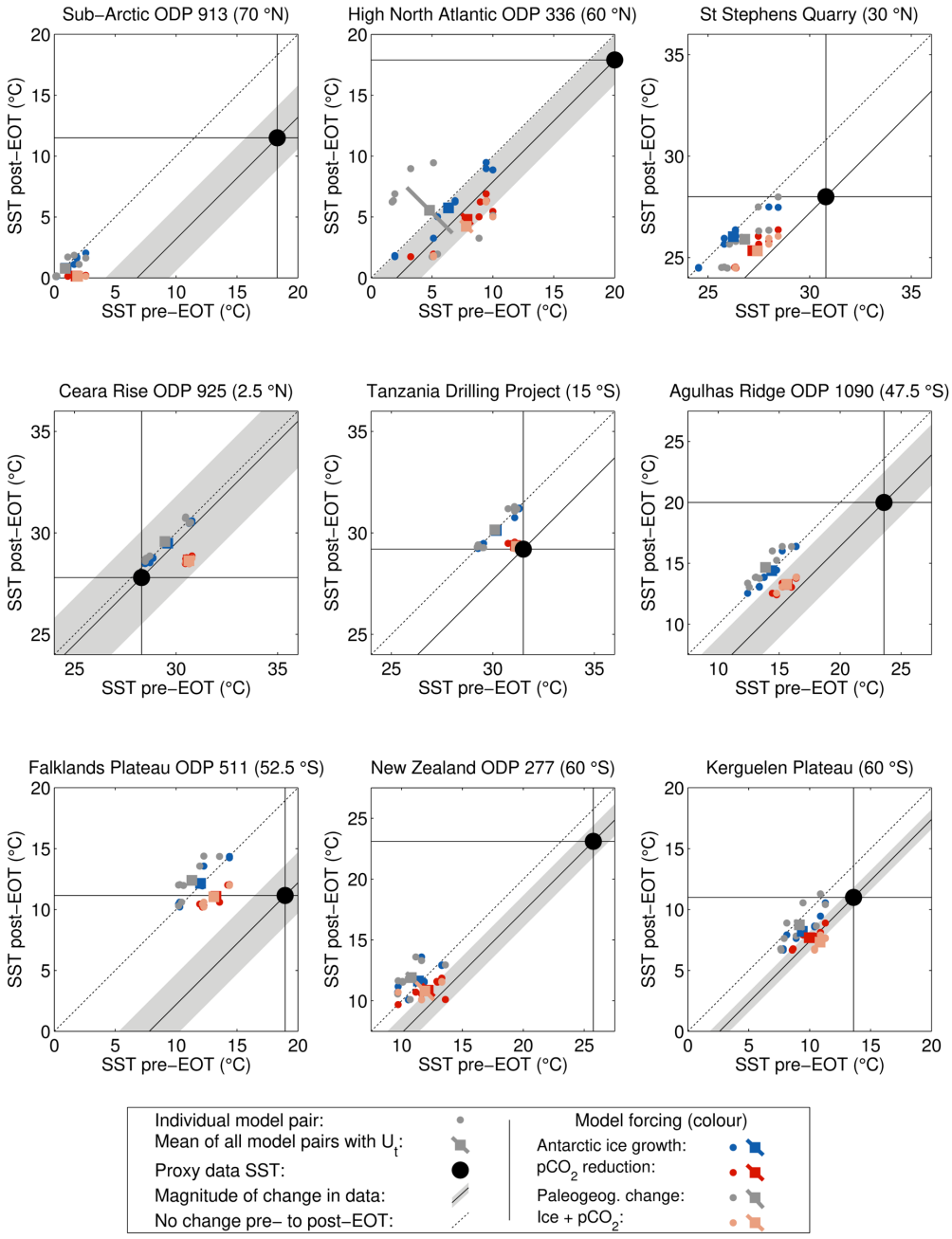

Figure 3.6: Comparison of the modelled SST pre- and post-EOT to proxy data for nine sites (Pearson et al., 2007; Liu et al., 2009; Bohaty et al., 2012; Wade et al., 2012). Individual pairs of model simulations are shown for the Antarctic ice growth, palaeogeographic change, pCO2 reduction and combined ice growth and pCO2 reduction forcings, with the mean for each of these forcings indicated by the squares with error bars of the same respective colors. The grey shading highlights the published uncertainty in the magnitude of change in the proxy data (where available) and the dotted line indicates no change across the EOT. Note: the axes ranges are different from the published figure in Kennedy-Asser et al. (2019).

before the EOT but close to the proxies after the EOT, while the Ceara Rise and Tanzania sites are close to the proxies both before and after the EOT, with Ceara Rise having a slight warm bias

(< 3 °C). The reasonable agreement with the low-latitude Ceara Rise and Tanzania sites highlights that the model is producing a steeper latitudinal SST gradient than is found in the data, with high latitudes being too cold as a result, a common issue in climate models (Huber & Caballero, 2011; Lunt et al., 2012).

In terms of magnitude of change, the model is generally found to be slightly conservative relative to the proxy records. Of the individual forcings tested here, pCO_2 halving is found to be the closest to the proxy records for most sites, only lying outside of the proxy uncertainty for the Falklands Plateau and sub-Arctic sites. The combined forcing of both ice growth and pCO_2 reduction (which could be expected to be the most realistic forcing for the EOT) also does a comparable job to pCO_2 reduction in isolation in terms of explaining the changes. Antarctic ice growth and palaeogeographic change generally result in very small changes (sometimes of opposite sign to the proxies), suggesting these forcings in isolation do a poor job of simulating the observed changes at the EOT; however, it is possible that these responses could change with increased spin-up. The only site at which ice growth and palaeogeographic change are closer to the change suggested by the proxy data is Ceara Rise, however, this site has very high uncertainty in the proxy itself and all forcings lie within the potential error.

In line with the generalised spatial patterns of U_t discussed in Section 3.4.1, the sites with the largest uncertainty in the mean model responses are New Zealand, the high North Atlantic, St Stephen's Quarry and the Kerguelen Plateau, all regions close to where the model has some deep water formation. For all of these sites there is overlap in the uncertainty in the magnitude of proxy change (where available) and the U_t of the mean pCO_2 reduction and combined ice growth and pCO_2 reduction forcings. In contrast, even with the wide U_t margin, palaeogeographic change does not have an effect similar to the proxy records at three of the sites, suggesting this U_t method does not simply increase tolerance so any model forcing can be described as 'good'. Again, however, these responses could change if the model simulations here were further spun-up. The New Zealand site in particular is close to the region that showed a reversal in the temperature anomaly in response to Antarctic ice growth for the spin-up ensemble (Figure 3.4a, b). Assuming a similar process could occur here with the boundary condition ensemble if the simulations were run for longer, it is possible that ice growth forcing could produce a more realistic change relative to the proxy records.

This analysis is reasonably simplistic as it looks only at idealised forcings and as such is not an attempt at a best guess of the actual climate transition that occurred at the EOT. In that regard, it is unsurprising that the modelled SSTs differ from the proxy data. In reality a combination of these forcings (and other processes that are not modelled here) would have been occurring at the EOT.

Missing or incorrectly represented processes must be responsible for at least some of the absolute model discrepancy from the data. It is possible that the pCO_2 could have been higher both before and after the EOT than the 1,120 and 560 ppmv values used here (Pearson et al., 2009; Zhang et al., 2013). This could account for some of the cold bias in the high latitude sites relative to the proxies, however it could not account for over 10 °C of warming without making the Ceara Rise and Tanzania sites much too hot relative to the proxies. Additionally, proxy bias (including issues resolving high temperatures or bias towards summer time conditions at high latitudes; Schouten et al., 2013) debatably could widen the uncertainties beyond the ranges given, while single proxy sites could be biased to localised conditions which are not resolved in the model, making like-for-like comparisons difficult.

Notwithstanding these potential sources of bias in proxy records, it is worth bearing in mind that HadCM3BL is shown to have extremely high seasonality over Southern Hemisphere high latitudes (a seasonal range of 30-60 °C), to the point that it would inhibit AIS growth even under favourable orbits unless pCO_2 is reduced considerably (Gasson et al., 2014). Assuming that this large seasonality in the model is the result of some unknown missing or incorrectly represented processes, it is plausible that similar unknown processes could account for at least part of the model-data discrepancy. Inclusion of such processes that could alter the modelled climate enough to fit the data would also likely have a huge impact on the modelled uncertainty looked at in this study. In that regard, the uncertainty results shown here are far from exhaustive.

3.5. Conclusions

Using two ensembles of fully-coupled GCM simulations, we generalise the Earth's atmospheric and oceanic response to various forcings typical of the EOT. The size of the ensembles used here allow the uncertainty in these responses due to boundary condition uncertainty, U_t, to be assessed using a *t*-distribution. Additionally, long spin-up simulations highlight which regions and forcings are particularly sensitive to a lack of spin-up (and so are less robust in shorter simulations).

For most climatic and oceanic variables, there is found to be significant variability in the impact of each of the forcings due to differences in boundary conditions. The growth of the Antarctic ice sheet causes a mixed SAT response (which is particularly uncertain due to a lack of spin-up), a minor global cooling, an increase in ACC flow through the Drake Passage and an increase in overturning and MLD in the Southern Ocean. Palaeogeographic change also increases ACC flow, with wider Southern Ocean gateways having greater flow through the Drake Passage, associated with a slight hemispheric redistribution of heat, with the ensemble agreeing on the Southern Hemisphere warming slightly particularly over the oceans. There is poor agreement as to how palaeogeographic change will affect ocean overturning in either hemisphere (although with increased spin-up the model agreement could possibly improve). Finally, atmospheric pCO_2 reduction has a clear cooling effect on global SAT, with good model agreement, and it has a modest effect of intensifying ACC flow through the Drake Passage. Of the three forcings, this is the most consistent between model simulations and the least susceptible to change with increased spin-up.

For mean annual SAT, the spatial patterns of U_t have similar characteristics for each forcing from both ensembles. Therefore, although the exact magnitude of U_t varies with the number of simulations used, the nature of the climate forcing and how far the model simulations are away from equilibrium (and will therefore vary for future studies), we can generalise where we have higher, medium and lower confidence in our modelling results. Low to mid-latitude oceans generally show the lowest uncertainties, most continental regions generally have slightly higher uncertainties while high latitude oceans (particularly deep-water formation regions) and mountainous regions have the highest uncertainties. The range in model responses to each forcing (an alternative method for portraying the uncertainty that does not make an assumption about the linearity of the modelled climate response) also shows similar spatial patterns of low-high uncertainty.

The modelled SAT response to various forcings can be profoundly affected by a lack of spin-up. Here, it is shown that the Antarctic ice growth forcing in particular has a reversal in the response in the Southern Ocean. In general, the absolute changes due to a lack of spin-up are of a similar magnitude (or greater) to the uncertainties due to different boundary conditions. However, it is harder to generalise how the model response (particularly in high latitude ocean regions) might change with a more complete spin-up. Again, high latitude oceans are found to be most susceptible to change due to a more complete spin-up, while responses in low to mid-latitude ocean regions where there is agreement early in the spin-up tend to be more stable, with the responses persisting through to the end of the spin-up.

In terms of the relative importance of each of the forcings on climate at the EOT, the boundary condition ensemble of model simulations shows pCO_2 reduction gives the best match to the magnitude of change recorded by proxy records of SST, compared to Antarctic ice growth or paleogeographic change forcings. A combined forcing of Antarctic ice growth and pCO_2 reduction also performs well, albeit with a smaller sample size. However, this analysis is reasonably simplistic as only idealized forcings are assessed and further work needs to be done to improve the match with data, as absolute biases in the temperature are generally found to be very high. It would also be of interest in future work to expand this analysis to other oceanic and terrestrial records (Pound & Salzmann, 2017; Li et al., 2018; Baatsen et al., 2018a).

These uncertainty patterns may be similar for other Cenozoic time periods when the palaeogeography had similar features to those assessed here for the late Eocene and early Oligocene (i.e. similar ocean gateways and continental positions), but this should be tested further. Deeper time periods when the palaeogeography was radically different may or may not behave in a similar way, requiring further study and assessment. The method used here with a medium sized ensemble and the uncertainty calculated with a *t*-distribution is one possible way to do this. If there are particular concerns about the linearity of the modelled climate response, other methods such as the range in responses can also be used to compliment this method. The generalised uncertainty highlighted by these model simulations should be considered when interpreting paleoclimate research when single or very few model simulations are used.

Chapter 4: Changes in the high latitude Southern Hemisphere through the Eocene-Oligocene Transition

4.1. Introduction

The previous chapters in this thesis highlighted that potentially large and uncertain changes could have occurred in the Southern Ocean and the climate of the high latitude Southern Hemisphere across the Eocene-Oligocene Transition (EOT) in response to both expansion of the Antarctic ice sheet (AIS) and reductions in atmospheric pCO_2 (e.g. Figures 2.3 and 3.1-3.4). The extreme HadCM3BL sea surface temperature (SST) response to Antarctic glaciation shown in Chapter 2 (Kennedy et al., 2015; Figure 2.3) is shown to not simply be an artefact of the island definition (Figure 2.11); however, the results of Chapter 3 suggest the response could be exaggerated due to a lack of model spin-up (Figure 3.4). It is important to note that these longer simulations still show small areas of fractional warming (or at least little cooling) in the Southern Ocean (Figure 3.4), indicating the regional SST response is heterogeneous. Additionally, other studies using different climate models also suggest some SST warming in response to Antarctic ice growth (e.g. Goldner et al., 2014; Knorr & Lohmann, 2014), but with markedly different spatial pattern to that shown in Figures 2.3 and 3.4. This calls into question what the true response of the climate in this region was at the EOT.

The Southern Ocean is of global importance for its connection between the other major global oceans. It is important in biogeochemical cycles, in terms of ventilation of atmospheric gases from the deep ocean (e.g. Schmittner & Galbraith, 2008; Waugh et al., 2013; Fyke et al., 2015), as well playing an important role in the thermohaline circulation in the formation of cold bottom waters (e.g. Hay et al., 2005; Marshall & Speer, 2012; Morrison & Hogg, 2012; Katz et al., 2011). Given the global importance of this region, but also its high sensitivity in model simulations, the general motivation of this chapter is to answer the question: how did the high latitude Southern Hemisphere climate change across the Eocene-Oligocene Transition?

While GCMs are useful tools for testing our understanding of the Earth system and forming plausible hypotheses, the uncertainty within them for this region highlighted in the previous chapters shows it is necessary to integrate proxy evidence to build up a more robust picture of what occurred across the EOT. Models are always approximations of what occurred during a past period, whereas the evidence in proxy records is 'real', albeit with many assumptions in the process

of deriving the actual climate signal they represent. The proxy records used in the model-data comparison in Chapter 3 (Figure 3.6) suggest there is too high a latitudinal temperature gradient, with higher latitudes showing a cold bias compared to lower latitude records, however the Southern Ocean was not focussed on in specific depth.

To investigate further what occurred across the EOT in the Southern Ocean, a large proxy database of temperature was compiled for the high latitude Southern Hemisphere, incorporating a multitude of different proxy records in terms of methods, sites and temporal coverage. The purpose of this compilation is somewhat as a review with as much data included as possible. Despite sometimes not being directly comparable, the inclusion of very different kinds of proxy evidence provides both qualitative and quantitative measures against which model simulations can be framed and tested. The quantitative elements of the dataset can also be used to describe general temperature patterns (e.g. in terms of the regional mean or latitudinal gradient), providing simple benchmarks against which the model simulations can be evaluated. Model simulations that perform relatively well can then be used in conjunction with the proxy dataset to start to explain what changes may have occurred in this region across the EOT.

Given that the HadCM3BL simulations from the boundary condition ensemble in Chapter 3 (Section 3.2.2) were shown to be potentially affected by a lack of spin-up in this region, these simulations will not be used in the analysis in this chapter. As a result, all of the HadCM3BL simulations used here were provided by P.J. Valdes (those from the spin-up ensemble; Section 3.2.3). These simulations are compared to results from other climate models (provided by modelling groups at different universities), to explore if the mechanisms and patterns of the temperature response are consistent beyond HadCM3BL.

4.1.1 Research questions

Two specific research questions are addressed in this chapter:

- What are the spatial patterns of temperature change inferred from proxy records for the high latitude Southern Hemisphere before, after and across the EOT?
- Which GCMs and model boundary conditions give the best fit to a range of qualitative and quantitative proxy records of temperature before, after and across the EOT?

A brief overview of the data synthesis follows in Section 4.2. Section 4.3 discusses the spatial patterns of temperature identified in the proxy data synthesis as well as giving a qualitative review of other significant changes in the Earth system. Section 4.4 outlines the methods and results of the model-data comparison. Finally, Sections 4.5 and 4.6 discuss the significance of the results and the potential scope of future research.

4.2. Data synthesis: methods

4.2.1. Spatial vs. temporal variability

A fundamental difference between the proxy records of past climate and the 'equilibrium' climate simulations carried out in this thesis, is how they can be used to reconstruct the temporal or spatial domain of climate. Proxy records, specifically sediment cores, are particularly good for reconstructing the temporal domain, showing changes through long time periods at a particular point in space (e.g. Zachos et al., 2001). By contrast, climate models generally cannot be run for long transient simulations and instead only provide snapshots of a single point in time but offer a complete spatial picture of how different regions compare to one another (e.g. Lunt et al., 2016).

This difference between the methods offers a key opportunity but also some major challenges. It offers the opportunity to use both methods to maximise each of their strengths, using models to build a complete spatial picture with proxies informing how this picture should change through time (Lear & Lunt, 2016). On the other hand, model-data comparisons can be difficult as there are few points in space and time at which the model and data intersect and can be directly compared and there are complications that proxy records might be a representation of a process that is not truly represented in the model (Crucifix, 2012). It is possible to explicitly model some proxy variables (such as oxygen isotopes; e.g. LeGrande et al., 2006), but this was not done here.

Because the research in this thesis has focussed primarily on equilibrium climate modelling, the aim of this data synthesis is to create a dataset that is comparable to the model simulations, i.e. can be used to validate the model in the spatial domain. This necessitates reducing the temporal variability of the proxy data into time slices, which was done for late Eocene absolute conditions (generally 36.4-34.0 Ma), early Oligocene absolute conditions (generally 33.2-32.0 Ma) and relative changes across the EOT (i.e. between the late Eocene and early Oligocene conditions). The definition of the time slices is reasonably crude, however, often dictated by what proxy data is available at a given site. The proxy records used will be on different age models and cover different specific periods in time. This introduces an element of uncertainty; it has been shown that there was variability throughout the EOT in the few million years either side of the Eocene-Oligocene Boundary (e.g. Scher et al. 2014; Galeotti et al. 2016). Time averaging approximately two million years prior to and after the Eocene-Oligocene Boundary will potentially lose this temporal variability (if a long record for a particular location is available) or potentially skew results (if for example a short-term excursion is captured in the record). However, this time

averaging is deemed necessary to make the proxy records of use for the model validation and is important to consider when interpreting the data compilation.

4.2.2. Proxy records used

Many different proxy records for in-situ SST are available. These include quantitative records using stable isotopes and trace metals (e.g. $\delta^{18}O$ and Mg/Ca, Bohaty et al., 2012; clumped isotopes, Δ_{47}, Petersen & Schrag, 2015) and organic biomarkers (e.g. TEX_{86} and $U^{K'}_{37}$; e.g. Liu et al., 2009; Douglas et al., 2014). Quantitative proxies can be used in conjunction with qualitative records, such as nannofossil or dinoflagellate species assemblage and size (e.g .Villa et al., 2013; Houben et al., 2013), to provide further evidence for temperature ranges or relative changes where or when quantitative data might be sparse. Some surface air temperature (SAT) records are also available, such as those derived from organic biomarkers in lignite (Naafs et al., 2017), from clay weathering products (S-index; e.g. Passchier et al., 2013) and from vegetation reconstructions (based on Nearest Living Relative, NLR, e.g. Francis et al., 2009; or the Coexistence Approach, e.g. Pound & Salzmann, 2017). These records may or may not be in-situ, with clay weathering products for example having been exported from terrestrial regions to where they are deposited in ocean sediment cores. These proxies all rely on various assumptions, resulting in uncertainty ranges that can be incorporated into the model-data comparison.

It is important to consider how the various different proxies used respond to the climate system in different ways and, as a result, do not all provide directly comparable records. Some proxies provide continuous quantitative data that can be directly compared to models or other records, e.g. absolute temperature estimates. Other proxies may provide ordinal (qualitative) data; that is, data that can be ranked into an order of greater or lesser magnitude but from which absolute values are not attainable. An example of such data is the abundance of the dinoflagellate species *S. antarctica*, which broadly suggests colder temperatures with higher abundance, while its general presence suggests mean annual SSTs < 10 °C (Zonnefeld et al., 2013). By using different proxies in combination, it may be possible to reduce some uncertainties. For example, if a continuous quantitative record suggests cooling temperatures, but with very large proxy calibration errors, a synchronous increase in *S. antarctica* from low to high abundance at the same site would add extra confidence that such a cooling trend is robust, even if the exact magnitude of cooling remains uncertain.

In addition to these temperature records, various proxy indicators of glaciation can also be valuable for the model evaluation. They not only provide some information about the terrestrial

climate, but they also can be used to constrain which boundary conditions in the model are most realistic for a specific time period in terms of the prescribed AIS size.

Ice rafted debris (IRD) in offshore sediments is a clear marker of glaciation (Breza & Wise, 1992). These are deposits of sand, gravel or larger stones in offshore sediments that could not have been transported by ocean currents or wind. Although IRD indicates the presence of marine calving ice, it does not provide evidence of how extensive glaciation might have been (Ehrmann & Mackensen, 1992). It also does not provide a precise location for the ice, as it is possible that ice bergs could travel long distances in the Southern Ocean; however, it can be possible to try to pinpoint its origin based upon the geology of the IRD (e.g. Ehrmann & Mackensen, 1992). It is also important to note that a lack of IRD does not exclude marine calving ice as it is possible that the direction of flow of the ice bergs might change or they could be melting at a different rate. However, if there is presence of IRD, there must be at least some coastal regions where there is net annual accumulation of snow, which can be checked against model simulations.

Erosion products, such as deposits of physically weathered clay minerals (e.g. illite and chlorite; Ehrmann & Mackensen, 1992), large deposits of eroded material (e.g. Huang et al., 2014) or large pulses or perturbations in neodymium in sediment cores (εNd; Scher et al., 2011), can be used to infer glaciation also. These can give a qualitative indication of the extent of glaciation, assuming that more extensive glaciation produces more weathering products and erosion deposits (shown in the thickness of sediment layers in seismic profiles for example; Huang et al., 2014). However, other factors could also be important for the supply rate of weathered material, such as the speed of ice flow (dictated by the ice temperature and availability of water at the bed amongst other factors; e.g. Harbor et al., 1988; Doyle et al., 2014; Koppes et al., 2015) and the availability of easily erodible regolith on top of the bedrock (e.g. Clark & Pollard, 1998; Piotrowski et al., 2004).

Finally, $\delta^{18}O$ can also be used to quantitatively constrain the ice volume (Shackleton, 1967). By understanding how much temperature at a particular location changed (using other independent proxies such as Mg/Ca), it is possible to calculate the change in $\delta^{18}O$ of global seawater (Lear et al., 2008; Bohaty et al., 2012). With some assumptions about the location of this ice (e.g. if it was only over Antarctica or if some also present in the Northern Hemisphere) and its isotopic composition, it is possible to calculate the volume of ice in the Antarctic ice sheet (e.g. DeConto et al., 2008). This usually provides a range of possible ice volumes, such as those calculated by Bohaty et al. (2012).

4.2.3. Combining records

Values and data are compiled from a range of sources within mostly published material (with the exception of an unpublished record for South Australia, provided by V. Lauretano, University of Bristol). Ideally, the data is available in supplementary material for the papers. In other cases, mean values might be quoted in tables or in the text of papers; however, it can be unclear over what time period these means are taken or how uncertainty values are calculated. Finally, on occasion some values are inferred from figures within papers (e.g. time series or scatter plots). This is not an accurate way of obtaining the data and so is avoided where possible; however, in some cases this might provide some of the only data available and so still warrants inclusion (e.g. the East Tasman Plateau record from Douglas et al., 2014).

Uncertainty in the proxy data records could arise due to calibration errors, proxy biases or could be due to temporal variability in the record (particularly the case here where temporal means are taken for each time slice). These various sources of uncertainty make rigorously defining it and how it should be quantified challenging. Generally, uncertainty is taken as the published values where available. If a calibration error for a given proxy is known, usually that value is taken as the uncertainty for absolute temperature estimates. If the calibration error is not known, two standard deviations of the temporal variability in the records are taken as the uncertainty. Some records are presented in terms of annual temperature range and these limits can be taken as the uncertainty around the annual mean (assumed to be the mean of the maximum and minimum of the range). Again, in some cases, it may be necessary (but undesirable) to obtain maximum or minimum values from figures which can be used as the uncertainty range.

Calculating the uncertainty range for the change across the EOT can be more complicated, as it is hard to know if calibration errors (for the absolute temperatures before and after the EOT) incorporate random variability or systematic biases. If the calibration errors cover a systematic bias, it could be assumed this bias persists across the EOT and so uncertainty in the change is more related to the uncertainty in the time averaging, trends and variability in the mean values before and after the EOT. In this case, the uncertainty in the change is taken as the maximum range between the highest and lowest temperature estimates before and after the EOT. If, however, the calibration error is reflective of random noise, the uncertainty in the change across the EOT could be much greater. If no published value is available, generally the former case is assumed, and the uncertainty is based on the range between the highest and lowest temperature estimates, although this can still produce a very large uncertainty range.

Some studies (e.g. Dowsett et al., 2012; Pound & Salzmann, 2017) devise metrics for the quality of proxy records, based upon factors such as preservation, dating quality, calibration errors etc. when compiling their datasets. Here, there is no formal assessment of the quality of individual proxies or records, nor is there any reinterpretation or recalculation of existing datasets, as this would beyond the scope of the chapter. Instead, here the dataset integrates as many independent proxies as possible for each site, and all are used to evaluate the model simulations. It is important to note that the same proxy is only used in the compilation once per site per time slice. If two or more records using the same proxy at the same site are available, generally the most recent value in the literature is used (e.g. Passchier et al., 2013 and 2016 both provide estimates for temperature using the S-index in Prydz Bay, so the 2016 value is used). Different proxies are generally weighted equally in the model evaluation, with sites where there are multiple records therefore becoming the locations for which it is most important for the model to perform well.

A detailed description of how each data point and its uncertainty were obtained are included in Appendix 3. Without obtaining all of the original data, it is hard to be consistent across all of the records. This chapter aims to test some of the possible methods for evaluating model simulations against a range of proxy records and while it would be ideal to have the best quality of data possible, with all uncertainty ranges rigorously included, due to time constraints this is not always the case. Future work could build upon this compilation and analysis as more higher quality data and model simulations become available.

4.2.4. Sites and coverage

Figure 4.1 shows the range of sites from which some evidence about the Earth system around the time of the EOT was compiled. The sites can broadly be broken into 3 sectors: the Atlantic, Indian and Pacific Ocean sectors. Although these regions sound broadly comprehensive, more than 90 ° of longitude in the Pacific Ocean off the West Antarctic coast are not covered, leaving a major data gap which would be of particular value for validating contradictory model results such as those in Kennedy et al. (2015). Nonetheless, this compilation offers the broadest coverage of the high Southern Hemisphere for this time period of which I am aware.

A potential spatial issue for some of these records (particularly some of those for terrestrial conditions) is that it is unclear as to where the signal originated. For example, a clay weathering record in offshore sediments could incorporate a signal from the continental interior, coastal

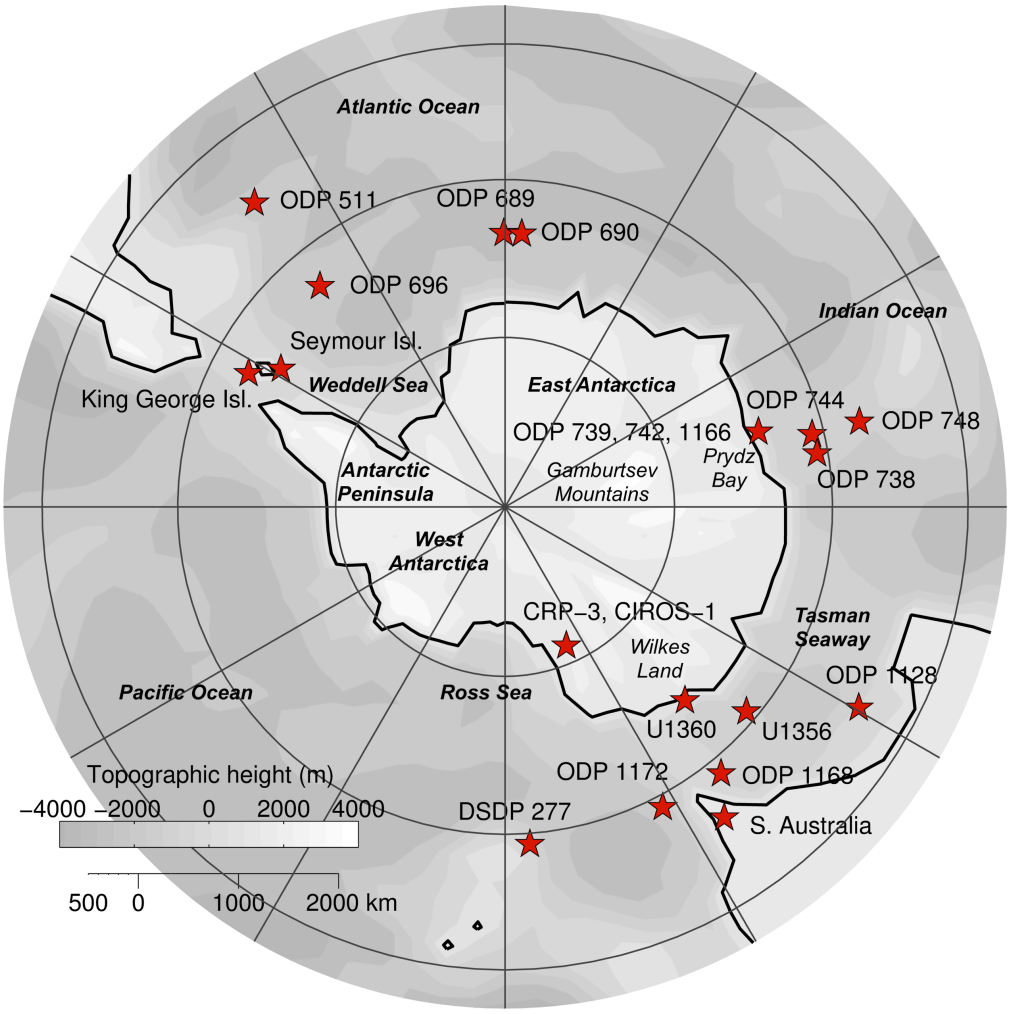

Figure 4.1: Location of proxy record sites used in the data compilation, overlaid on the Getech Rupelian land-sea mask with some key regions labelled.

regions or both. For this reason, the model comparison to the records must account for some spatial variability. Here, the modelled temperature is taken as the mean over a three by three grid cell area surrounding each proxy location, with the maximum and minimum modelled temperature also taken from these nine grid cells as the modelled uncertainty. While this likely does not cover the exact region of origin of terrestrial proxies, it at least accounts for some spatial variability. A potential spatio-temporal issue also occurs in a few cases when the exact sites for a location change between the time slices. This is particularly the Ross Sea, which uses the CIROS-1 core (Wilson et al., 1998; Passchier et al., 2013) and an erratic of unknown origin (located at McMurdo; Pole et al., 2000; Francis et al., 2009) for the late Eocene reconstructions and the CRP-3 core (Raine & Askin, 2001; Passchier et al., 2013) for the early Oligocene reconstructions. It is possible that this introduces errors into the change across the EOT that is included in the dataset, and this must be kept in mind.

In total, evidence was taken from 15 sites, ranging in palaeolatitude from 51 to 77 °S and palaeolongitude from 63 °W to 156 °E. These proxy records are described qualitatively in Section 4.3, with the compiled temperature records shown for the late Eocene in Figure 4.2 and for the early Oligocene and Figure 4.3 for the change across the EOT.

4.3. Data synthesis: results

4.3.1. Atlantic sector

Sites with proxy records in the Atlantic sector include the Weddell Sea (ODP site 696, Houben et al., 2013; and SHALDRIL-3C, Anderson et al., 2011), Maud Rise (ODP sites 689 and 690; Ehrmann & Mackensen, 1992; Bohaty et al., 2012; Petersen & Schrag, 2015; etc.), the Falklands Plateau (ODP site 511; Liu et al., 2009) and a spatially disperse vegetation compilation from the western high South Atlantic (Pound & Salzmann, 2017). Additionally, there are two sites off the tip of the Antarctic Peninsula, on Seymour Island (east of the peninsula; Cantrill & Poole, 2005; Douglas et al., 2014) and King George Island (west of the peninsula; Birkenmajer & Zastawniak, 1989). Both of these sites are included in the Atlantic sector due to their relative proximity, despite the fact that King George Island is in the Pacific. These sites on the islands are terrestrial sections; however, Seymour Island has records that were deposited in a shallow coastal setting, which is now above sea level (Douglas et al., 2014).

In the Weddell Sea, there is evidence of iceberg calving from both West and East Antarctica from approx. 36.5 Ma (Ehrmann & Mackensen, 1992; Carter et al., 2017) and low concentrations of *S. antarctica*, suggesting temperatures less than 10 °C (Houben et al., 2013). At the northern tip of the Antarctic Peninsula marine and terrestrial taxa suggest cool but not polar conditions in the late Eocene, with increased physical weathering towards the end of the period (Anderson et al., 2011). After Oi-1 there is an approximate doubling in sedimentation rates suggesting increased erosion, but not enough to suggest the West Antarctic Ice Sheet (WAIS) was expanded to modern proportions (Huang et al., 2014). There is also an increase in *S. antarctica* concentration at site 696, with some low abundance lower-latitude taxa, suggesting there was cooling and an increase in seasonal sea ice coverage (Houben et al., 2013). This is supported further by the presence of algae species associated with modern day Arctic sea ice at the SHALRDIL 3-C site, as well as sedimentological evidence for increased (but not exclusive) physical weathering on the Antarctic Peninsula in the Oligocene (Anderson et al., 2011).

At Maud Rise, prior to the EOT (from approx. 37 Ma onwards), cooling pulses and ice growth are suggested by spikes in chlorite and kaolinite weathering products (Ehrmann & Mackensen, 1992) and cool water taxa spikes (Villa et al., 2013). Deep surface temperatures based on clumped isotopes dropped from 22.0 °C to 12.3 °C between 35.8 Ma and 35.3-34.2 Ma (Petersen & Schrag,

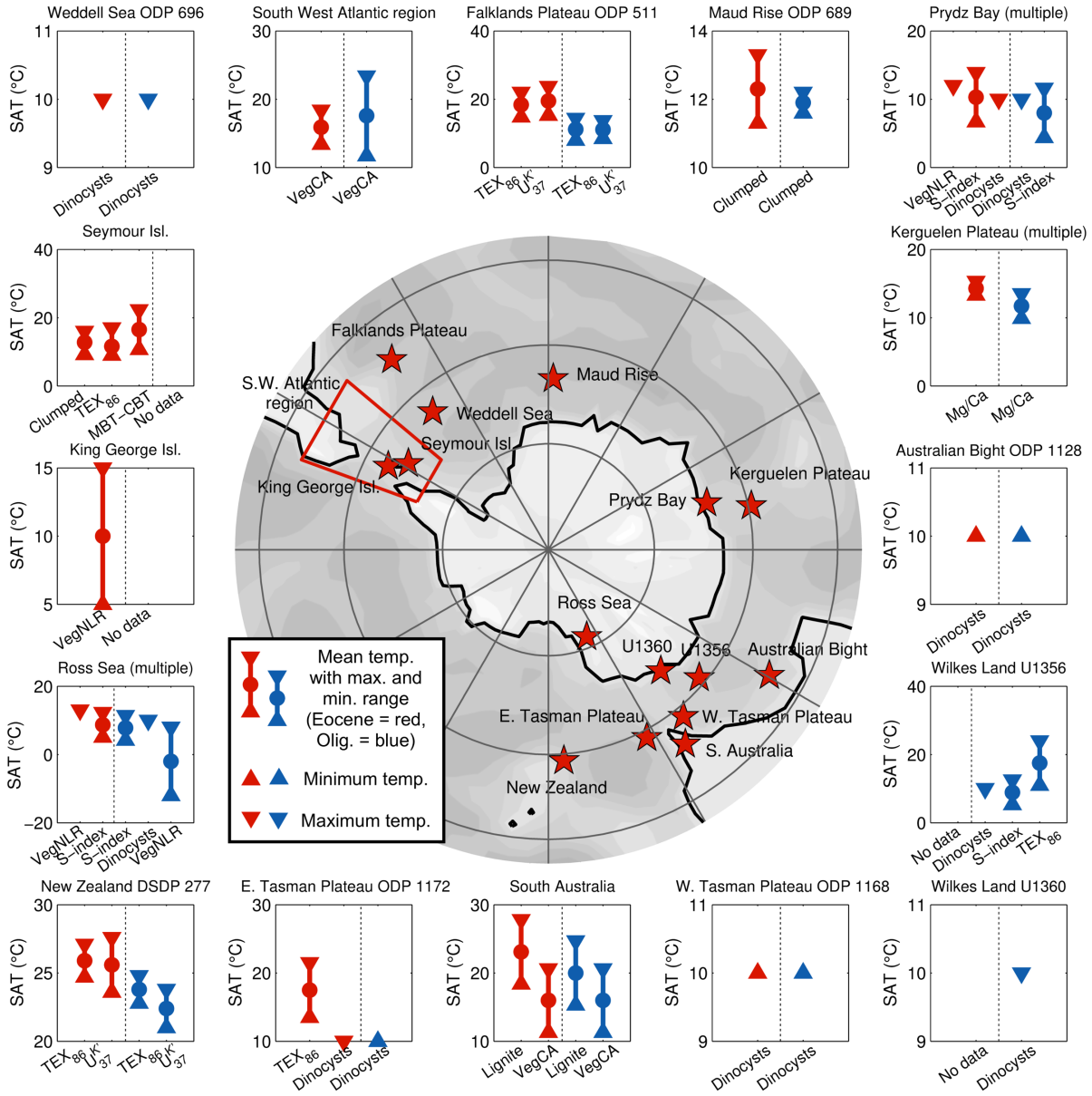

Figure 4.2: Mean annual temperature (°C) from proxy records for all sites during the late Eocene and early Oligocene. The mean values (circles) are shown with maximum and minimum values (error bars), while ordinal limits are shown by upwards (greater than) or downwards (less than) pointing triangles. Late Eocene records are in red and early Oligocene records in blue.

2015), while temperature reconstructions based on vegetation for the western high South Atlantic region also suggest that temperatures cooled prior to the EOT; by approx. 2.1-2.9 °C at around 35 Ma (Pound & Salzmann, 2017).

At the EOT diversity drops at Maud Rise and there is a pulse of sedimentary IRD (either from West Antarctica or the Beacon Supergroup in East Antarctica; Ehrmann & Mackensen, 1992), synchronous with a further shift to cold water taxa (Villa et al., 2013) and physically weathered

clay minerals (reduced smectite and increased illite concentrations; Ehrmann & Mackensen, 1992). However, this IRD pulse is not as large as that at the Kerguelen Plateau and wind deposition cannot be ruled out (Ehrmann & Mackensen, 1992). There are also large divergences in the εNd and the $\delta^{13}C$ records, suggesting a large weathering flux or deep-water pulse (Scher & Martin, 2004). Oxygen isotopes suggest a two-step change over the EOT in planktic and benthic species, but Mg/Ca trends are not clear and the foraminifera are notably poorly preserved, with only a short-term cooling anomaly compared to the Kerguelen Plateau records (Bohaty et al., 2012). This short-term cooling is somewhat in agreement with clumped isotopes, which suggest there is a slightly lower temperature at the EOT (34.1-33.9 Ma) of 11.6 °C relative to the late Eocene or early Oligocene (Petersen & Schrag, 2015).

After the EOT there is a slight, short recovery in the clay weathering products (Ehrmann & Mackensen, 1992), but cool water taxa remain dominant (Villa et al., 2013) and IRD remains high but of a different origin (likely East Antarctica; Ehrmann & Mackensen, 1992). There is another later εNd spike at approx. 28.2-27.13 Ma, possibly suggesting more weathering or another deep-water formation pulse (Scher & Martin, 2004). Temperatures from clumped isotopes, are not much lower than the late Eocene, at 11.9 °C (Petersen & Schrag, 2015). Throughout these records there are timing differences with Kerguelen Plateau, suggesting dating uncertainties and/or zonally heterogeneous changes (Ehrmann & Mackensen, 1992; Villa et al., 2013).

Records of Seymour Island and King George Island off the Antarctic Peninsula assess some terrestrial and some coastal ocean conditions but are limited to the mid-late Eocene. On the east side (Seymour Island), vegetation contains a mixture of conifers and angiosperms in the mid-late Eocene suggesting a cool temperate climate (Cantrill & Poole, 2005; Francis et al., 2009). This becomes cooler, drier and frostier around the EOT with increased physical weathering (Dingle et al., 1998) and declining leaf sizes (Francis et al., 2009). Coastal conditions inferred from TEX_{86} and clumped isotopes suggest temperatures between 9 and 17 °C, slightly cooler than nearby terrestrial temperatures inferred with the MBT-CBT index (10.7-22.3 °C; Douglas et al., 2014). On the west side of the Antarctic Peninsula, throughout the mid-late Eocene (possibly around 40 Ma) there are some till layers possibly from alpine glaciers (Birkenmajer et al., 2005). Southern Beech dominates the vegetation record (Cantril & Poole, 2005), with vegetation proxies based upon nearest living relative methods suggesting temperatures between 11.7-15.0 °C (Birkenmajer & Zastawniak, 1989), although this estimate has been argued to be too high (Francis et al., 2009; based upon Francis & Hill, 1996). The different dominant tree species suggest zonal temperature and precipitation gradients across the peninsula, like in Patagonia today (Cantrill & Poole, 2005).

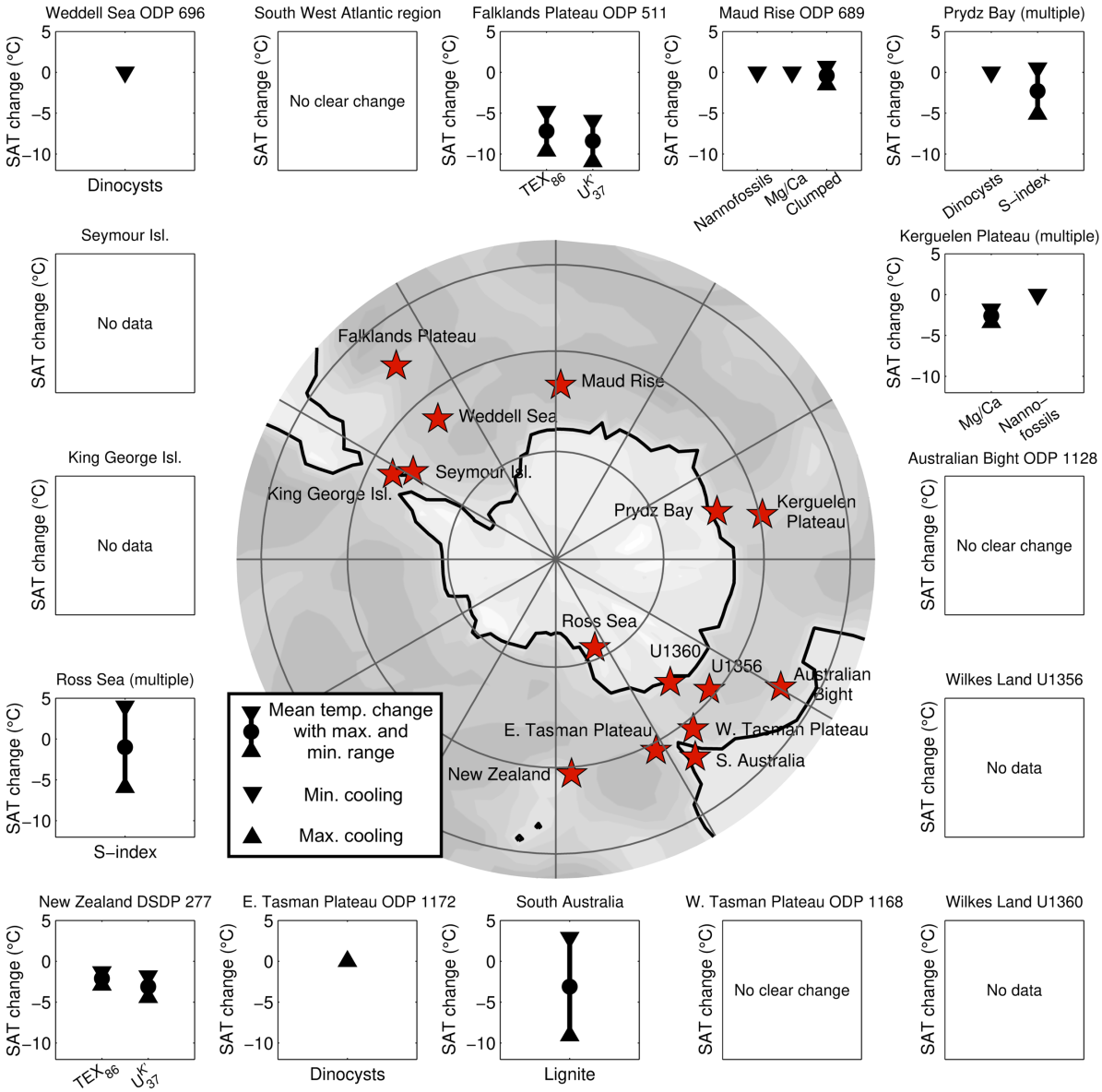

Figure 4.3: Changes in mean annual temperature (°C) from proxy records for all sites across the EOT. The mean values (circles) are shown with maximum and minimum values (error bars), while ordinal limits are shown by upwards or downwards pointing triangles.

Further north at the Falklands Plateau (ODP site 511), SSTs are found to drop significantly across the EOT, by approx. 8 °C (Liu et al. 2009; Plancq et al., 2014). This is the largest change of any of the sites included in the dataset, suggesting either a localised or very heterogeneous temperature response across the EOT. It is also important to note that the clumped isotope record for Maud Rise showed a comparable cooling earlier in the record (Petersen & Schrag, 2015), suggesting this could be due to dating issues or could be a slow northward propagation of the signal.

4.3.2. Indian sector

Sites in the Indian Sector include Prydz Bay (ODP sites 739, 742 and 1166; Macphail & Truswell, 2004; Passchier et al., 2013; 2016; Scher et al., 2014 etc.), close to the Antarctic margin at the Lambert Graben, and the more offshore Kerguelen Plateau (ODP sites 738, 744 and 748; Zachos et al., 1992; Bohaty et al., 2012; Villa et al., 2013).

There is evidence for an early polar climate around the region inland from Prydz Bay and the Lambert Graben, with a pre-cursor glaciation 0.5 Ma prior to the EOT (Scher et al., 2014), variable temperature excursions (of up to 3 °C; Passchier et al., 2016) and orbitally paced depositional sequences, suggesting a sensitive, accumulation driven cryosphere system (Passchier et al., 2016). Vegetation records suggest a cool-temperate shrubland existed at lower altitudes near the coast (Pound & Salzmann, 2017), with Southern Beech pollen taken to suggest temperatures around or below 12 °C (Macphail & Truswell, 2004). Dinoflagellates also suggest this area was also cool prior to the major glaciation at Oi-1, with some *S. antarctica* present before the EOT (i.e. SSTs below 10 °C; Houben et al., 2013). At the EOT, records show the ice extending to the outer continental shelf and temperatures dropping approx. 3 °C (Passchier et al., 2016). In agreement with this record of terrestrial cooling, *S. antarctica* also increases in abundance, although other species remain present suggesting the conditions were not fully polar (however, the authors argue this could be the result of reworking in the sediments; Houben et al., 2013).

At the Kerguelen Plateau, during the late Eocene the sediments are rich in carbonates and smectite is dominant but declining (Ehrmann & Mackensen, 1992). There is a pulse of IRD prior to the EOT (Ehrmann & Mackensen, 1992) and a perturbation in εNd (Scher et al., 2011), likely related to the small precursor glaciation (Scher et al., 2014). Nannofossil species suggest decreasing warm-water and increasing cool-water taxa throughout the late Eocene (Villa et al., 2013) Using information about the temperature gradient of approx. 2 °C between the Kerguelen Plateau and Maud Rise based upon Mg/Ca records (Bohaty et al., 2012) and absolute temperature values from Maud Rise based upon clumped isotopes (Petersen & Schrag, 2015), deep surface ocean temperatures are taken to be 14.3 °C prior to the EOT.

At the EOT there is a large, short excursion in IRD for around 100 ka that coincides with a large oxygen isotope shift (Zachos et al., 1992), an increase in kaolinite, illite and chlorite clay weathering products (Ehrmann & Mackensen, 1992) and a large weathering pulse inferred from εNd (Scher et al., 2011). Deep surface ocean temperature shows a 2.6 °C cooling across the EOT in Mg/Ca records, with the excursion lasting around 1 Ma (Bohaty et al., 2012), and there is a

shift towards cold-water taxa, with temperate and warm-water taxa remaining low or negligible for the majority of the early Oligocene (Villa et al., 2013). In the early Oligocene, there are cyclical variations in the productivity (Diester-Haass, 1996), oxygen isotopes (Zachos et al., 1996) and carbonate preservation (Ehrmann & Mackensen, 1992), which could be related to pulses of warm and cool water influencing the region.

4.3.3. Pacific sector

This sector contains regions in the Tasman Seaway, South Australia, the western South Pacific and the Ross Sea. The Tasman Seaway includes sites further north (ODP sites 1128 and 1168 off the south Australian coast; Houben et al., 2013) and further south (U1356 and U1360 off the Wilkes Land coast, Antarctica; Houben et al., 2013; Hartman et al., 2018). The South Australia terrestrial sites include lignite records (V. Lauretano, unpublished data) and vegetation records (Pound & Salzmann, 2017) from multiple sites. The western South Pacific sites include ODP 1172 on the East Tasman Plateau (Houben et al., 2013; Douglas et al., 2014) and DSDP 277 south of New Zealand (Liu et al., 2009), while the Ross Sea records include CRP-3 (Raine & Askin, 2001; Galeotti et al., 2016), CIROS-1 (Passchier et al., 2013) and some data from an Eocene erratic at McMurdo (Francis et al., 2009)

In the Tasman Seaway, records generally paint a complex picture of changes extending across the EOT. The records from the southern Tasman Seaway off the Wilkes Land coast do not extend back to sufficiently describe the late Eocene but suggest cold conditions (less than 10 °C) with seasonal sea ice in the early Oligocene (Houben et al., 2013; Passchier et al., 2013). However, TEX_{86} records stretching further into the Oligocene suggest warmer temperatures (~17.5 °C), suggesting these cold conditions might be short lived (Hartman et al., 2018). Records on the northern side of the seaway (ODP 1128 in the Australian Bight and 1168 on the West Tasman Plateau) are absent of *S. antarctica* species before and after the EOT, suggesting they are consistently warmer than 10 °C (Houben et al., 2013). On the other side of the Tasman Gateway at site 1172, *S. antarctica* are present during the late Eocene but not during the late Oligocene, suggesting temperatures were cooler there but then warmed after the EOT (Houben et al., 2013). The presence of *S. antarctica* is inconsistent with TEX_{86} reconstructions for site 1172, which suggest SSTs were in the region of 21 °C (Douglas et al., 2014); however, this record is dated earlier (38.5-36.5 Ma) than the *S. antarctica* record (35.5-33.7 Ma), so it is possible this difference is due to a large cooling prior to the EOT, followed by warming after the EOT. Nearby terrestrial records in South Australia suggest there is cooling before and/or across the EOT (V. Lauretano, unpublished

data; Pound & Salzmann, 2017), although the absolute temperature records from the lignite and the temperature range from the vegetation proxies are also inconsistent, with the vegetation record suggesting cooler temperatures than the lignite.

The presence of *S. antarctica* and the potential warming across the EOT has been explained by some authors as a local effect due to changes in the gateway (Stickley et al., 2004; Houben et al., 2013). Opening of the Tasman gateway started before but finished after the EOT, with deepening events generally associated with hiatuses and increased erosion from increased bottom water flow (Stickley et al., 2004). It is suggested that during the late Eocene, the very shallow Tasman Seaway had a limited connection between the Antarctic-Australian Gulf and the South Pacific (Stickley et al., 2004). This would have allowed the proto-Ross Sea gyre to have been bigger, extending further north towards Australia and potentially carrying Antarctic taxa such as *S. antarctica* with it (Stickley et al., 2004; Houben et al., 2013). This hypothesised ocean state seems similar to the ice free Priabonian climate model simulation in Chapter 2 (Kennedy et al., 2015). As the gateway opened, flow from the Indian Ocean (the proto-Leeuwin current) brought warmer water (and associated cosmopolitan taxa to the region), with the sites becoming more similar and starting to converge with New Zealand sites (Scher et al., 2015). These mechanisms are plausible, but this highlights that there are complications in compiling the dataset with sometimes contradictory records.

The New Zealand sites, which are further from the Antarctic margin, show warmer SSTs around 26 °C before the EOT (Liu et al., 2009), with waters coming from Pacific circulation or source (Scher et al., 2015). SSTs cool by approx. 3 °C over the EOT (Liu et al., 2009), before becoming influenced by a proto-ACC and Indian Ocean waters after the EOT, around 30 Ma (Scher et al., 2015).

Finally, in the Ross Sea there are a range of records available. Terrestrial temperature estimates for the CIROS-1 core using S-index suggest the temperature in the late Eocene was approx. 8.7 °C (Passchier et al., 2013), broadly in agreement with fossil wood from a McMurdo glacial erratic that puts the maximum temperature at 13 °C (Francis et al., 2009). The temperature for the early Oligocene is approx. 1 °C colder, based upon an S-index record for the nearby CRP-3 core, while interpretations of the magnitude of cooling based on the dominant vegetation vary significantly between different studies (Francis & Hill, 1996; Raine & Askin, 2001; Passchier et al., 2013). In the ocean, dinoflagellate assemblages at CRP-3 show *S. antarctica* after the EOT (the record does not cover the late Eocene), suggesting at least seasonal sea ice, colder conditions and SSTs less than 10 °C (Houben et al., 2013).

On land, there is generally tundra-like vegetation with no clear period of more temperate vegetation during the late Eocene (Raine & Askin, 2001; Pound & Salzmann, 2017). The lack of vegetation change and the small temperature change could be due to the record starting after some cooling had already occurred (Raine & Askin, 2001), with the Atlantic Ocean, Indian Ocean and Australian vegetation records all showing some cooling prior to the EOT as discussed above. There are some occasional pollen data points suggesting the temperature had been warmer as well as a gradual cooling trend and diversity reduction through the Oligocene, but these warm species are very scarce and could be due to reworking of sediments (Askin & Raine, 2000; Raine & Askin, 2001).

The ice sheet is thought to have been variable from Oi-1 through to Oi-1a (32.8 Ma), at which point it expanded to the outer Ross Sea shelf and became more stable (Galeotti et al., 2016). There is also seismic evidence suggesting that the ice during this early period came from areas of West Antarctica such as Marie Byrd Land (Sorlien et al., 2007; Olivetti et al., 2015), with potentially large ice expansions around 32 and 30 Ma. The 32 Ma expansion correlates with a decrease in smectite, also suggesting an increase in glacial activity (Olivetti et al., 2015).

4.3.4. Overview

Although there is regional variation in the temperature patterns shown here, all of the sites in the Southern Ocean from the different sectors generally show agreement with the 2-3 °C benthic cooling inferred from oxygen isotope records (with a glacial expansion of ice to 60-130 % of the present-day East Antarctic ice sheet (EAIS) volume; Bohaty et al., 2012). Given that deep ocean waters are expected to have formed in the Southern Ocean (e.g. Katz et al., 2011), the change in Southern Ocean SST and benthic temperatures should be expected to be similar. The mean cooling across all sites for the EOT dataset (i.e. for records that are available both before and after the EOT) is ~3.4 °C, while the difference between the mean of each absolute dataset is ~2.8 °C. The mean temperature (change) and linear best fit using ordinary least squares through the mean temperatures (or temperature change) with palaeolatitude from all proxies and sites are shown in Figure 4.4 for each time slice.

The absolute temperature profiles in the late Eocene and early Oligocene datasets show colder temperatures at higher latitudes than mid-latitudes, as would be expected. The latitudinal gradient

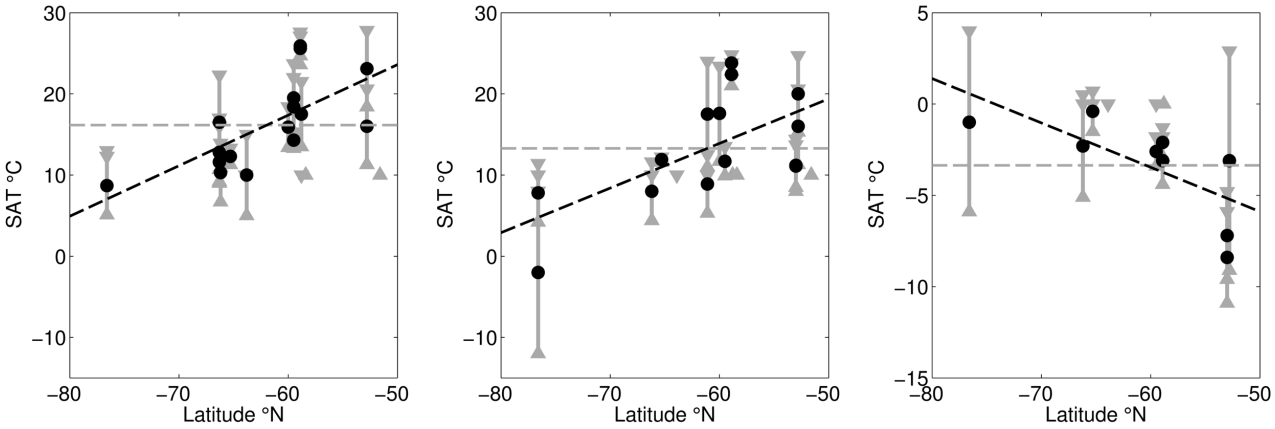

Figure 4.4: Latitudinal profiles of a) late Eocene absolute temperature, b) early Oligocene absolute temperature and c) EOT temperature change from proxy records. The mean values are plotted in grey dotted lines and latitudinal gradients (calculated using ordinary least squares) in black dotted lines. As with Figures 4.2 and 4.3, circles show mean values, uncertainty ranges and maximum/minimum limits are shown by the bars and triangles.

is shallower in the early Oligocene (0.55 °C °N^{-1}) compared to the late Eocene (0.62 °C °N^{-1}). The change in temperature across the EOT has a negative slope, suggesting that cooling is greater at mid-latitudes and is less at higher latitude sites, which could reflect a qualitative agreement with modelling results (Kennedy et al., 2015; this thesis Chapter 3; Goldner et al., 2014; Knorr & Lohmann, 2014), where the heterogeneous temperature response saw some high latitude areas warming or cooling less. The steepness of the gradient for the EOT dataset (-0.24 °C °N^{-1}) is partially enhanced by the strong cooling at the low latitude Falklands Plateau and the weak signal at the higher latitude Maud Rise and Ross Sea sites; however, even if all of these points were to be omitted from the fit, the latitudinal gradient would still be weakly negative (-0.06 °C °N^{-1}; figure not shown). Implications of this latitudinal gradient change across the EOT will be discussed further in Section 4.5.

Generally, a reasonably consistent picture can be built up between proxies at each site. The site which has the most contradictory records is at ODP 1172 on the East Tasman Plateau (Houben et al., 2013; Douglas et al., 2014); however, as discussed this could be due some localised oceanographic changes (Stickley et al., 2004) or due to differences in the timing of the proxies. There are a number of sites where cooling appears to pre-date the EOT, for example in the Weddell Sea terrestrial records (Carter et al., 2017), Maud Rise SST records (Petersen & Schrag, 2015) or the vegetation records from South Australia or the South Atlantic (Pound & Salzmann, 2017). The use of time averaging in the dataset might therefore be an over-simplification. While it would be ideal to subdivide the time slices further into mid-late Eocene, pre-EOT, post-EOT and early Oligocene for example, given the amount of data available at this stage this is not possible. This

work provides a template that future work can build upon and include more data as more proxies, sites and temporal coverage becomes available.

Finally, it is important to comment on the evidence for glacial expansion at the EOT. This work does not explicitly model the AIS, and instead it is prescribed in the climate models. This means that there are no results that can test in depth how the ice sheet expands, flows or its erosional capability. The balance of proxy evidence here shows that some glacial activity and cold terrestrial conditions existed before the EOT. There then appears to have been a relatively major glacial expansion over East Antarctica in the build up to and across the EOT. It then took a further million years or so for the ice sheet to fully expand over East Antarctica and also parts of West Antarctica (particularly into areas in Marie Byrd Land near the Ross Sea; Sorlien et al., 2007; Olivetti et al., 2015). However, glaciation does not seem to have covered all of West Antarctica, with erosion being less than in more recent time periods (Huang et al., 2014) and relatively diverse vegetation biomes still present around most of the coastal regions of the continent (Francis et al., 2009). This seems to be consistent with estimates of ice sheet volume based upon approximations using oxygen isotopes (e.g. DeConto et al., 2008; Bohaty et al., 2012; Wilson et al., 2013).

4.4. Comparison of proxies to GCM output

4.4.1. Methods

4.4.1.1. Metrics of comparison

The first metric used to evaluate the GCMs against the dataset is the root mean square error (RMSE), which simply finds the mean difference between the models and the data for all comparable points. The RMSE is calculated for the temperature fields in the model and is done in two ways. Firstly, the 'standard' RMSE is calculated from the maximum or minimum of the uncertainty range of the proxy data (if the model is too warm or cold, respectively), with the error taken as zero if the model lies within the range of proxy uncertainty. This can be calculated for continuous data or ordinal data that provides an upper or lower range for the temperature, such as the presence of *S. antarctica*.

Secondly, the RMSE is calculated once the mean temperature of all data points/sites (either in the proxy dataset or for a given model simulation) has been removed. The purpose of removing the mean is so the model performance is not primarily judged against systematic warm or cold biases, which are typical at high latitudes (Huber & Caballero, 2011; Lunt et al., 2012). This 'normalised' RMSE instead evaluates the spatial patterning of relatively warm or cold sites within the Southern Ocean, for example if the Pacific sites are consistently warmer than the Atlantic sites. This metric is used with continuous data where a mean value is available, again with the error taken from the upper or lower range of the uncertainty.

Count metrics can also be used for the absolute and relative change data comparisons, potentially allowing a large range of proxy records to be incorporated. These can count how many of the data points the model is consistent with in terms of magnitude (i.e. within the error bars of).

Alternatively, for the change across the EOT, the number of records for which the model simulations correctly predict the direction of change across the EOT can be counted. This can allow ordinal data (such as increasing cold water taxa) to contribute to the comparison. The proxy dataset only has one point that shows warming (East Tasman Plateau; based on Houben et al., 2013; although this could be contentious as discussed in Section 4.3.3), with all of the other sites showing cooling. This metric therefore generally penalises simulation pairs that suggest warming across the EOT, the opposite response to the vast majority of proxy data.

To judge the simulations across multiple criteria, if the metric scores have comparable units (e.g. the two RMSE metrics) they can simply be summed or averaged. If metrics with different units are to be incorporated (e.g. using the RMSE and count metrics together), their ranked score in terms of their performance for each metric (with 1 being the best performer and *n* being the worst performer, where *n* is the number of simulations) can be summed across all metrics for each time slice. Although this method could be useful for integrating many different kinds of proxy, it will not be independent of the model simulations used (as the choice of simulations will affect their ranked score), and so it is not discussed here.

To further expand upon the idealised model-data comparison in Chapter 3, it is important to consider not just if the simulated change across the EOT is realistic, but also if the starting and ending state are realistic compared to the late Eocene and early Oligocene datasets. This is done by combining the metric scores for a pair of simulations that describe the change across the EOT (compared to the EOT dataset) with metric scores for the pre- and post-EOT simulations that make up that pairing (compared to the late Eocene and early Oligocene datasets). This combined score can change the order of which model simulation pairs would be perceived as the best, compared to just evaluating against the EOT data alone. If the datasets had a consistent spatial coverage for each of the time slices, the difference between the late Eocene and early Oligocene absolute datasets would be the same as the EOT relative change dataset. However, because there are some sites with records available only before or after the EOT, and some relative changes for which absolute values are not available, the pair of simulations that gives the best fit before and after the EOT is not necessarily the same pair as gives the best bit for the observed change across the EOT. Which metric is used to evaluate across the time slices and if there is any weighting put on the absolute or relative change datasets is subjective. Here, the combined rank score for each time slice is based upon only the two RMSE metrics and the three time slices are weighted equally.

4.4.1.2. Benchmarks for evaluation

For the model simulations to be described as performing particularly 'well' or 'poorly', it is necessary to have some sort of benchmark to compare the model's performance against. For the three time slices, two benchmarks are used. First, the mean temperature (or temperature change) of all sites and proxies is taken as a homogeneous value at all sites. Second, the ordinary least squares linear fit through the mean temperatures (or temperature change) with palaeolatitude from all proxies and sites, shown in Figure 4.4, is taken to produce a synthetic, latitudinally varying temperature field for the region. If model simulations perform better than both benchmarks, they

can be described as showing *good* performance as they are correctly modelling zonal and regional variation beyond this general latitudinal trend. If the simulations perform worse than both metrics, they show *poor* performance and are failing to identify even the most basic variation in the dataset. If the simulations outperform the homogeneous benchmark but not the latitudinal gradient benchmark, they are described as showing *moderate* performance.

4.4.1.3. Simulations used

The proxy datasets compiled here are compared to the fully spun-up HadCM3BL-M2.1aE simulations outlined in Chapter 3 and other simulations from three different models: FOAM (a low resolution GCM; simulations from Ladant et al., 2014a), UVic (an EMIC with a 3-D ocean but a simplified atmosphere; simulations from Sijp et al., 2016) and GENESIS (a slab ocean GCM; simulations from Pollard & DeConto, 2005). These models are all relatively low resolution and are less complex than some others that have been used in recent studies (e.g. Hutchinson et al., 2018; Baatsen et al., 2018a); however, they are still regularly used in palaeoclimate research of this period. The simulations used are outlined in Table 4.1.

Table 4.1: Brief overview of other models used and the boundary conditions varied for each, with HadCM3BL shown again for reference.

Model	Atmos. resolution	Ocean resolution	Palaeogeog. vars.	pCO_2 vars. (ppmv)	Ice sheet vars.	Simulation length (years)	Reference
HadCM3BL-M2.1aE	96x73x19	96x73x20	Open/closed Drake Passage	840/ 560	No ice/ EAIS	>6,000	Section 3.2.3
UVic	150x100x1	150x140x40	Open/closed Drake Passage	1,600	No ice	9,000	Sijp et al., 2016
GENESIS	96x48x18	Slab	None	1,120/ 560	No ice/ EAIS	30	Pollard & DeConto, 2005
FOAM	48x40x18	128x128x24	None	1,120/ 840/ 560	No ice/ small EAIS/ EAIS/ full AIS	2,000	Ladant et al., 2014a

To evaluate against the proxy dataset of relative changes across the EOT, pairs of model simulations must be selected that represent the forcing changes occurring across the EOT. These pairs of model simulations represent a before and after state, with the difference in the boundary conditions between the pairs described as the forcing and the difference in the modelled climate representing the change across the EOT.

The model data comparison in Chapter 3 is reasonably idealised in that mostly isolated changes in the model setup were taken as the forcing across the EOT; for example, a change in palaeogeography but no change in pCO_2 or ice sheet extent. Given that the vast majority of proxy data discussed in Section 4.3 gives evidence of glacial expansion, here the modelled forcing must include some sort of ice expansion. The simulation pairs may additionally include other forcing changes that are potentially relevant to describe the state of the Earth system before and after the EOT. Simulation pairs were chosen that represented:

- An expansion of ice over Antarctica from an ice-free state to either an EAIS of full AIS, with all other boundary conditions remaining the same
- A similar expansion of ice over Antarctica but also combined with a simultaneous drop in pCO_2, with palaeogeographic boundary conditions remaining the same
- A similar expansion of ice over Antarctica but also combined with a simultaneous change in palaeogeography (an opening of the Drake Passage), with pCO_2 boundary conditions remaining the same

This produced 8 pairs of simulations from HadCM3BL, 9 pairs from FOAM and 3 pairs from GENESIS. There were no glaciated UVic simulations available, so it cannot be compared to the EOT dataset.

4.4.2. Quantitative comparisons

4.4.2.1. Late Eocene temperatures

The RMSE, normalised RMSE and count metrics for all of the ice-free simulations and the benchmarks in comparison to the late Eocene data are shown in Figure 4.5. The standard RMSE scores show that absolute temperature biases are quite large. The standard RMSE scores are better for simulations at higher pCO_2 levels, showing there is a cold bias in the model simulations. As a result, only one HadCM3BL simulation outperforms the homogeneous benchmark (3x pre-

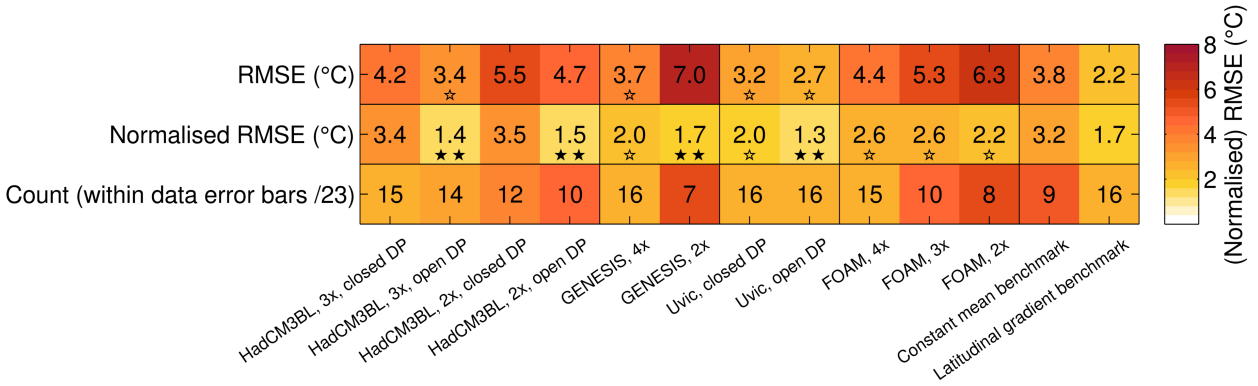

Figure 4.5: RMSE (°C), normalised RMSE (°C) and count metrics for all ice free model simulations and the benchmarks compared against the late Eocene dataset. Labels on the x-axis refer to the pCO_2 level ('2x', '3x' or '4x' pre-industrial levels) and state of the Drake Passage ('DP'). For a given metric, simulations marked with a single star show *moderate* performance, those with two stars show *good* performance. The colour scale of the count metric is normalised to match that of the RMSE metrics.

industrial pCO_2 levels and an open Drake Passage). The lowest standard RMSE scores are from the UVic simulations, likely due to their higher pCO_2 levels (1,600 ppmv) compared to the other models. The GENESIS simulation with 4x pre-industrial (PI) pCO_2 also outperforms the constant mean benchmark, while the 2x PI pCO_2 simulation has the lowest standard RSME of all simulations. No simulations from any model outperform the latitudinal gradient benchmark in terms of the standard RMSE.

When the mean temperature bias is removed for the normalised RMSE, most of the simulations outperform the constant mean benchmark and some outperform the latitudinal gradient benchmark. Although the general cold bias in the simulations means that the high pCO_2 simulations perform better than the low pCO_2 equivalents for the standard RMSE, with the bias removed, the low pCO_2 simulations perform as well or better than the high pCO_2 simulations. The best simulations are the UVic simulation with an open Drake Passage, those from HadCM3BL with an open Drake Passage and the GENESIS simulation at 2x PI pCO_2. The only simulations not to outperform either benchmark are the HadCM3BL simulations with a closed Drake Passage, suggesting this palaeogeographic configuration has a major influence on the spatial patterns of temperature. The UVic simulations also perform worse when the Drake Passage is closed, although it should be noted that the UVic simulation with a closed Drake Passage still outperforms the constant mean benchmark, as well as the FOAM simulations with an open Drake Passage.

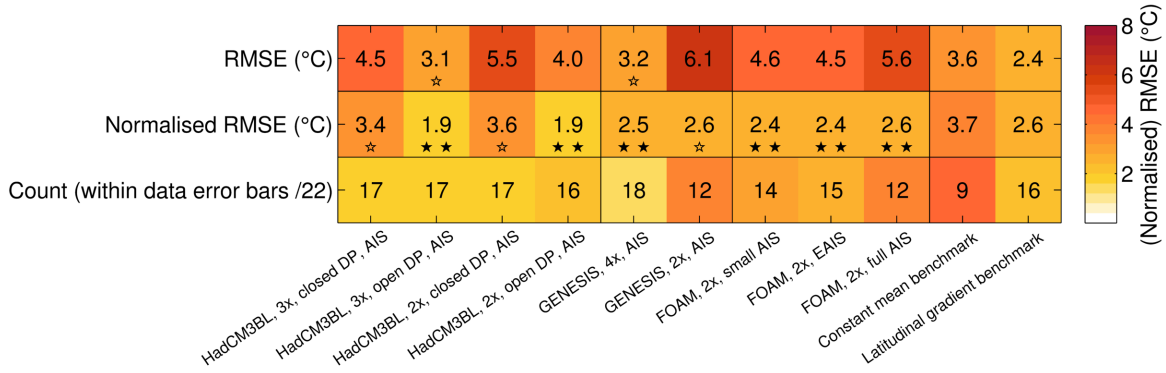

Figure 4.6: RMSE (°C), normalised RMSE (°C) and count metrics for all glaciated model simulations and the benchmarks compared against the late Eocene dataset. Labels on the x-axis refer to the pCO_2 level ('2x', '3x' or '4x' pre-industrial levels), state of the Drake Passage ('DP') and the size of the Antarctic ice sheet (AIS) in the FOAM simulations. For a given metric, simulations marked with a single star show *moderate* performance, those with two stars show *good* performance. The colour scale of the count metric is normalised to match that of the RMSE metrics.

No simulations outperform both benchmarks for both RMSE metrics, so none can be described as *good*. However, the HadCM3BL simulation at 3x PI pCO_2 with an open Drake Passage and the UVic simulation with an open Drake Passage outperform the homogenous benchmark for both metrics and the latitudinal gradient benchmark for the normalised RMSE, so can be described as *moderate-good*. The 4x PI pCO_2 GENESIS simulation and the UVic simulation with a closed Drake Passage can also be described as *moderate* as they outperform the homogeneous benchmark for both metrics.

4.4.2.2. Early Oligocene temperatures

Figure 4.6 shows the standard RMSE, normalised RMSE and count metrics for all glaciated simulations against the early Oligocene dataset. Again, there is a general cold bias indicated by the poorer standard RMSE scores for the lower pCO_2 simulations, although generally the standard RMSE values are slightly better compared to the late Eocene comparison. Only two simulations outperform the constant mean benchmark: HadCM3BL at 3x PI pCO_2 with an open Drake Passage and GENESIS at 4x PI pCO_2, with no simulations outperforming the latitudinal gradient benchmark for this metric. The FOAM simulation with the largest ice sheet configuration has a poorer RMSE compared to the FOAM simulations with smaller ice sheets, likely due to the cooling (and hence cold bias) being greater with a large ice sheet.

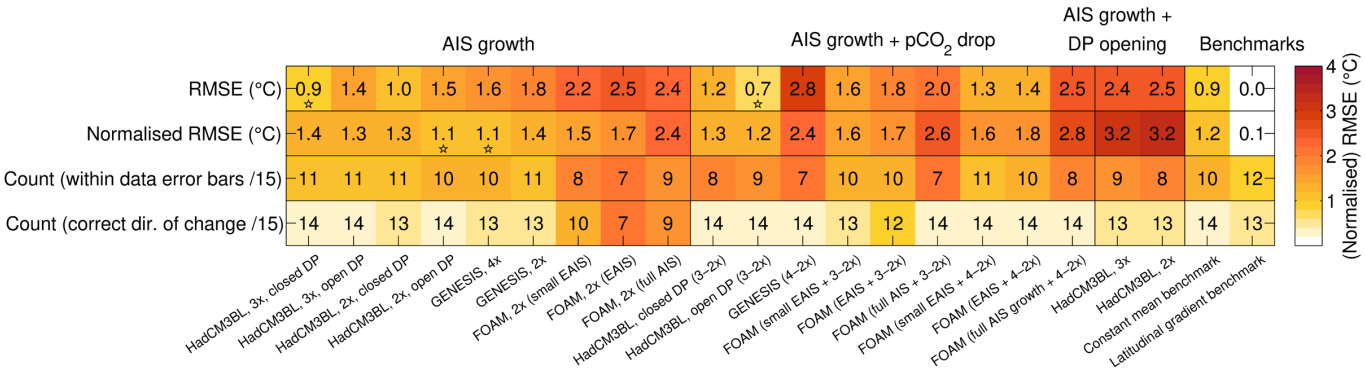

Figure 4.7: RMSE (°C), normalised RMSE (°C) and count metrics for all pairs of model simulations representing the forcing across the EOT and the benchmarks compared against the EOT dataset. The simulation pairs are grouped by forcing. Labels on the x-axis refer to the pCO_2 level ('2x', '3x' or '4x' pre-industrial levels) and state of the Drake Passage ('DP'); brackets in the labels specify the size of AIS added or magnitude of pCO_2 drop. For a given metric, simulation pairs marked with a single star show *moderate* performance, those with two stars show *good* performance. The colour scale of the count metrics are normalised to match that of the RMSE metrics.

For the normalised RMSE, all simulations outperform the constant mean benchmark and several simulations perform better than both benchmarks. The HadCM3BL simulations with an open Drake Passage at either pCO_2 level are the joint best, with the 4x pre-industrial pCO_2 GENESIS simulation and the FOAM simulations with only an EAIS also performing better than both benchmarks. Again, as with the late Eocene temperature data, the HadCM3BL simulations with the closed Drake Passage perform much worse than the equivalent open Drake Passage simulations in terms of the both RMSE metrics.

Like for the late Eocene, no simulation can be described as *good* for both RMSE metrics; however, the glaciated HadCM3BL simulation at 3x PI pCO_2 with an open Drake Passage and the glaciated GENESIS simulation at 4x PI pCO_2 can be described as *moderate-good*.

4.4.2.3. EOT temperature change

All pairs of model simulations representing the change that occurred across the EOT are shown in Figure 4.7. It is important to note that, generally, the uncertainties in the EOT dataset are much greater relative to the magnitude of change, compared to the uncertainties relative to the absolute

values in the late Eocene and early Oligocene datasets. As a result, the latitudinal gradient benchmark provides a remarkably good fit for the data covering the EOT, lying almost entirely within the data uncertainty. No model simulations performs nearly as well as this benchmark but again, because the uncertainty in the change relative to its magnitude is greater than in the absolute datasets, generally the model RMSE scores are lower for this dataset than the late Eocene or early Oligocene datasets.

Two simulation pairs outperform the constant mean change benchmark for the standard RMSE metric (HadCM3BL with an open Drake Passage in response to AIS growth and a pCO_2 drop and HadCM3BL with a closed Drake Passage at 3x PI pCO_2 in response to AIS growth) and two simulation pairs outperform the constant mean change benchmark for the normalised RMSE metric (HadCM3BL with a closed Drake Passage at 2x PI pCO_2 in response to AIS growth and GENESIS at 4x PI pCO_2 in response to AIS growth).

In contrast to what was shown for the absolute temperature dataset comparisons for the late Eocene and early Oligocene, the HadCM3BL simulation pairs with a closed Drake Passage (both before and after the EOT) perform relatively well across all metrics. This shows that although simulations can be far from the proxies in absolute terms, they can still produce promising results in other ways.

Similarly to what was shown for the late Oligocene, the FOAM simulations generally fit the dataset best in terms of the RMSE and normalised RMSE when they have smaller ice sheets added.

In terms of the forcings across all model simulation pairs, the AIS growth forcing in isolation in general produces the best normalised RMSE and has the highest count of points within error bars of the data. The combined AIS growth and pCO_2 drop forcing produces a fractionally better standard RMSE and correctly identifies the direction of change at most sites. The AIS growth forcing in combination with an opening of the Drake Passage gives the poorest fit for all four metrics shown in Figure 4.7.

No simulations from any model perform better than either benchmark for both RMSE metrics, with the best HadCM3BL simulation pairing (with an open Drake Passage in response to both AIS growth and pCO_2 drop) coming the closest (its normalised RMSE being 0.04 °C worse than the constant mean benchmark). All simulation pairs can therefore only be described as *moderate-poor* or *poor*. The reasoning for this poor performance is discussed further in Section 4.5.1.

4.4.2.4. Evaluation across time slices

As noted in Section 4.4.1.1, it is possible to evaluate the model simulations and model simulation pairs across various metrics. The best five simulations (or simulation pairs) for the late Eocene, early Oligocene and for the change across the EOT based on the two RMSE metrics are shown in Table 4.2. As well as taking the average RMSE for each time slice, the average RMSE can be taken across all three time slices. It is not always the case that simulation pairs that perform well for the observed EOT change also perform well when the late Eocene and early Oligocene data are incorporated. As was noted in sections 4.4.2.1 and 4.4.2.2, for the absolute temperatures, simulations with a closed Drake Passage perform relatively poorly. As a result, when the combined ranked performance score is calculated across all three time slices, the pairings with a closed Drake Passage are not found to perform as well, highlighting the importance of incorporating the absolute values into this model-data comparison. The best five simulations in terms of the average RMSE and normalised RMSE across all three datasets are also listed in Table 4.2.

Table 4.2: The top five model simulations (or simulation pairs) in terms of combined RMSE performance for each proxy dataset, plus the top five simulation pairs across all three datasets.

Rank	Model	pCO_2 (ppmv)	AIS state	Drake Passage
		Late Eocene absolute		
1	UVic	1,600	No ice	Open
2	HadCM3BL	840	No ice	Open
3	UVic	1,600	No ice	Closed
4	GENESIS	1,120	No ice	N/A$^{\Delta}$
5	HadCM3BL	560	No ice	Open
		Early Oligocene absolute		
1	HadCM3BL	840	AIS*	Open
2	GENESIS	1,120	AIS*	N/A$^{\Delta}$
3	HadCM3BL	560	AIS*	Open
4	FOAM	560	EAIS	Open†
5	FOAM	560	Small EAIS	Open†
		EOT change		
1	HadCM3BL	840 – 560	No ice – AIS*	Open – Open
2	HadCM3BL	840 – 840	No ice – AIS*	Closed – Closed
3	HadCM3BL	560 – 560	No ice – AIS*	Closed – Closed
4	HadCM3BL	840 – 560	No ice – AIS*	Closed – Closed
5	HadCM3BL	560 – 560	No ice – AIS*	Open – Open
		Late Eocene absolute + EOT change + Early Oligocene absolute		
1	HadCM3BL	840 – 840	No ice – AIS*	Open – Open
2	HadCM3BL	840 – 560	No ice – AIS*	Open – Open
3	GENESIS	1,120 – 1,120	No ice – AIS*	N/A$^{\Delta}$
4	HadCM3BL	560 – 560	No ice – AIS*	Open – Open
5	FOAM	1,120 – 560	No ice – small EAIS	Open† – Open†

Notes:

**AIS resembles an EAIS configuration, it is the only configuration available for these models*

$^{\Delta}$*GENESIS Drake Passage is listed as N/A as it does not have a dynamic ocean*

†*This is the only gateway configuration for this model*

4.5. Discussion

This model-data comparison shows that the most realistic representation of the high latitude Southern Hemisphere climate before, after and across the EOT would be simulated by an expansion of an AIS, possibly with some combination of atmospheric pCO_2 decline. However, there is still clear room to improve the models' performance relative to the data. For the late Eocene and early Oligocene, generally the models provide a better representation of the relative spatial patterns of temperature (i.e. for the normalised RMSE metric) compared to the absolute temperatures (i.e. for the standard RMSE metric). Given that the simulations were run with relatively arbitrary orbital configurations and pCO_2 levels (although they are of a plausible magnitude; Pearson et al., 2009; Pagani et al., 2011; Foster et al., 2017), it is perhaps unsurprising that the absolute temperature values are not a good fit for the data. It could be possible to attempt to scale the modelled temperature assuming a linear fit between the few pCO_2 levels simulated here (as was carried out in the model-data comparison for an upcoming review paper; Hutchinson et al., in prep.). However, this would still provide just a simple approximation of the climate as it would not account for non-linear responses. A more rigorous model-data comparison would vary the pCO_2 levels by more subtle increments, but this would require significantly greater computing resources.

However, despite these limitations in the modelled absolute temperature before and after the EOT, incorporating this information into the comparison influences which simulation pairs are identified as best at representing how the climate might have changed across the EOT. Without accounting for the absolute data, simulation pairs with a closed Drake Passage perform well, whereas for the absolute data these simulations perform poorly.

The marked reduction in performance by HadCM3BL and UVic when the Drake Passage is closed supports the conclusions of Goldner et al. (2014) that changes in ocean gateways around the EOT are not the best way to describe the changes observed in the proxy record. This is in support of the general shift in consensus away from the gateway hypothesis as the cause of the changes at the EOT, at least in terms of the direct climatic implications (DeConto & Pollard, 2003a; Huber & Nof, 2006; Sijp et al., 2011; Ladant et al., 2014a etc.). There is inconclusive evidence in the literature for fundamental changes in Drake Passage around the EOT (e.g. Lagabrielle et al., 2009 and references therein), in agreement with the Getech palaeogeographic reconstructions, which have the gateway open throughout the period (see Supplementary Figure 3.1). Proxy evidence and reconstructions suggest the Tasman Seaway changed close to the EOT (e.g. Stickley et al., 2004;

Scher et al., 2015) and it could be of interest to focus on this gateway with future model comparisons.

The better fit with proxy data by FOAM when the AIS is not at its full extent also would be consistent with the other glaciological evidence presented in Section 4.3. Various sites showed the maximum EOT expansion occurring around ~32 Ma (Olivetti et al., 2015; Galeotti et al., 2016), significantly after the EOT, while sedimentological evidence from the Weddell Sea suggests that region of West Antarctica was not fully glaciated until much more recently (~15 Ma; Huang et al., 2014). If this climatic fingerprint of a smaller AIS is robust, given that this signal already appears to be present in the data even with only limited site locations, there could be potential in future work to be able to constrain the extent of the AIS using only a climate model and proxy temperature records, which could then be used to independently verify other estimates from ice sheet modelling or proxy estimates using $\delta^{18}O$.

Preliminary results using the HadCM3BL simulations from the boundary condition ensemble from Chapter 3 (those with the Getech palaeogeographic reconstructions; Section 3.2.2) also show a similar result, with simulations with a smaller EAIS fitting the data better (figure not shown). However, as was shown in Figure 3.4, these simulations are potentially not properly spun-up and so they are not included in the analysis of this chapter. It should be noted that the FOAM simulations have a relatively short spin-up of 2,000 years (Table 4.1) and without deeper investigation into the time series of the model spin-up, it is not possible to say if this model is yet fully in equilibrium.

4.5.1. Changes in the latitudinal temperature gradient

A major concern identified in the model-data comparison is that the simulation pairs for all models do a poor job at recreating the change across the EOT compared to the latitudinal gradient benchmark or even the constant mean benchmark. This suggests that these simulation pairs are having issues recreating the latitudinal profile of temperature that is indicated by the data. The zonal mean temperature for each of the best pairs of simulations from HadCM3BL, GENESIS and FOAM (across all three time slices) are shown in Figure 4.8 along with the proxy records previously plotted in Figure 4.4.

Generally for the late Eocene, the latitudinal gradients produced by all of the models are reasonably similar to the gradient shown in the proxy records, although the models generally have

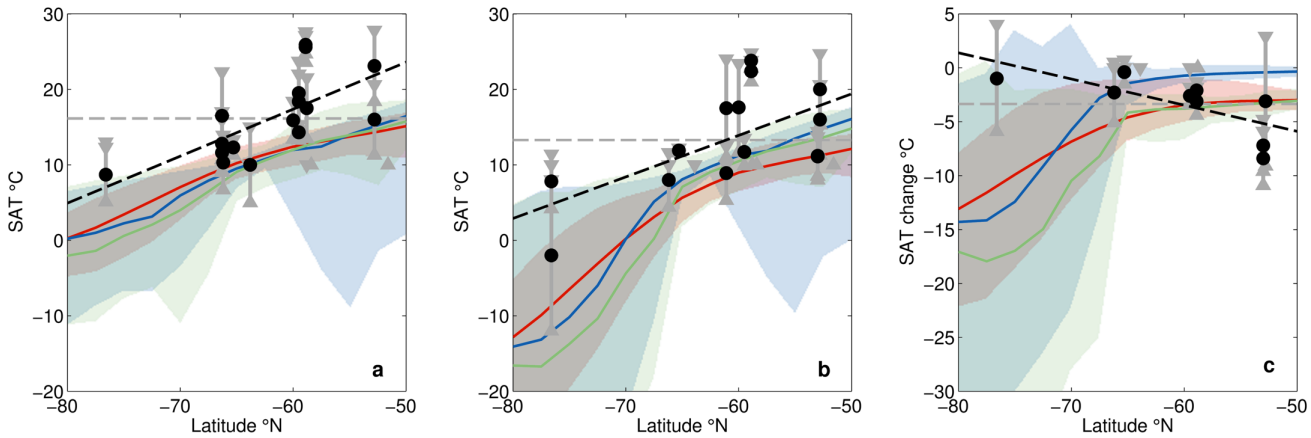

Figure 4.8: Zonal mean temperature profiles for the best HadCM3BL (green), GENESIS (blue) and FOAM (red) simulation pairs compared to the data for the a) late Eocene, b) early Oligocene and c) EOT time slices respectively. Shading around the zonal mean shows the maximum and minimum range for that latitude; black and grey markers show the proxy record mean values and uncertainty ranges respectively (the same data as Figure 4.4).

a cold bias of around 5 °C (Figure 4.8a). As discussed previously, however, it is unsurprising that there is some absolute bias as the pCO_2 levels used in the simulations are relatively arbitrary. For the early Oligocene, this cold bias generally reduces between 50-65 °S to ~2-3 °C; however, all models show an inflection in their latitudinal gradients around 65 °S (Figure 4.8b). Between 65-80 °S there is a steeper latitudinal gradient, which fits only with the relatively uncertain vegetation temperature reconstruction for the Ross Sea during this period (Raine & Askin, 2001). The S-index record for the Ross Sea suggests much warmer temperatures for the region (Passchier et al., 2013). The cooler zonal mean temperatures in the models between 65-80 °S are due to the presence of the AIS having a cooling effect through albedo and elevation changes, as discussed in Chapters 2 and 3. However, even the warmer S-index record lies close the maximum limit of temperature for that latitude for the HadCM3BL and GENESIS simulations (latitudinal maximum and minimum range for each model showed by the coloured shading), suggesting that these models do find some localised areas that are consistent with the data at that latitude.

The zonal mean of the modelled change in temperature across the EOT is very different from the proxies for all models. From 50-65 °S, the HadCM3BL and FOAM simulations are mostly in agreement with the mean change observed in the proxy records, while GENESIS shows slightly less cooling (closer to zero change, as the best GENESIS pairing did not have a pCO_2 drop). However, south of 65 °S there is a strong increase in cooling with poleward latitude, again due to the cooling effect of the ice sheet. All models suggest zonal mean cooling in the range of 11-18 °C at 75 °S while at the Ross Sea site the S-index proxy suggests only minor cooling of 1 ±5 °C

(Passchier et al., 2013). The vegetation records would suggest greater cooling at this site but given the extremely large uncertainty in this proxy (Francis & Hill, 1996; Raine & Askin, 2001), this data point is not trusted for the comparison.

Critically assessing the proxy records that are included in the compilation could explain some of the differences between the records and the models. Although the dataset used here was as large as could be compiled at the time of writing, there are still large gaps spatially and temporally with no data. A number of the proxies, such as the absolute temperature estimates based on vegetation, have extremely high uncertainties and cannot necessarily be used to constrain the temperature change across the EOT. It is also unclear as to what area the terrestrial proxies such as the S-index represent. It is possible the sites around the Ross Sea are part of very localised microclimates, which are not representative of the large areas covered by a model grid cell.

Similarly, as noted in Section 4.3.4, the particular gradient of the EOT change as recorded in the data may be partly due to some extreme values that are included in the compilation. For example, the strong cooling at the Falklands Plateau (Liu et al., 2009; Plancq et al., 2014) is significantly greater than any cooling recorded at any other Southern Ocean site, or at any other site in the Atlantic more broadly (Liu et al., 2009; also see Figure 3.6 of Chapter 3). This major cooling is hard to explain by any large-scale oceanic process. Even if there were to be a shift in the ACC and the Antarctic convergence, resulting in cold Southern Ocean waters reaching the site, surface waters 8 °C cooler lie more than 15 ° further south. As a result, the model simulations presented here would suggest that the major cooling that occurred at this site (assuming it is not due to some other error or bias in the record processing) is due to a highly localised feature, such as becoming influenced by an upwelling of cold deep water. Such a feature is below the resolution of these models and cannot be expected to be captured.

A second option that could partly explain the model-data discrepancy is that that the local-regional scale warming signals in response to Antarctic glaciation shown in Goldner et al. (2014), Knorr & Lohmann (2014), various HadCM3BL simulations (e.g. Kennedy et al., 2015; Figure 3.1) and some of the FOAM simulations used here from Ladant et al. (2014a; shown in Figures 4.9) due to enhanced circulation, deep water formation and sea ice feedbacks are robust, and this could be compensating for some of the cooling. When this warming is combined with a pCO_2 decline, the models do suggest that some very localised areas (i.e. < 5 grid cells) show little cooling or even warming, while other regions around the world cool more (figure not shown). This could at least be consistent with the data around 65 °S, with the single higher latitude site in the Ross Sea perhaps being misleading. Further data at very high latitude sites might show greater cooling, more

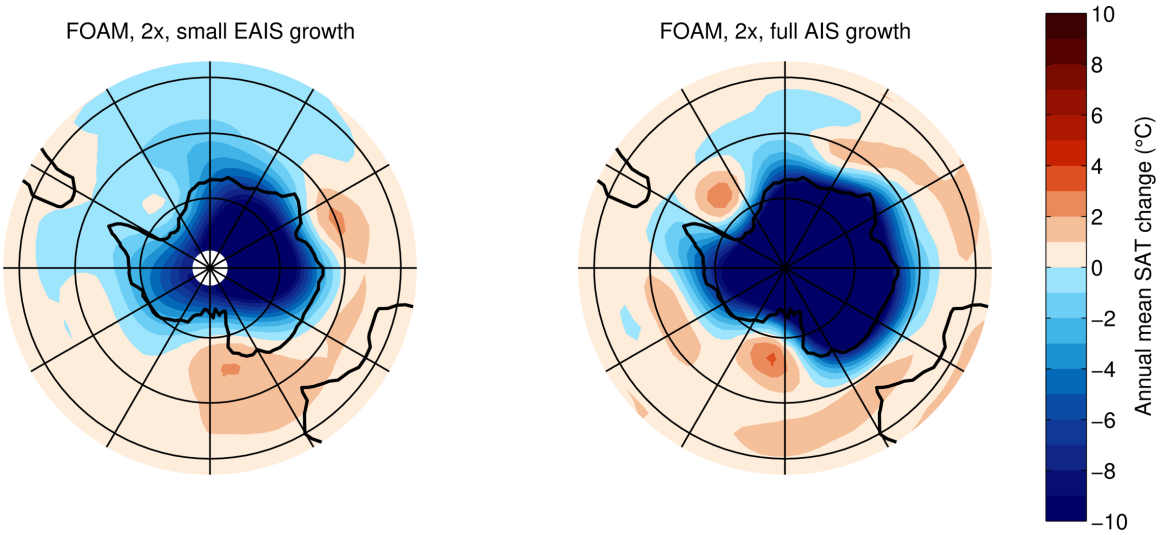

Figure 4.9: Changes in sea surface/surface air temperature (°C) for two FOAM simulation pairings with some ice growth at constant pCO_2 levels.

consistent with the generalised latitudinal temperature profiles suggested by the models in Figure 4.8c. It is therefore possible that the models are producing a qualitatively realistic result, however they do not get the location to match the proxy datasets. An issue with this hypothesis is that the modelled warming with glaciation was shown in Chapter 3 to be largely reduced with increasing spin-up, suggesting a similar effect could negate the at least some of the warming found in the other models (with the spin-up lengths of Goldner et al., 2014, Knorr & Lohmann, 2014 and Ladant et al., 2014a all ranging between 2,000-3,500 years).

A third factor that could be affecting the localised climate near the Antarctic margin recorded at the Ross Sea site could be isostatic changes. In Figure 4.8c the maximum range of the GENESIS simulation pairs shows the least cooling and even showing some warming between ~70-75 °S. This is broadly related to changes in the palaeogeographic reconstruction of the glaciated simulation, as shown in Figure 4.10, which suggests an isostatic depression of the topography around some margins of the ice sheet (Figure 4.10a), with the resultant drop in altitude resulting in warming due to the lapse rate effect (Figure 4.10b). Over all model grid points (interpolated to HadCM3BL resolution), there is a strong altitude-temperature relationship, as shown in Figure 4.10c. For the gird cells that show warming, shown in Figure 4.10d, the altitude-temperature relationship is not as clear, with some grid cells showing strong warming but also increasing in height; however, this is possibly due to an interpolation issue as the topography and modelled climate were initially on different resolution grids. It is possible that the relatively low cooling in the Ross Sea proxy records could reflect a localised factor such as this.

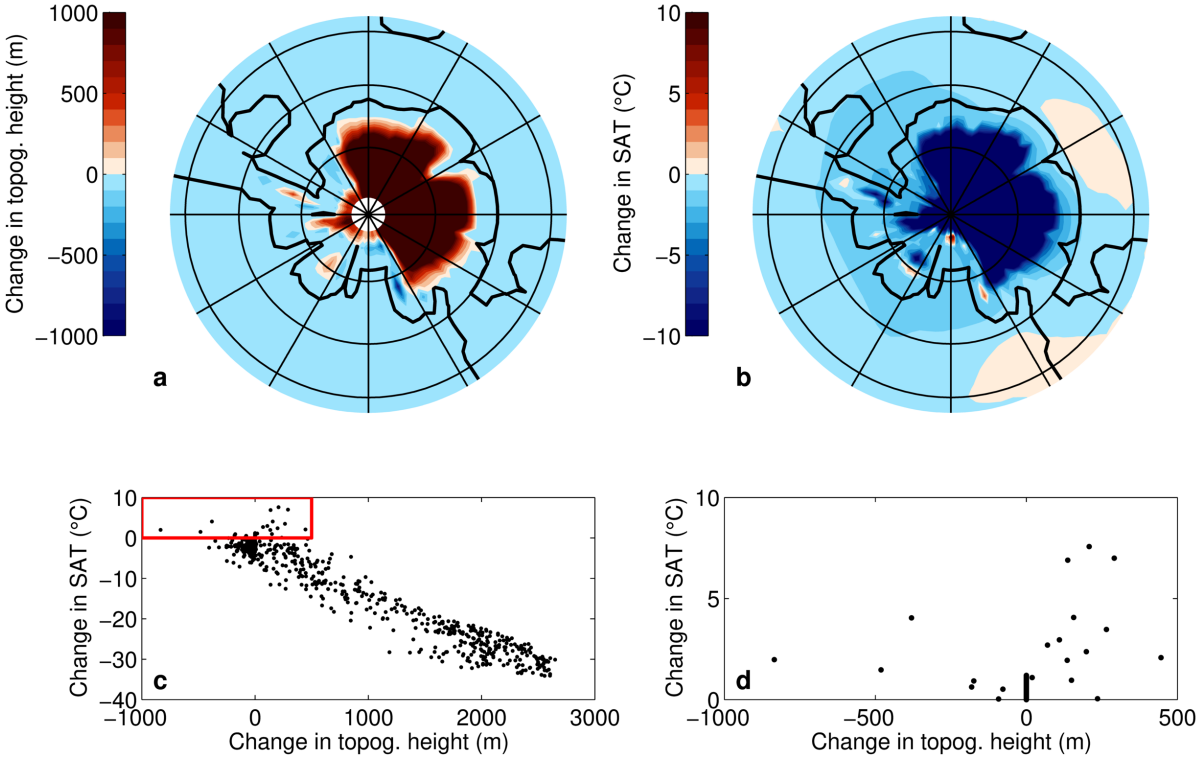

Figure 4.10: a) Changes in the topographic height (m) used in the GENESIS simulations between the glaciated and unglaciated simulations; b) Change in surface air temperature (°C) between the glaciated and unglaciated GENESIS simulations at high pCO_2; c) Changes in surface air temperature with changing topographic height globally; d) as (c), enlarged to the area in the red box.

A final important consideration is that the temporal averaging of the dataset carried out here could be inappropriate. A number of studies referenced in Section 4.3 suggested there was cooling in the several million years prior to the EOT, particularly at high latitudes (e.g. Raine & Askin, 2001; Petersen & Schrag, 2015; Passchier et al., 2016; Carter et al., 2017; Pound & Salzmann, 2017). Even in the high Northern Hemisphere changes have been identified occurring prior to the EOT (e.g. Coxall et al., 2018). These changes could all have a range of different forcings; however, it is possible that some of them are related. Even a global forcing such as atmospheric pCO_2 decline could potentially have a signal that is shown first at higher latitudes. If there is polar amplification of the cooling signal (as was shown in Figure 3.4), and if there is a threshold of magnitude at which temperature changes could be identified in the proxy record (or other elements of the Earth system start to respond to the temperature change; e.g. changes in vegetation, weathering or precipitation), then even with a gradual decline in pCO_2 there could appear to be temporal heterogeneity in the response.

If cooling started near the poles prior to the EOT and propagated equatorwards, it is likely that the Ross Sea site also experienced cooling prior to the EOT. This would support evidence of some tundra vegetation in the region recorded prior to the EOT (Raine & Askin, 2001). It therefore might be necessary to include older records and further split the dataset into additional time slices to capture the climate of Antarctica before any cooling occurred. The only record of this age included in the current dataset is the McMurdo erratic, which suggested temperatures of less than 13 °C (Francis et al., 2009); however, the original location of this fossilised section is unknown and it could represent an area further south or at higher altitude, and thus introduce a cold temperature bias and is not suitable to use in isolation.

Currently, the data compilation is not big enough at this stage to allow for such analysis to be carried out; however, this could potentially offer a more appropriate comparison with the equilibrium climate model simulations used here, which are broadly 'warm and ice-free' or 'cool and glaciated'. If this hypothesis is correct, if more comparable records were included for the period pre-cooling and glaciation (e.g. dating from 40 Ma), it is possible that the high latitude change across the EOT would be greater than that which is shown in Figure 4.8, closer in line with the model simulations.

4.6. Conclusions and future work

An extensive review of temperature proxy records for the high latitude Southern Hemisphere region before, after and across the EOT was presented and used to evaluate model simulations of the EOT. These simulations came from four different GCMs with different sets of boundary conditions. The best simulations were able to capture spatial patterning of absolute temperature recorded in the late Eocene and early Oligocene proxy datasets. The performances were not as good for the dataset of relative changes across the EOT, due to the models inadequately capturing changes in the latitudinal gradient shown by the data. The latitudinal gradients shown by the data are possibly related to the paucity of data in certain regions (particularly at very high latitude), the time averaging of the proxy records into time slices (with some of the higher latitude changes possibly occurring prior to the EOT), localised climatic effects (e.g. ocean upwelling or isostatic changes) or possibly because the glaciation of Antarctica results in some localised warming that approximately balances the general cooling across the EOT (e.g. due to pCO_2 decline). If the latter in the case, it would qualitatively support the conclusions found in Chapters 2 and 3 of this thesis, as well as by multiple other models (Goldner et al., 2014; Knorr & Lohmann, 2014; Ladant et al., 2014a). If this is correct, the poorer results in the model-data comparison carried out here may be because the models are simply mis-identifying the areas where the warming occurs.

The best pairs of simulations for modelling the absolute temperatures and relative changes were found by assessing the individual simulations' performance across all time slices for various metrics. This suggests that the best simulations for representing the EOT were by HadCM3BL with an open Drake Passage, AIS expansion and possibly a drop in atmospheric pCO_2 levels. The poorer fit with the data for the late Eocene and early Oligocene when the Drake Passage is closed suggests the gateway was open for the duration of this period, and so the opening of the Drake Passage was an unlikely driver of the EOT (in agreement with the results of DeConto & Pollard, 2003a; Goldner et al., 2014 etc.). This result was particularly pronounced in the HadCM3BL simulations. The UVic model also had worse performance when the Drake Passage was closed, but the difference was not as great.

The performance of FOAM for the early Oligocene time slice was better with smaller ice sheet configurations over Antarctica, potentially in agreement with proxy records of ice volume and extent (e.g. Bohaty et al., 2012; Huang et al., 2014; Galeotti et al., 2016). A similar finding is also seen in the HadCM3BL simulations using the Getech palaeogeographies (not shown); however, as these simulations could be affected by a lack of spin-up, they were not included in the analysis.

Further spinning-up those HadCM3BL simulations with multiple ice sheet sizes could provide some interesting insights into whether this climatic fingerprint of a smaller AIS is robust.

An important consideration in interpreting this model-data comparison is the relative paucity of data available for the region during the EOT, in combination with records generally showing heterogeneous temperature patterns. Particularly for the normalised RMSE, an important measure for determining if the model is showing the correct spatial patterns, there are only a handful of sites which can be used across all sectors of the Southern Ocean. With the relatively limited data coverage available here, it is possible that these latitudinal profiles could be biased by anomalous values. To attempt to account for this uncertainty, this model-data comparison could be repeated, systematically omitting different sites or proxy data points. However, as noted in Section 4.3.4, this was done for the calculation of the latitudinal gradient in the change across the EOT, with all permutations still showing a negative slope. Based on these provisional results, this kind of analysis would not be expected to fundamentally affect the model-data comparison across the EOT.

Future research by the palaeoclimate community will inevitably produce new records in new locations, potentially correcting older, spurious results or having an impact on the inferred spatial patterns shown in the proxy record. Future work on the research carried out here towards publication could improve the consistency of the data used, for example in terms of using the same proxy calibrations, age models and definitions of uncertainty. Additionally, future work can also expand upon this analysis by including more model simulations and trialling other metrics and scoring techniques. The challenge in synthesising the many changes that occurred in this highly uncertain region across the EOT is huge, but this chapter shows that with increased modelling and proxy data results, some convergence of ideas within the palaeoclimate community appears possible.

Chapter 5: Concluding thoughts

5.1. Conclusions from this research

This research set out to address a series of core and sub-research questions:

- What impact does the Antarctic ice sheet have on regional and global climate?
  - How does the impact of glaciation vary between two different palaeogeographic reconstructions?
  - How does the island definition in the model affect the climatic responses shown?
  - Why do the results differ from those of Hill et al. (2013) in terms of the change in Antarctic Circumpolar Current flow in response to Antarctic glaciation?

- How sensitive are palaeoclimate model simulations to subtle changes in boundary conditions?
  - What are the impacts and relative importance of three forcings on global and Antarctic climate at the EOT (including pCO_2 drop and palaeogeographic change)?
  - For each of these forcings, what is the range of uncertainty in the magnitude of certain modelled variables resulting from differences in the model boundary conditions?
  - How does the simulation spin-up time affect the modelled impacts associated with these forcings?

- How did the high latitude Southern Hemisphere climate change across the Eocene-Oligocene Transition?
  - What are the spatial patterns of temperature change inferred from proxy records for the high Southern Hemisphere before, after and across the EOT?
  - Which GCMs and model boundary conditions give the best fit to a range of qualitative and quantitative proxy records of temperature before, after and across the EOT?

Framed against a background of research into the Eocene-Oligocene Transition (EOT), the three results chapters of this thesis each address one of the core questions and its sub-research questions.

The first question was addressed in Chapter 2 by using equilibrium climate simulations with and without an Antarctic ice sheet (AIS) and described the processes through which the AIS can affect the Earth's climate and oceans. The results suggested that for some palaeogeographic reconstructions it is possible to greatly warm the Southern Ocean by including an ice sheet, or more correctly that it is possible to generate very cold Southern Ocean states (particularly in the Ross Sea) when Antarctica is ice-free. Although the exact results presented in Chapter 2 (Kennedy et al., 2015) were shown to be affected by the island definition of Antarctica in HadCM3BL, the modelled response mechanisms described in Kennedy et al. still appear plausible and relevant for a situation with a very narrow Tasman Seaway. Other model simulations with HadCM3BL were shown in Chapters 2 and 3 to behave in a similar way, even with the correct island definition used, and other studies using different climate models show qualitatively similar responses to those presented in Kennedy et al. (e.g. Goldner et al., 2014; Knorr & Lohmann, 2014; Ladant et al., 2014a). While the data compilations used in Chapter 4 do not strongly support this Southern Ocean warming, they do suggest limited cooling in the high latitude Southern Ocean, possibly indicating a similar process could be occurring in tandem with other cooling mechanisms (such as declining atmospheric pCO_2).

The model dependence of the results and the idealised nature of the experiment shown in Chapter 2 mean it is hard to definitively show the exact and comprehensive impact of the AIS on global climate. It is also vital to separate the reality of the Earth's climate system from what is represented in a model and, as such, modelling alone cannot 'prove' an answer to this research question. However, the work in this thesis builds on previous research by expanding the analysis with many more model simulations, to show that the responses described are at least not simulation specific.

Additionally, an important technical conclusion from Chapter 2 is to ensure that the island definition used in HadCM3BL is correct for palaeogeographies. Although the exact implications are not comprehensively investigated, it is shown that incorrect island definition can have a fundamental impact on the ocean circulation once an ocean gateway becomes narrower than two grid cells. This makes it very hard to realistically model subtle changes in ocean gateways, such as those on the scale described by Stickley et al. (2004) for the Tasman Seaway at the EOT. Higher resolution modelling could be a solution for this issue but would require a step back in terms of how long the simulations could be run for, potentially introducing issues with the model being insufficiently spun-up and thus being far from equilibrium.

Finally, differences in the findings of Kennedy et al. (2015) and Hill et al. (2013) in terms of the impact of Antarctic glaciation on the strength of the (proto-) Antarctic Circumpolar Current were

reconciled by investigating differences in the spin-up of the model simulations used in the two studies. Although the published results of Hill et al. show a small reduction in flow through the Drake Passage when an ice sheet is added to the model, the simulations used in that study had quite markedly different lengths of spin-up. Continuations of the Hill et al. simulations with a comparable length of total spin-up for both the ice-free and glaciated simulations show a response similar to that shown by Kennedy et al., with increasing flow through the Drake Passage in the presence of an AIS.

The second core research question was designed to test the validity of the results of Kennedy et al. (2015) by expanding the number of simulations carrying out qualitatively similar experiments. Model simulation pairs were shown to vary significantly in their response to similar forcings, with high latitude oceans where there is deep water formation shown to be the most uncertain regions. It is therefore unsurprising that the results in Kennedy et al. for two different palaeogeographies vary so greatly in the temperature response for the Ross Sea and Southern Ocean. Chapter 3 presents the mean response of all simulation pairs for each forcing and aims to quantify the uncertainty of this mean climate state using a *t*-distribution. This bases the uncertainty on the standard error and assumes the climatic response has a normal distribution, requiring the climatic response to be approximately linear. This may not be the case for the high latitude oceans where the many feedback mechanisms associated with deep water formation may result in a non-linear or multi-stable climate state. However, this would likely cause the uncertainty presented here to be an underestimation, meanwhile other methods of expressing the variability in the response which do not assume linearity (such as the range in responses) also show similar spatial patterns of uncertainty.

Three forcings of the climate were investigated: AIS expansion, palaeogeographic change and pCO_2 reduction. In terms of the mean annual temperature response to these forcings, pCO_2 reduction showed the greatest cooling globally and for all regions. AIS growth and palaeogeographic change both showed a mixed cooling and warming signal, with palaeogeographic change generally producing warmer temperatures throughout the Southern Hemisphere. When compared to a collection of sea surface temperature proxy records from around the world, the pCO_2 reduction (or pCO_2 reduction in combination with AIS growth) gave the best fit between the data and the model, while AIS growth in isolation and palaeogeographic change generally poorly fitted the data.

A second important conclusion from this work is that the uncertainty in a single model simulation (or pair of model simulations if looking at a forcing and climate response) can vary significantly in

space as a result of subtle changes in the model boundary conditions. Consequently, a degree of scepticism should be taken when interpreting the results of a single simulation or model setup. Additionally, this chapter concluded that the length of the model spin-up can radically affect the modelled climate response to forcings, with the response to Antarctic ice growth shown to be significantly different in simulations 1,000 years into their spin-up compared to once they are more fully equilibrated (>6,000 years into their spin-up). This presents a great challenge to palaeoclimate modelling research in general, showing both long simulations and wider sampling of boundary conditions are important.

Finally, the third core research question could not be addressed by modelling alone due to the high uncertainty shown in the model for this region. Instead, this was addressed by drawing together previously published proxy data records for the high latitude Southern Hemisphere to use in conjunction with the fully spun-up model simulations from Chapter 3 and simulations using different models from other research groups. The proxy data was compiled into time slices for the late Eocene absolute temperature, early Oligocene absolute temperature and the relative change in temperature across the EOT. Records were reasonably heterogeneous with the largest changes of ~8 °C across the EOT (Liu et al., 2009; Plancq et al., 2014) and other changes of less than 1 °C (Petersen & Schrag, 2015). The cooling across the EOT was found to be lesser at higher latitudes and greater at lower latitudes. This could have been partly due to issues with the data; for example, due to the paucity of records in certain locations biasing the trends to single (potentially anomalous) points, due to proxies recording highly localised signals (again biasing the recorded patterns), or due to the simplification of compiling the data into time slices, resulting in a loss of temporal variability with many records suggesting changes occurring prior to the EOT (e.g. Petersen & Schrag, 2015; Carter et al., 2017; Pound & Salzmann, 2017). However, the observed latitudinal temperature change across the EOT could also qualitatively support the results shown in Chapter 2 that there can be warming (or at least limited cooling) in response to Antarctic ice growth (also shown by various other climate models; e.g. Goldner et al., 2014; Ladant et al., 2014a; Knorr & Lohmann, 2014). Although the models do not match the exact spatial variability of the data shown here, it is possible they are showing a realistic result in terms of the mechanisms behind the response, but just in the wrong location.

HadCM3BL performed the best across all three time slices (i.e. in terms of capturing both the absolute and relative changes) when the Drake Passage was open and the AIS expanded possibly in combination with a drop in atmospheric pCO_2. This suggests that based on this data, a drop in pCO_2 seems to be a more realistic driver of the EOT rather than an opening of the Drake Passage, in support of previous work (e.g. DeConto & Pollard, 2003a; Huber & Nof, 2006; Goldner et al.,

2014). The other models showed similar results, with GENESIS showing the best fit to data without a drop in pCO_2, FOAM showing the best fit with a drop in pCO_2 and expansion of a small AIS and UVic also performing worse for the late Eocene when the Drake Passage was closed. Based on these conclusions, it appears that the 'CO_2 hypothesis' is the more likely driver of the changes observed across the EOT, not the traditional 'gateway hypothesis'.

5.2. Outlook for future research

Future work could expand this analysis from both the proxy data and model sides of the comparison. Further data points could be included as they become available, meanwhile greater consistency across proxy records in terms of calibrations used, age models and method of quantifying their uncertainty could remove the potential for spurious temperature signals between sites. From the modelling perspective, the results of Chapter 3 show that ideally more simulations should be run to verify the conclusions as to which boundary condition combinations (i.e. open or closed Drake Passage, high or low pCO_2) give the best fit to the data in this highly sensitive region. Additionally, the results from other GCMs could be included (e.g. Goldner et al., 2014; Hutchinson et al., 2018; Baatsen et al., 2018a) to investigate if they find comparable results to the models evaluated here. Due to the time commitment these tasks would take however, they are beyond the scope of this thesis.

There are also other indirectly related fields of inquiry that pose interesting questions for future EOT research.

In terms of climate modelling, interesting questions not addressed in this thesis include the impact of ocean gateways in the Northern Hemisphere. Preliminary results using HadCM3BL suggest that connections into the Arctic ocean can have an impact on ocean overturning in the North Atlantic and Southern Ocean (University of Bristol Masters thesis by Li, 2017), potentially impacting on regional temperatures. Modelling studies by other research groups have suggested similar important effects of the connection to the Arctic (e.g. Hutchinson et al., 2018; Vahlenkamp et al., 2018) and this could explain changes in the North Atlantic proxy records observed for this period (e.g. Coxall et al., 2018). Some additional simulations are underway at the University of Bristol continuing on the simulations used in Li (2017), although as shown in this thesis, clearly it would be beneficial to greatly expand the boundary conditions sampled and ensure that these simulations are all adequately spun-up.

Additionally, increased coupling of the climate model with other elements of the Earth system clearly offers the best method to fully understand the changes occurring at the EOT. For example, coupling with a carbon cycle model (e.g. Lefebvre et al., 2013; Fyke et al., 2016) helps to properly explain the driving effect on atmospheric pCO_2, rather than taking it as a forcing which is a large idealisation in the simulations used here. Alternatively, simpler relationships with the carbon cycle or carbon cycle models could be investigated offline from climate model simulations to suggest

plausible mechanisms for the drawdown of atmospheric pCO_2 around the EOT (e.g. Armstrong McKay et al., 2016; Elsworth et al., 2017).

Coupling with an ice sheet model (which themselves vary significantly in complexity) would also be necessary to further explore the exact response of the climate across the EOT, potentially allowing (semi-)transient simulations which could be compared to the data used in Chapter 4 without aggregating it into time slices. However, this would require a significant increase in computational power. Various statistical approaches could be utilised to sample the variety of changes that possibly occurred across the EOT without explicitly modelling them in transient simulations, such as the matrix or emulator approaches used in other studies to drive ice sheet models with a varying climate (e.g. Pollard et al., 2013; Ladant et al., 2014a; Lord et al., 2017). This provides a feasible mechanism for exploring the links between ice sheets and climate across the EOT, and with only limited examples of this with a few models used in the literature, there is plenty of scope for other modelling groups, such as at the University of Bristol, to explore these methods.

Standalone, offline ice sheet modelling could also provide some interesting new insights into the early AIS, as this field is always developing. Although not included in this thesis, a significant amount of time was spent assessing the viability of using a state-of-the-art ice sheet model, BISICLES (Cornford et al., 2013), to model the early AIS, with results presented at the International Conference on Paleoceanography (Utrecht, 2016) and American Geophysical Union Fall Meeting (New Orleans, 2017). The proxy database complied here in Chapter 4 was originally intended that it could also incorporate variables to validate ice sheet models and could yet be expanded for this purpose.

BISICLES models the flow of ice, with its unique feature being that it has an adaptive mesh resolution (Cornford et al., 2013). This allows it to model certain features in extremely high resolution where that is necessary, for example near to the grounding line or along ice streams where local shear stresses become important, whereas the slow-moving interior can be modelled at lower resolution and thus save computing time (Cornford et al., 2013). While a model like BISICLES will not fundamentally change our understanding of when or where snow might accumulate over the interior of Antarctica with a cooling climate (as it uses the same snow accumulation equations as most simpler models), its improved resolution of ice flow dynamics could impact how the early AIS could expand or collapse following its initiation at the EOT. This could potentially affect our understanding of hysteresis in the feedbacks between the Earth's climate and ice sheets (Pollard & DeConto, 2005).

The issue with this model is that it has extremely high data requirements to produce realistic results, for example in terms of the basal topography or ice sheet size, with modern day and future simulations tuned through inverse modelling to fit the best data available (e.g. Cornford et al., 2016). Preliminary experiments attempting to model the modern day AIS but with reduced data quality similar to that available for the EOT suggested the uncertainties were unfeasibly large to produce meaningful results with BISICLES at this stage. Improving the availability of quality data is the main challenge in utilising state-of-the-art models such as this for such a deep-time period.

There are still great uncertainties remaining in palaeoclimate and paleo-ice sheet research over what happened even during the Pleistocene glacial cycles (Clark et al., 2006; Masson-Delmotte et al., 2010). Given the amount of unknown variables for deeper-time periods such as the EOT, in what remains an ice covered, inhospitable region, the challenge in fully understanding the nature of the early AIS will present a considerable task for many years to come.

5.3. *Terra Australis Incognita*

The Earth system holds complexity beyond the realms of the human imagination or the greatest computing power. Grappling with their understanding of this world, cartographers centuries ago put together the pieces of information they had and used artistic license to fill in the unmapped gaps that explorers had yet to reach. From the 17th Century, this map by Blaeu includes the *Terra Australis Incognita*, or 'Unknown Southern Continent'. While modern science would not approve of such guess work, purely by chance, the connection between Australia and Antarctica is remarkably similar to early Eocene palaeogeographic reconstructions.

Exploring the history of the Earth system, is an equal step into the unknown, with palaeoceanographers and palaeoclimatologists having to build the picture around what limited information they have. From 1646, when Blaeu's map was published, it was a further 174 years before the first humans saw the Antarctic continent. Now, nearly 200 years on from that first sighting, the Unknown Southern Continent still holds many secrets.

Figure 5.1: A section of the map by Blaeu (1645-1646), showing the as yet uncharted and hence imagined *Terra Australis Incognita*. Image courtesy of Special Collections, University of Bristol Library.

References

Abernathey, R., Marshall, J. & Ferreira, D. 2011. The Dependence of Southern Ocean Meridional Overturning on Wind Stress. *Journal of Physical Oceanography*, 41, pp. 2261-2278, DOI: 10.1175/JPO-D-11-023.1.

Alley, R.B., Clark, P.U., Huybrechts, P. & Joughin, I., 2005. Ice-sheet and sea-level changes. *Science*, 310, pp. 456-460, DOI: 10.1126/science.1114613.

Allison, L.C., Johnson, H.L., Marshall, D.P. & Munday, D.R. 2010. Where do winds drive the Antarctic Circumpolar Current? *Geophysical Research Letters*, 37, L12605, DOI: 10.1029/2010GL043355.

Anderson, J.B., Warny, S., Askin, R.A., Wellner, J.S., Bohaty, S.M., Kirshner, A.E., Livsey, D.N., Simms, A.R., Smith, T.R., Ehrmann, W., Lawver, L.A., Barbeau, D., Wise, S.W., Kulhanek, D.K., Weaver, F.M. & Majewski, W., 2011. Progressive Cenozoic cooling and the demise of Antarctica's last refugium. *Proceedings of the National Academy of Science*, 108, 39, pp. 11356-11360, DOI: 10.1073/pnas.1014885108.

Arakawa, A. & Lamb, V. R., 1977. Computational Design of the Basic Dynamical Processes of the UCLA General Circulation Model. In: General Circulation Models of the Atmosphere, edited by: Chang, J., Vol. 17, *Methods in Computational Physics: Advances in Research and Applications*, pp. 173–265, Elsevier, DOI: 10.1016/B978-0-12-460817-7.50009-4.

Armstrong, E., Valdes, P., House, J. & Singarayer, J., 2017. Investigating the Impact of CO2 on Low-Frequency Variability of the AMOC in HadCM3. *Journal of Climate*, pp. 7863-7883, DOI: 10.1175/JCLI-D-16-0767.1.

Armstrong McKay, D.I., Tyrrell, T. & Wilson, P.A., 2016. Global carbon cycle perturbation across the Eocene-Oligocene climate transition. *Paleoceanography*, 31, pp. 311-329, DOI: 10.1002/2015PA002818.

Askin, A.R. & Raine, J.I., 2000. Oligocene and Early Miocene Terrestrial Palynology of the Cape Roberts Drillhole CRP-2/2A, Victoria Land Basin, Antarctica. *Terra Antarctica*, 7, 4, pp. 493-501.

Assmann, K.M. & Timmermann, R. 2005. Variability of deep water formation in the Ross Sea. *Ocean Dynamics*, 55, pp. 68-87, DOI: 10.1007/s10236-004-0106-7.

Baatsen, M.J.L., van Hinsbergen, D.J.J., von der Heydt, A.S., Dijkstra, H.A.; Sluijs, A., Abels, H.A. & Bijl, P.K., 2016. Reconstructing geographical boundary conditions for palaeoclimate modelling during the Cenozoic. *Climate of the Past,* Volume 12, pp. 1635-1644, DOI: 10.5194/cp-12-1635-2016.

Baatsen, M.J.L., von der Heydt, A.S., Huber, M., Kliphuis, M.A., Bijl, P.K., Sluijs, A. & Dijkstra, H.A., 2018a. Equilibrium state and sensitivity of the simulated middle-to-late Eocene climate. *Climate of the Past Discussions*, DOI: 10.5194/cp-2018-43

Baatsen, M.J.L., von der Heydt, A.S., Kliphuis, M., Viebahn, J. & Dijkstra, H.A., 2018b. Multiple states in late Eocene ocean circulation. *Global and Planetary Change*, 163, pp. 18-28, DOI: 10.1016/j.gloplacha.2018.02.009.

Bamber, J.L. & Aspinall, W.P., 2013. An expert judgement assessment of future sea level rise from the ice sheets. DOI: 10.1038/NCLIMATE1778.

Barker, P.F. & Thomas, E. 2004. Origin, signature and palaeoclimatic influence of the Antarctic Circumpolar Current. *Earth-Science Reviews*, 66, pp. 143-162, DOI: 10.1016/j.earscirev.2003.10.003.

Barker, P.F., Filippelli, G.M., Florindo, F., Martin, E.E. & Scher, H.D. 2007. Onset and role of the Antarctic Circumpolar Current. *Deep Sea Research II*, 54, pp. 2388-2398, DOI: 10.1016/j.dsr2.2007.07.028.

Beerling, D.J. & Osborne, C.P., 2006. The origin of the savanna biome. *Global Change Biology*, 12, pp. 2023-2031, DOI: 10.1111/j.1365-2486.2006.01239.x.

Berger, A., Gallee, H., Fichefet, T., Marsiat, I. & Tricot, C. 1990. Testing the astronomical theory with a coupled climate-ice-sheet model. *Palaeogeography, Palaeoclimatology, Palaeoecology. Global and Planetary Change Section*, 89, 3, pp. 125-141.

Bernard, T., Steer, P., Gallagher, K., Szulc, A., Whitham A. & Johnson, C., 2016. Evidence for Eocene–Oligocene glaciation in the landscape of the East Greenland margin. *Geology*, DOI: 10.1130/G38248.1.

Birkenmajer, K. & Zastawniak, E., 1989. Late Cretaceous–Early Tertiary floras of King George Island, West Antarctica: their stratigraphic distribution and palaeoclimatic significance. In: Crame, J.A. (Ed.), Origins and Evolution of the Antarctic Biota, Geological Society Special Publication 147, pp. 227–240.

Birkenmajer, K., Gaździcki, A., Krajewski, K.P., Przybycin, A., Solecki, A., Tatur, A. & Yoon, H.I., 2005. First Cenozoic glaciers in West Antarctica. *Polish Polar Research*, 26, 2, pp. 3-12.

Blackmon, M. et al., 2001. The Community Climate System Model. *Bulletin of the American Meteorological Society*, 82, 11 pp. 2357-2376

Blaeu, W., 1645-1646. *Theatrum orbis terrarum, sive, Atlas novus: in quo tabulae et descriptiones omnium regionum*. Image courtesy of Special Collections, University of Bristol Library.

Bohaty, S.M., Zachos, J.C. & Delaney, M.L. 2012. Foraminiferal Mg/Ca evidence for Southern Ocean cooling across the Eocene-Oligocene transition. *Earth and Planetary Science Letters*, 317-318, pp. 251-261, DOI: 10.1016/j.epsl.2011.11.037.

Breza, J.R. & Wise, S.W., 1992. Lower Oligocene ice-rafted debris on the Kerguelen Plateau: Evidence for East Antarctic continental glaciation. *Proceedings of the Ocean Drilling Program, Scientific Results*, 120, pp. 161-177.

Bryan, K. & Cox, M. D., 1972. An Approximate Equation of State for Numerical Models of Ocean Circulation. *Journal of Physical Oceanography*, 2, pp. 510–514, DOI: 10.1175/1520-0485(1972)002<0510:AAEOSF>2.0.CO;2.

Burt, J., Barber, G. & Rigby, D., 2009. Elementary statistics for geographers. 3 ed. New York: Guildford Press.

Bushell, A., 1998. Unified Model User Guide, chap. Clouds, p. 27, in: Matthews (1998), available at: http://www.ukscience.org/_Media/UM_User_Guide.pdf (last accessed: 8 September 2017).

Caldeira, K. & Kasting, J. F., 1992. The life span of the biosphere revisited, *Nature*, 360, 721-723.

Cantrill, D.J. & Poole, I., 2005. Taxonomic turnover and abundance in Cretaceous to Tertiary wood floras of Antarctica: implications for changes in forest ecology. *Palaeogeography, Palaeoclimatology, Palaeoecology*, 215, pp. 205-219, DOI: 10.1016/j.palaeo.2004.09.004.

Carter, A., Riley, T.R., Hillenbrand, C.D. & Rittner, M., 2017. Widespread Antarctic glaciation during the Late Eocene. *Earth and Planetary Science Letters*, 458, pp. 49-57, DOI: 10.1016/j.epsl.2016.10.045.

Church, J.A., Clark, P.U., Cazenave, A., Gregory, J.M., Jevrejeva, S., Levermann, A., Merrifield, M.A., Milne, G.A., Nerem, R.S., Nunn, P.D., Payne, A.J., Pfeffer, W.T., Stammer D. & Unnikrishnan, A.S., 2013. Sea Level Change. In: *Climate Change 2013: The Physical Science Basis. Contribution of Working Group I to the Fifth Assessment Report of the Intergovernmental Panel on Climate Change* [Stocker, T.F., D. Qin, G.-K. Plattner, M. Tignor, S.K. Allen, J. Boschung, A. Nauels, Y. Xia, V. Bex and P.M. Midgley (eds.)]. Cambridge University Press, Cambridge, United Kingdom and New York, NY, USA.

Clark, P.U. & Pollard, D., 1998. Origin of the middle Pleistocene transition by ice sheet erosion of regolith. *Paleoceanography*, 13, 1, pp. 1-9.

Clark, P.U., Archer, D., Pollard, D., Blum, J.D., Rial, J.A., Brovkin, V., Mix, A.C., Pisias, N.G. & Roy, M., 2006. The middle Pleistocene transition: characteristics, mechanisms, and implications for long-term changes in atmospheric pCO2. *Quaternary Science Reviews*, 25, pp. 3150-3184, DOI: 10.1016/j.quascirev.2006.07.008.

Coccione, R., 1988. The genera Hantkenina and Cribrohantkenina (foraminifera) in the Massignano Section (Ancona, Italy). *International Subcommission on Paleogeography and Stratigraphy, Eocene/Oligocene Meeting*, 81–96.

Cohen, K.M., Finney, S.C., Gibbard, P.L. & Fan, J.-X., 2018 (2013; updated). The ICS International Chronostratigraphic Chart. Episodes 36: 199-204.

Cornford, S.L., Martin, D.F., Graves, D.T., Ranken, D.F., Le Brocq, A.M., Gladstone, R.M., Payne,. A.J., Ng, E.G. & Lipscomb, W.H., 2013. Adaptive mesh, finite volume modeling of

marine ice sheets. *Journal of Computational Physics*, 232, pp. 529-549, DOI: 10.1016/j.jcp.2012.08.037.

Cornford, S.L., Martin, D.F., Lee, V., Payne, M.J. & Ng, E.G., 2016. Adaptive mesh refinement versus subgrid friction interpolation in simulations of Antarctic ice dynamics. *Annals of Glaciology*, DOI: 10.1017/aog.2016.13.

Costa, E., Garcés, M., Sáez, A., Cabrera, L. & López-Blanco, M., 2011. The age of the "Grande Coupure" mammal turnover: New constraints from the Eocene–Oligocene record of the Eastern Ebro Basin (NE Spain). *Palaeogeography, Palaeoclimatology, Palaeoecology*, 301, pp. 97–107, DOI: 10.1016/j.palaeo.2011.01.005

Cox, P. M., 2001. Description of the TRIFFID dynamic global vegetation model. Tech. Note 24, Hadley Centre, Met Office, UK, 16 pp.

Cox, P.M., Betts, R.A., Jones, C.D., Spall, S.A. & Totterdell, I.J., 2001. Modelling vegetation and the carbon cycle as interactive elements of the climate system, in *Meteorology at the Millennium*, edited by Pearce, R., pp. 259-279, Academic Press, San Diego, California.

Coxall, H.K. & Pearson, P.N., 2007. The Eocene-Oligocene transition, in Williams, M., Hayward, A., Gregory, J., and Schmidt, D. N., eds., Deep time perspectives on climate change: Marrying the signal from computer models and biological proxies: London, Geological Society Publishing House, p. 351-387.

Coxall, H.K., Wilson, P.A., Pälike, H., Lear, C.H. & Backman, J., 2005. Rapid stepwise onset of Antarctic glaciation and deeper calcite compensation in the Pacific Ocean. *Nature*, 433, pp. 53-57, DOI: 10.1038/nature03135.

Coxall, H.K., Huck, C.E., Huber, M., Lear, C.H., Legarda-Lisarri, A., O'Regan, M., Sliwinska, K.K., van de Flierdt, T., de Boer, A.M., Zachos, J.C. & Backman, J., 2018. Export of nutrient rich Northern Component Water preceded early Oligocene Antarctic glaciation. *Nature Geoscience*, 11, pp. 190-196, DOI: 10.1038/s41561-018-0069-9.

Crucifix, M., 2012. Traditional and novel approaches to palaeoclimate modelling. *Quaternary Science Reviews*, 57, pp. 1-16, DOI: 10.1016/j.quascirev.2012.09.010.

DeConto, R. M. & Pollard, D., 2003a. Rapid Cenozoic glaciation of Antarctica induced by declining atmospheric CO_2. *Nature*, 421, pp. 245-249.

DeConto, R. M. & Pollard, D., 2003b. A coupled climate-ice sheet modeling approach to the Early Cenozoic history of the Antarctic ice sheet. *Palaeogeography, Palaeoclimatology, Palaeoecology*, 198, pp. 39-52, DOI: 10.1016/S0031-0182(03)00393-6.

DeConto, R. M. & Pollard, D., 2016. Contribution of Antarctica to past and future sea-level rise. *Nature*, 531, pp. 591-597, DOI: 10.1038/nature17145.

DeConto R.M., Pollard, D., Wilson, P.A., Pälike, H., Lear, C.H. & Pagani, M., 2008. Thresholds for Cenozoic bipolar glaciation. *Nature*, 455, pp. 652-656, DOI: 10.1038/nature07337.

de Boer, B., Dolan, A.M., Bernales, J., Gasson, E., Goelzer, H., Golledge, N.R., Sutter, J., Huybrechts, P., Lohmann, G., Rogozhina, I., Abe-Ouchi, A., Saito, F. & van de Wal, R.S.W., 2015. Simulating the Antarctic ice sheet in the late-Pliocene warm period: PLISMIP-ANT, an ice-sheet model intercomparison project. *The Cryosphere*, 9, pp. 881-903, DOI: 10.5194/tc-9-881-2015.

Diester-Haass, L., 1996. Late Eocene-Oligocene paleoceanography in the southern Indian Ocean (ODP Site 744). *Marine Geology*, 130, pp. 99-119.

Dingle, R.V., Marenssi, S.A. & Lavelle, M., 1998. High latitude Eocene climate deterioration: evidence from the northern Antarctic Peninsula. *Journal of South American Earth Sciences*, 11, 6, pp. 571-579.

Donnadieu, Y., Godderis, Y. & Bouttes, N.,2009. Exploring the climatic impact of the continental vegetation on the Mesozoic atmospheric CO_2 and climate history. *Climate of the Past*, 5, pp. 85-96, DOI: 10.5194/cp-5-85-2009.

Douglas, P.M.J., Affek, H.P., Ivany, L.C., Houben, A.J.P., Sijp, W.P., Sluijs, A., Schouten, S. & Pagani, M., 2014. Pronounced zonal heterogeneity in Eocene southern high-latitude sea surface temperatures. *PNAS*, 111, 18, pp. 6582-6587, DOI: 10.1073/pnas.1321441111.

Dowsett, H.J., Robinson, M.M., Haywood, A.M., Hill, D.J., Dolan, A.M., Stoll, D.K., Chan, W.L., Abe-Ouchi, A., Chandler, M.A., Rosenbloom, N.A., Otto-Bliesner, B.L., Bragg, F.J., Lunt, D.J., Foley, K.M. & Riesselman, C.R., 2012. Assessing confidence in Pliocene sea surface temperatures to evaluate predictive models. *Nature Climate Change*, 2, pp. 365-371, DOI: 10.1038/NCLIMATE1455.

Doyle, S.H., Hubbard, A., Fitzpatrick, A.A.W., van As, D., Mikkelsen, A.B., Pettersson, R. & Hubbard, B., 2014. Persistent flow acceleration within the interior of the Greenland ice sheet. *Geophysical Research Letters*, 41, pp. 899-905, DOI: 10.1002/2013GL058933.

Dutton, A., Carlson, A.E., Long, A.J., Milne, G.A., Clark, P.U., DeConto, R., Horton, B.P., Rahmstorf, S. & Raymo, M.E., 2015. Sea-level rise due to polar ice-sheet mass loss during past warm periods. *Science*, 349, aaa4019, DOI: 10.1126/science.aaa4019.

Edwards, J., 1998. "Radiation" Unified Model User Guide. Version 4.4., Report, Met Office, UK, available at: http://www.ukscience.org/_Media/UM_User_ Guide.pdf (last accessed: 8 September 2017).

Edwards, J. M. & Slingo, A., 1996. Studies with a flexible new radiation code. I: Choosing a configuration for a largescale model. *Quarterly Journal of the Royal Meteorological Society*, 122, pp. 689–719, DOI: 10.1002/qj.49712253107.

Edwards, E.J., Osborne, C.P., Strömberg, C.A.E., Smith, S.A., and C4 Grasses Consortium, 2010. The Origins of C4 Grasslands: Integrating Evolutionary and Ecosystem Science. *Science*, 328, pp. 587-591, DOI: 10.1126/science.1177216.

Ehrmann, W.U. & Mackensen, A., 1992. Sedimentological evidence for the formation of an East Antarctic ice sheet in Eocene/Oligocene time. *Palaeogeography, Palaeoclimatology, Palaeoecology*, 93, pp. 85-112.

Eldrett, J.S., Greenwood, D.R., Harding, I.C. & Huber, M., 2009. Increased seasonality through the Eocene to Oligocene transition in northern high latitudes. *Nature*, 459, pp. 969-973, DOI: 10.1038/nature08069.

Elsworth, G., Galbraith, E., Halverson, G. & Yang, S., 2017. Enhanced weathering and CO2 drawdown caused by latest Eocene strengthening of the Atlantic meridional overturning circulation. *Nature Geoscience*, 10, pp. 213-216, DOI: 10.1038/NGEO2888.

England, M.H., 1993. Representing the Global-Scale Water Masses in Ocean General Circulation Models. *Journal of Physical Oceanography*, 23, pp. 1523-1552, DOI: 10.1175/1520-0485(1993)023<1523:RTGSWM>2.0.CO;2

Essery, R. L. H., Best, M. J., Betts, R. A., Cox, P. M. & Taylor, C. M., 2003. Explicit Representation of Subgrid Heterogeneity in a GCM Land Surface Scheme. *Journal of Hydrometeorology*, 4, pp. 530–543, DOI: 10.1175/1525-7541(2003)004<0530:EROSHI>2.0.CO;2.

Foreman, S. J., 2005. Unified Model Documentation Paper Number 40, The Ocean Model, Report, The Met. Office, available at: http://cms.ncas.ac.uk/documents/vn4.5/p040.pdf (last access: 14 November 2018).

Foster, G.L. & Rohling, E.J. 2013. Relationship between sea levels and climate forcing by CO_2 on geological timescales. *PNAS*, 110, 4, pp. 1209-1214, DOI: 10.1073/pnas.1216073110.

Foster, G.L., Royer, D.L. & Lunt, D.J., 2017. Future climate forcing potentially without precedent in the last 420 million years. *Nature Communications*, 8:14845, DOI: 10.1038/ncomms14845.

Francis, J.S. & Hill, R.S., 1996. Fossil Plants from the Pliocene Sirius Group, Transantarctic Mountains: Evidence for Climate from Growth Rings and Fossil Leaves. *Palaios*, 11, 4, pp. 389-396.

Francis, J.E. & Poole, I., 2002. Cretaceous and early Tertiary climates of Antarctica: evidence from fossil wood. *Palaeogeography, Palaeoclimatology, Palaeoecology*, 182, pp. 47-64.

Francis, J.E., Marenssi, S., Levy, R., Hambrey, M, Thorn, V.T., Mohr, B., Brinkhuis, H., Warnaar, J., Zachos, J.C., Bohaty, S.M., & DeConto, R.M., 2009. From Greenhouse to Icehouse – The Eocene/Oligocene in Antarctica. In: Developments in Earth & Environmental Sciences, 8, F. Florindo and M. Siegert (Editors), DOI 10.1016/S1571-9197(08)00008-6.

Fyke, J.G., D'Orgeville, M. & Weaver, A.J., 2015. Drake Passage and Central American Seaway controls on the distribution of the oceanic carbon reservoir. *Global and Planetary Change*, 128, pp. 72-82, DOI: 10.1016/j.gloplacha.2015.02.011.

Galeotti, S., DeConto, R.M., Naish, T., Stocchi, P., Florindo, F., Pagani, M., Barrett, P., Bohaty, S.M., Lanci, L., Pollard, D., Sandroni, S., Talarico, F.M. & Zachos, J.C., 2016. Antarctic Ice Sheet variability across the Eocene-Oligocene boundary climate transition. *Science*, 352, 6281, pp. 76-80, DOI: 10.1126/science.aab0669.

Ganopolski, A., Calov, R. & Claussen, M. 2010. Simulation of the last glacial cycle with a coupled climate-ice sheet model of intermediate complexity. *Climate of the Past*, 6, pp. 229-244.

Gasson, E., Lunt, D.J., DeConto, R., Goldner, A., Heinemann, M., Huber, M., Legrande, A.N., Pollard, D., Sagoo, N., Siddall, M., Winguth, A. & Valdes, P.J., 2014. Uncertainties in the modelled CO_2 threshold for Antarctic glaciation. *Climate of the Past*, 10, pp. 451-466, DOI: 10.5194/cp-10-451-2014.

Gent, P. R. & McWilliams, J. C., 1990. Isopycnal Mixing in Ocean Circulation Models, *Journal of Physical Oceanography*, 20, pp. 150–155.

Gent, P. R., Danabasoglu, G., Donner, L. J., Holland, M. M., Hunke, E. C., Jayne, S. R., Lawrence, D. M., Neale, R. B., Rasch, P. J., Vertenstein, M.,Worley, P. H., Yang, Z. L. & Zhang, M., 2011. The community climate system model version 4. *Journal of Climate*, 24, pp. 4973–4991, DOI: 10.1175/2011JCLI4083.1, 2011.

Gill, A.E. & Bryan, K., 1971. Effects of geometry on the circulation of a three-dimensional southern-hemisphere ocean model. *Deep Sea Research*, 18, 7, pp. 685-721.

Goldner, A., Huber, M. & Caballero, R., 2013. Does Antarctic glaciation cool the world? *Climate of the Past*, 9, pp. 173-189, DOI: 10.5194/cp-9-173-2013.

Goldner, A., Herold, N. & Huber, M., 2014. Atlantic glaciation caused ocean circulation changes at the Eocene-Oligocene transition. *Nature*, 511, pp. 574-577, DOI: 10.1038/nature13597.

Golledge, N.R., Kowalewski, D.E., Naish, T.R., Levy, R.H., Fogwill, C.J. & Gasson, E.G.W., 2015. The multi-millennial Antarctic commitment to future sea-level rise. *Nature*, 526, pp. 421-425, DOI: 10.1038/nature15706.

Gordon, C., Cooper, C., Senior, C.A., Banks, H., Gregory, J.M., Johns, T.C., Mitchell, J.F.B. & Wood, R.A., 2000. The simulation of SST, sea-ice extents and ocean heat transports in a version of the Hadley Centre coupled model without flux adjustments. *Climate Dynamics*, 16, pp. 147-168.

Grant, A., 1998. Unified Model User Guide, chap. Convection, p. 32, in: Matthews (1998), available at: http://www.ukscience.org/_Media/UM_User_Guide.pdf (last accessed: 8 September 2017).

Gregory, D., Kershaw, R. & Inness, P. M., 1997. Parametrization of momentum transport by convection. II: Tests in single-column and general circulation models. *Quarterly Journal of the Royal Meteorological Society*, 123, pp. 1153–1183, DOI: 10.1002/qj.49712354103.

Gregory, D., Shutts, G. J. & Mitchell, J. R., 1998. A new gravity-wavedrag scheme incorporating anisotropic orography and low-level wave breaking: Impact upon the climate of the UK Meteorological Office Unified Model. *Quarterly Journal of the Royal Meteorological Society*, 124, pp. 463–493, DOI: 10.1002/qj.49712454606.

Hammer, C.U., Clausen, H.B. & Dansgaard, W., 1980. Greenland ice sheet evidence of post-glacial volcanism and its climatic impact. *Nature*, 288, pp. 230-235.

Harbor, J.M., Hallet, B. & Raymond, C.F., 1988. A numerical model of landform development by glacial erosion. *Nature*, 333, pp. 347-349.

Hartman, J.D., Sangiorgi, F., Salabarnada, A., Peterse, F., Houben, A.J.P., Schouten, S., Brinkhuis, H., Escutia, C. & Bijl, P.K., 2018. Paleoceanography and ice sheet variability offshore Wilkes Land, Antarctica – Part 3: Insights from Oligocene–Miocene TEX_{86}-based sea surface temperature reconstructions. *Climate of the Past*, 14, pp. 1275-1297, DOI: 10.5194/cp-14-1275-2018.

Hawkings, J.R., Wadham, J.L., Tranter, M., Raiswell, R., Benning, L.G., Statham, P.J., Tedstonw, A., Nienow, P., Lee, K. & Telling, J., 2014. Ice sheets as a significant source of highly

reactive nanoparticulate iron to the oceans. *Nature Communications*, 5:3929, DOI: 10.1038/ncomms4929.

Hay, W.W., Flögel, S. & Söding, E., 2005. Is the initiation of glaciation on Antarctica related to a change in the structure of the ocean? *Global and Planetary Change*, 45, pp. 23-33, DOI: 10.1016/j.gloplacha.2004.09.005.

Hays, J.D., Imbrie, J. & Shackleton, N.J., 1976. Variations in the Earth's Orbit: Pacemaker of the Ice Ages. *Science*, 194, 4270, pp.1121-1132.

Hewitt, H.T., Copsey, D., Cluverwell, I.D., Harris, C.M., Hill, R.S.R., Keen, A.B., McLaren, A.J. & Hunke, E.C., 2011. Design and implementation of the infrastructure of HadGEM3: the next-generation Met Office climate modelling system. *Geoscientific Model Development* 4, pp. 223-253, DOI: 10.5194/gmd-4-223-2011.

Hill, D.J., Haywood, A.M., Valdes, P.J., Francis, J.E., Lunt, D.J., Wade, B.S. & Bowman, V.C. 2013. Paleogeographic controls on the onset of the Antarctic circumpolar current. *Geophysical Research Letters*, 40, pp. 5199-5204, DOI: 10.1002/grl.50941.

Hohbein, M.W., Sexton, P.F. & Cartwright, J.A., 2012. Onset of North Atlantic Deep Water production coincident with inception of the Cenozoic global cooling trend. *Geology*, 40, 3, pp. 255-258, DOI: 10.1130/G32461.1.

Houben, A.J.P., Bijl, P.K., Pross, J., Bohaty, S.M., Passchier, S., Stickley, C.E., Röhl, U., Sugisaki, S., Tauxe, L., van de Flierdt, T., Olney, M., Sangiorgi, F., Sluijs, A., Escutia, C., Brinkhuis, H.A. & the Expedition 318 Scientists, 2013. Reorganization of Southern Ocean Plankton Ecosystem at the Onset of Antarctic Glaciation. *Science*, 340, pp. 341-344, DOI: 10.1126/science.1223646.

Huang, X., Gohl, K. & Jokat, W., 2014. Variability in Cenozoic sedimentation and paleo-water depths of the Weddell Sea basin related to pre-glacial and glacial conditions of Antarctica. *Global and Planetary Change*, 118, pp. 25-41, DOI: 10.1016/j.gloplacha.2014.03.010.

Huber, M. & Caballero, R., 2011. The early Eocene equable climate problem revisited. *Climate of the Past*, Volume 7, pp. 603-633, DOI: 10.5194/cp-7-603-2011.

Huber, M. & Nof, D., 2006. The ocean circulation in the southern hemisphere and its climatic impacts in the Eocene. *Palaeogeography, Palaeoclimatology, Palaeoecology*, 231, pp. 9-28.

Huber, M., Brinkhuis, H., Stickley, C.E., Doos, K., Sluijs, A., Warnaar, J., Schellenberg, S.A. & Williams, G.L., 2004. Eocene circulation of the Southern Ocean: Was Antarctica kept warm by subtropical waters? *Paleoceanography*, 19, PA4026, doi: 10.1029/2004PA001014.

Hutchinson, D.K., de Boer, A.M., Coxall, H.K., Caballero, R., Nilsson, J. & Baatsen, M.J.L. 2018. Climate sensitivity and meridional overturning circulation in the late Eocene using GFDL CM2.1. *Climate of the Past,* Volume 14, pp. 789-810, DOI: 10.5194/cp-14-789-2018.

Hutchinson, D.K., et al., in prep. A review of marine and terrestrial changes across the Eocene-Oligocene Transition: insights from geological data, models, and model-data comparisons.

Inglis, G.N., Farnsworth, A., Lunt, D.J., Foster, G.L., Hollis, C.J., Pagani, M., Jardine, P.E., Pearson, P.N., Markwick, P.J., Raynman, L., Galsworthy, A.M.J. & Pancost, R.D. Descent towards the Icehouse: Eocene sea surface cooling inferred from GDGT distributions, 2015. *Paleoceanography*, 30, pp. 1000-1020, DOI: 10.1002/2014PA002723.

Ingram,W. S.,Woodward, S. & Edwards, J., 1997. Unified Model Documentation Paper: Radiation, Report 23, Met Office, UK.

IPCC: Climate Change 2007: The Physical Science Basis. Contribution of Working Group I to the Fourth Assessment Report of the Intergovernmental Panel on Climate Change, edited by: Solomon, S., Qin, D., Manning, M., Chen, Z., Marquis, M., Avery, K., Tignor, M. & Miller, H., Cambridge University Press, 2007.

Jacob, R., Schafer, C., Foster, I., Tobis, M. & Anderson, J., 2001. Computational Design and Performance of the Fast Ocean Atmosphere Model, Version One. In: Proc. 2001 International Conference on Computational Science (Eds.: Alexandrov, V. N., Dongarra, J. J. & Tan, C. J. K.), Springer-Verlag, pp. 175-184.

Jones, C., 2003. A fast ocean GCM without flux adjustments. *Journal of Atmospheric and Oceanic Technology*, 20, pp. 1857-1868.

Joughin, I. & Alley, R.B., 2011. Stability of the West Antarctic ice sheet in a warming world. *Nature Geoscience*, 4, pp. 506-513, DOI: 10.1038/NGEO1194.

Katz, M.E., Miller, K.G., Wright, J.D., Wade, B.S., Browning, J.V., Cramer, B.S. & Rosenthal, Y. 2008. Stepwise transition from the Eocene greenhouse to the Oligocene icehouse. *Nature Geoscience*, 1, 329-334, DOI: 10.1038/ngeo179.

Katz, M.E., Cramer, B.S., Toggweiler, J.R., Esmay, G., Liu, C., Miller, K.G., Rosenthal, Y., Wade, B.S. & Wright, J.W., 2011. Impact of Antarctic Circumpolar Current Development on Late Paleogene Ocean Structure. *Science*, 332, pp. 1076-1079, DOI: 10.1126/science.1202122.

Kennedy A.T., Farnsworth A., Lunt D.J., Lear C.H., & Markwick P.J., 2015. Atmospheric and oceanic impacts of Antarctic glaciation across the Eocene–Oligocene transition. *Phil. Trans. R. Soc. A*, 373, 20140419, DOI:10.1098/rsta.2014.0419.

Kennedy-Asser, A.T., Lunt, D.J., Farnsworth, A. & Valdes, P.J., 2019. Assessing mechanisms and uncertainty in modelled climatic change at the Eocene-Oligocene Transition. *Paleoceanography and Paleoclimatology*, 34, pp. 16-34, DOI: 10.1029/2018PA003380.

Kennett, J.P., 1977. Cenozoic evolution of Antarctic glaciation, circum Antarctic ocean, and their impact on global paleoceanography. *Journal of Geophysical Research*, 82, pp. 3843-3860, DOI: 10.1029/JC082i027p03843.

Kennett, J.P., & Shackleton, N.J., 1976. Oxygen isotopic evidence for the development of the psychrosphere 38 Myr ago. *Nature*, 260, pp. 513-515, DOI: 10.1038/260513a0.

Knorr, G. & Lohmann, G., 2014. Climate warming during Antarctic ice sheet expansion at the Middle Miocene transition. *Nature Geoscience*, 7, pp. 376-381, DOI: 10.1038/ngeo2119.

Koppes, M., Hallet, B., Rignot, E., Mouginot, J., Wellner, J.S. & Boldt, K., 2015. Observed latitudinal variations in erosion as a function of glacier dynamics. *Nature*, 526, pp. 100-103, DOI: 10.1038/nature15385.

Kraatz, B.P. & Geisler, J.H., 2010. Eocene–Oligocene transition in Central Asia and its effects on mammalian evolution. *Geology*, 38, pp. 111-114, DOI: 10.1130/G30619.1.

Ladant, J.B. & Donnadieu, Y., 2016. Palaeogeographic regulation of glacial events during the Cretaceous supergreenhouse. *Nature Communications*, 7:12771, DOI: 10.1038/ncomms12771.

Ladant, J.B., Donnadieu, Y., Lefebvre, V. & Dumas, C., 2014a. The respective role of atmospheric carbon dioxide and orbital parameters on ice sheet evolution at the Eocene-Oligocene transition. *Paleoceanography*, DOI: 10.1002/2013PA002593.

Ladant, J.B., Donnadieu, Y. & Dumas, C., 2014b. Links between CO2, glaciation and water flow: reconciling the Cenozoic history of the Antarctic Circumpolar Current. *Climate of the Past*, 10, pp. 1957-1966, DOI: 10.5194/cp-10-1957-2014.

Lagabrielle, Y., Goddéris, Y., Donnadieu, Y., Malavieille, J. & Suarez, M., 2009. The tectonic history of Drake Passage and its possible impacts on global climate. *Earth and Planetary Science Letters*, 279, pp. 197-211, DOI: 10.1016/j.epsl.2008.12.037.

Laskar, J., Robutel, P., Joutel, F., Gastineau, M., Correia, A. C. M. & Levrard, B. 2004. A long-term numerical solution for the insolation quantities of the Earth. *Astronomy & Astrophysics,* 428**,** 261-285**,** DOI: 10.1051/0004-6361:20041335.

Lear, C.H. & Lunt, D.J., 2016. How Antarctica got its ice. *Science*, 352, pp. 34-36, DOI: 10.1126/science.aad6284.

Lear, C.H., Rosenthal, Y., Coxall, H.K. & Wilson, P.A., 2004. Late Eocene to early Miocene ice-sheet dynamics and the global carbon cycle. *Paleoceanography*, 19, PA4015, DOI: 10.1029/2004PA001039.

Lear, C.H., Bailey, T.R., Pearson, P.N., Coxall, H.K., & Rosenthal, Y., 2008. Cooling and ice growth across the Eocene–Oligocene transition. *Geology*, 36, pp. 251-254, DOI: 10.1130/G24584A.1.

Lear, C.H., Mawbey, E.M., & Rosenthal, Y., 2010. Cenozoic benthic foraminiferal Mg/Ca and Li/Ca records: Toward unlocking temperatures and saturation states. *Paleoceanography*, 25, PA4215, DOI: 10.1029/2009PA001880.

Lefebvre, V., Donnadieu, Y., Sepulchre, P., Swingedouw, D. & Zhang, Z.S., 2012. Deciphering the role of southern gateways and carbon dioxide on the onset of the Antarctic Circumpolar Current. *Paleoceanography*, 27, PA4201, DOI: 10.1029/2012PA002345.

Lefebvre, V., Donnadieu, Y., Goddéris, Y, Fluteau, F. & Hubert-Théou, L., 2013. Was the Antarctic glaciation delayed by a high degassing rate during the early Cenozoic? *Earth and Planetary Science Letters*, 371-372, pp. 203-211, DOI: 10.1016/j.epsl.2013.03.049.

LeGrande, A.N., Schmidt, G.A., Shindell, D.T., Field, C.V., Miller, R.L., Koch, D.M., Faluvegi, G. & Hoffman, G., 2006. Consistent simulations of multiple proxy responses to an abrupt climate change event. *Proceedings of the National Academy of Sciences*, 103, 4, pp. 837-842, DOI: 10.1073_pnas.0510095103.

Li, Y., 2017. The climates responses to the closure of the Turgai Strait during the Eocene-Oligocene transition. MSc thesis, University of Bristol.

Li, S, Xing, Y., Valdes, P.J., Huang, Y., Su, T., Farnsworth, A., Lunt, D.J., Tang, H., Kennedy, A.T. & Zhou, Z., 2018. Oligocene climate signals and forcings in Eurasia revealed by plant macrofossil and modelling results. *Gondwana Research*, 61, pp. 115-127, DOI: 10.1016/j.gr.2018.04.015.

Liakka, J., Colleoni, F., Ahrens, B. & Hickler, T., 2014. The impact of climate-vegetation interactions on the onset of the Antarctic ice sheet. Geophysical Research Letters. 41, pp. 1269-1276, DOI: 10.1002/2013GL058994

Liebrand, D., de Bakker, A.T.M., Beddow, H.M., Wilson, P.A., Bohaty, S.M., Ruessink, G., Pälike, H., Batenburg, S.J., Hilgen, F.J., Hodell, D.A., Huck, C.E., Kroon, D., Raffi, I., Saes, M.J.M, van Dijk, A.E. & Lourens, L.J., 2017. Evolution of the early Antarctic ice ages. *Proceedings of the National Academy of Sciences*, DOI: 10.1073/pnas.1615440114.

Liu, Z., Pagani, M., Zinniker, D., DeConto, R., Huber, M., Brinkhuis, H., Shah, S.R., Leckie, R.M., & Pearson, A., 2009. Global cooling during the Eocene–Oligocene climate transition. *Science*, 323, pp. 1187-1190, DOI: 10.1126/science.1166368.

Lord, N.S., Crucifix, M., Lunt, D.J., Thorne, M.C., Bounceur, N., Dowsett, H., O'Brien, C.L. & Ridgwell, A.J., 2017. Emulation of long-term changes in global climate: Application to the late Pliocene and future. *Climate of the Past*, 13, pp. 1539-1571, DOI: 10.5194/cp-13-1539-2017.

Lucarini, V. & Bódai, T., 2017. Edge states in the climate system: exploring global instabilities and critical transitions. *Nonlinearity*, 30, pp. R32-R66, DOI: 10.1088/1361-6544/aa6b11.

Lunt, D.J., Ross, I., Hopley, P.J., Valdes, P.J. (2007) Modelling Late Oligocene C4 grasses and climate. *Palaeogeography, Palaeoclimatology, Palaeoecology*, 251, 239-253.

Lunt, D.J., Dunkley Jones, T., Heinemann, M., Huber, M., LeGrande, A., Winguth, A., Lopston, C., Marotzke, J., Roberts, D.C., Tindall, J., Valdes, P.J. & Winguth, C., 2012. A model–data comparison for a multi-model ensemble of early Eocene atmosphere–ocean simulations: EoMIP. *Climate of the Past*, 8, pp. 1717-1736, DOI :1 0.5194/cp-8-1717-2012.

Lunt, D. J., Farnsworth, A., Lopston, C., Foster, G.L., Markwick, PJ., O'Brien, C.L., Pancost, R.D., Robinson, S.A. & Wrobel, N., 2016. Palaeogeographic controls on climate and proxy interpretation. *Climate of the Past*, 12, pp. 1181-1198, DOI: 10.5194/cp-12-1181-2016.

Lyle, M., Gibbs, S., Moore, T.C. & Rea, D.K., 2007. Late Oligocene initiation of the Antarctic Circumpolar Current: Evidence from the South Pacific. *Geology*, 35, pp.691-694, DOI: 10.1130/G23806A.1.

Macphail, M.K., & Truswell, E.M., 2004. Palynology of Site 1166, Prydz Bay, East Antarctica. In: *Proceedings of the Ocean Drilling Program, Scientific Results Volume 188*, Cooper, A.K., O'Brien, P.E. & Richter, C. (Eds.), pp. 1-43.

Marchitto T. M., Curry, W. B., Lynch-Stieglitz, J., Bryan, S. P., Cobb, K.M. & Lund, D. C., 2014. Improved oxygen isotope temperature calibrations for cosmopolitan benthic foraminifera, *Geochimica et Cosmochimica Acta* 130 1–11.

Markwick, P.J., 2007. The palaeogeographic and palaeoclimatic significance of climate proxies for data-model comparisons, in *Deep-time perspectives on climate change: Marrying the signal from computer models and biological proxies*, edited by Williams, M. et al. pp. 251-312, Micropalaeontological Society, Special Publications, The Geological Society, London.

Marshall, J. & Speer, K., 2012. Closure of the meridional overturning circulation through Southern Ocean upwelling. *Nature Geoscience*, 5, pp. 171-180, DOI: 10.1038/NGEO1391.

Marshall, J. & Speer, K., 2012. Closure of the meridional overturning circulation through Southern Ocean upwelling. *Nature Geoscience*, 5, pp. 171-180, DOI: 10.1038/NGEO1391.

Masson-Delmotte, V. et al., 2010. EPICA Dome C record of glacial and interglacial intensities. *Quaternary Science Reviews*, 29, pp. 113-128, DOI: 10.1016/j.quascirev.2009.09.030.

Mellor, G.L., 1996. Introduction to Physical Oceanography. Springer, New York, USA.

Meng, J., & McKenna, M.C., 1998. Faunal turnovers of Palaeogene mammals from the Mongolian Plateau. *Nature*, 394, pp. 364-367.

Meredith, M.P., Woodworth, P.L., Hughes, C.W. & Stepanov, V., 2004. Changes in the ocean transport through the Drake Passage during the 1980s and 1990s, forced by changes in Southern Annular mode. *Geophysical Research Letters*, 31, L21305, DOI: 10.1029/2004GL021169.

Miller, K.G., Wright, J., Katz, M., Browning, J., Cramer, B., Wade, B.S. & Mizintseva, S., 2008. A view of Antarctic ice-sheet evolution from sea-level and deep-sea isotope changes during the Late Cretaceous-Cenozoic, in *Antarctica: A Keystone in a Changing World*, pp. 55-70, Natl. Acad., Washington D.C.

Milton, S.F. & Wilson, C.A., 1996. The Impact of Parameterized Subgrid-Scale Orographic Forcing on Systematic Errors in a Global NWP Model. *Monthly Weather Review*, 124, pp. 2023-2045, DOI: 10.1175/1520-0493(1996)124<2023:TIOPSS>2.0.CO;2.

Morrison, A.K. & Hogg, A.M., 2012. On the Relationship between Southern Ocean Overturning and ACC Transport. *Journal of Physical Oceanography*, 43, pp. 140-148, DOI: 10.1175/JPO-D-12-057.1.

Munday, D.R., Johnson, H.L. & Marshall, D.P., 2015. The role of ocean gateways in the dynamics and sensitivity to wind stress of the early Antarctic Circumpolar Current. *Paleoceanography*, 30, DOI: 10.1002/2014PA002675.

Naafs, B.D.A. et al., 2017. Introducing global peat-specific temperature and pH calibrations based on brGDGT bacterial lipids. *Geochimica et Cosmochimica Acta*, 208, pp. 285–301, DOI: 10.1016/j.gca.2017.01.038.

New, M., Lister, D., Hulme, M. & Makin, I., 2002. A high-resolution data set of surface climate over global land areas, *Clim. Res.*, 21, pp. 1–25, DOI: 10.3354/cr021001, 2002.

Nocchi, M., et al., 1986. The Eocene-Oligocene Boundary in the Umbrian Pelagic Sequences, Italy. *termbal eocene events*, C. Pomerol and I.B.T.-D. in P. and S. Premoli-Silva, Eds., Vol. 9 of, Elsevier, 25–40.

Oerlemans, J., 2002. On glacial inception and orography. *Quaternary International*, 95-96, pp. 5-10, DOI: 10.1016/S1040-6182(02)00022-8.

Olivetti, V., Balestrieri, M.L., Rossetti, F., Thomson, S.N., Talarico, F.M. & Zattin, M., 2015. Evidence of a full West Antarctic Ice Sheet back to the early Oligocene: insight from double dating of detrital apatites in Ross Sea sediments. *Terra Novai*, pp. 238-246, DOI: 10.1111/ter.12153.

Ozsvárt, P., Kocsis, L., Nyerges, A., Gyori, O. & Pálfy, J., 2016. The Eocene-Oligocene climate transition in the Central Paratethys. *Palaeogeography, Palaeoclimatology, Palaeoecology*, 459, pp. 471-487. DOI: 10.1016/j.palaeo.2016.07.034.

Pacanowski, R. 1995. MOM 2 Documentation User's Guide and Reference Manual, GFDL Ocean Group Technical Report. NOAA, GFDL. Princeton. 232 pp.

Pagani, M., Huber, M., Liu, Z., Bohaty, S.M., Henderiks, J., Sijp, W., Krishnan, R. & DeConto, R.M. 2011. The Role of Carbon Dioxide During the Onset of Antarctic Glaciation. *Science*, 334, pp. 1261-1264, DOI: 10.1126/science.1203909.

Pälike, H., Norris, R.D., Herrle, J.O., Wilson, P.A., Coxall, H.K., Lear, C.H., Shackleton, N.J., Tripati, A.K. & Wade, B.S., 2006. The Heartbeat of the Oligocene Climate System. *Science*, 314, pp. 1894-1898, DOI: 10.1126/science.1133822.

Pälike, H. et al., 2012. A Cenozoic record of the equatorial Pacific carbonate compensation depth. *Nature*, Volume 488, pp. 609-614, DOI: 10.1038/nature11360.

Parish, T.R. & Waight, K.T., 1987. The Forcing of Antarctic Katabatic Winds. *Monthly Weather Review*, 115, pp. 2214-2226.

Passchier, S., Bohaty, S.M., Jiménez-Espejo, F., Pross, J., Röhl, U., van de Flierdt, T., Escutia, C. & Brinkhuis, H., 2013. Early Eocene to middle Miocene cooling and aridification of East Antarctica. *Geochemistry, Geophysics, Geosystems*, 14, 5, pp. 1399-1410, DOI: 10.1002/ggge.20106.

Passchier, S., Ciarletta, D.J., Miriagos, T.E., Bijl, P.K. & Bohaty, S.M., 2016. An Antarctic stratigraphic record of stepwise ice growth through the Eocene-Oligocene transition. *GSA Bulletin*, DOI: 10.1130/B31482.1.

Pearson, P.N., van Dongen, B.A., Nicholas, C.J., Pancost, R.D., Schouten, S., Singano, J.M. & Wade, B.S., 2007. Stable warm tropical climate through the Eocene Epoch. *Geology*, 35, 3, pp. 211-214, DOI: 10.1130/G23175A.1.

Pearson, P.N., McMillan, I.K., Wade, B.S., Dunkley Jones, T., Coxall, H.K., Bown, P.R., & Lear, C.H., 2008. Extinction and environmental change across the Eocene–Oligocene boundary in Tanzania. *Geology*, 36, pp. 179-182, DOI: 10.1130/G24308A.1.

Pearson, P.N., Foster, G.L., & Wade, B.S., 2009. Atmospheric carbon dioxide through the Eocene-Oligocene climate transition. *Nature*, 461, pp. 1110-1113, DOI: 10.1038/nature08447.

Peck, V.L., Yu, J., Kender, S. & Riesselman, C.R., 2010. Shifting ocean carbonate chemistry during the Eocene-Oligocene climate transition: Implications for deep-ocean Mg/Ca paleothermometry. *Plaeoceanography*, 25, PA4219, DOI :10.1029/2009PA001906.

Petersen, S.V. & Schrag, D.P., 2015. Antarctic ice growth before and after the Eocene-Oligocene transition: New estimates from clumped isotope paleothermometry. *Paleoceanography*, 30, pp. 1305-1317, DOI: 10.1002/2014PA002769.

Petty, A.A., Holland, P.R. & Feltham, D.L., 2014. Sea ice and the ocean mixed layer over the Antarctic shelf seas. *The Cryosphere*, 8, pp. 761-783, DOI: 10.5194/tc-8-761-2014.

Pfuhl, H.A. & McCave, I.N., 2005. Evidence for late Oligocene establishment of the Antarctic Circumpolar Current. *Earth and Planetary Science Letters*, 235, pp. 715-728, DOI: 10.1016/j.epsl.2005.04.025.

Piotrowski, J.A., Larsen, N.K. & Junge, F.W., 2004. Reflections on soft subglacial beds as a mosaic of deforming and stable spots. *Quaternary Science Reviews*, 23, pp. 993-1000, DOI: 10.1016/j.quascirev.2004.01.006.

Plancq, J., Mattioli, E., Pittet, B., Simon, L. & Grossi, V., 2014. Productivity and sea-surface temperature changes recorded during the late Eocene–early Oligocene at DSDP Site 511 (South Atlantic). *Palaeogeography, Palaeoclimatology, Palaeoecology*, 407, pp. 34-44, DOI: 10.1016/j.palaeo.2014.04.016.

Pole, M., Hill, B. & Harwood, D., 2000, Eocene plant macrofossils from erratics, McMurdo Sound, Antarctica. In: Paleobiology and paleoenvironments of Eocene Rocks, McMurdo Sound, East Antarctica. *Antarctic Research Series*, 76, pp. 243-251.

Pollard, D. & DeConto, R.M., 2005. Hysteresis in Cenozoic Antarctic ice-sheet variations. *Global and Planetary Change*, 45, pp. 9-21, DOI: 10.1016/j.gloplacha.2004.09.011.

Pollard, D. & DeConto, R.M., 2012. Description of a hybrid ice sheet-shelf model, and application to Antarctica. *Geoscientific Model Development*, 5, pp. 1273-1295, DOI: 10.5194/gmd-5-1273-2012.

Pollard, D., DeConto, R.M. & Nyblade, A.A., 2005. Sensitivity of Cenozoic Antarctic ice sheet variations to geothermal heat flux. *Global and Planetary Change*, 49, pp. 63-74, DOI: 10.1016/j.gloplacha.2005.05.003.

Pollard, D., Kump, L.R. & Zachos, J.C., 2013. Interactions between carbon dioxide, climate, weathering, and the Antarctic ice sheet in the earliest Oligocene. *Global and Planetary Change*, 111, pp. 258-267, DOI: 10.1016/j.gloplacha.2013.09.012.

Poole, I., Cantrill, D.J. & Utescher, T., 2005. A multi-proxy approach to determine Antarctic terrestrial palaeoclimate during the Late Cretaceous and Early Tertiary. *Palaeogeography, Palaeoclimatology, Palaeoecology*, 222, pp. 95-121, DOI: 10.1016/j.palaeo.2005.03.011.

Pound, M.J. & Salzmann, U., 2017. Heterogeneity in global vegetation and terrestrial climate change during the late Eocene to early Oligocene transition. *Scientific Reports*, 7, p. 43386, DOI: 10.1038/srep43386.

Pross, J., Contreras, L., Bijl, P.K., Greenwood, D.R., Bohaty, S.M., Schouten, S., Bendle, J.A., Röhl, U., Tauxe, L., Raine, J.I., Huck, C.E., van de Flierdt, T., Jamieson, S.S.R, Stickley, C.E., van de Schootbrugge, B., Escutia, C., Brinkhuis, H. & IODP Exp. 318 Scientists, 2012. Persistent near-tropical warmth on the Antarctic continent during the early Eocene epoch. *Nature*, 488, pp. 73-77, DOI: 10.1038/nature11300.

Prothero, D.R., 1994. The Late Eocene-Oligocene Extinctions. *Annu. Rev. Earth Planet. Sci.,* 22, pp. 145-65.

Pusz, A.E., Thunell, R.C. & Miller, K.G., 2011. Deep water temperature, carbonate ion, and ice volume changes across the Eocene-Oligocene climate transition. *Paleoceanography*, 26, PA2205, DOI: 10.1029/2010PA001950.

Rahmstorf, S. & England, M.H., 1997. Influence of Southern Hemisphere Winds on North Atlantic Deep Water Flow. *Journal of Physical Oceanography*, 27, pp. 2040-2054.

Raine, J.I. & Askin, R.A., 2001. Terrestrial Palynology of Cape Roberts Project Drillhole CRP-3, Victoria Land Basin, Antarctica. *Terra Antarctica*, 8, pp. 389-400.

Retallack, G.J., 2000. Cenozoic Expansion of Grasslands and Climatic Cooling. *The Journal of Geology*, 109, pp. 407-426.

Rickard, G. & Foreman, S., 2000. Fourier Filtering in the Ocean Model, Unified Model Version 4.5. The Met. Office, available at: http://cms.ncas.ac.uk/documents/vn4.5/p060.ps (last access: 20/12/2018).

Ridgwell, A., Hargreaves, J.C., Edwards, N.R., Annan, J.D., Lenton, T.M., Marsh, R., Yool, A. & Watson, A., 2007. Marine geochemical data assimilation in an efficient Earth System Model of global biogeochemical cycling. *Biogeosciences*, 4, pp. 87-104, DOI: 10.5194/bg-4-87-2007

Robock, A., 2000. Volcanic eruptions and climate. *Reviews of Geophysics*, 38, pp. 191-219.

Rögl, F., 1999. Mediterranean and Paratethys. Facts and hypotheses of an Oligocene to Miocene paleogeography (short overview). *Geologica Carpathica*, 50, 4, pp. 339-349.

Rugenstein, M., Stocchi, P., von der Heydt, A.S., Dijkstra, H.A. & Brinkhuis, H., 2014. Emplacement of Antarctic ice sheet mass affects circumpolar ocean flow. *Global and Planetary Change*, 118, pp. 16-24, DOI: 10.1016/j.gloplacha.2014.03.011.

Rutt, I.C., Hagdorn, M., Hulton, N.R. & Payne, A.J., 2009. The Glimmer community ice sheet model. *Journal of Geophysical Research*, 114, F02004, DOI: 10.1029/2008JF001015.

Scher, H.D., 2017. Carbon-ocean gateway links. *Nature Geoscience*, 10, pp. 164-165.

Scher, H.D. & Martin, E.E., 2004. Circulation in the Southern Ocean during the Paleogene inferred from neodymium isotopes. *Earth and Planetary Science Letters*, 228, pp. 391-405, DOI: 10.1016/j.epsl.2004.10.016.

Scher, H.D., Bohaty, S.M., Zachos, J.C. & Delaney, M.L., 2011. Two-stepping into the icehouse: East Antarctic weathering during progressive ice-sheet expansion at the Eocene–Oligocene transition. *Geology*, 39, 4, pp. 383-386, DOI: 10.1130/G31726.1.

Scher, H.D., Bohaty, S.M., Smith, B.W. & Munn, G.H., 2014. Isotopic interrogation of a suspected late Eocene glaciation. *Paleoceanography*, 29, pp. 628-644, DOI: 10.1002/2014PA002648.

Scher, H.D., Whitaker, J.M., Williams, S.E., Latimer, J.C., Kordesch, W.E.C. & Delaney, M.L., 2015. Onset of Antarctic Circumpolar Current 30 million years ago as Tasmanian Gateway aligned with westerlies. *Nature*, 523, pp. 580-583, DOI: 10.1038/nature14598.

Schmittner, A. & Galbraith, E.D., 2008. Glacial greenhouse-gas fluctuations controlled by ocean circulation changes. *Nature*, 456, pp. 373-376, DOI: 10.1038/nature07531.

Schouten, S., Hopmans, E. & Sinninghe Damsté, J., 2013. The organic geochemistry of glycerol dialkyl glycerol tetraether lipids: A review. *Organic Geochemistry,* Volume 54, pp. 19-61, DOI: 10.1016/j.orggeochem.2012.09.006.

Shackleton, N., 1967. Oxygen Isotope Analyses and Pleistocene Temperatures Re-assessed. *Nature*, 215, pp. 15-17.

Sheldon, N.D. & Retallack, G.J., 2004. Regional Paleoprecipitation Records from the Late Eocene and Oligocene of North America. *The Journal of Geology*, 112, pp. 487-494.

Shakun, J.D., Clark, P.U., He, F., Marcott, S.A., Mix, A.C., Liu, Z., Otto-Bliesner, B., Schmittner, A. & Bard, E. 2012. Global warming preceded by increasing carbon dioxide concentrations during the last deglaciation. *Nature*, 484, pp. 49-54, DOI: 10.1038/nature10915.

Sijp, W.P. & England, M.H., 2004. Effect of Drake Passage Throughflow on Global Climate. *Journal of Physical Oceanography*, 34, pp. 1254-1266.

Sijp, W.P. & England, M.H., 2009. Southern Hemisphere Westerly Wind Control over the Ocean's Thermohaline Circulation. *Journal of Climate*, 22, pp. 1277-1286, DOI: 10.1175/2008JCLI2310.1.

Sijp, W.P., England, M.H. & Huber, M., 2011. Effect of deepening the Tasman Gateway on the global ocean. *Paleoceanography*, 26, PA4207, DOI: 10.1029/2011PA002143.

Sijp, W.P., von der Heydt, A.S., Dijkstra, H.A., Flögel, S., Douglas, P.M.J & Bijl, P.K., 2014. The role of ocean gateways on cooling climate on long time scales. *Global and Planetary Change*, 119, pp. 1-22, DOI: 10.1016/j.gloplacha.2014.04.004.

Sijp, W.P., von der Heydt, A.S. & Bijl, P.K., 2016. Model simulations of early westward flow across the Tasman Gateway during the early Eocene. *Climate of the Past*, 12, pp. 807-817, DOI: 10.5194/cp-12-807-2016.

Silva, I. P., and D. G. Jenkins, 1993: Decision on the Eocene-Oligocene boundary stratotype. *Episodes*, 16, 379–382.

Sorlien, C.C., Luyendyk, B.P., Wilson, D.S., Decesari, R.C., Bartek, L.R. & Diebold, J.B., 2007. Oligocene development of the West Antarctic Ice Sheet recorded in eastern Ross Sea strata. *Geology*, 35, 5, pp. 467-470, DOI: 10.1130/G23387A.1.

Spicer, R.A., Ahlberg, A., Herman, A.B., Hofmann, C.C., Raikevich, M., Valdes, P.J. & Markwick, P.J., 2008. The Late Cretaceous continental interior of Siberia: A challenge for

climate models. *Earth and Planetary Science Letters*, 267, pp. 228-235, DOI: 10.1016/j.epsl.2007.11.049.

Stap, L.B., van de Wal, R.S.W., de Boer, B., Bintanja, R. & Lourens, L.J., 2017. The influence of ice sheets on temperature during the past 38 million years inferred from a one-dimensional ice sheet–climate model. *Climate of the Past*, 13, pp. 1243-1257, DOI: 10.5194/cp-13-1243-2017.

Stickley, C.E., Brinkhuis, H., Schellenberg, S.A., Sluijs, A., Rohl, U., Fuller, M., Grauert, M., Huber, M., Warnaar, J. & Williams, G.L., 2004. Timing and nature of the deepening of the Tasmanian Gateway. *Paleoceanography*, 19, PA4027, DOI: 10.1029/2004001022.

Sun, J. & Windley, B.F., 2015. Onset of aridification by 34 Ma across the Eocene-Oligocene transition in Central Asia. *Geology*, 43, 11, pp. 1015-1018 DOI: 10.1130/G37165.1.

Thorn, V.C. & DeConto, R., 2006. Antarctic climate at the Eocene/Oligocene boundary — climate model sensitivity to high latitude vegetation type and comparisons with the palaeobotanical record. *Palaeogeography, Palaeoclimatology, Palaeoecology*, 231, pp. 134-157, DOI: 10.1016/j.palaeo.2005.07.032.

Thompson, S.L. & Pollard, D., 1997. Greenland and Antarctic Mass Balances for Present and Doubled Atmospheric CO2 from the GENESIS Version-2 Global Climate Model. *Journal of Climate*, 10, pp. 871-900.

Torsvik, T. H., Van der Voo, R., Preeden, U., Niocaill, C. M., Steinberger, B., Doubrovine, P. V., van Hinsbergen, D. J. J., Domeier, M., Gaina, C., Tohver, E., Meert, J. G., McCausland, P. J. A., and Cocks, L. R. M., 2012. Phanerozoic polar wander, palaeogeography and dynamics. Earth-Science Reviews, 114, 325–368, DOI:10.1016/j.earscirev.2012.06.002.

Tripati, A. & Darby, D., 2018. Evidence for ephemeral middle Eocene to early Oligocene Greenland glacial ice and pan-Arctic sea ice. *Nature Communications*, 9:1038, DOI: 10.1038/s41467-018-03180-5.

UKESM, The UK Earth System Modelling Project – Development and Community Release of UKESM1, available at: https://ukesm.ac.uk (last accessed: 9/12/2018), 2018.

Vahlenkamp, M., Niezgodzki, I., De Vleeschouwer, D., Bickert, T., Harper, D., Kirtland Turner, S., Lohmann, G., Sexton, P., Zachos, J.C. & Pälike, H., 2018. Astronomically paced changes in deep-water circulation in the western North Atlantic during the middle Eocene. *Earth and Planetary Science Letters*, 484, pp. 329-340, DOI: 10.1016/j.epsl.2017.12.016.

Valdes, P.J., 2011. Built for stability. *Nature Geoscience*, 4, pp.414-416.

Valdes, P.J., Armstrong, E., Badger, M.P.S., Bradshaw, C.D., Bragg, F., Crucifix, M., Davies-Barnard, T., Day, J.J., Farnsworth, A., Gordon, C., Hopcroft, P.O., Kennedy, A.T., Lord, N.S., Lunt, D.J., Marzocchi, A., Parry, L.M., Pope, V., Roberts, W.G.H., Stone, E.J., Tourte, G.J.L. & Williams, J.H.T., 2017. The BRIDGE HadCM3 family of climate models: HadCM3@Bristol v1.0. *Geoscientific Model Development*, 10, pp. 3715-3743, DOI: 10.5194/gmd-10-3715-2017.

Vaughan, D.G., Comiso, J.C., Allison, I., Carrasco, J., Kaser, G., Kwok, R., Mote, P., Murray, T., Paul, F., Ren, J. Rignot, E., Solomina, O., Steffen, K. & Zhang, T., 2013. Observations: Cryosphere. In: *Climate Change 2013: The Physical Science Basis. Contribution of Working Group I to the Fifth Assessment Report of the Intergovernmental Panel on Climate Change* [Stocker, T.F., D. Qin, G.-K. Plattner, M. Tignor, S.K. Allen, J. Boschung, A. Nauels, Y. Xia, V. Bex and P.M. Midgley (eds.)]. Cambridge University Press, Cambridge, United Kingdom and New York, NY, USA.

Via, R.K. & Thomas, D.J., 2006. Evolution of Atlantic thermohaline circulation: Early Oligocene onset of deep-water production in the North Atlantic. *Geology*, 34, 6, pp. 441-444, DOI: 10.1130/G22545.1.

Villa, G., Fioroni, C., Persico, D., Roberts, A.P. & Florindo, F., 2013. Middle Eocene to Late Oligocene Antarctic glaciation/deglaciation and Southern Ocean productivity. *Paleoceanography*, 29, pp. 223-237, DOI: 10.1002/2013PA002518.

von der Heydt, A.S., Dijkstra, H.A., van de Wal, R.S.W., Caballero, R., Crucifix, M., Foster, G.L., Huber, M., Köhler, P., Rohling, E., Valdes, P.J., Ashwin, P., Bathiany, S., Berends, T., van Bree, L.G.J., Ditlevsen, P., Ghil, M., Haywood, A.M., Katzav, J., Lohmann, G., Lohmann, J., Lucarini, V., Marzocchi, A., Pälike, H., Ruvalcaba Baroni, I., Simon, D., Sluijs, A., Stap, L.B., Tantet, A., Viebahn, J. & Ziegler, M., 2016. Lessons on Climate Sensitivity From Past Climate Changes. *Current Climate Change Reports*, 2, pp. 148-158, DOI: 10.1007/s40641-016-0049-3.

Wade, B.S., Houben, A.J.P., Quaijtaal, W., Schouten, S., Miller, K.G., Katz, M.E., Wright, J.D. & Brinkhuis, H., 2012. Multiproxy record of abrupt sea-surface cooling across the Eocene-Oligocene transition in the Gulf of Mexico. *Geology*, 40, 2, pp. 159-162, DOI:10.1130/G32577.1.

Watson, A.J., Bakker, D.C.E., Ridgwell, A.J., Boyd, P.W. & Law, C.S., 2000. Effect of iron supply on Southern Ocean CO2 uptake and implications for glacial atmospheric CO_2. *Nature*, 407, pp. 730-733.

Waugh, D.W., Primeau, F., DeVries, T. & Holzer, M., 2013. Recent Changes in the Ventilation of the Southern Oceans. *Science*, 339, pp. 568-570, DOI: 10.1126/science.1225411.

Weaver, A.J., Eby, M., Wiebe, E.C., Bitz, C.M., Duffy, P.B., Ewen, T.L., Fanning, A.F., Hollands, M.M., MacFadyen, A., Matthews, H.D., Meissner, K.J., Saenko, O., Schmittner, A., Wang, H. & Yoshimori, M., 2001. The UVic earth system climate model: Model description, climatology, and applications to past, present and future climates, Atmosphere-Ocean, 39:4, 361-428, DOI: 10.1080/07055900.2001.9649686.

Weertman, J., 1976. Milankovitch solar radiation variations and ice age ice sheet sizes. *Nature*, 261, pp. 17-20.

White, A. A. & Bromley, R. A., 1995. Dynamically consistent, quasihydrostatic equations for global models with a complete representation of the Coriolis force. *Quarterly Journal of the Royal Meteorological Society*, 121, pp. 399–418, DOI: 10.1002/qj.49712152208.

Wilson, D., 1998. Unified Model User Guide, chap. Precipitation, p. 32, in: Matthews (1998), available at: http://www.ukscience.org/_Media/UM_User_Guide.pdf (last accessed: 8 September 2017).

Wilson, G.S., Roberts, A.P., Verosub, K.L., Florindo, F. & Sagnotti, L., 1998. Magnetobiostratigraphic chronology of the Eocene–Oligocene transition in the CIROS-1 core, Victoria Land margin, Antarctica: Implications for Antarctic glacial history. *GSA Bulletin*, 10, 1, pp. 35-47

Wilson, D.S., Jamieson, S.S.R., Barrett, P.J., Leitchenkov, G., Gohl, K. & Larter, R.D., 2012. Antarctic topography at the Eocene-Oligocene boundary. *Palaeogeography, Palaeoclimatology, Palaeoecology*, 335-336, pp. 24-34, DOI: 10.1016/j.palaeo.2011.05.028.

Wilson, D.S., Pollard, D., DeConto, R.M., Jamieson, S.S.R. & Luyendyk, B.P., 2013. Initiation of the West Antarctic Ice Sheet and estimates of total Antarctic ice volume in the earliest Oligocene. *Geophysical Research Letters*, 40, pp. 4305-4309, DOI: 10.1002/grl.50797.

Wolff, E.W., Shepherd, J.G., Shuckburgh, E. & Watson, A.J., 2015. Feedbacks on climate in the Earth system: introduction. *Philosophical Transactions of the Royal Society A*, 373, 20140428, DOI: 10.1098/rsta.2014.0428.

Zachos, J.C. & Kump, L.R., 2005. Carbon cycle feedbacks and the initiation of Antarctic glaciation in the earliest Oligiocene. *Global and Planetary Change*, 47, pp. 51-66, DOI: 10.1016/j.gloplacha.2005.01.001.

Zachos, J.C., Breza, J.R. & Wise, S.W., 1992. Early Oligocene ice-sheet expansion on Antarctica: Stable isotope and sedimentological evidence from Kerguelen Plateau, southern Indian Ocean. *Geology*, 20, pp. 569-573.

Zachos, J.C., Quinn, R.M., & Salamy, K., 1996. High resolution (104 yr) deep-sea foraminiferal stable isotope records of the Eocene–Oligocene climate transition. *Paleoceanography*, 11, pp. 251-266, DOI: 10.1029/96PA00571.

Zachos, J.C., Shackleton, N.J., Revenaugh, J.S., Pälike, H. & Flower, B.P., 2001. Trends, Rhythms, and Aberrations in Global Climate 65 Ma to Present. *Science*, 292, pp. 686-693, DOI: 10.1126/science.1059412.

Zachos, J.C., Dickens, G.R. & Zeebe, R.E., 2008. An early Cenozoic perspective on greenhouse warming and carbon cycle dynamics, *Nature*, 551 (7176), pp. 279-283, DOI: 10.1038/nature06588.

Zanazzi, A., Kohn, M.J., MacFadden, B.J. & Terry, D.O., 2007. Large temperature drop across the Eocene–Oligocene transition in central North America. *Nature*, 445, pp. 639-642, DOI: doi:10.1038/nature05551.

Zhang, Z., Nisancioglu, K.H., Flatøy, F., Bentsen, M., Bethke, I. & Wang, H., 2011. Tropical seaways played a more important role than high latitude seaways in Cenozoic cooling. *Climate of the Past*, 7, pp. 801-813, DOI: 10.5194/cp-7-801-2011.

Zhang, Y.G., Pagani, M., Liu, Z., Bohaty, S.M. & DeConto, R.M., 2013. 40-million year history of atmospheric CO2. *Philosophical Transactions of the Royal Society A*, 371, p. 20130096, DOI: 10.1098/rsta.2013.0096.

Zonneveld, K.A.F., Marret, F., Versteegh, G.J.M., Bogus, K., Bonnet, S., Bouimetarhan, I., Crouch, E., de Vernal, A., Elshanawany, R., Edwards, L., Esper, O., Forke, S., Grøsfjeld, K., Henry, M., Holzwarth, U., Kielt, J.F., Kim, S.Y., Ladouceur, S., Ledu, D., Chen, L., Limoges, A., Londeix, L., Lu, S.H., Mahmoud, M.S., Marino, G., Matsouka, K., Matthiessen, J., Mildenhal, D.C., Mudie, P., Neil, H.L., Pospelova, V., Qi, Y., Radi, T., Richerol, T., Rochon, A., Sangiorgi, F., Solignac, S., Turon, J.L., Verleye, T., Wang, Y., Wang, Z. & Young, M., 2013. Atlas of modern dinoflagellate cyst distribution based on 2405 data points. *Review of Palaeobotany and Palynology*, 191, pp. 1-197, DOI: 10.1016/j.revpalbo.2012.08.003.

List of abbreviations

ACC: Antarctic Circumpolar Current

AIS: Antarctic Ice Sheet

DP: Drake Passage

E/O: Eocene-Oligocene Boundary

E-P: Evaporation-Precipitation

EAIS: East Antarctic Ice Sheet

EMIC: Earth system Model of Intermediate Complexity

EOT: Eocene-Oligocene Transition

ESM: Earth System Model

GCM: General Circulation Model

IRD: Ice Rafted Debris

IS: Indonesian Seaway

Ma: Million years ago

MLD: Mixed Layer Depth

NLR: Nearest Living Relative

P: Atmospheric Pressure

PI: Pre-Industrial

PS: Panama Seaway

SAT: Surface Air Temperature

SST: Sea Surface Temperature

SO: Southern Ocean

TDP: Tanzania Drilling Project

TS: Tasman Seaway

UM: Unified Model

U_t: Model uncertainty (based on *t*-distribution)

WAIS: West Antarctic Ice Sheet

Δ_{glac}: Model response to glaciation

Appendix 1: Description of model simulations

Table A1.1: Description of simulations carried out by A.T. Kennedy-Asser during this PhD, including those not used in the thesis. Note: all simulations are continuations of simulations by D.J. Lunt and A. Farnsworth.

Expt. name	Stage	pCO_2	AIS state	Islands	*Other changes/purpose & description (*including paper/ chapter if used*)	Spin-up phase	Length (ave. period)	Ancil code	Atmos. restart	Ocean restart
TDWQE	Rup.	2	EAIS	Correct	Ice sheet sensitivity (*Kennedy et al. 2015; Chapter 2, 3*)	4	1,000 (30)	rup_040	tdlcla@dam69c1	ocean.restart_rup_025
TDWQF	Cha.	2	Full	Correct	Ice sheet sensitivity (*Kennedy et al. 2015; Chapter 2, 3*)	4	1,000 (30)	cha_040	tdlcma@dam69c1	ocean.restart_cha_025
TDWQJ	Pri.	2	No ice	Incorrect	Ice sheet sensitivity (*Kennedy et al. 2015; Chapter 2*)	4	1,000 (30)	pri_010	tdlcga@dam72c1	ocean.restart_pri_010
TDWQK	Pri.	2	No ice	Correct	Correcting island definition of TDWQJ (*Chapter 2, 3*)	4	1,000 (30)	pri_011	tdlcga@dam72c1	ocean.restart_pri_011
TDWQL	Pri.	2	Full	Incorrect	Ice sheet sensitivity (*Kennedy et al. 2015; Chapter 2*)	4	1,000 (30)	pri_045	tdlcka@dam69c1	ocean.restart_pri_025
TDWQM	Pri.	2	EAIS	Incorrect	Ice sheet sensitivity (*Kennedy et al. 2015; Chapter 2*)	4	1,000 (30)	pri_040	tdlcka@dam69c1	ocean.restart_pri_025
TDWQP	Rup.	2	Full	Correct	Continuation to produce more stash/output	4+	50 (40)	rup_025	tdlupa@daw74c1	tdlupo@daw74c1
TDWQQ	Cha.	2	EAIS	Correct	Continuation to produce more stash/output	4+	50 (40)	cha_025	tdluqa@daw74c1	tdluqo@daw74c1
TDWQV	Pri.	2	Full	Correct	Correcting island definition of TDWQL (*Chapter 2, 3*)	4	1,000 (30)	pri_046	tdlcka@dam69c1	ocean.restart_pri_046
TDZSA	Pri.	2	Full*	Incorrect	*Ice sheet surface/ albedo changes only – rerunning end of TDZSM that corrupted	4	195 (30)	pri_045a	tdzsma@dau79c1	tdzsmo@dau79c1
TDZSC	Pri.	4	No ice	Correct	Boundary condition ensemble (*Chapter 3*)	4	1,000 (30)	pri_011	tdlcga@dam72c1	ocean.restart_pri_011
TDZSD	Pri.	4	Full	Correct	Boundary condition ensemble (*Chapter 3*)	4	1,000 (30)	pri_046	tdlcka@dam69c1	ocean.restart_pri_046
TDZSE	Cha.	4	Full	Correct	Boundary condition ensemble (*Chapter 3*)	4	1,000 (30)	cha_040	tdlcma@dam69c1	ocean.restart_cha_025

TDZSI	Pri.	2	No Ice	Ant.-Aus. Isl.*	* Antarctica and Australia defined as one island (*Chapter 2*)	4	1,000 (30)	pri_012	tdlcga@dam72c1	ocean.restart_pri_012
TDZSJ	Pri.	2	Full	Ant.-Aus. Isl.*	* Antarctica and Australia defined as one island (*Chapter 2*)	4	1,000 (30)	pri_048	tdlcka@dam69c1	ocean.restart_pri_048
TDZSM	Pri.	2	Full*	Incorrect	*Ice sheet surface/ albedo changes only	4	1,000 (30)	pri_045a	tdlcka@dam69c1	ocean.restart_pri_045a
TDZSN	Pri.	2	Full*	Incorrect	*Ice sheet elevation changes only	4	1,000 (30)	pri_045b	tdlcka@dam69c1	ocean.restart_pri_045b
TDZSO	Rup.	4	No ice	Correct	Turgai control (standard Rupelian)	5-alt	3,000 (50)	rup_012	tenjda@daw74c1	tenjdo@daw74c1
TDZSP	Rup.	4	No ice	Correct	Idealised lake added for Turgai	5-alt	3,000 (50)	rup_011	tenjca@daw74c1	tenjco@daw74c1
TDZSQ	Rup.	4	No ice	Correct	Idealised lake/strait added for Turgai	5-alt	3,000 (50)	rup_013	tenjea@daw74c1	tenjeo@daw74c1
TDZSS	Rup.	4	No ice	Correct	Turgai control (standard Rupelian) – continuation of TDZSO	5-alt	3,000 (50)	rup_012	tdzsoa@dau00c1	tdzsoo@dau00c1
TDZST	Rup.	4	No ice	Correct	Idealised lake added for Turgai – continuation of TDZSP	5-alt	3,000 (50)	rup_011	tdzspa@dau00c1	tdzspo@dau00c1
TDZSU	Rup.	4	No ice	Correct	Idealised lake/strait added for Turgai – continuation of TDZSQ	5-alt	3,000 (50)	rup_013	tdzsqa@dau00c1	tdzsqo@dau00c1
TEVDA	Rup.	2	No ice	Correct	Continuing Kennedy et al. 2015 simulations	5-alt	3,000 (50)	rup_010	tdluta@daw75c1	tdluto@daw75c1
TEVDB	Rup.	2	Full	Correct	Continuing Kennedy et al. 2015 simulations	5-alt	3,000 (50)	rup_025	tdlupa@daw74c1	tdlupo@daw74c1
TEVDE	Pri.	2	No ice	Correct	Continuing Kennedy et al. 2015 simulations	5-alt	3,000 (50)	pri_011	tdwqka@daw74c1	tdwqko@daw74c1
TEVDF	Pri.	2	Full	Correct	Continuing Kennedy et al. 2015 simulations (crashed)	5-alt	1,903 (50)	pri_046	tdwqva@daw74c1	tdwqvo@daw74c1
TEVDG	Pri.	2	Full	Correct	Continuing Kennedy et al. 2015 simulations (restarted, crashed)	5-alt	597 (50)	pri_046	tevdfa@dai03c1	tevdfo@dai03c1
TEVDH	Pri.	2	Full	Correct	Continuing Kennedy et al. 2015 simulations (restarted, completed)	5-alt	500 (50)	pri_046	tevdga@dap00c1	tevdgo@dap00c1

Table A1.2: Simulations used in the analysis carried out by other researchers. Note: all Getech Phase 4 simulations are continuations of simulations by D.J. Lunt and A. Farnsworth (Phases 1-3).

Expt. name	Stage	pCO_2	AIS state	Islands/ Drake Passage	Description (*including paper/ chapter where used*)	Spin-up phase	Length (ave. period)	Owner
TECQN	Rup. Alt.	2	AIS	DP open	Robertsons simulation (*Chapter 3, 4*)	N/A	6,550 (100)	P.J. Valdes
TECQO	Rup. Alt.	2	AIS	DP closed	Robertsons simulation (*Chapter 3, 4*)	N/A	9,350 (100)	P.J. Valdes
TECQP	Rup. Alt.	2	No ice	DP closed	Robertsons simulation (*Chapter 3, 4*)	N/A	10,182 (100)	P.J. Valdes
TECQQ	Rup. Alt.	2	No ice	DP open	Robertsons simulation (*Chapter 3, 4*)	N/A	6,121 (100)	P.J. Valdes
TECQS	Rup. Alt.	3	AIS	DP open	Robertsons simulation (*Chapter 3, 4*)	N/A	6,921 (100)	P.J. Valdes
TECQT	Rup. Alt.	3	AIS	DP closed	Robertsons simulation (*Chapter 3, 4*)	N/A	13,557 (100)	P.J. Valdes
TECQU	Rup. Alt.	3	No ice	DP closed	Robertsons simulation (*Chapter 3, 4*)	N/A	10,385 (100)	P.J. Valdes
TECQV	Rup. Alt.	3	No ice	DP open	Robertsons simulation (*Chapter 3, 4*)	N/A	6,493 (100)	P.J. Valdes
TDLUP	Pri.	2	Full	Correct	Original Getech Phase 4 (*Kennedy et al. 2015; Chapter 2, 3*)	4	1,000 (30)	A. Farnsworth
TDLUQ	Rup.	2	EAIS	Correct	Original Getech Phase 4 (*Chapter 3*)	4	1,000 (30)	A. Farnsworth
TDLUT	Rup.	2	No ice	Correct	Original Getech Phase 4 – continuation of TDLUN which crashed (*Kennedy et al. 2015; Chapter 2, 3*)	4	416 (30)	A. Farnsworth
TDLUU	Cha.	2	Full	Correct	Original Getech Phase 4 – continuation of TDLUO which crashed (*Chapter 3*)	4	489 (30)	A. Farnsworth
TDLUV	Rup.	4	No ice	Correct	Original Getech Phase 4 (*Chapter 3*)	4	1,000 (30)	A. Farnsworth
TDLUW	Rup.	4	Full	Correct	Original Getech Phase 4 (*Chapter 3*)	4	1,000 (30)	A. Farnsworth
TDLUX	Cha.	4	EAIS	Correct	Original Getech Phase 4 (*Chapter 3*)	4	1,000 (30)	A. Farnsworth
TDLUY	Cha.	4	No ice	Correct	Original Getech Phase 4 (*Chapter 3*)	4	1,000 (30)	A. Farnsworth

Appendix 2: Supplementary model data summary included in Kennedy-Asser et al. (2019)

Table A2.1: Summary of model setup, spin-up and mean values from various climate variables for all simulations included in Chapters 3.

Simulation name	Averaging period/run length (years)	Annual mean global TOA energy imbalance (W m^{-2})	Global annual mean SAT (°C)	Global annual mean SST (°C)	Drake Passage through-flow (Sv)	Annual mean Southern Ocean SST (°C)	Antarctic total annual precip. (mm)	Gamburtsev summer (DJF) mean SAT (°C)	Max. Southern Ocean MLD (m)	Max. southern overturn-ing (Sv)	Max. North Atlantic MLD (m)	Max northern overturn-ing (Sv)	Annual mean Antarctic SAT (°C)	Antarctic winter sea ice extent (km^2)
TDLUY	30/1,422	0.31	21.84	24.98	69.74	10.28	659.58	17.96	543.28	21.03	347.36	10.35	-4.24	75558
TDLUX	30/1,422	0.01	21.16	24.67	90.93	9.60	470.76	-14.02	879.19	30.74	357.30	10.59	-18.13	109183
TDZSE	30/1,422	-0.05	21.04	24.65	99.39	9.48	436.30	-18.13	971.23	32.59	305.44	8.67	-21.19	136688
TDLUU	30/1,422	-0.20	18.91	22.91	77.96	8.10	610.74	13.72	609.78	24.98	379.87	12.64	-8.21	159273
TDLUQ	30/1,422	-0.49	18.35	22.72	103.52	7.71	406.68	-18.43	833.60	33.62	352.22	10.37	-22.15	172244
TDWQF	30/1,422	-0.55	18.25	22.72	107.03	7.70	372.91	-22.34	1007.94	33.85	320.60	10.78	-25.25	119979
TDLUV	30/1,422	0.28	21.40	24.46	45.77	8.14	598.14	13.16	791.05	19.22	368.29	12.71	-6.01	250985
TDLUW	30/1,422	0.02	20.79	24.45	62.80	9.36	426.96	-17.44	990.67	30.31	113.66	4.00	-21.27	178231
TDLUT	30/1,422	-0.19	18.60	22.58	46.19	7.18	546.42	7.66	684.14	27.39	350.55	11.94	-9.53	283253
TDWQE	30/1,422	-0.39	17.94	22.30	64.46	7.18	382.34	-19.21	936.98	34.92	371.05	11.32	-23.02	219187
TDLUP	30/1,422	-0.45	17.88	22.33	68.00	7.22	342.01	-22.86	1145.65	37.39	292.19	11.94	-26.13	104858
TECQS	100/6,921	-0.07	22.20	24.43	56.18	5.93	301.09	-18.20	461.67	11.68	129.89	7.57	-24.96	1585357
TECQV	100/6,493	-0.07	23.58	25.27	43.32	8.21	557.10	16.32	317.31	14.10	169.43	12.35	-5.08	567223
TECQN	100/6,550	-0.11	20.02	22.80	60.67	4.11	240.57	-21.85	553.05	13.17	131.37	6.89	-28.47	3246863
TECQQ	100/6,121	-0.03	20.97	23.29	49.68	5.64	486.19	12.34	387.42	13.06	143.13	8.86	-9.37	1785803
TECQT	100/13,557	-0.01	22.37	24.62	0.00	6.46	334.76	-16.83	689.98	17.09	133.26	5.67	-23.11	1600795
TECQU	100/10,385	0.14	23.92	25.73	0.00	10.08	652.23	19.09	365.31	18.88	133.88	6.05	-2.32	262160
TECQO	100/9,350	-0.09	20.20	22.98	0.00	4.12	274.61	-20.09	825.02	18.04	126.14	5.09	-26.37	3291955
TECQP	100/10,182	0.08	21.37	23.75	0.00	7.21	566.35	15.03	499.88	16.97	130.55	5.48	-6.31	1078409
TDZSC	30/1,422	0.32	21.59	24.53	27.31	7.56	574.70	13.70	386.54	17.47	493.53	15.44	-5.98	406952
TDZSD	30/1,422	0.14	20.66	24.18	45.70	8.05	389.85	-18.10	785.46	32.02	392.08	13.33	-22.53	336800
TDWQK	30/1,422	-0.04	18.52	22.44	38.41	6.54	524.41	6.88	819.93	24.43	450.19	15.26	-10.29	693624
TDWQV	30/1,422	-0.45	18.02	22.41	62.71	7.43	345.59	-21.57	1080.12	33.77	467.95	13.50	-25.64	114177

Appendix 3: Data compilations used in Chapter 4 (in simplified format, with a detailed source).

Table A3.1: Compilation of temperature proxy records for the late Eocene.

Site	Palaeo-Lat.	Palaeo-Long.	Mean annual temp. (MAT; °C)	Max. MAT (°C)	Min. MAT (°C)	Proxy description	Age max. (Ma)	Age min. (Ma)	Source
Maud Rise	-65.3	1.6	12.3	13.3	11.3	Clumped isotopes	35.3	34.2	Value from Petersen & Schrag, 2015 (Table 2)
Prydz Bay	-66.2	73.5		12.0		Veg. NLR	39.0	34.0	Maximum value given in Trusswell & Macphail, 2009 (p. 100)
Prydz Bay	-66.2	73.5	10.3	13.9	6.7	S-index	35.8	33.7	Value from Passchier et al., 2016 (supp. info.), error from main text (p. 2)
Prydz Bay	-66.2	73.5		10.0		Dinocysts	35.4	33.6	Value from Houben et al., 2013, (Figure 3) and Zonnefeld et al., 2013 (Figure 208)
Kerguelen Plateau	-59.5	77.8	14.3	15.3	13.3	Mg/Ca	35.3	34.2	Offset from Maud Rise by 2°C, value in Bohaty et al., 2012, (Section 4.1)
Australian Bight	-51.6	119.6			10.0	Dinocysts	34.1	33.7	Value from Houben et al., 2013, (Figure 3) and Zonnefeld et al., 2013 (Figure 208)
Wilkes Land U1356	-61.1	130.3				No data			
Wilkes Land U1360	-66.2	137.1				No data			
West Tasman Plateau	-58.4	141.0			10.0	Dinocysts	35.6	33.6	Value from Houben et al., 2013, (Figure 3) and Zonnefeld et al., 2013 (Figure 208)
S. Australia	-52.8	144.8	23.1	27.8	18.4	Lignite	37.6	34.0	Value, calibration error and dating from V. Lauretano (University of Bristol, pers. comm.)
S. Australia (region)	-52.8	144.8	16.0	20.6	11.3	Veg. Coexist.	36.6	34.0	Max. and min. values quoted in Pound and Salzmann, 2017 (p.4), location assumed the same as Lauretano data; mean taken between the max. and min. may be unrealistic
East Tasman Plateau	-58.8	152.3	17.5	21.5	13.5	TEX_{86}	38.5	36.5	Value from Douglas et al., 2014 (Figure S3; reading off TEX86L), with standard 4°C error for TEX86L
East Tasman Plateau	-58.8	152.3		10.0		Dinocysts	35.5	33.7	Value from Houben et al., 2013, (Figure 3) and Zonnefeld et al., 2013 (Figure 208)

Ross Sea	-76.6	156.2		13.0		Veg. NLR	41.0	34.0	Value from Francis et al., 2009 (p.333), location assumed the same as CRP-3 and age assumed 41-34 Ma (Bartonian/Priabonian)
Ross Sea	-76.6	156.2	8.7	12.3	5.1	S-index	36.2	34.2	Value from Passchier et al., 2013 (supp. info.; MAT sheet), error from main text (p. 1403)
New Zealand	-58.9	175.8	25.9	27.1	24.7	TEX_{86}	35.4	33.6	Value and error from Liu et al., 2009 (supp. info.), error of 2 stan. dev.
New Zealand	-58.9	175.8	25.6	27.6	23.6	$U^{K'}_{37}$	35.4	33.6	Value and error from Liu et al., 2009 (supp. info.), error of 2 stan. dev.
King George Isl.	-63.8	-62.5	10.0	15.0	5.0	Veg. NLR	41.0	34.0	Max. value from Birkenmajer & Zastawniak, 1989, main text (p. 238), date from main text (p. 234, discussion of loc. 7); Min. value from Francis et al. 2009 (p.330-331); mean taken between the max. and min. may be unrealistic
Seymour Isl.	-66.3	-58.4	12.8	16.0	9.2	Clumped isotopes	37.5	34.0	Value from Douglas et al., 2014 (supp. info., Table S3: mean of 34, 37.4 and 37.5 Ma values for both *Cucullaea* and *Eurhomalea*), error from maximum range of these values with their external error
Seymour Isl.	-66.3	-58.4	11.6	17.0	9.0	TEX_{86}	37.5	34.0	Value from Douglas et al., 2014 (supp. info., Table S4: mean of 34, 37.4 and 37.4 Ma TEX86L and TEX86' values), error from main text (p.4)
Seymour Isl.	-66.3	-58.4	16.5	22.3	10.7	MBT-CBT	37.5	34.0	Values from Douglas et al., 2014, (supp. info., Table S4: mean of 34, 37.4 and 37.5 Ma values). Two calibrations give very different values, taken here as a max. and min. range; mean (of max. and min.) may therefore be unrealistic
Weddell Sea	-63.9	-40.0		10.0		Dinocysts	36.6	33.6	Value from Houben et al., 2013, (Figure 3) and Zonnefeld et al., 2013 (Figure 208)
Falklands Plateau	-59.5	-39.4	18.4	22.0	14.8	TEX_{86}	37.1	33.3	Value and error from Liu et al., 2009 (supp. info.), error of 2 stan. dev.
Falklands Plateau	-59.5	-39.4	19.5	23.7	15.3	$U^{K'}_{37}$	37.1	33.3	Value and error from Liu et al., 2009 (supp. info.), error of 2 stan. dev.
S.W. Atlantic (region)	-60.0	-60.0	15.9	18.4	13.4	Veg. Coexist.	37.0	34.0	Max. and min. values quoted in Pound & Salzmann, 2017 (p.5), location is very large/unspecified, mean taken between the max. and min. may be unrealistic

Table A.3.2: Compilation of temperature proxy records for the early Oligocene.

Site	Paleo-Lat.	Palao-Long.	Mean annual temp. (MAT; °C)	Max. MAT (°C)	Min. MAT (°C)	Proxy description	Age max. (Ma)	Age min. (Ma)	Source
Maud Rise	-65.3	1.6	11.9	12.2	11.6	Clumped isotopes	33.0	31.9	Value from Petersen & Schrag, 2015 (Table 2)
Prydz Bay	-66.2	73.5		10.0		Dinocysts	33.6	33.3	Value from Houben et al., 2013, (Figure 3) and Zonnefeld et al., 2013 (Figure 208)
Prydz Bay	-66.2	73.5	8.0	11.6	4.4	S-index	33.7	32.9	Value from Passchier et al., 2016 (supp. info.; error from main text, p.2)
Kerguelen Plateau	-59.5	77.8	11.7	13.5	9.9	Mg/Ca	34.0	33.2	Value from Bohaty et al., 2012 (Section 4.2), taken away from inferred late Eocene temp. (see Table A3.1); max. and min. allowing for error in absolute values (from Petersen & Schrag, 2015) and change (Bohaty et al., 2012)
Australian Bight	-51.6	119.6			10.0	Dinocysts	33.6	30.6	Value from Houben et al., 2013, (Figure 3) and Zonnefeld et al., 2013 (Figure 208)
Wilkes Land U1356	-61.1	130.3		10.0		Dinocysts	33.5	30.5	Value from Houben et al., 2013, (Figure 3) and Zonnefeld et al., 2013 (Figure 208)
Wilkes Land U1356	-61.1	130.3	8.9	12.5	5.3	S-index	33.6	30.0	Value from Passchier et al., 2013 (supp. info.; MAT sheet), error from main text (p. 1403)
Wilkes Land U1356	-61.1	130.3	17.5	24.0	11.0	TEX_{86}	33.1	32.9	Value from Hartman et al., 2018 (reading first three points in record shown in Figure 3), with 4°C calibration error based on main text (p. 1285)
Wilkes Land U1360	-66.2	137.1		10.0		Dinocysts	33.6	32.4	Value from Houben et al., 2013, (Figure 3) and Zonnefeld et al., 2013 (Figure 208)
West Tasman Plateau	-58.4	141.0			10.0	Dinocysts	33.6	30.6	Value from Houben et al., 2013, (Figure 3) and Zonnefeld et al., 2013 (Figure 208)
S. Australia	-52.8	144.8	20.0	24.7	15.3	Lignite	33.9	33.7	Value, calibration error and dating from V. Lauretano (University of Bristol, pers. comm.)
S. Australia (region)	-52.8	144.8	16.0	20.6	11.3	Veg. Coexist.	33.0	30.0	Max. and min. values quoted in Pound and Salzmann, 2017 (p.4), location assumed the same as Lauretano data; mean taken between the max. and min. may be unrealistic
East Tasman Plateau	-58.8	152.3			10.0	Dinocysts	30.7	30.3	Value from Houben et al., 2013, (Figure 3) and Zonnefeld et al., 2013 (Figure 208)

Ross Sea	-76.6	156.2	7.8	11.4	4.2	S-index	33.6	33.0	Value from Passchier et al., 2013 (supp. info.; MAT sheet), error from main text (p. 1403)
Ross Sea	-76.6	156.2		10.0		Dinocysts	32.5	31.0	Value from Houben et al., 2013, (Figure 3) and Zonnefeld et al., 2013 (Figure 208)
Ross Sea	-76.6	156.2	-2.0	8.0	-12.0	Veg. NLR	32.0	31.0	Max. value from Passchier et al., 2013 (supp. info.; vegetation sheet), based on their interpretation of similar modern ecosystem. Min. value based on interpretations of Francis & Hill, 1996. Mean taken between both. Approx. age from Prebble et al., 2006
New Zealand	-58.9	175.8	23.8	24.8	22.8	TEX_{86}	33.6	33.4	Value and error from Liu et al., 2009 (supp. info.), error of 2 stan. dev.
New Zealand	-58.9	175.8	22.4	23.8	21.0	$U^{K'}_{37}$	33.6	33.4	Value and error from Liu et al., 2009 (supp. info.), error of 2 stan. dev.
King George Isl.	-63.8	-62.5				No data			
Seymour Isl.	-66.3	-58.4				No data			
Weddell Sea	-63.9	-40.0		10.0		Dinocysts	33.6	33.2	Value from Houben et al., 2013, (Figure 3) and Zonnefeld et al., 2013 (Figure 208)
Falklands Plateau	-53.0	-39.5	11.2	14.4	8.0	TEX_{86}	33.7	33.1	Value and error from Liu et al., 2009 (supp. info.), error of 2 stan. dev.
Falklands Plateau	-53.0	-39.5	11.1	13.7	8.5	$U^{K'}_{37}$	33.7	33.1	Value and error from Liu et al., 2009 (supp. info.), error of 2 stan. dev.
S.W. Atlantic (region)	-60.0	-60.0	17.6	23.4	11.7	Veg. Coexist.	31.1	30.9	Max. and min. values quoted in Pound & Salzmann, 2017 (p.5), location is very large/unspecified, mean taken between the max. and min. may be unrealistic

Table A3.3: Compilation of temperature proxy records across the Eocene-Oligocene Transition.

Site	Palaeo-Lat.	Palaeo-Long.	Mean temp. change (°C)	Max. temp. change (°C)	Min. temp. change (°C)	Proxy description	Source
Maud Rise	-65.3	1.6			0.0	Nannofossils	General cooling suggested from Villa et al., 2013 (Figures 5 and 6)
Maud Rise	-65.3	1.6			0.0	Mg/Ca	General cooling suggested from Bohaty et al., 2012 (Figure 4b)
Maud Rise	-65.3	1.6	-0.4	-1.5	0.7	Clumped isotopes	Value from Petersen & Schrag, 2015 (Table 2)
Prydz Bay	-66.2	73.5			0.0	Dinocysts	*S. antarctica* increase shown in Houben et al., 2013 (Figure 3 and in supplementary dataset)
Prydz Bay	-66.2	73.5	-2.3	-5.1	0.5	S-index	Mean from difference in Passchier et al., 2016 (supp. info.); range taken from difference between max. and min. of each period based on 2 stan. dev.
Kerguelen Plateau	-59.5	77.8	-2.6	-3.4	-1.8	Mg/Ca	Value from Bohaty et al., 2012 (Section 4.2)
Kerguelen Plateau	-59.5	77.8			0.0	Nannofossils	General cooling suggested from Villa et al., 2013 (Figures 2, 3 and 4)
Australian Bight	-51.6	119.6				No clear change	No change shown in Houben et al., 2013 (Figure 3)
Wilkes Land U1356	-61.1	130.3				No data	
Wilkes Land U1360	-66.2	137.1				No data	
West Tasman Plateau	-58.4	141.0				No clear change	No change shown in Houben et al., 2013 (Figure 3)
S. Australia	-52.8	144.8	-3.1	-9.1	2.9	Lignite	Value from difference in V. Lauretano data; range taken from difference between max. and min. of each period based on 2 stan. dev.
S. Australia (region)							Max. and min. values quoted in Pound & Salzmann, 2017 (p.4) suggest a drop in MATR before the EOT, no change across EOT, then rising to same values after; location assumed the same as Lauretano data

East Tasman Plateau	-58.8	152.3		0.0		Dinocysts	*S. antarctica* disappearance shown in Houben et al., 2013 (Figure 3 and in supplementary dataset)
Ross Sea	-76.6	156.2	-1.0	-5.9	4.0	S-index	Value from difference in Passchier et al., 2013 (supp. info.; MAT sheet), range taken from difference between max. and min. of each period based on 2 stan. dev.
New Zealand	-58.9	175.8	-2.1	-2.9	-1.3	TEX_{86}	Value and error from Liu et al., 2009 (supp. info.)
New Zealand	-58.9	175.8	-3.1	-4.4	-1.8	$U^{K'}_{37}$	Value and error from Liu et al., 2009 (supp. info.)
King George Isl.	-63.8	-62.5				No data	
Seymour Isl.	-66.3	-58.4				No data	
Weddell Sea	-63.9	-40.0			0.0	Dinocysts	*S. antarctica* increase shown in Houben et al., 2013 (Figure 3 and in supplementary dataset)
Falklands Plateau	-53.0	-39.5	-7.2	-9.6	-4.8	TEX_{86}	Value and error from Liu et al., 2009 (supp. info.)
Falklands Plateau	-53.0	-39.5	-8.4	-10.9	-5.9	$U^{K'}_{37}$	Value and error from Liu et al., 2009 (supp. info.); similar value recorded by Plancq et al., 2014
S.W. Atlantic (region)	-60.0	-60.0				No clear change	Max. and min. values quoted in Pound & Salzmann, 2017 (p.5) suggest a drop in MATR before the EOT, no change across EOT, then rising to same values after; location is very large/unspecified

Table A3.4: Proxy record location information. The Getech ranges are taken from back rotations of the present day site locations using the Getech plate model, which is based on the paleomagnetic reference frame (Torsvik et al., 2012). Ranges show the maximum and minimum values of longitude and latitude of all sites at each location across the Priabonian, Rupelian and Chattian.

Location	Site	Accepted Palaeo-Lat. (°S)	Accepted Palaeo-Long. (°E)	Getech Palaeo-Lat. range (°S)	Getech Palaeo-Long. range (°E)	Previously published Palaeo-Lat.	Previously published Palaeo-Long.
Maud Rise	ODP 689 + 690 average	65.3	1.6	65.0 – 65.6	-0.6 – 3.9	ODP 689: 64 °S (Bohaty et al., 2012, table 1)	None available
Prydz Bay	ODP 739, 742 + 1166 average	66.2	73.5	66.1 – 66.3	72.5 – 74.5	None available	None available
Kerguelen Plateau	ODP 738, 744 + 748 average	59.5	77.8	56.1 – 61.4	75.7 – 81.2	ODP 738: 63 °S, ODP 744: 62 °S, ODP 748: 58 °S (Bohaty et al., 2012, table 1)	None available
Australian Bight	ODP 1128	51.6	119.6	48.8 – 54.4	118.0 – 121.2	None available	None available
Wilkes Land	U1356	61.1	130.3	60.9 – 61.3	129.5 – 131.1	None available	None available
Wilkes Land	U1360	66.2	137.1	66.0 – 66.4	136.2 – 138.0	None available	None available
West Tasman Plateau	ODP 1168	58.4	141.0	55.6 – 61.2	140.9 – 141.1	None available	None available
S. Australia	Traralgon	52.8	144.8	50.3 – 55.3	144.7 – 144.9	None available	None available
S. Australia (region)	Multiple sites	52.8	144.8	Multiple sites are included in this vegetation record (Pound & Salzmann, 2017): the location is assumed the same as the other S. Australia site			
East Tasman Plateau	ODP 1172	58.8	152.3	56.2 – 61.4	151.2 – 153.4	None available	None available

Ross Sea	CRP-3, CIROS-1 + McMurdo average	76.6	156.2	76.3 – 76.9	155.2 – 157.2	None available	None available
New Zealand	DSDP 277	58.9	175.8	57.9 – 59.9	174.4 – 177.2	59 °S (Liu et al., 2009, table S1)	175 °W (Liu et al., 2009, table S1)
King George Isl.	Breccia Crag	63.8	-62.5	63.7 – 63.9	-62.3 – -62.7	None available	None available
Seymour Isl.	La Meseta	66.3	-58.4	66.1 – 66.5	-58.1 – -58.7	None available	None available
Weddell Sea	ODP 696	63.9	-40.0	63.8 – 64.0	-39.6 – -40.4	None available	None available
Falklands Plateau	ODP 511	53.0	-39.5	52.8 – 53.2	-37.7 – -41.3	52.5 °S (Liu et al., 2009, table S1)	39 °W (Liu et al., 2009, table S1)
S.W. Atlantic (region)	Multiple sites	60.0	-60.0	Multiple sites are included in this vegetation record (Pound & Salzmann, 2017): the location is taken at an arbitrary point within the region.			